Department of Chemical Engineering
Centre for Fuels and Energy

Catalytic Partial Oxidation of Propylene to Acrolein: The Catalyst Structure, Reaction Mechanisms and Kinetics

Hamzah Fansuri

This thesis is presented for the Degree of
Doctor of Philosophy
of
Curtin University of Technology

June 2005

Declaration

This thesis contains no material which has been accepted for the award of any other degree or diploma in any university.

To the best of my knowledge and belief this thesis contains no material previously published by any other person except where due acknowledgment has been made.

Signature: …….

Date: ……...

Acknowledgments

First, I would like to thank The AusAID for sponsoring my studies at Curtin University of Technology; AINSE for grants awarded (grant AINGRA03132, AINGRA04177 and AINGRA 04191) which enable me to carry out neutron diffraction experiments at ANSTO and CHEMEQ Company for funding which has partially supported the research. I would also like to thank Institute of Technology Sepuluh November (ITS), Surabaya and Direktorat Jenderal Pendidikan Tinggi (DIKTI) who gave me the opportunity to pursue a higher degree education. However, this dissertation could not have been completed without the assistance and support of many people and institutions.

Countless thanks to Professor Dong-ke Zhang, the Supervisor of my research, for his intense interest and patience in supervising my research, and his valuable guidance as well as his constructive comments at all stages of the research. In addition, his financial support enabled me to attend conferences, giving me opportunities to expand my knowledge about research and to exchange ideas with other scholars. I would also like to thank Dr. Gia Hung Pham of CHEMEQ Company for his invaluable help at the early stage of my candidature.

Both Professor Dong-ke Zhang and Dr. Gia Hung Pham are my guru in this research and always be my guru. I am very lucky to have been associated with them, because without their encouragement, invaluable advice and criticism, this thesis could never have come into existence.

I would also like to thank other students who were involved in the same project. To be mentioned here are: Ms Sandra Wibawanta, Ms Linlin Yang, Ms Audrey Boehly, Mr. Jasson Muirhead, and Mr. Bendan Lynch. Thank you all for your contribution in the lab work, preparation, and discussions regarding the research

subjects. I would also like to thank my colleagues in the CHEMEQ, including Andrew Huxham, Steve Jarkovic, and Ben De Pinto for their insightful discussions.

I also need to acknowledge the useful assistance provided by all academic and administrative staff in the Centre for Fuels and Energy and Department of Applied Physics at Curtin University of Technology and Bragg Institute at ANSTO. In particular Ms Angelina Rositter for the lab support, Mr. Geoffrey Han for his computer and network support, Ms Elaine Miller for her assistance with my SEM work, Professor Brian O'Connor and Dr. Suminar Pratapa for their assistance with XRD analyses, Dr. Margaret Elcombe, Dr. Andrew Studer and Mr. Michael Prior for assistance with my Neutron Diffraction analysis, and Dr. David French for his help with high temperature X-ray Diffraction analysis.

This thesis will also not exist without support, understanding, patience, and love from my family, my wife Nurul Widiastuti and my son Zahrul Atharinafi. Without their unconditional support, endless patience and constant encouragement during my stay in Perth, Western Australia, it would have been very difficult for me to finish this work.

Finally, this work would not have been possible without the previous works of other researchers cited within the body of the thesis. For this, I am also grateful.

Dedications

High above all be Allah, the King, the Truth! be not in haste with the Quran before its revelation to thee is completed but say, "O my Lord! Advance me in knowledge."

The Holy Quran - Thaha 114.

For Nurul and Zahrul,
my beloved wife and son

Publications

Journals

1. Fansuri, H., G. H. Pham, S. Wibawanta, D.K. Zhang and D. French, *The Relationship Between Structural Change in a and g-Bismuth Molybdate at High Temperature and Their Selectivity and Activity on Catalytic Partial Oxidation of Propylene to Acrolein*, Surface Review and Letters, Vol. 10 Nos. 2-3 (2003) 549-553.

2. Fansuri, H., G. H. Pham, S. Wibawanta, R. Radford, and D.K. Zhang, *Catalytic Activity of Propylene to Acrolein: The Activity of Bismuth Molybdate Catalysts under Oxygen-Rich Conditions*, DCEMP, vol 12 No 3/4 (2004) 333-340

Conference Proceedings

1. Fansuri, H., D.K. Zhang, D. French, M. Elcombe, A. Studer, An X-ray and Neutron Diffraction Study of the Structure of α-$Bi_2Mo_3O_{12}$ as Catalyst for Partial Oxidation of Propylene to Acrolein, CHEMECA 2004, Sydney, 26-29 September 2004.

2. Fansuri, H., G. H. Pham, S. Wibawanta, D. K. Zhang, *The Effect of Phosphorous Addition on the Activity of Bismuth Molybdate Catalyst for Partial Oxidation of Propylene to Acrolein*, Australian Symposium on Combustion and The 8th Australian Flames Days, Melbourne, December 2003.

3. Fansuri, H., D. K. Zhang, M. Elcombe, and A. Studer, In-Situ Neutron Diffraction Study of α-Bismuth Molybdate, CHEMECA 2003, Adelaide-Australia, September 2003.

4. Fansuri, H., G. H. Pham, S. Wibawanta, R. Radford, and D.K. Zhan, Catalytic Activity of Propylene to Acrolein: The Activity of Bismuth Molybdate Catalysts

under Oxygen-Rich Conditions, 9th APCChE Congress and CHEMECA 2002, Christchurch-New Zealand, September 2002.

Power point Presentation and Posters

1. Fansuri, H., D.K. Zhang, M. Elcombe, A. Studer, *In-situ Structural Studies of Bismuth Molybdate Catalysts for Partial Oxidation of Propylene to Acrolein using Neutron Diffraction*, SSC 2004, Praha, 12-15 September 2004.

2. Fansuri, H., D.K. Zhang, M. Elcombe, A. Studer, D. French, *Structure Determination of Powder α-$Bi_2Mo_3O_{12}$ by Joint Refinements of its Cu and Co Source X-ray and Neutron Diffractogram*, EPDIC-IX, Praha, 2-5 September 2004.

3. Fansuri, H., D.K. Zhang, M. Elcombe, A. Studer, *In-situ Neutron Diffraction Study of alpha Bismuth Molybdate*, (Poster), EPDIC-IX, Praha, 2-5 September 2004.

4. Fansuri, H., G. H. Pham, S. Wibawanta, D.K. Zhang and D. French, *The Relationship Between Structural Change in a and g-Bismuth Molybdate at High Temperature and Their Selectivity and Activity on Catalytic Partial Oxidation of Propylene to Acrolein*, (Poster), ICSOS 7, Newcastle, 21-27 July 2002.

Table of content

List of Figures

List of Tables

Abbreviations

AES	Auger Electron Spectroscopy
AINSE	Australian Institute of Nuclear Science and Engineering
ANSTO	Australian Nuclear Science and Technology Organisation
BET	Brunauer-Emmett-Teller
DTA	Differential Thermal Analysis
ED	Electron Diffraction
EXAFS	Extended X-ray Absorption Fine Structure
FID	Flame Ionisation Detector
FT-IR	Fourier-Transform Infra Red
GC	Gas Chromatography
GOF	Goodness of Fit
HIFAR	High Flux Australian Reactor
HRPD	High-Resolution Powder Diffractometer
ICSD	Inorganic Crystal Structure Database
ISS	Ion-Scattering Spectroscopy
MRPD	Medium-Resolution Powder Diffractometer
ND	Neutron Diffraction
NMR	Nuclear Magnetic Spectroscopy
SEM	Scanning Electron Microscopy

TCD	Thermal Conductivity Detector
TEM	Transmission Electron Microscopy
TGA	Thermogravimetry Analysis
UPS	Ultraviolet Photoelectron Spectroscopy
XANES	X-ray Absorption at Near Edges Spectroscopy
XPS	X-ray Photoelectron Spectroscopy
XRD	X-ray Diffraction

Summary

Bismuth molybdates have long been known as active catalysts for selective oxidation of olefins. There are several phases of bismuth molybdates but only three of them are known to be active for partial oxidation of propylene to acrolein, namely, α, β and γ bismuth molybdates. A significant amount of work has been carried out and reported in the literature, aiming to understand the reaction mechanisms so as to control the reaction process. It has been revealed that the oxidation reaction follows the redox mechanisms and lattice oxygen plays a key role as the main oxygen source for the reaction and controls the catalyst performance. The properties of the lattice oxygen are influenced by the bulk crystalline structure of the catalyst. Therefore, it is possible that the crystal structure influences the performance of the catalyst in promoting the partial oxidation reaction. However, there appears to be a lack of detailed reports in the literature on the relationship between the bulk crystal structure and the activity and selectivity of the catalyst for the partial oxidation reaction.

The work reported in this thesis has been designed to achieve an improved understanding of the catalyst structure in relation to the activity and selectivity of the catalyst for the partial oxidation of propylene to acrolein. In order to fulfil the objectives of this study, several investigation steps have been taken, namely 1) acquiring and analysing the catalyst structural parameters under real reaction conditions as well as at room temperature by means of neutron diffraction and X-ray diffraction, 2) obtaining kinetics from experimentation using a packed-bed reactor operating under differential reactor mode so as to eliminate the mass diffusion effect, and 3) developing and proposing reaction mechanisms which contain events that occur on the crystalline structure of the catalysts, particularly lattice oxygen, during the reaction.

Characterisation of the structure of the catalysts has been carried out by means of *In-situ* neutron diffraction, which has the ability to probe the crystal

structure at atomic level. The structure is characterised under simulated reaction conditions to investigate the dynamics of the crystal structure, particularly lattice oxygen, during the reaction.

The *In-situ* diffraction studies have uncovered the relationship between the crystal structure of bismuth molybdates and their selectivity and activity towards the catalytic partial oxidation of propylene to acrolein. The possible active lattice oxygen in the bismuth molybdate structures has been identified. The active lattice oxygen ions are responsible for maintaining redox balance in the crystal lattice and thus control the catalyst activity and selectivity.

Mobile oxygen ions in the three bismuth molybdate crystal phases are different. The mobile oxygen ions are O(1), O(11), and O(12) in the α phase; O(3), O(11), O(16), and O(18) in the β phase; and O(1) and O(5) in the γ phase. The mobile lattice oxygen ions are proposed to be the source of the oxidising oxygen responsible for the selective oxidation of propylene to acrolein. One common feature of all mobile oxygen ions, from a catalyst crystal structure point of view, is that they are all related to molybdenum ions rather than bismuth ions in the lattice. By modifying the physical and chemical environment of the molybdenum oxide polyhedra, it is possible to modify the catalyst selectivity and activity.

The diffraction diagnoses have also shown that molybdenum oxide polyhedra in all bismuth molybdate are unsaturated. In contrast, the bismuth oxide polyhedra are over charged. The co-existence of molybdenum ions that are co-ordinately unsaturated with bismuth ions that are over valence-charged promote the formation of allyl radical such as those found in the partial oxidation of propylene to acrolein. The molybdenum ions become propylene-adsorbing sites while the bismuth ions are the active sites to attract hydrogen from the adsorbed propylene, leading to the formation of the allyl intermediate.

Oxygen ions from the mobile lattice oxygen are a more moderate oxidant than molecular oxygen. With their mild activity, the partially oxidised products are the main products such as acrolein and formaldehyde when oxygen ions react with the allyl intermediate while more complete combustion products such as carbon oxides and organic acids become the side products.

Investigation into the kinetics and reaction mechanisms has revealed the aforementioned evidence to support the role of the mobile lattice oxygen ions in the partial oxidation of propylene to acrolein. The kinetic experiments have employed the power rate law to model the kinetic data. The model shows that the reaction orders in propylene and oxygen concentrations are a function of the reaction temperature. The reaction order in propylene increases with reaction temperature, from 0.6 at 300^{o}C to 1.0 at 450^{o}C for all the bismuth molybdate catalysts, while the reaction order in oxygen decreases from 0.6 at 300^{o}C to 0 at 450^{o}C. The activation energies are 99.7, 173, and 97.7 kJ.mol^{-1} for α-$Bi_2Mo_3O_{12}$, β-$Bi_2Mo_2O_9$, and γ-Bi_2MoO_6, respectively. The changes in reaction orders with respect to propylene and oxygen indicate that the reaction occurs through the redox mechanisms, using the mobile lattice oxygen.

The structural dynamics identified earlier explains the decrease in the acrolein selectivity at high temperatures (ca above 390^{o}C). At these temperatures, the mobile oxygen becomes more mobile and more active. As a result, as the mobility of the oxygen ions increase, their reactivity also increases. The increase in the oxygen reactivity leads to unselective, complete oxidation reaction, forming the complete oxidation products CO_2 and H_2O. The reduction-reoxidation of bismuth molybdate is controlled by the diffusion of oxygen ions in the lattice, because the reduction sites do not have to be adjacent to the oxidation sites. The oxygen diffusion rate is in turn controlled by how mobile the lattice oxygen ions are. Hence, the mobile oxygen ions discussed earlier control the catalyst activity in catalysing the reaction of propylene partial oxidation.

The examination of several reaction mechanism models has given further evidence that the propylene partial oxidation to acrolein occurs via the redox mechanism. In this mechanism, the rate of acrolein formation depends on the degree of fully oxidised sites in the bismuth molybdate. The oxidised sites affect the apparent reaction orders in propylene and oxygen and thus control the kinetics of partial oxidation of propylene to acrolein. The more easily the reduced catalysts are reoxidised, the more active the catalysts in converting propylene to acrolein. A set of reaction steps has been proposed, which adequately reassembles the reaction mechanism. Side product reactions are also identified and included in the mechanisms.

The present thesis has revealed a much detailed insight into the role of lattice oxygen in the catalytic partial oxidation of propylene to acrolein over bismuth molybdates and established the relationship between structure and activity and selectivity of the catalyst. This work has laid a foundation for future catalyst design to be based on structural knowledge of the catalysts.

Chapter 1

INTRODUCTION

More than one third of worldwide chemical products, are produced by catalysed reactions with oxides types of catalysts (Centi & Perathoner 2001). Among the catalysts, selective oxidation can be considered the most typical example of metal oxide-type materials as heterogenous catalysts, which produce around one quarter of total organic chemicals worldwide.

The use of metal oxide catalysts began with the realisation of the need to convert low molecular-weight hydrocarbons, such as natural gas and refinery off-gas, to larger molecules of higher value. It was Hearne and Adams (Adams & Jennings 1963) in 1948 who first reported that cuprous oxide could selectively oxidise propylene into acrolein. Acrolein has broad industrial and agricultural applications and had been produced by silica supported sodium catalysing vapour-phase condensation of acetaldehyde and formaldehyde at temperatures between 300^{o}C and 320^{o}C (Takahasi Ohara et al. 1987). Large-scale production of acrolein process was later commercialised by SOHIO (Standard Oil of OHIO) in 1950s using the Hearne and Adams' catalytic process. Later, Veatch and co-workers (Veatch et al. 1960) discovered that bismuth molybdate-based catalysts (bismuth phosphomolybdates) are more superior to cuprous oxide. The bismuth molybdate-based catalysts have since become the major catalysts in commercial processes worldwide to produce acrolein (Bielanski & Haber 1991; Callahan et al. 1970; Cullis & Hucknall 1981; Hock Seng Tan 1986).

Since the discovery of the process, a huge amount of reports of studies on the process have been published, mainly focusing on reaction mechanisms and catalyst

characterisation to reveal the mystery behind the selective oxidation. The most important findings are the fact that the acrolein was formed via the formation of allyl intermediate on the catalyst surface and the reaction uses lattice oxygen. In terms of bismuth molybdate, it was also found that only three phases of pure bismuth molybdate, namely alpha, beta, and gamma phases ($Bi_2Mo_3O_{12}$, $Bi_2Mo_2O_9$, and Bi_2MoO_6, respectively) are active and selective for the reaction.

While catalyst characterisation and reaction mechanisms have been relatively well studied, perhaps in qualitative terms, no sufficient attention has been paid to the reaction kinetics. Among a limited number of kinetic studies, the most comprehensive one has been that performed by Krenzke (Leonard David Krenzke 1977), which covers a wide range of temperature and composition and uses pure phases of bismuth molybdates (alpha and gamma bismuth molybdate, bismuth iron molybdate, and uranyl-antimony oxide). Another report using pure bismuth molybdate phase was by Keulks et al. (Keulks, Rosyneck & Daniel 1971). Other kinetic reports were mainly written for a supported, mixture or multi phase bismuth molybdate-based catalysts that make the data less universal.

Research into partial oxidation of propylene to acrolein in the past decades has been focused on more fundamental understanding of the mechanisms at molecular levels, particularly the events that take place on the surface of catalysts. Several surface characterisation methods, particularly under in-situ or near in-situ conditions have been employed, such as in-situ XPS and UPS (Ayame et al. 2000; Ayame et al. 2002; R. Grzybowska et al. 1976), in-situ NMR (Bemis, Douskey & Munson 1997; Douskey & Munson 1997) and FT-IR (Carrazan et al. 1996a). The in-situ research has proven the previous hypotheses of surface formation of allyl intermediates, interaction of allyl species with surface species such as Mo, Bi, and O, and the state of the surface species, etc. The most important finding is that the lattice oxygen has been shown as the oxygen source (Han, Ueda & Moro-Oka 1999) and the activity of catalysts depends on how they effectively provide selective oxygen to the reactions and transfer oxygen from the bulk of the catalyst to its surface (D. J. Buttrey, Jefferson & Thomas 1986). In addition, Keulks and co-workers (Hoefs, Monnier & Keulks 1979), after studying the bismuth molybdate catalysts using IR

and Raman spectroscopy and $^{18}O_2$ labelling, found that all types of lattice oxygen ions participated in propylene oxidation.

Despite the fruitfulness of surface analysis, all surface spectroscopic techniques (e.g., infrared, Raman, EXAFS, XANES) would only provide bulk structural information due to extremely low surface areas of these oxides (typically ~0.1 to 1.0 $m^2.g^{-1}$). The small contribution of the surface component to the spectroscopic signal will generally be overshadowed by the significantly stronger contribution of the bulk component (Arora et al. 1996). Arora et al (Arora et al. 1996) revealed that attempts to characterise the surface of metal oxide using the well known surface analysis means such as XPS, AES, and ISS actually did not characterise the surface, but the thin layers of bulk at the surface since the surface information is averaged over an escape depth of approximately 30-50 Å. With that depth, very little is actually known about the outermost layer of bulk metal oxides and essentially no molecular level structural information is available about this layer from XPS. Consequently, most of the researchers have assumed the last layer to be just an extension of the bulk structure and composition.

All the aforementioned work has aimed to understand the reaction mechanisms so as to control the reaction process. However, further research is still required to be able to better understand the working of the catalysts so that the design of new catalysts can be based on sound science and their performance can be well predicted and controlled.

The research in this thesis is designed to achieve an improved understanding in the catalyst's structure characteristics, reaction mechanisms and kinetics. The aim of structural characterisation is to explain the role of the bulk catalyst structure in the catalytic activity for the partial oxidation of propylene to acrolein and to investigate which oxygen in the bulk structure actually plays the key role in the catalyst's selectivity and how the differences in the crystal structure affect the catalyst's selectivity and activities.

Diffraction is known as one of the best techniques to look at the details of the crystal structure, particularly the movement of all oxygen species in the catalyst crystal. There are three main diffraction techniques, namely, x-ray diffraction

(XRD), neutron diffraction (ND), and electron diffraction (ED), each of which has its own advantages and disadvantages, depending on their interaction with the materials. XRD is very good in looking at the crystal structure and the atomic position of heavy atoms, and the instrument is easily available in most major physics laboratories. ND, on the other hand, is the best diffraction instrument to look at atomic position in the crystal structure for almost all elements, including light elements such as oxygen, nitrogen, and even hydrogen. However, the instrument can only be found in certain specialised laboratories. Electron diffraction is a good technique to determine the unit cell and the characterisation can be done simultaneously with electron microscopy in investigating the catalyst's morphology and microstructure.

Kinetic studies can yield rate equations to quantify the performance of bismuth molybdate catalysts for partial oxidation of propylene to acrolein. A differential reactor system, which gives direct kinetic parameters in the power rate law model, is employed to study the kinetics. The kinetic parameters obtained experimentally can also help interpreting the reaction mechanisms by comparing and fitting the experimental data with alternative hypotheses of the reaction mechanisms.

This thesis is written in seven chapters which are interlinked with each other as depicted in Figure 1.1. The present chapter (Chapter One) establishes the overall scope of this thesis and the need for further research into the catalytic partial oxidation of propylene to acrolein. Chapter Two reviews the current state of knowledge on this subject, the techniques previously used for catalyst characterisation and reaction kinetic studies, and identifies the gaps in the literature, some of which form the objectives of the present effort. The review also provides foundation for experimental arrangements and result discussion. Chapter Three describes the general experimental techniques, arrangements and procedures, while the specific procedures are described in more detail in relevant discussion chapters.

The results and their analysis and interpretation are presented in three chapters. The physical characterisation of the catalysts is discussed in length in Chapter Four, which covers global characterisation such as surface area, particle size, catalysts morphology, microstructure, and crystal structure at room temperature and discusses the structure dynamics under in-situ conditions.

Chapter Five presents the results of kinetic experiments using the differential reactor system and develops the rate equations using the power rate law model. The kinetic results are used to fit with the theoretical model in Chapter Six.

Several reaction models are proposed and employed to reveal the reaction mechanisms by fitting with the experimental results. The models are derived from four main models, namely, the Langmuir-Hinshelwood, the Eley-Rideal, Redox, and the stationary adsorption models.

The final chapter (Chapter 7) provides a concise account of the conclusions and recommendations for future research and development.

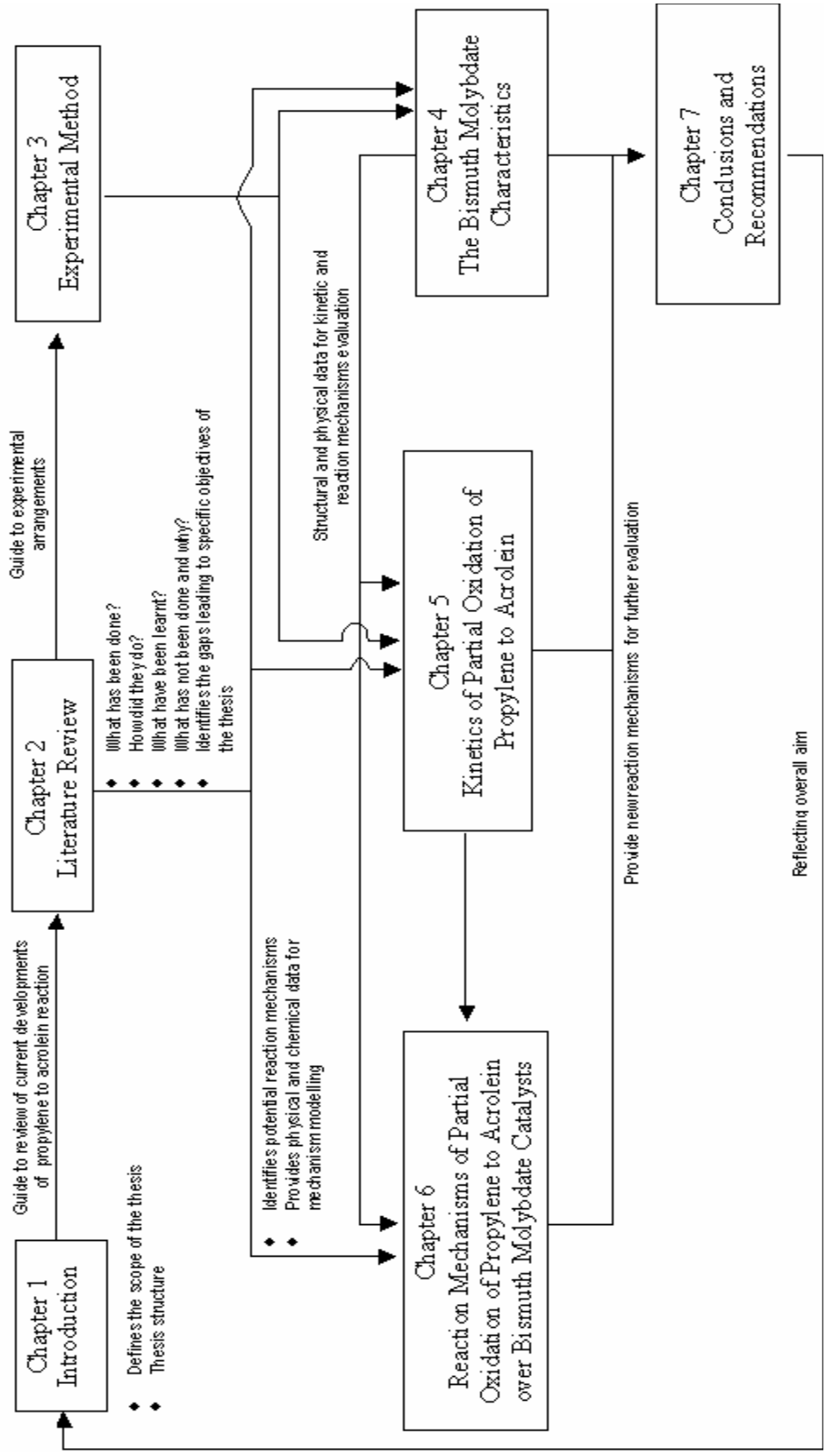

Figure 1.1 The thesis Map

Chapter 2

LITERATURE REVIEW

Following the general scope of the present research provided in Chapter 1, this chapter considers in detail the underlying theories behind catalytic partial oxidation of propylene to acrolein over bismuth molybdate catalysts. It contains historical background of the reaction discussion in depth of the bismuth molybdates, how they work in catalysing partial oxidation of propylene to acrolein and the background of the kinetic and the mechanisms of the reaction.

2.1 Acrolein

Acrolein is a chemical that is widely known as a biocide. Due to its biocidal activity, acrolein is commonly applied as an aquatic herbicide and slimicide (International Agency for Research on Cancer 1995). It is also an important intermediate for many industrial chemicals such as D,L-methionine (Takahasi Ohara et al. 1987), acrylic acid, 1,3 propanediol, and glutaraldehyde. According to the report from Occupational Safety and Health Administration of US Department of Labour, 50% of acrolein production is for glycerine, 25% for methionine, and the rest for other applications (U.S Department of Labor 1989).

The molecular structure of acrolein is shown in Figure 2.1. Note that acrolein has two conjugative unsaturated carbon bonding, one from the vinyl group and the other from aldehyde group. Due to the existence of these groups, acrolein undergoes reactions characteristic of both an unsaturated and an aldehyde compounds. Some

examples of reaction characteristics of acrolein are Diels-Alder reaction between two acrolein molecules, addition to carbon-carbon double bond, polymerisation, and reaction with amine compounds (Takahasi Ohara et al. 1987).

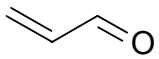

Figure 2.1 Molecule structure of acrolein

The activity of the aldehyde group to attack an amine-containing molecule makes it reactive to a protein molecule. The reaction underlies the activity of acrolein as an anti microbial and biocide, where the reaction of acrolein with protein on a cell wall can cause damage to the cell and kill it.

Acrolein is very toxic and flammable. It also undergoes polymerisation easily and exothermally. The polymerisation can be initiated by light, heat, air or peroxides. It is also polymerised in the existence of alkaline solution such as amines, ammonia, and caustic soda or by mineral acids such as sulphuric acid. Acrolein polymerisation, initiated by alkaline or acids, is very exothermic and no inhibitors can stop the polymerisation once it is initiated. Acrolein reacts with water and therefore addition of water to stored acrolein must be avoided, as the acrolein-containing water layer is particularly prone to polymerisation. Acrolein vapour polymerises upon condensation (Takahasi Ohara et al. 1987).

2.2 Partial Oxidation of Propylene to Acrolein

Acrolein occurs naturally in foods and is formed during combustion of fossil fuels, wood and tobacco and during the heating of cooking oils (International Agency for Research on Cancer 1995). For industrial applications, acrolein is commercially produced by heterogeneously catalysed gas-phase oxidation of propylene (Takahasi Ohara et al. 1987).

The catalytic partial oxidation of propylene to form acrolein follows the reaction equation below. The reaction is exothermic and produces 340.8 kJ of heat per mol of reacted propylene. The Gibbs free energy (ΔG) shows that the reaction will spontaneously occur, once the reaction is initiated.

$$CH_3CH{=}CH_2 + O_2 \rightarrow CH_2{=}CHCHO + H_2O \qquad \text{R1}$$

$$\Delta_r H^o = 340.8 \text{ kJ mol}^{-1}$$

$$\Delta_r G^o = -180.19 \text{ kJ mol}^{-1}$$

Although the reaction is energetically spontaneous, acrolein is not the only product when propylene is reacted with oxygen. Several other products such as CO_2, CO, acetaldehyde, formaldehyde, carboxylic acids etc can also form. Some possible products and their thermodynamic parameters are listed in Table 2.1.

Table 2.1 Thermodynamic parameters of the formation of other propylene oxidation products.

Reactions	**$\Delta_r G^o_{700}$ * kJ mol^{-1}**	**$\Delta_r H^o_{298}$ kJ mol^{-1}**
$C_3H_6(g) + 4.5O_2(g) \rightarrow 3CO_2(g) + 3H_2O(l)$	-1942.089	-2058.43
$C_3H_6(g) + 3O_2(g) \rightarrow 3CO(g) + 3H_2O(l)$	-1276.765	-1209.48
$C_3H_6(g) + O_2(g) \rightarrow C_3H_4O_2(l) + H_2O(l)$	-550.2293	-404.21
$C_3H_6(g) + O_2(g) \rightarrow C_3H_4O(l) + H_2O(l)$	-338.7959	-426.24

* data taken from Grasselli (Robert Karl Grasselli 1982)

The thermodynamic parameters shown in Table 2.1 reveal that the formation of side products (such as CO_2 and CO) is more thermodynamically favourable than the formation of acrolein.

2.3 Acrolein Production

Commercial production of acrolein by heterogenous catalytic partial oxidation of propylene started in 1948, when Hearne and Adams patented cuprous oxide catalysts for Shell Chemical Company (Hearne, Cerrito & Adams 1948). The acrolein yield from the patented process, however, was less than 50% from the total input of propylene, which left enormous opportunity to develop better catalysts than cuprous oxide.

In the 1950s, SOHIO (Standard Oil of Ohio) initiated an extensive research into catalytic vapour phase oxidation of unsaturated hydrocarbons to produce useful products such as acrolein, acrylonitrile, methacrylonitrile, and acrylic acid (Callahan et al. 1970). The research was developed based on the Lewis concept (Lewis, Gilliland & Reed 1949), in that lattice oxygen of reducible metal oxide would serve as a better oxidant for hydrocarbon partial oxidation than the gas phase oxygen. Several catalysts, either single metal oxide or a mixture of two or more metal oxides were tested for their activity towards acrolein formation from propylene.

In the early stages of the development, the catalytic activity was tested using fluidised bed reactors where the propylene was flushed to the reactor without oxygen, followed by steps of catalyst regeneration cycle by allowing oxygen to flow through the catalyst without propylene. Precaution had to be maintained to avoid reaction between propylene and molecular oxygen because it can lead to undesired oxidation products such as carbon dioxide and carbon monoxide. With the fluidised bed reactor system, SOHIO found that some mixtures of metal oxides gave good selectivity as well as yield of acrolein. However, the catalysts did not work properly in the existent of molecular oxygen in the feed stream.

The extensive research led the SOHIO team to discover bismuth-molybdate, which had better selectivity for acrolein than cuprous oxide (Takahasi Ohara et al. 1987), even when the feed stream contained molecular oxygen. Since then, the bismuth-molybdate system has been significantly improved by adding some metal oxides to form multicomponent catalysts. These catalyst systems have even better activity and selectivity for the oxidation of propylene to acrolein. Some examples of bismuth-molybdate based multi-component catalysts are presented in Table 2.2.

Table 2.2 Some examples of multi-component BiMo based catalysts

Catalyst composition	$T_{Reaction}$ (^oC)	Conversion (%)	One Pass Yield (mol %)	Ref.*)
$Mo_{12}Bi_{1.2}Fe_{1.2}Co_{4.5}W_{2.4}K_{0.07}Si_{1.62}$	325	96	79	1
$Mo_{12}Bi_{1.2}Fe_{1.2}Co_{5.8}K_{0.05}Ce_{1.2}Nb_{0.5}\ Si_{1.62}$	325	96	77.8	1
$Mo_{12}Bi_1Fe_1Ni_{10.5}P_1$	300	98	71.0	2
$Mo_{12}Bi_1Fe_2Co_3Ni_1P_2K_{0.2}$	305	96	88.0	3
$Mo_{10}Bi_1Fe_1Co_4W_2K_{0.06}Si_{1.35}$	320	97	90.2	4
$Mo_{12}Bi_1In_{0.4}Fe_2Ni_8Co_{0.3}W_{0.1}P_1$	350	89	74	5

*)Reference 1 (Tanimoto, Nakamura & Kawajiri 2003), Reference 2 (Yamaguchi & Takenaka 1969), Reference 3 (Takenaka et al. 1973), Reference 4 (Takashi Ohara et al. 1974), Reference 5 (Krabetz et al. 1977)

2.4 Active Catalyst Systems

As mentioned above, the catalysts are the supplier of oxygen for the partial oxidation of propylene, where the oxygen comes from the lattice. To meet this requirement, the catalysts must have the ability to perform internal oxidation-reduction processes. Copper oxide is one of many examples of metal oxides that have such ability. It is also the only single component metal oxide that has good activity and selectivity for partial oxidation of olefin. In cuprous oxide, the copper exists in three-oxidation state, namely Cu metal, Cu^+ and Cu^{2+}, allowing internal reduction-oxidation. These ions constitute a mixture of Cu-Cu_2O-CuO system. An electron diffraction study on a thin layer of copper film showed that the cuprous oxide is responsible for the activity of the catalyst (Leonard David Krenzke 1977). Bettahar (Bettahar et al. 1996) reported in a review that a stoichiometric or copper rich Cu_2O is the most active catalyst for the partial oxidation of propylene to acrolein while oxygen rich Cu_2O favours CO_2 and H_2O, which is in agreement with the report by Krenzke (Leonard David Krenzke 1977).

Extensive studies on copper oxide catalysts led to the conclusion that metal oxides catalysts for partial oxidation reactions should contain two metal ion species in the form of $M^{I}M^{II}O_x$. The M^{I} ion is normally a heavy metal and M^{II} from transition metal groups, which have variable oxidation numbers. From this requirement, tin antimonite, uranium antimonite and bismuth molybdate are among the most active and extensively studied binary metal oxide catalysts. Individual metal oxides do not have sufficient activity to convert propylene to acrolein, but mixtures can have very good activity and selectivity.

Uranium antimonite, as reported by Krenzke (Leonard David Krenzke 1977), has excellent selectivity towards acrolein over a wide range of reaction temperatures. There are two phases found in this catalyst system, namely USb_3O_{10} and $USbO_5$ (Robert K. Grasselli & Suresh 1972) where only Sb^{V} and U^{V} species are contained in the catalyst (Evans 1976). The first phase is selective and active for acrolein formation and hence, its concentration determines the overall performance of catalyst (Hayden & Higgins 1976), while the second phase has lower selectivity towards acrolein. Matsuura (Matsuura 1974) reported that the catalyst has special oxygen mobility, which favours surface reaction of propylene partial oxidation to acrolein. However, due to its highly radioactive nature, this catalyst has little scope for commercial application.

Tin antimonite is a mixture of SnO_2 and a solid solution of α-Sb_2O and β-Sb_2O_4 where none of them, as individual, is active as a catalyst for propylene oxidation to acrolein (Vittorio Fattore et al. 1975b). It has been reported that the addition of only 6.8% Sb to tin(IV) oxide increased the conductivity by three orders of magnitude (Leonard David Krenzke 1977). This is attributed to the substitution of Sb^{5+} for Sn^{4+} ions in the tin(IV) oxide lattice. It is believed that the catalytic activity of these mixed oxides is related to the presence of the solid solution and the Sb_2O_4 species lying on the surface of SnO_2 (Boudeville et al. 1979).

Bismuth molybdates are the second most studied catalyst after copper oxide and serve as the main ingredient in almost all commercial catalysts for propylene oxidation to acrolein. There are several known phases of binary bismuth molybdates but only three phases are active and selective for the partial oxidation of propylene to

acrolein (Bielanski & Haber 1991; Carson et al. 1983; R. Grzybowska et al. 1976; Kumar & Ruckenstein 1976; Olier et al. 1989). The ratios of Bi to Mo in these catalysts are within the range of 2:3 and 2:1, namely α-$Bi_2Mo_3O_{12}$, β-$Bi_2Mo_2O_9$, and γ-Bi_2MoO_6.

2.5 Bismuth Molybdates

2.5.1 Crystal Structure of Bismuth Molybdates

The fact that only certain phases of known bismuth molybdate are active as selective oxidation catalysts means that the bulk structure determines the activity of bismuth molybdate. Before discussing the relation between structure and catalytic activity, the crystal structures of the three phases of active bismuth molybdate, namely α-$Bi_2Mo_3O_{12}$, β-$Bi_2Mo_2O_9$, and γ-Bi_2MoO_6 are briefly reviewed.

i) α-$Bi_2Mo_3O_{12}$

There are numerous reports on the crystal structure of α-$Bi_2Mo_3O_{12}$. One of the widely accepted reports is of van den Elzen and Rieck (van den Elzen & Rieck 1973a) who used a single crystalline X-ray diffraction technique and revealed that the structure was derived from naturally occurring mineral $CaWoO_4$ (scheelite). A neutron diffraction study on a powder sample of α-$Bi_2Mo_3O_{12}$ by Theobald et al (Theobald, Laarif & Hewat 1985) confirmed the structure found by van den Elzen and Rieck (van den Elzen & Rieck 1973a).

Scheelite crystalline structure is built from stacking up of Ca^{2+} and WO_4^{2-} ions. In the case of α-$Bi_2Mo_3O_{12}$, Ca^{2+} is replaced by Bi^{3+} ion while WO_4^{2-} is replaced by MoO_4^{2-} ion. Both WO_4^{2-} and MoO_4^{2-} have the same structure. To maintain the charge balance within the crystal due to the replacement of a +2 ion (Ca^{2+}) with a +3 ion (Bi^{3+}), the structure contains an ordered arrangement of vacancies in the Bi positions corresponding to the formation of $Bi_2□,Mo_3O_{12}$. Figure 2.2 shows the projection of the crystal along *b* axis and the bismuth vacation sites on the structure.

All MoO_4 tetrahedra in α-$Bi_2Mo_3O_{12}$ are in Mo_2O_8 form (van den Elzen & Rieck 1973a). There are two forms of Mo_2O_8, one of which possesses a central symmetry while the other does not. In addition, all Bi have 8 oxygen neighbours. However, the Bi-O distances are not equal and range from 2.12 to 2.93 Å. The unit cell structure of α-$Bi_2Mo_3O_{12}$ according to van den Elzen and Rieck is shown in Figure 2.3.

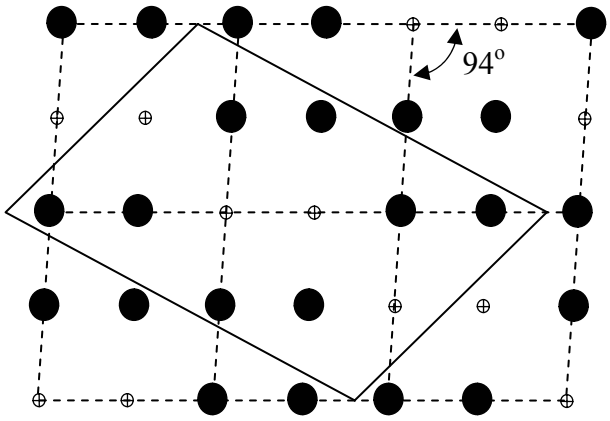

Figure 2.2 Bismuth vacant sites in α-$Bi_2Mo_3O_{12}$ along *b* axis projection. The solid lines show the α-$Bi_2Mo_3O_{12}$ unit cell while the dashed line is a unit cell of scheelite. Large solid circles represent occupied Bi sites while the small circles are the empty Bi sites (Adapted from van den Elzen and Rieck, (van den Elzen & Rieck 1973a)).

ii) β-$Bi_2Mo_2O_9$

Growing a single crystal of β-$Bi_2Mo_2O_9$ to the size suitable for single crystalline X-ray diffraction was not an easy task. This is the reason why the crystal structure of β-$Bi_2Mo_2O_9$ was not well understood until 1975. In 1974, Chen (Tu Chen & Smith 1975) grew a single crystalline β-$Bi_2Mo_2O_9$, but the crystal was twinned and not suitable for accurate X-ray structure analysis. Due to the difficulties, van den Elzen and Rieck (van den Elzen & Rieck 1975) did a comprehensive powder X-ray diffraction analysis on a high purity β-$Bi_2Mo_2O_9$ and obtained its structure. The crystal was prepared according to the method developed by Batist (Batist et al. 1968). van den Elzen and Rieck noted that Bi^{3+} had octahedral coordination to oxygen anions at various distances as in the alpha phase, while Mo^{6+} had tetrahedral coordination with oxygen. van den Elzen and Rieck further proposed that Mo^{6+}

tetrahedral might be strongly distorted and linked together in pairs as in the alpha phase.

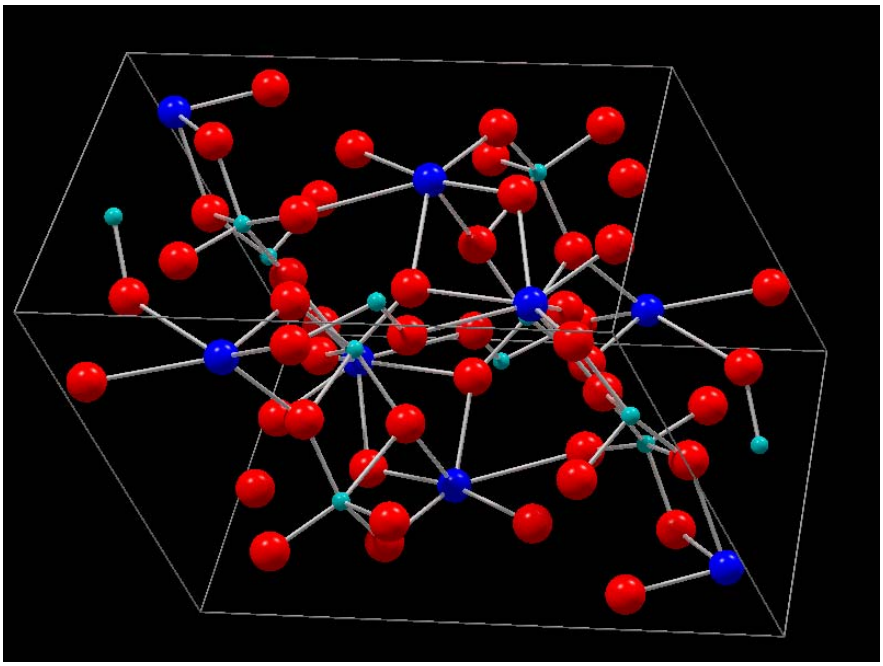

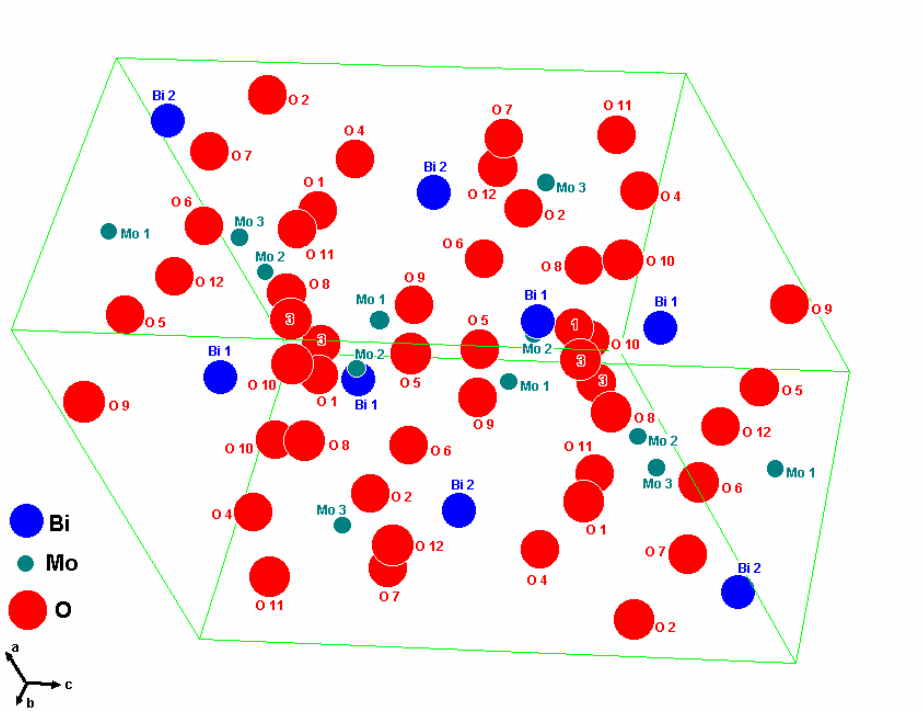

Figure 2.3 The unit cell structure of α-$Bi_2Mo_3O_{12}$ (upper figure) and atom map of the unit cell (lower figure). (Adapted from van den Elzen and Rieck, (van den Elzen & Rieck 1973a)).

In 1986, Chen and Sleight (Horng-Yih Chen & Sleight 1986) crystallised β-$Bi_2Mo_2O_9$ from a mixture of Bi_2O_3 and MoO_3 with a molar ratio of 27.5/72.5 using the Czochralski method (West 1989). Although the crystal was twinned, they successfully isolated a clear yellow, twinned free-fragment of crystalline β-$Bi_2Mo_2O_9$. Subsequent single crystal X-ray diffraction analysis using the Patterson and Fourier method (Stout & Jensen 1989) revealed that the crystal structure was remarkably close to that outlined by van den Elzen and Rieck. The crystal is monoclinic and belongs to the space group $P2_1/n$ with a = 11.972(3) Å, b = 10.813(4) Å, c = 11.899(2), β= 90.13(2), and Z = 8. This structure may be represented by the formula $Bi(Bi_3O_2)(MoO_4)_4$. The Bi_3O_2 chains are parallel to the *b*-axis and Bi ions bound only to MoO_4 tetrahedra. Contrary to an earlier report by van den Elzen and Rieck (van den Elzen & Rieck 1975), the isolated MoO_4 tetrahedra are very regular. A neutron diffraction study on β-$Bi_2Mo_2O_9$ by Antonio et al (Antonio et al. 1988) showed very little discrepancy with the structure proposed by Chen and Sleight (Horng-Yih Chen & Sleight 1986). In addition, Antonio et al suggested that the lack of Mo-O_4 distortion was attributed to their isolation from each other.

The structure of β-$Bi_2Mo_2O_9$ is built with square clusters of four MoO_4 tetrahedra to become Mo_4O_{16}. They bound together by Bi ions located halfway on the axis passing through the centre of the squares (Bielanski & Haber 1991). Some Bi cations are surrounded by eight oxygen ions from the MoO_4 tetrahedra. There are also some oxygen ions associated only with Bi cation in the coordination sphere of others. Thus, the structure may be visualised as composed of rows of oxygen ions, connected only to Bi cations, running parallel to the (Mo_4O_{16})-Bi-(Mo_4O_{16}) units. These resemble the ribbons of Bi_2O from the Bi_2O_2 layers in koechlinite. However, not all Bi sites are filled. One in every four Bi sites is empty. The structure may be thus represented by $Bi(Bi_3\square O_2)(Mo_4O_{16})$, where the first Bi is associated only with the (Mo_4O_{16}) units and the Bi cations in parentheses are bonded to the oxygen atoms associated only with Bi as well as to those shared with the (Mo_4O_{16}) units. The structure of a unit cell of β-$Bi_2Mo_2O_9$ and its crystal representation along the (010) face are shown in Figure 2.4 and 2.5, respectively.

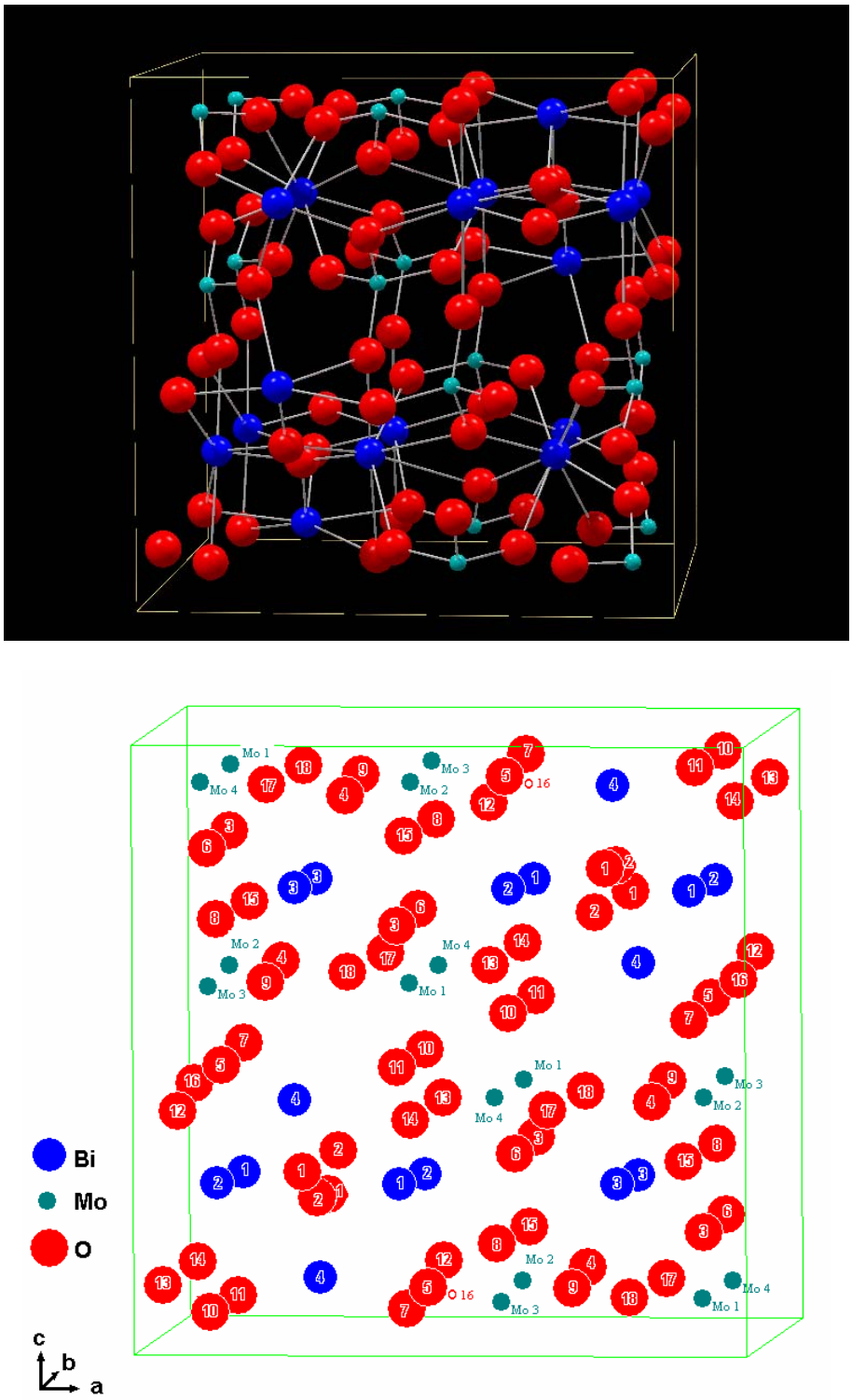

Figure 2.4 A unit cell of β-$Bi_2Mo_2O_9$ (upper figure) and atom map of the unit cell (lower figure). (Adapted from H.-Y. Chen and A.W. Sleight (Horng-Yih Chen & Sleight 1986)).

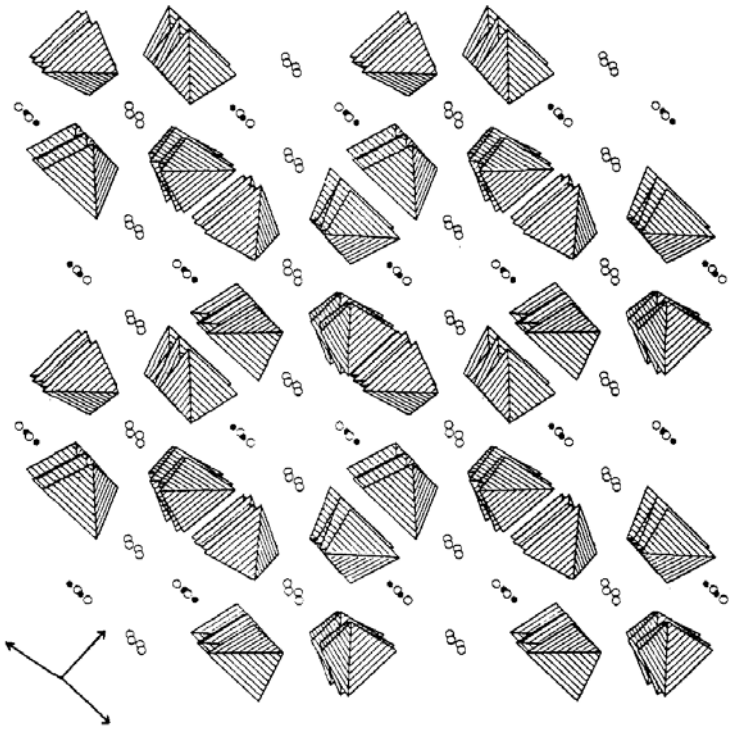

Figure 2.5 Representation of the β-$Bi_2Mo_2O_9$ structure projected along (010) (Antonio et al. 1988). The figure shows clusters of MoO_4 tetrahedral to form Mo_4O_{16}. The small circle represents a bismuth atom.

c. γ–Bi_2MoO_6

The gamma phase of bismuth molybdate is found naturally as mineral koechlinite. The structure was firstly determined by Zemann in 1956 (Zeeman 1956). In 1973, van den Elzen and G.D Rieck (van den Elzen & Rieck 1973b) redetermined the structure using single crystal X-ray diffraction because they found that the crystal model from Zemann was inaccurate due to a large linear absorption coefficient as a result of irregular and poorly defined specimen. Using the single crystal X-ray diffraction technique, they found that the actual symmetry was *$Pca2_1$* rather than *Cmca* as suggested by Zemann. However, the model developed by van den Elzen and Rieck has two oxygen atoms that are separated by only 2.2 Å in O-O distance. The distance is a physically unrealistic feature, because the closest distance allowable for two-unbounded oxygen is 2.4Å, based on the effective ionic radii of oxygen (Shannon & Prewitt 1969). The structure of γ-Bi_2MoO_6 in Zeeman and van den

Elzen and Rieck's work were determined from crystals of natural koechlinite mineral.

In order to make a correction to the flaw in the van den elzen and Rieck model, Teller et al (Teller, Brazdil & Grasselli 1984) collected diffraction data from synthetic γ-Bi_2MoO_6 powder using a high intensity time-of-flight (TOF) neutron diffraction. Their work corrected the flaw in O-O distance but agreed that the crystal has a *Pca2₁* symmetry as reported by van den Elzen and Rieck.

Theobald et al (Theobald, Laarif & Hewat 1984) published a similar structure a couple months earlier than Teller et al.. They reported the results of their structural study of synthetic γ-Bi_2MoO_6 by constant wavelength neutron diffraction and found that the structure has a *Pca2₁* symmetry. The short O-O distance found in van den Elzen and Rieck structure was resolved as well.

The crystalline structure model developed by Teller et al (Teller, Brazdil & Grasselli 1984) and Theobald et al (Theobald, Laarif & Hewat 1984) was based on Zeeman (Zeeman 1956) and van den Elzen and Rieck's (van den Elzen & Rieck 1973b) work. It contains series of layers made up of $(Bi_2O_2)^{2+}_n$ and $(MoO_2)^{2+}_n$ octahedron units connected by O^{2-} ions in the arrangement of $(Bi_2O_2)^{2+}_n$ O^{2-}_n $(MoO_2)^{2+}_n$ O^{2-}_n. An overview of the structure is given in Figure 2.6.

Three types of oxygen ions exist in the structure. The first type of oxygen ions are within the Mo octahedral layer, bridging only two Mo atoms. The second type of oxygen ions are entirely within the Bi layer, bridging four metal atoms. The third type bridges the Mo and Bi layers.

The structure model developed by Teller et al (Teller, Brazdil & Grasselli 1984) has asymmetry coordination around the Bi atom in the BiO_6 unit. The asymmetry allows the lone pair electrons of Bi to be directed toward MoO_6 octahedron. With steric considerations, the position of Mo in the MoO_6 octahedron should be distorted away from the lone pair, which is opposite to their experiment result in which Mo is distorted to the lone pair direction. The opposite finding is associated with the Lewis acid-base interaction between the lone pair and the *d* orbital on the transition metal (Mo).

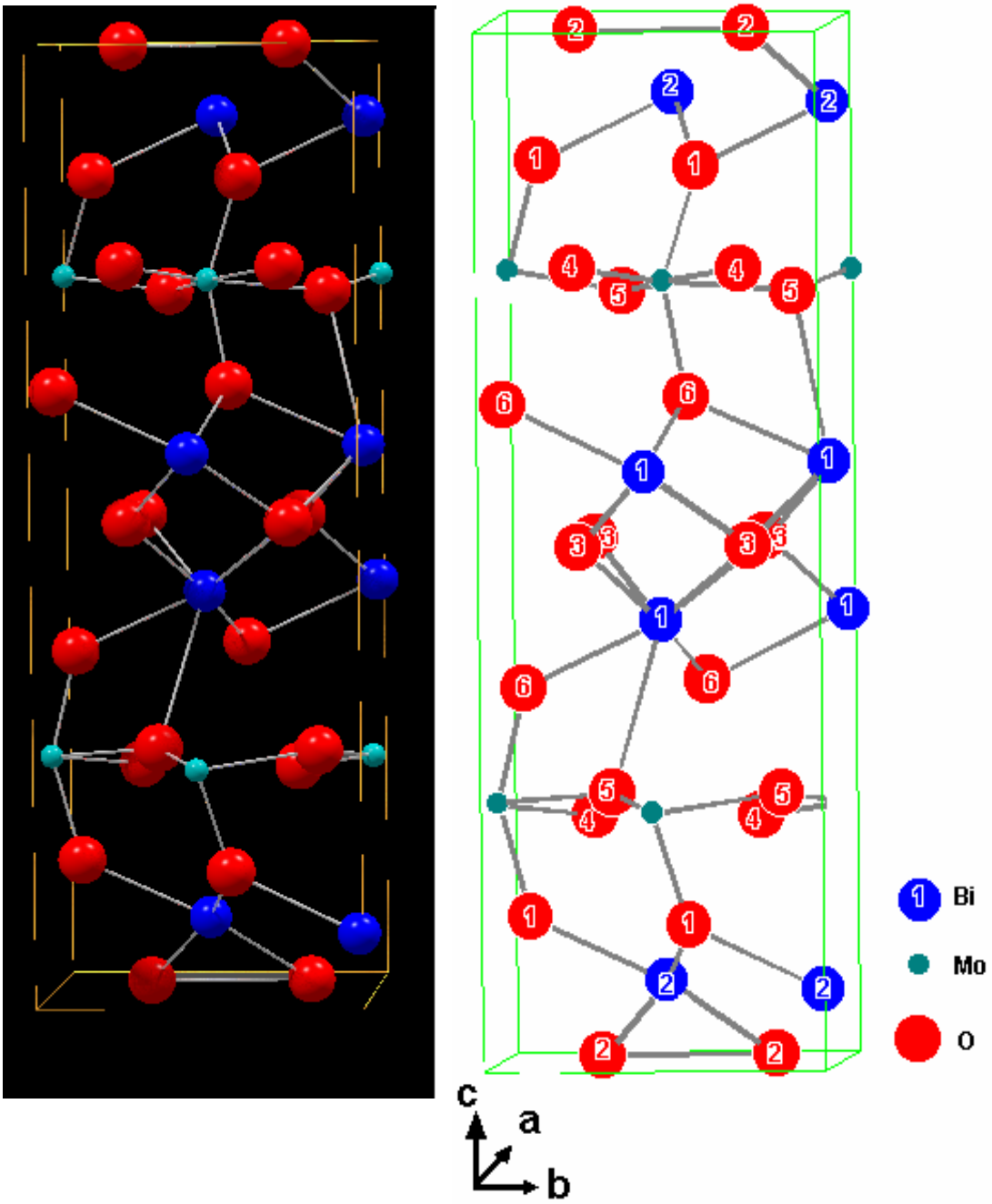

Figure 2.6 From left to right, a unit cell of γ-Bi_2MoO_6 and its atom map. The figure is adapted from Teller et al (Teller, Brazdil & Grasselli 1984).

Unlike the alpha and beta phases, the gamma phase of bismuth molybdate has three polymorphs, namely, γ, γ', and γ''. The structure discussed above is the lowest temperature polymorph. At 570°C, the γ polymorph is reversibly turned into the γ'

polymorph and further to the irreversible γ" polymorph if it is heated to 670°C (Balessi et al. 1999; D. J. Buttrey et al. 1994; Catlow 1997). Thus, caution should be taken when preparing γ-Bi_2MoO_6 since only the γ polymorph is active for partial oxidation of propylene to acrolein

2.5.2 Relationship between Structure of Bismuth Molybdate and Catalytic Activity

According to the literature on phase equilibria studies (Douglas J. Buttrey 2001; Egashira et al. 1979; Hriljac, Torardi & Vogt 1995; Tomasi et al. 1997), there are eight phases known on binary bismuth molybdenum oxides, prepared by high temperature synthesis. Among the eight phases, only three of them are active and selective toward partial oxidation of olefin. Hriljac et al (Hriljac, Torardi & Vogt 1995) reported a possible fourth active binary bismuth-molybdenum oxide prepared under mild hydrothermal conditions, but no catalytic activity was reported.

Among the family of active bismuth molybdenum catalysts, several arguments have been raised in deciding which one has the best activity and selectivity. At least there are three opinions about the order of activity of the α, β, and γ phases. The first comes from Beres et al. (Beres, Janik & Wasilewski 1969), Millet et al (Millet et al. 1993) and also Monnier and Keulks (Monnier & Keulks 1981) who found that the β-phase was the most active and selective, followed by α and γ. The second comes from Batist et al. (Batist et al. 1968; Batist et al. 1971) who observed that γ phase was equally good as the beta phase. Yet another opinion from more recent studies by Agaquseinova et al (in Cullis and Hucknall (Cullis & Hucknall 1981)) who observed that the order of propene activity decreased in the order of α>β>γ whereas the order of selectivity was β>α>γ.

In all active bismuth molybdate catalysts, lattice oxygen plays the key role in the catalytic activity for partial oxidation of propylene. The role of lattice oxygen has been proven by tracer studies using ^{18}O (Leonard David Krenzke 1977; Miura et al. 1979; Ono, Ogata & Kuczkowski 1998) as well as photoelectron characterisation of the catalyst surface (Ayame et al. 2000; Ayame et al. 2002; R. Grzybowska et al. 1976; Han, Ueda & Moro-Oka 1999). The importance of lattice oxygen in the

catalytic partial oxidation led to the conclusion that an active catalyst has to be able to provide lattice oxygen for oxidation.

Batist et al. (Batist et al. 1968) attempted to correlate the Bismuth-Molybdate activity and selectivity with the bulk crystal structure. In their opinion, the catalytic activity for selective oxidation of olefin was connected with the corner-sharing Mo-O octahedra, while the catalytic activity was largely absent in compounds containing edge-shared octahedra. They believed that in the 1:1 bismuth to molybdenum ratio compound, Mo ion has an octahedral coordination, which allows a high catalytic activity. In addition, they suggested that the interlinking of Mo-O octahedra by edge sharing is responsible for the low activity of the 2:3 molybdate. However, detailed studies (Theobald, Laarif & Hewat 1985; van den Elzen & Rieck 1973a) have shown that in the 2:3 compound, the molybdenum ion is surrounded by a distorted tetrahedron. Infrared and ultraviolet investigations by kumar and Ruckenstein (Kumar & Ruckenstein 1976) revealed the presence of both tetrahedral and octahedral oxomolybdenum species on the surface of the 2:1 and 1:1 active Bismuth-Molybdates.

The importance of edge sharing Mo-O octahedral was also reported in Haber's review (Haber 1985). When the reaction occurred on the bismuth molybdate surface, the uptake of oxygen from the surface caused oxygen vacancies. The oxygen vacancies generated electrophilic oxygen, which then led to total oxidation products. The oxygen vacancies, surprisingly, were not found on the reacting surface. The absence of elecrophilic surface oxygen is now believed to be caused by the so-called "shear plane", where the corner-sharing Mo-O turned into the edge-sharing Mo-O. The ability of bismuth molybdate to serve the change of the sharing is believed to be the source of their selectivity for partial oxidation reaction.

Buttrey et al (D. J. Buttrey, Jefferson & Thomas 1986) mentioned that the event that is taking place on the surface could lead to the structural reorganisation. They investigated the structure of $Bi_2O_3.nMoO_3$ crystal, covering n=3 (alpha phase), n=2 (beta phase) and n=1 (gamma phase) to find the relation between the structure and catalytic activity and concluded that all active phases were actually derived from the fluorite structure. They further concluded that fluorite structure was possibly responsible for the accommodation of either cation or anion vacancies in the crystal

framework for the n = 2 and 3 and determined the catalyst activity toward the catalytic partial oxidation of olefin. For the phase with n = 1, fluorite-related structure did not exist and its activity was due to the facile path of lattice oxygen (O^{2-}) diffusion through MoO_2 and Bi_2O_2 layers (Robert Karl Grasselli 1982).

Buttrey et al, however, confessed that the structure identified in their study might be different from the real structure under actual reaction conditions. This raises a question about the role of the structure of the catalyst under the reaction condition. This will be further investigated in more detail in this thesis. The following section outlines the diffraction techniques used in the investigation in the crystal structure of the catalysts.

2.6 Diffraction Techniques for Characterisation of Heterogeneous Catalyst

Physical and chemical characteristics of catalysts are normally studied by spectroscopic-surface analysis instruments such as XPS, NMR, EPR, EXAFS and etc. These techniques, however, only give local surface information or near surface structure and about certain elements in the catalysts. The important role of the bulk structure of bismuth molybdate in providing lattice oxygen for the oxidation reaction led to the need to investigate the bulk structure of bismuth molybdate in great detail.

Diffraction is the main technique for investigation of bulk structure and a very useful technique in solid-state chemistry. There are three means of diffraction, depending on the nature of the diffracted beam, namely X-ray, neutron and electron diffraction. X-ray diffraction has been used as a useful tool for fingerprint characterisation of crystalline materials and determination of their crystal structures.

The diffraction of X-rays by crystals was discovered by von Laue (West 1989) in 1912. Later, Bragg derived a simple equation by treating diffraction as “reflection” from planes in the lattice (West 1989). Bragg deduced the relation between the inter-planar distance (d) and the incident beam angle (θ) and the wavelength of the X-ray as represented by equation (2.1), where n is an integer. For a given set of planes, several solution of the Bragg’s Law are usually possible, for n=1,

2, 3, etc. The Bragg relation between crystal spacing and wavelength is also applicable to neutron and electron diffraction.

$$2d\sin\theta = n\lambda \qquad 2.1$$

Powder diffraction is the most common technique for characterising the bulk structure of catalysts since most of them are in the form of powder. In the past, the powder method was rarely used for structural characterization because the technique was regarded as inferior for structure refinement as compared to the single crystal method (Robert Alan Young 1993). Significant improvements in instrumentation and availability of more powerful computers and refinement methods have made it possible to use the diffraction technique for structural analysis. The diffraction technique has now not only been used for fingerprint analysis of crystal phases but also for structural refinement since Hugo Rietveld (Rietveld 1967) proposed and published a method for structure refinement from powder diffraction data in the late 1960s. The method was based on the full-profile fitting from neutron powder diffraction data, which was later successfully adapted for the refinement of X-ray powder diffraction data by Malmros and Thomas (Malmros & Thomas 1977), Khattak and Cox (Khattak & Cox 1977), and Young et al (R. A. Young, Mackie & von Dreele 1977). The refinement method developed by Rietveld is well known as Rietveld analysis (Robert Alan Young 1993). The method gained its momentum when it was successfully applied to refine the structure of high temperature superconductor (T_c = 90K) $YBa_2Cu_3O_{7-x}$ (Robert Alan Young 1993).

With the advances in the diffraction technique and the rise of the Rietveld method, very wide applications of the technique have been opened for catalyst characterisation. The Rietveld analysis can extract structural information such as lattice parameters, occupancy factors, atomic coordinates, and thermal vibration of each atom in the catalyst lattice. The advances in instrumentation also make possible the in-situ diffraction analysis although it still has some limitations. One of the limitations is that the timescale of data acquisition is much slower than the dynamics of the structure evolution.

2.7 The Rietveld Analysis

The Rietveld analysis is a method widely used to refine a whole powder diffraction pattern (Kisi 1994; Perego 1998; Pratapa 2003; Sitepu 1998). The pattern is considered as a collection of individual *hkl* reflection profiles, which are not all resolved but partially overlap one over another (Perego 1998). Each reflection is characterised by a peak height, a peak position, a peak broadening, and an integrated area proportional the Bragg intensity (I_{hkl}). In order to resolve the structure of a sample, a pattern from a postulated structural model, which has to be very close to the actual structure, is generated. After that, the structure of the model is refined until its pattern becomes exactly the same as the pattern of the actual structure. In a Rietveld analysis, the refinement is undertaken by the least-squares method (Rietveld 1967).

The basis of the Rietveld method is minimising the residual, S_y, of the least-square procedure. In the procedure, a model is presumed to be optimal when the sum (S) of the squares of the differences between the measured and the calculated patterns is the lowest, that is, when the value of S_y reaches a minimum, as given in equation 2.2 below:

$$S_y = \sum_i w_i \left(y_i - y_{ci}\right)^2 \qquad 2.2$$

where y_i is the observed step intensity, y_{ci} is the corresponding calculated value, and w_i is the weighting factor of point i in the pattern which is normally set as the reciprocal of the variance of the measured intensity at point i, i.e. $w_i = 1/y_i$. The calculated intensity is given by summing the contributions from (i) neighbouring Bragg reflections and (ii) background (assuming the crystallites are randomly oriented). The general expression for the calculated intensity y_{ci} is given by:

$$y_{ci} = s\sum_K L_K \left|F_K\right|^2 \phi\left(2\theta_i - 2\theta_K\right) P_K A + y_{bi} \qquad 2.3$$

where i is index of the point being calculated, s is the scale factor, K represents the Miller indices (West 1989), h, k, l for a Bragg peaks, L_K contains the Lorentz (West 1989), polarisation and multiplicity factors, $\left|F_K\right|$ is the structure factor for K^{th} Bragg reflection, ϕ is the peak shape function, $2\theta_i$ and $2\theta_K$ are the detector angles with

respect to point *i* and Bragg peak *K*, P_K is the preferred orientation function, *A* is an absorption factor and y_{bi} is the background contribution. The "*s*" parameter is the scale factor which is very useful for quantitative analysis (Robert Alan Young 1993).

The structure factor F_K is given by equation 2.4, where *h, k, l* are Miller indices, x_j, y_j, z_j are relative position parameters of j^{th} atom in the unit cell, N_j is the site occupancy multiplier for the j^{th} atom site, and f_j is the scattering factor which is proportional to atomic number (Z) and decreases with increasing the Bragg angle.

$$F_K = \sum_j N_j f_j e^{\left[2\pi i(hx_j+ky_j+lz_j\right]} e^{-M_j} \qquad 2.4$$

The scattering factor of atoms in X-ray and neutron diffraction is different. In X-ray, the beam is scattered by electrons surrounding the nuclei while in neutron, the beam is scattered by nucleus. The result is that the X-ray scattering factors are dependent on the atomic number (*Z*) and fall off quickly over the range of (sin θ)/λ. In contrast to X-ray, the atomic scattering factor in neutron diffraction is effectively constant and there is no regular progression with Z (Robert Alan Young 1993).

M_j in equation 2.4 is the thermal factor, which is mathematically represented by equation 2.5. This factor is determined by the mean square root of thermal displacements of the j^{th} atom site represented by $\overline{u_s^2}$. For isotropic thermal motion, the term $8\pi^2\overline{u_s^2}$ is known as temperature factor B_j. Thus, by knowing the temperature factor, the vibration of atoms/ions in a crystal lattice can be calculated.

$$M_j = 8\pi^2 \overline{u_s^2} \sin^2 \frac{\theta}{\lambda^2} \qquad 2.5$$

Various mathematical peak profile functions ϕ_{ijk} are available in the Rietveld softwares. The Voigt function, a convolution of Gaussian and Lorentzian functions (Robert Alan Young 1993), was used for all refinements in this study. The function is given by equation 2.6,

$$\phi(2\theta_i - 2\theta_j) = \frac{1}{H_{Gj}} \left(\frac{C_1}{\pi}\right)^{\frac{1}{2}} \mathrm{Re}\left[\omega\left(C_1^{\frac{1}{2}} X_{ij} + iC_2 \frac{H_{Lj}}{H_{Gj}}\right)\right] \qquad 2.6$$

where $C_1 = 2\ln 2$, $C_2 = \sqrt{\ln 2}$, H_{Gj} is the FWHM (Full Width of Half Maximum) of the contributing Gaussian, H_{Lj} is the FWHM of the contributing Lorentzian, ω is the complex error function, defined as $\omega(z) = \exp(-z^2)erfc(-iz)$ and Re denotes the real part of the complex expression. The dependence of breadth H of the reflection profiles measured as Gaussian FWHM varies with the diffraction angle θ according to the expression given by equation 2.7 while the Lorentzian H of FWHM is according to equation 2.8.

$$H^2 = U\tan^2\theta + V\tan\theta + W \qquad 2.7$$

$$H_{Lj} = \frac{180}{\pi}\frac{\lambda}{D}\sec\theta + \frac{180}{\pi}S\tan\theta \qquad 2.8$$

One has to bear in mind that the Rietveld method is not a structure solution method, but a structure refinement method. This means that the method needs a very good structural model to begin with.

2.8 The Reaction Mechanisms of Partial Oxidation of Propylene to Acrolein on Bismuth Molybdate Catalysts

2.8.1 Propylene Activation

It is probably Adams and Jennings (Adams & Jennings 1963) (Adams & Jennings 1964) who first started the studies of the reaction mechanisms of propylene partial oxidation to acrolein over bismuth moybdate catalysts. In they work, Adam and Jenning used propylene labelled with deuterium and used a kinetic isotope effect analysis to find out the probability of deuterium atoms being abstracted relative to hydrogen atoms. The conclusions of their work were:

1. The first step in the oxidation of propylene is the abstraction of a hydrogen atom from the methyl group and the process is the rate-determining step.
2. The hydrocarbon intermediate formed after the abstraction is a symmetrical structure, probably similar to the π-allylic species. This species is not cyclic

because no deuterium was found in the middle of carbon atoms of the resulting acrolein.

3. Propylene underwent two successive hydrogen abstractions before the addition of oxygen.

The existence of the symmetrical intermediate was also found by Voge et al. (Voge, Wagner & Stevenson 1963) by using propylene labelled with ^{13}C on a cuprous oxide catalyst at 300°C. The same conclusion was also made by Sachtler and DeBoer (after Krenze, (Leonard David Krenzke 1977)). Report on studies where allyl radicals were generated *in-situ*, either by allyl iodide (B. Grzybowska, Haber & Janas 1977) or from gas phase radicals (Driscoll & Lunsford 1985; Martir & Lunsford 1981), confirmed the existence of the symmetrical allyl intermediate. Figure 2.7 gives the reaction path of the propylene activation via the formation of allylic intermediate.

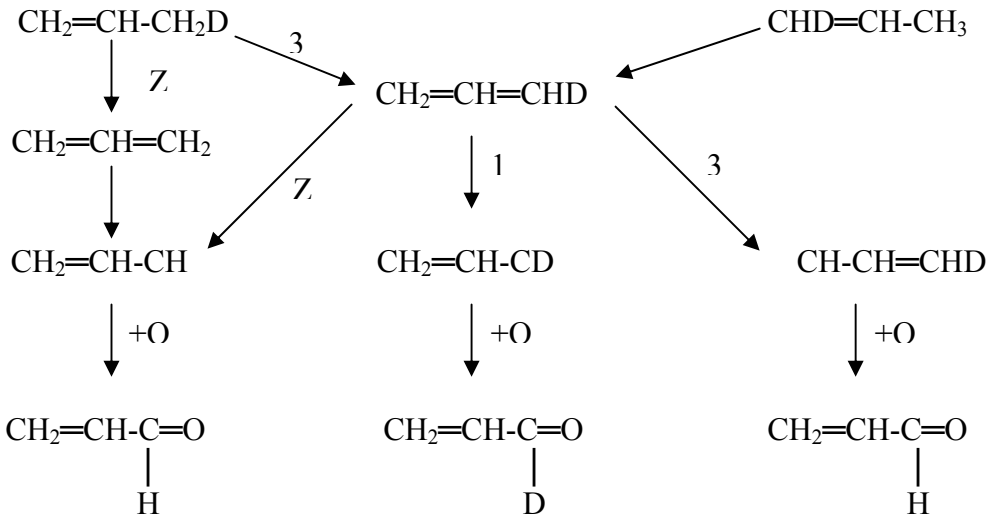

Figure 2.7 The reaction paths of the partial oxidation of deuterium-labelled propylene, $Z=k_D/k_H$, while 1 and 3 are the numbers of carbon atoms where hydrogen is abstracted. The value of Z was calculated from the distribution of deuterium in acrolein. Deuterated carbon was only found on terminal carbon atoms of the products (Leonard David Krenzke 1977).

Transient response and spectroscopy methods have also been used to prove the existence of the allylic radical. Kobayashi (Kobayashi & Futaya 1979) used a transient response method on a bismuth molybdate with Bi:Mo ratio of about 1.0 and comprised of alpha, beta and gamma phases, and revealed the existence of the allylic intermediate. The allylic intermediate was also reported by Martir and Lundsford (Martir & Lunsford 1981) using an EPR spectroscopy method, and by Schultz and Beauchamp (Schultz & Beauchamp 1983) using a photoelectron spectroscopy. The study by Carrazan et al. (Carrazan et al. 1996a) using an FT-IR spectroscopy technique on a multiphase Bi, Mo, and Co catalyst and proposed a mechanism which is in agreement with those of Cullis and Hucknall (Cullis & Hucknall 1981) and Bettahar et al. (Bettahar et al. 1996). A more recent study by Ono, Ogata, and Kuczkowski (Ono, Ogata & Kuczkowski 1998) using labelled oxygen and microwave spectroscopy also supported the existence of allylic intermediate.

Several studies (Gorshkov et al. 1970; Gorshkov et al. 1969; Gorshkov et al. 1968) on the formation of side products also confirmed the allylic intermediate mechanism. The side products normally accompany the selective oxidation of propylene to acrolein. Keulks and Daniel (Daniel & Keulks 1972) investigated the oxidation of ^{14}C labelled and unlabelled acrolein. They found that the carbon dioxide is formed almost exclusively from the further oxidation of acrolein. The same result was also found earlier by Russian researchers (Gorshkov et al. 1970; Gorshkov et al. 1969; Gorshkov et al. 1968). Figure 2.8 shows the reaction path of the formation of some side products.

All of the above studies using indirect methods concluded the formation of the allylic radical. The formation of allylic intermediate in the reaction of partial oxidation of propylene over bismuth molybdate catalysts has been widely accepted although the isolation of the allylic and allyl-peroxiradicals was only proven in 1981 by Martir and Lundsford (Martir & Lunsford 1981) in their matrix isolation-EPR studies on α-$Bi_2Mo_3O_{12}$ and γ-Bi_2MoO_3.

2.8.2 Oxygen Insertion

The step after propylene activation is the abstraction of second hydrogen and the oxygen insertion into allyl group. The abstraction of the second hydrogen is

unlikely to occur at the same time as the allylic formation is taking place because the reaction is energetically rate-determining step. Studies using self-generating allylic species (James D. Burrington, Kartisek & Grasselli 1980; B. Grzybowska, Haber & Janas 1977) have showed that the second hydrogen was abstracted from the allylic intermediate.

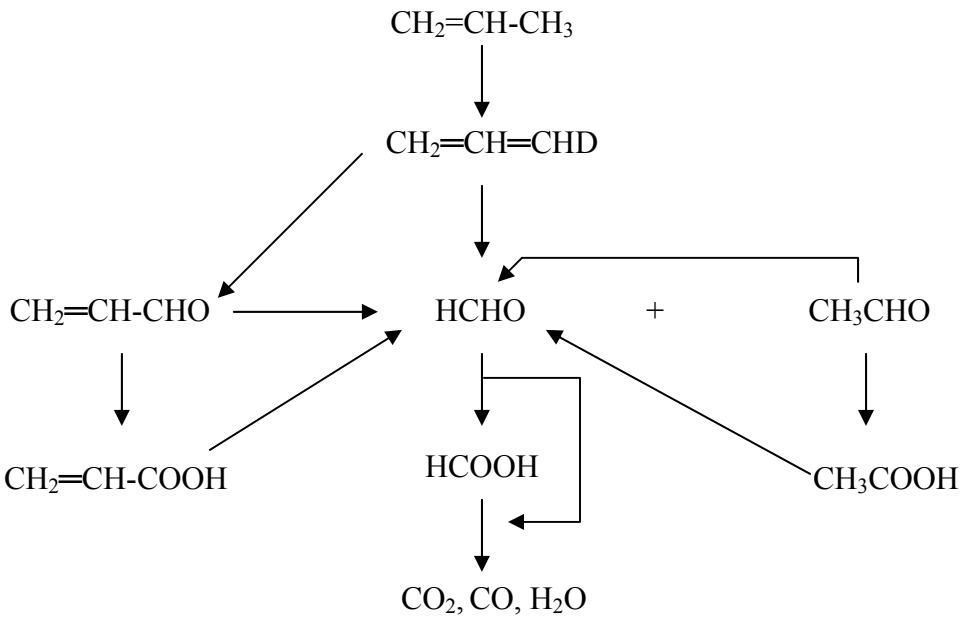

Figure 2.8 The reaction paths of the formation of side products (Leonard David Krenzke 1977).

The insertion of oxygen occurs before the second abstraction of hydrogen from the allylic intermediate. In order to elucidate the key aspects of selective partial oxidation of propylene to acrolein over bismuth molybdate and related catalysts, Burrington et al. (James D. Burrington, Kartisek & Grasselli 1980) used allyl alcohol-1,1-d2 and -3,3-d2 in their investigation. They concluded that the insertion of oxygen occurs before the abstraction of the second hydrogen and facilitated by the presence of a C─O bond.

So far, no mention has been made of the source of oxygen for oxygen insertion into the allylic intermediate. For the formation of acrolein, there are two possible sources of oxygen. One involves the use of lattice oxygen and the other an adsorbed form of molecular or gas phase oxygen. The first mechanism is referred to

as the redox mechanism where the catalyst itself acts as the oxidising agent. In this mechanism, molecular oxygen serves only to re-oxidise the reduced catalyst. The second type of oxygen reacts with the allylic intermediate to form hydroperoxide. The hydroperoxide then decomposes to acrolein and water.

The redox mechanism was first proposed by Mars and van Krevelen (Thomas & Thomas 1997) and has since been known as the Mars and van Krevelen mechanism. In early 1954, Mars and van Krevelen (Mars & van Krevelen 1954) concluded that the catalytic oxidation of hydrocarbon took place in two steps: *(a)* the reaction between hydrocarbon and the oxide in which the latter is reduced and the former is oxidised, followed by *(b)* reoxidation of the reduced catalyst by gaseous oxygen to the original state of activity and selectivity. The Mars and van Krevelen mechanism is schematically given in Figure 2.9. The concept where the lattice oxygen of a reducible metal oxide could serve as a useful oxidising agent for hydrocarbons was actually the basis of the early work at SOHIO which led to the development of bismuth molybdate catalyst (Callahan et al. 1970).

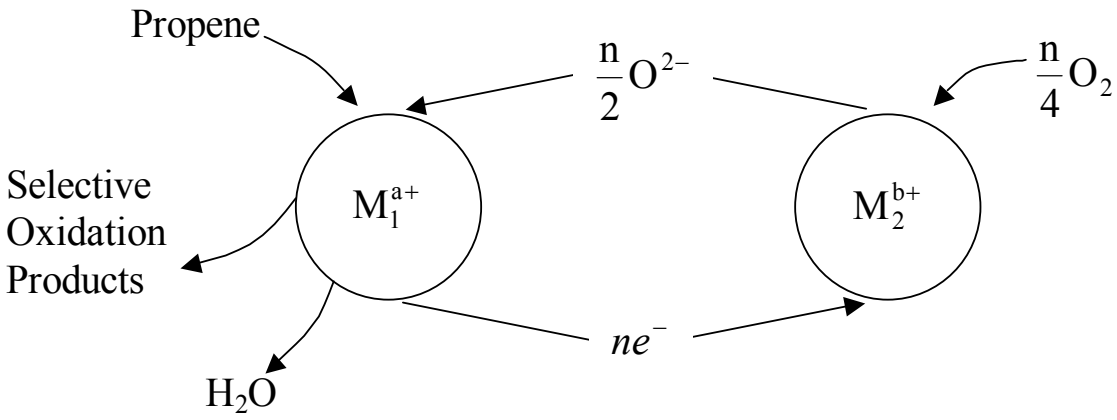

Figure 2.9 A schematic of the Mars and van Krevelen mechanism on bismuth molybdate catalysts (Thomas & Thomas 1997).

The usefulness of lattice oxygen as the source of oxygen for oxidation reactions is due to the fact that the oxygen is relatively easy to be removed from the lattice. Burlamacchi et al. (Burlamacchi, Martini & Ferroni 1971) gave evidence that the lattice oxygen ions on γ-Bi_2MoO_6 surface could be easily removed by applying high vacuum at temperatures above 300^{o}C. Fattore et al. (Fittorio Fattore et al.

1975a; Vittorio Fattore et al. 1975b) observed that acrolein could be formed without any gaseous oxygen over bismuth molybdate and several other metal oxides catalysts.

2.8.3 Active Site for the Source of Lattice Oxygen

The evidence of the formation of allylic intermediate and the involvement of lattice oxide ions led to further questions how the propylene is activated on the surface of bismuth molybdate catalysts and which oxide ions are responsible for the oxidation of the allylic intermediate. In order to answer these questions, many studies have been taken to find out the active sites on bismuth molybdate catalysts.

Otsubo et al. (Otsubo et al. 1975) used γ-$Bi_2{}^{18}O_3.MoO_3$ and γ-$Bi_2O_3.Mo^{18}O_3$ to investigate which oxygen ions are actually taken from the lattice. They reacted bismuth molybdate with hydrogen and found that the products contain mainly ^{18}O on the γ-$Bi_2{}^{18}O_3.MoO_3$ but not found on γ-$Bi_2O_3.Mo^{18}O_3$. From the finding, they concluded that oxide ions in $(Bi_2O_2)^{2+}_n$ layers are responsible for olefin oxidation. Later, they further discovered that the oxide ions consumed by the reaction are replenished by gaseous oxygen through $(MoO_2)^{2+}_n$ layer (Miura et al. 1979) and supported the former investigation results of Grzybowska and his co-workers (B. Grzybowska, Haber & Janas 1977; R. Grzybowska et al. 1976). Miura et al (Miura et al. 1979) also found that the oxide ions in the beta and gamma phases of bismuth molybdate are more mobile than those in the alpha phase. The different extent of lattice oxygen participation in the three bismuth molybdate phases was also revealed by Hoefs et al. (Hoefs, Monnier & Keulks 1979).

Ono et al. (Ono, Ogata & Kuczkowski 1998) reported that initial hydrogen abstraction to produce an allylic intermediate involves an oxygen atom associated with bismuth. They also found that the second hydrogen abstraction was facilitated by the presence of molybdenum oxide polyhedra on γ-Bi_2MoO_6. The allylic radicals formed on the surface of γ-Bi_2MoO_6 are found in the rapid equilibrium form of π-allyl and σ-allyl on the surface of α-$Bi_2Mo_3O_{12}$. The study by Batist in 1979 (Batist 1979) also revealed the importance of redox couples in a catalyst for the selective oxidation of olefin.

Evidence of dual sites for propylene adsorption was also reported in the most recent studies by Ayame et al. (Ayame et al. 2000; Ayame et al. 2002). Using an *in-situ* XPS method on the alpha and gamma phases of bismuth molybdates, they found the propylene molecule interact simultaneously with two different lattice oxygen ions to result in almost equivalent amounts of Mo^{4+} and Mo^{5+}, but the reduced species of bismuth were not found. Abstraction of bridging oxygen led to the formation of Mo^{5+} species, while abstraction of double bonded oxygen led to the formation of Mo^{4+} (Ayame et al. 2000; Ayame et al. 2002; Gualtieri & Venturelli 1999). The results of the investigation by Ayame et al (Ayame et al. 2000; Ayame et al. 2002) indicate that propylene interacted with two different oxygen ions on the surface of bismuth molybdate at the same time to produce acrolein and water. The first oxygen ion bridges Bi^{3+} and Mo^{6+} while the other is the oxygen ion doubly bonded to Mo^{6+} where the former is structurally and laterally distinct from the latter. A study on adsorption equilibrium of propylene on γ-Bi_2MoO_6, reviewed in reference (Bettahar et al. 1996) showed that the propylene was adsorbed on a dual site. The reaction scheme of bridges and doubly bonded oxide ions is given in Figure 2.10.

All above evidence has led one to draw all molecular level mechanisms of propylene oxidation to acrolein over bismuth molybdate catalysts as articulated in Figures 2.11 to 2.13.

2.9 Kinetics of Propylene Oxidation to Acrolein

Although there has been a vast amount of research into the reaction mechanisms of partial oxidation of propylene to acrolein over bismuth molybdate catalysts, very few kinetic experiments have been reported. One of the earliest reports on the kinetics is by Adams et al. (Adams et al. 1964). They reported that the reaction was first order in propylene and independent of oxygen and products. The conclusions of the report were derived from their kinetic experiments using an integral reactor operating at atmospheric pressure and 450 to 550^{o} C. The first order in propylene and zero order in oxygen were also reported by Gel'bstein et al. (Gel'bstein et al. 1965) using an externally recirculated reactor with beta phase of bismuth molybdate supported on silica as a catalyst.

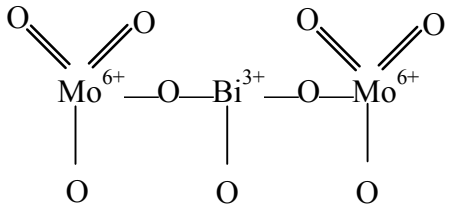

Figure 2.10 A schematic of bridges and doubly bonded oxygen ions on bismuth molybdate catalysts (Bettahar et al. 1996).

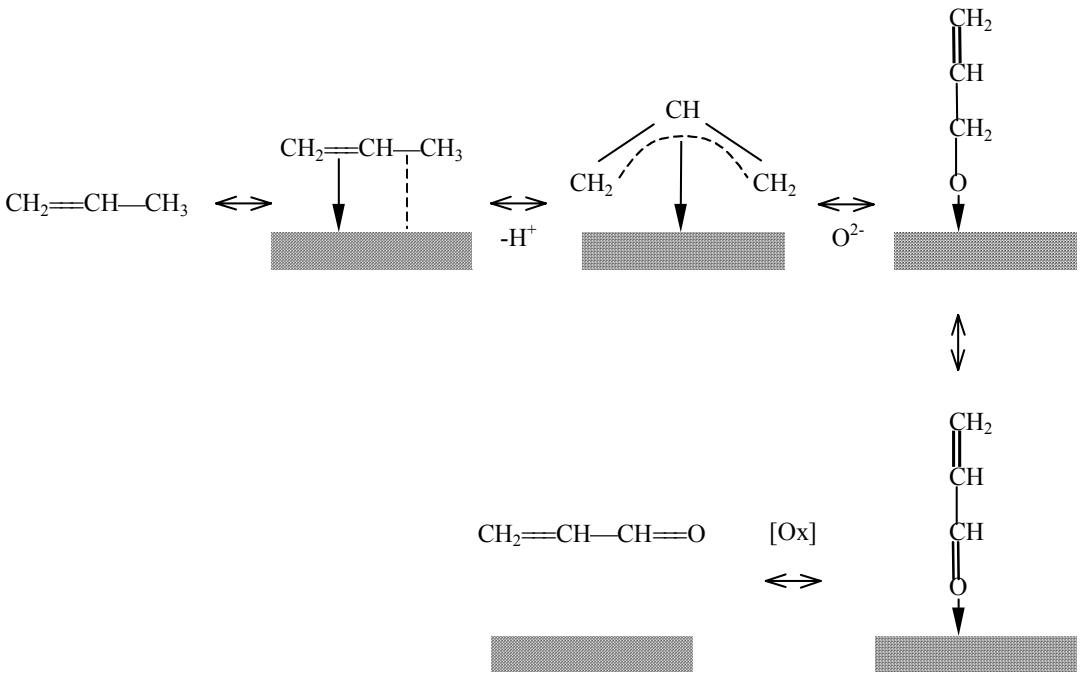

Figure 2.11 A schematic of steps in propylene oxidation into acrolein over bismuth molybdate catalyst (Carrazan et al. 1996a).

The oxidation of propylene over bismuth molybdate as had been done by Adams et al. and Gel'bstein et al. yielded, in addition to acrolein, some considerable amounts of carbon monoxide, carbon dioxide and lesser amounts of ethylene, formaldehyde and acetaldehyde. The carbon oxides (CO and CO_2) appeared to come from either direct reaction of propylene with oxygen as well as oxidation of acrolein. In order to gain further insight into the reaction mechanism and to find out the origin of carbon oxides, Keulks et al. (Keulks, Rosyneck & Daniel 1971) undertook a

kinetic study on propylene oxidation over bismuth molybdate using a single pass, integral flow reactor at 350^{o} to 475^{o}C and atmospheric pressure. They found that: i) the kinetics showed the first order in propylene and zero order in oxygen; ii) the activation energy was 121.42 kJ mol^{-1} over the temperature range; iii) the side products, such as acetaldehyde, formaldehyde, ethylene, carbon monoxide, and carbon dioxide were formed almost exclusively via oxidation of acrolein or its surface precursor species when excess oxygen was present and the direct oxidation propylene to carbon dioxide only became important when there oxygen was deficient. They also found that the homogeneous-gas phase oxidation of acrolein became important when the post catalytic volume of the reactor was increased.

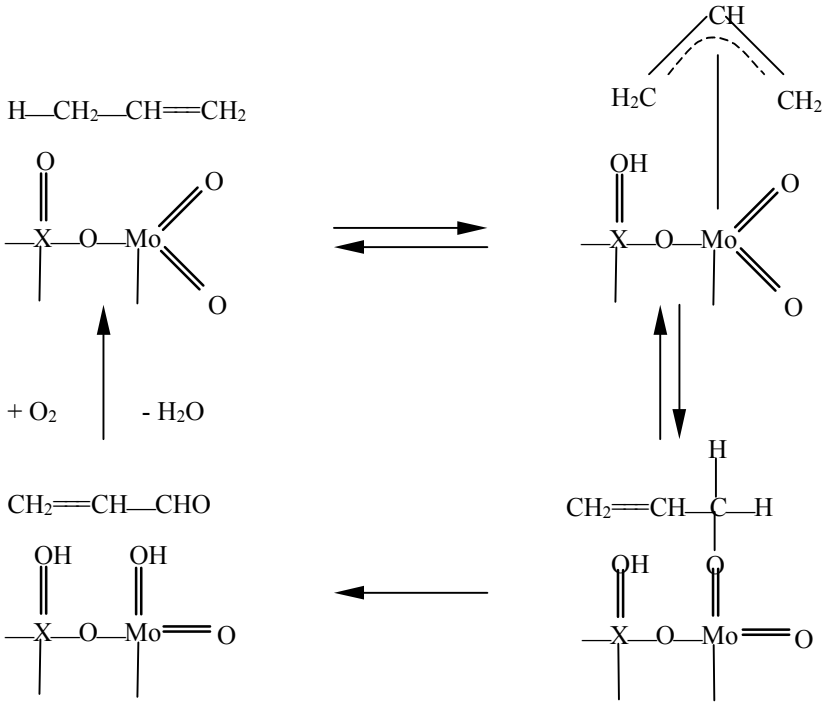

Figure 2.12 The detailed reaction mechanism of propylene oxidation into acrolein over bismuth molybdate catalysts, X = Bi (Cullis & Hucknall 1981) and Bi, Co (Carrazan et al. 1996a).

More recent studies of the kinetics of propylene oxidation to acrolein were reported by Keulks and co-workers (L. David Krenzke & Keulks 1980b; Monnier & Keulks 1981), Tan et al. (H. S. Tan, Downie & Bacon 198819891990) and Kremenic et al (Kremenic et al. 1987). Keulks and co-workers put more emphasis on the

kinetics of the redox mechanism over bismuth molybdate while Tan et al concentrated more on statistically accepted data.

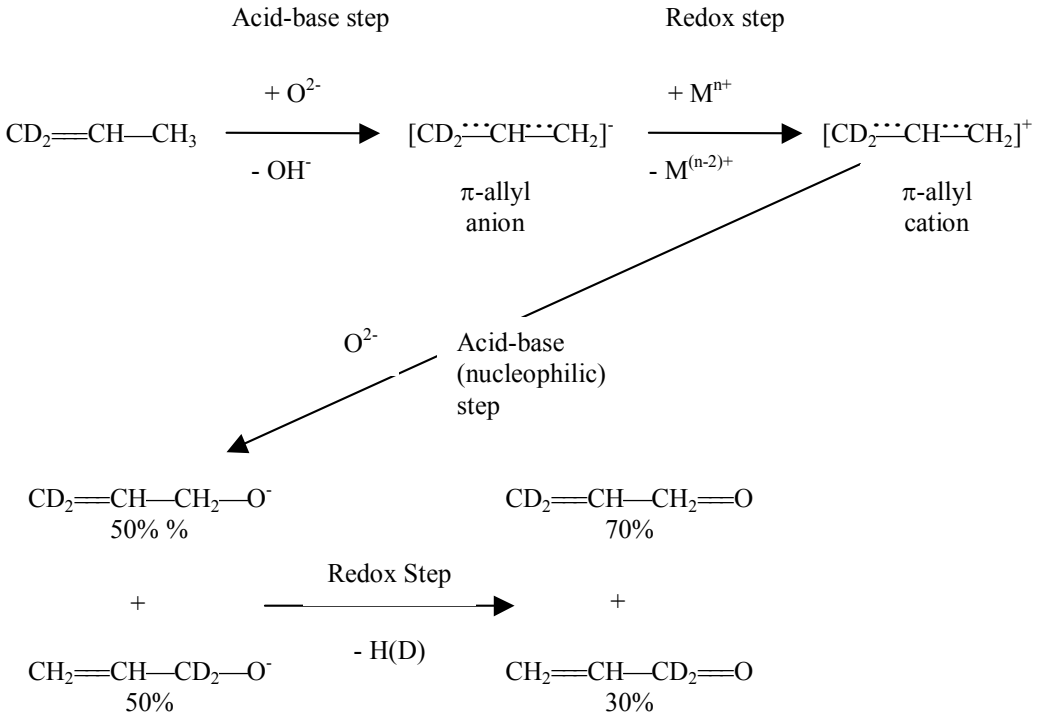

Figure 2.13 A reaction mechanism of propylene oxidation into acrolein, showing acid-base and redox steps (Bettahar et al. 1996).

Keulks and co-workers (Keulks & Lo 1986; Keulks, Rosyneck & Daniel 1971; Leonard David Krenzke 1977; L. David Krenzke & Keulks 1980b; Monnier & Keulks 1981) found that there were two apparent activation energies, depending on the reaction temperature for the acrolein formation from partial oxidation of propylene on α, β and γ-bismuth moybdate. The apparent activation energies on α-$Bi_2Mo_3O_{12}$, β-$Bi_2Mo_2O_9$ and γ-Bi_2MoO_6 found by Keulks and co-workers are given in Table 2.3. They also found that the kinetics of acrolein and carbon dioxide formation over bismuth molybdate appear to be complicated by the fact that the dependencies on both oxygen and propylene tend to change with temperature. However, they have successfully explained the kinetic behaviour by the redox mechanism.

Table 2.3 Apparent Activation Energies of Partial Oxidation of Propylene to Acrolein over Bismuth Molybdate Catalysts (L. David Krenzke & Keulks 1980b; Monnier & Keulks 1981).

Catalyst	Temperature Range	E_A	
		kJ mol^{-1}	kcal mol^{-1}
α-$Bi_2Mo_3O_{12}$	>410°C	75.36	18
	<410°C	221.90	53
β-$Bi_2Mo_2O_{12}$	>400	83.74	20
	<400	180.03	43
γ-Bi_2MoO_6	>419°C	62.80	15
	<419°C	180.03	43

The kinetic equation of the redox model developed by Keulks and co-workers (Leonard David Krenzke 1977; L. David Krenzke & Keulks 1980ab) is given in equation 2.1. The model is in qualitative agreement with the observed kinetics of acrolein and carbon dioxide formations.

$$-\frac{d[C_3H_6]}{dt} = k_{\mathrm{Red}} P_{C_3H_6}^{x} \left[\frac{k_{Ox} P_{O_2}^{y} k_R P_{C_3H_6}^{x}}{1 + \left(k_{Ox} P_{O_2}^{y} / k_R P_{C3H6}^{x} \right)} \right] \qquad 2.1$$

where:

- k_{Red} = rate constant for catalyst reduction
- P_{C3H6} = partial pressure of propylene
- x = reaction order in propylene
- k_{Ox} = rate constant for catalyst reoxidation
- P_{O2} = partial pressure of oxygen
- y = reaction order in oxygen

The first order in propylene was also reported by Kremenec et al. (Kremenic et al. 1987) for a Mo-Pr-Bi catalyst. The apparent reaction order with respect to oxygen was relatively low and decreased from 0.4 to 0.1 as the temperature increased from 320° to 380°C, and the apparent activation energy was calculated from Arrhenius plot to be 117 kJ mol^{-1}. In addition, they fitted their experimental data using the Least Squares method (*Mathematica in Engineering*) to find the best-fit of

the experimental data to several kinetic models widely used for catalytic reactions such as the power rate law, Langmuir-Hinshelwood, Eley-Rideal kinetics, redox, and stationary state. Combination of the best-fit models and the information on adsorption of propylene and oxygen on the Mo-Pr-Bi catalysts led them to the conclusion that the reaction followed the Mars and van Krevelen mechanisms as founded by Keulks and co-workers using bismuth molybdate catalysts (Kremenic et al. 1987; Kremenic et al. 1988).

The agreement on the redox mechanisms of the partial oxidation of propylene to acrolein on bismuth molybdate catalysts was also reported by Tan et al. (Hock Seng Tan 1986; H. S. Tan, Downie & Bacon 19881989). Tan firstly criticised the earlier work (Hock Seng Tan 1986). For instance, the work of Keulks and co-workers (Keulks 1970; Keulks, Krenzke & Notermann 1978; Keulks & Lo 1986; Keulks, Rosyneck & Daniel 1971; Leonard David Krenzke 1977; L. David Krenzke & Keulks 1980b; Monnier & Keulks 1981) was limited in number and range of reactant concentration, and the rate parameters associated with the model were not evaluated. Using statistical methods for model discrimination and parameter estimation, they found that the partial oxidation of propylene to acrolein followed a redox steady state model with a half-order in oxygen concentration, involving oxygen adsorption and reaction with propylene from the gas phase. Moreover, the disappearance of propylene occurred through parallel reactions to acrolein, carbon oxides, and acetaldehyde, with subsequent oxidation of the acrolein to carbon oxide.

2.10 Conclusions from Literature Review

From the discussion thus far, it is obvious that the relationship between structure, reaction kinetics and mechanisms is complex. Indeed, there has been no such kind of research, which took into account these three subjects on catalytic partial oxidation of propylene to acrolein over bismuth molybdate in a single research. In most case, these subjects were studied separately.

From the viewpoint of reaction mechanisms, the allylic intermediate formation as the first step for the selective partial oxidation reaction and oxygen ions

of the catalyst lattice being the source of oxygen for the reaction has been widely accepted. Ono et al. (Ono, Ogata & Kuczkowski 1998) and Ayame et al. (Ayame et al. 2000; Ayame et al. 2002) have tried to investigate the relations between the bismuth molybdate crystal structure and the reaction mechanism by proposing that certain oxygen types in the lattice are more active and selective than others. However, they could not conclude more definitively because their experiments were based only on surface characterisation techniques.

Attempts have been made to reveal the relation between structure and catalytic activity and selectivity of bismuth molybdate catalysts. Buttrey et al. (D. J. Buttrey, Jefferson & Thomas 1986) gave an example on how the structure can be related to their catalytic activity. Buttrey et al (D. J. Buttrey, Jefferson & Thomas 1986) mentioned that all active phases were actually derived from fluorite structure except the γ-Bi_2MoO_6. However, the structure identified in their study might be different from the one under actual reaction conditions. This is a fundamental reason why an *in-situ* characterisation is needed and will be investigated in more detail in this thesis.

With the advances in diffraction techniques and the availability of the Rietveld method, catalyst characterisation under *in-situ* conditions has been possible, although there are still some limitations such as the timescale of data acquisition necessary for more adequate evaluation of the dynamics of the structure.

Although the reaction mechanisms at molecular level have been widely accepted, the measured kinetics of propylene oxidation to acrolein has never been directly derived from the mechanisms. All reported kinetics uses the surface mechanisms rather than the molecular mechanism although it has already given acceptable explanation of the experimental data. The redox mechanism has so far been accepted as the only mechanism that can satisfactorily explain the kinetic data over bismuth molybdate catalysts as mentioned by Keulks and co-workers (Keulks & Lo 1986; Keulks, Rosyneck & Daniel 1971; Leonard David Krenzke 1977; L. David Krenzke & Keulks 1980b; Monnier & Keulks 1981) and Tan et al. (Hock Seng Tan 1986; H. S. Tan, Downie & Bacon 1988).

2.11 Objectives of the Present Research

All the aforementioned literature studies have aimed to understand the reaction mechanisms so as to control the reaction process. However, further research is still required to be able to better understand the working of the catalysts so that the design of new catalysts can be based on sound science and their performance can be well predicted and controlled.

The research in this thesis is designed to achieve an improved understanding of the catalyst structure characteristics, reaction mechanisms and kinetics. The aim of structural characterisation is to explain the role of the bulk catalyst structure in the catalytic activity for the partial oxidation of propylene to acrolein and to investigate which oxygen in the bulk structure actually plays the key role in the catalyst's selectivity and how the differences in the crystal structure affect the catalyst's selectivity and activities. The structural studies will involve *in-situ* experiments where the catalyst structure will be studied in their active conditions.

The *in-situ* studies are designed to reveal which oxygen in the bismuth molybdate lattice is particularly taking control of the catalysts activity as well as selectivity. For example, oxygen No. 4 and 5 in α-$Bi_2Mo_3O_{12}$ are the most likely oxygen ions who are responsible for the catalyst activity for selective oxidation of propylene to acrolein. It is also aimed to find out the relationship between different bismuth molybdate crystal structure and their activity with a hope to achieve better understanding of how they work and, in the future, to engineer the structure in such a way so that one could fully control the catalyst activity and selectivity towards certain useful products.

To give more support on the relation, the kinetics will also be investigated. The kinetic investigations will be conducted using unsupported powder-form of high purity, in-house prepared bismuth molybdate catalysts. The unsupported forms are chosen to annihilate the synergetic effects that might be given by the supports, reducing the external factors. The kinetics will also be studied using a quartz reactor which has proven to be inert under reaction conditions.

The kinetic data will then be analysed to model the kinetics based on molecular level mechanisms as well as surface mechanisms.

Chapter 3

EXPERIMENTAL METHOD

In order to achieve the objectives set out for the present thesis as detailed in Chapters 1 and 2, several analytical and experimental techniques have been chosen or developed to investigate the partial oxidation of propylene to acrolein on three bismuth molybdate catalysts namely α-$Bi_2Mo_3O_{12}$, β-$Bi_2Mo_2O_9$ and γ-Bi_2MoO_6. There are three facets in this investigation, namely, structural characterisation, reaction kinetics, and reaction mechanisms. This chapter describes in detail these techniques and their procedures.

3.1 Catalyst Preparation and Characterisation

The chemicals used for the catalyst preparation were bismuth nitrate pentahydrate $Bi(NO_3)_3.5H_2O$ from Aldrich Chemical Company, Inc (Cat. No. 24,859-2), and ammonium paramolybdate $(NH_4)_6Mo_7O_{24}.4H_2O$ from AR (Cat. No. CA3885). Both chemicals were purchased from Rowe Scientific, Australia. The bismuth-molybdate catalysts were prepared using the so-called co-precipitation method based on the literature (Carrazan et al. 1996b; Fittorio Fattore et al. 1975a; R. Grzybowska et al. 1976; Millet et al. 1993; Ono, Ogata & Kuczkowski 1998). The chemical compositions to make ca 100 grams of the targeted α, β, and γ-bismuth molybdate are listed in Table 3.1.

Bismuth nitrate, $Bi(NO_3)_3.5H_2O$ and ammonium paramolybdate, $(NH_4)_6Mo_7O_{24}.4H_2O$ were dissolved separately in minimum amounts of hot, distilled water (70°C). The bismuth nitrate solution was then dropped slowly into the vigorously stirred ammonium paramolybdate solution, producing a yellowish suspension. The suspension was kept in a water bath at 70°C and stirred well to evaporate the liquid slowly until it became an almost dry paste. The paste was then put into an oven at 120°C for 20 hours in air. The dried paste was then crushed and calcined at 250°C for 2 hours in an air oven to transpose all metal salts into metal oxides precursors.

Table 3.1 The chemicals for preparing ca. 100 gram of targeted catalysts

Targeted Catalyst	**$Bi(NO_3)_3.5H_2O$**	**$(NH_4)_6Mo_7O_{24}.4H_2O$**
α-$Bi_2Mo_3O_{12}$	110.279 gram	59.000 gram
γ-Bi_2MoO_6	162.312 gram	28.947 gram
β-$Bi_2Mo_2O_9$	131.320 gram	46.841 gram

The catalyst precursors were then grinded to a powder prior to further calcination. The calcination temperature and duration were different for each catalyst, depending on the results from DTA-TGA analyses of the precursors and x-ray diffraction phase analyses of the calcined precursors. Table 3.2 gives the optimised calcination program for each targeted catalyst.

Table 3.2 Calcination temperature and duration for catalyst precursors

Targeted Catalyst	**Calcination Temperature (°C)**	**Duration (hours)**
α-$Bi_2Mo_3O_{12}$	480	20
γ-Bi_2MoO_6	480	20
β-$Bi_2Mo_2O_9$	650	24

The catalysts surface area and porosity were determined by the BET method using N_2 as the adsorbate at the liquid nitrogen temperature. The chemical composition of the catalysts was semi-quantitatively determined using X-ray

spectroscopy with an EDAX detector on the Philips XL-500 SEM. The SEM instrument was also used to study the morphology of the catalysts.

3.2 Diffraction Analyses

The diffraction analyses were aimed to determine the phase and crystalline structure of the catalysts, either at room temperature or at high temperatures with different atmospheres. Two diffraction techniques were employed to reveal the catalysts structure, namely, x-ray and neutron diffraction.

3.2.1 X-ray diffraction (XRD)

The room temperature XRD analyses were undertaken using a Siemens XRD type D-500 equipped with a Bragg-Brentano optical system, available in the Applied Physics Department at Curtin University of Technology. X-ray radiation was Cu K_α generated from a Cu source operating at 40 kV and 30 mA. The details of data collection are given in Table 3.3. The phase search and match were carried out using the JADE^{TM} software (version 6.0).

Table 3.3 XRD Pattern Measurement Conditions

Radiation:	Cu-anode tube type FF Cu4KE 60kV 1.5kW Operating Voltage and Current were 40kV and 30mA Effective focal spot size, 0.04 x 8 mm^2 Unfiltered, wavelength: $CuK\alpha_1$=1.5406Å and $CuK\alpha_2$=1.54439Å
Optics:	Bragg-Brentano, measuring circle diameter = 401mm Incident beam divergence = 1^o, receiving slit = 0.05^o Scatter slits divergence = 1^o, soller Slit divergence = 1^o
Specimen:	Holder = circular format, diameter = 23 mm Holder were rotated in all measurements
Detection:	Graphite diffracted beam monochromator set for CuKα NaI scintillator with pulse height analysis
Acquisition:	Angular range in 2θ, 5^o – 120^o Step size, 0.02^o Step speed, $0.5^o.min^{-1}$

3.2.2 Neutron Diffraction (ND)

The Neutron Diffraction experiments were carried out using the HIFAR (High Flux Australian Reactor) situated at the Bragg Institute-ANSTO, Lucas Heights Science and Technology Centre, New South Wales. The experiments used two neutron diffraction instruments, namely, the High Resolution Powder Diffractometer (HRPD) and the Medium Resolution Powder Diffractometer (MRPD).

The HRPD instrument has been described by Howard et al. (Howard et al. 1983), Howard and Kennedy (Howard & Kennedy 1994), and Knott (Knott 1998). Figure 3.1.a shows a schematic diagram of the instrument. It has 24 ^{3}He detectors, separated by 5^o in 2θ. This detector arrangement provides an effective angular range of 0^o to 150^o. A Ge crystal monochromator was used to produce a monochrome neutron beam at the wavelength of 1.495Å. The wavelength was chosen because it was close to the laboratory XRD wavelength, i.e 1.5418Å. The step size of 0.05^o over a 2θ range between 0 and 150^o was chosen to obtain sufficient steps through each peak.

The HRPD experiments were carried out in air at room temperature. As counting times for the data collection was sample dependent (Sitepu 1998), HRPD experiments was undertaken over 12 hour for α-$Bi_2Mo_3O_{12}$ and 24 hour for β-$Bi_2Mo_2O_9$ and γ-Bi_2MoO_6 to provide a good counting statistics. Specimens were contained in a vanadium can with 10 mm OD and 60 mm high. The specimens were rotated during the analyses to assure that the diffraction could result from random particles in the sample. Details of the instrument setting for the data collection are given in Table 3.4.

The MRPD instrument had 32 detector channels and gave medium resolution over an angular range from 4^o to 138^o of 2θ. A germanium crystal monochromator was used to provide a monochrome neutron beam at a wavelength of 1.665 Å. The wavelength was closest to the laboratory Cu-XRD among the possible wavelengths, which could be provided by the monochromator system (Howard & Hunter 1997).

The MRPD experiments were carried out at temperature between 300 and 400^{o}C in air and in the real reaction atmosphere. The reaction atmosphere comprised

of 1% C_3H_6, 2% O_2 and 97% He. The supply of reactant gasses was provided by controlling the flow rates of high purity helium and oxygen, and polymer grade propylene from BOC Australia. The helium and oxygen were used as they were supplied, while the propylene was premixed with high purity helium to bring the concentration to around 20%. Three MKS™ mass flow controllers were used to introduce the reaction gasses into the sample cell chamber at a constant total flow rate of 120 ml min^{-1}. Data were collected for six hours for α-$Bi_2Mo_3O_{12}$ and eight hour for β-$Bi_2Mo_2O_9$ and γ-Bi_2MoO_6 to obtain sufficiently high diffraction intensity. Details of the instrument setting are given in Table 3.5.

Table 3.4 HRPD Pattern Measurement Conditions

Monochromator:	Ge single crystal, take-off angle = 120^o Wavelength = 1495 Å
Optics:	Debye-Scherrer
Specimen:	Vanadium can (10 mm diameter and 60 mm high) Holder were rotated in all measurements
Detection:	24 ^{3}He detectors, separated by 5^o in 2θ
Acquisition:	Angular range of 2θ: 0^o – 150^o Step size: 0.05^o Twelve-hour data acquisition for α-$Bi_2Mo_3O_{12}$ and 24 hour for β-$Bi_2Mo_2O_9$ and γ-Bi_2MoO_6.

A special sample cell (reactor), made of quartz, was designed to enable the *in-situ* MRPD analyses (Figure 3.2). The cell was placed inside a furnace with 75 mm (ID). The quartz tube was 60mm in diameter at the bottom and 40mm at the top. Each catalyst sample was placed inside the vanadium can. The bottom part of the can was perforated to allow the reactant gas to flow freely through the sample and glass wool was placed on the perforated section to avoid the sample being blown through by the gas. A small quartz tube was connected to the perforated vanadium can inside the sample cell to enable the reactant gas to flow from the top of the can to the bottom. The neutron beam went through the middle of the 40mm section of the can. Figure 3.1.b illustrates the schematic diagram of MRPD instrument.

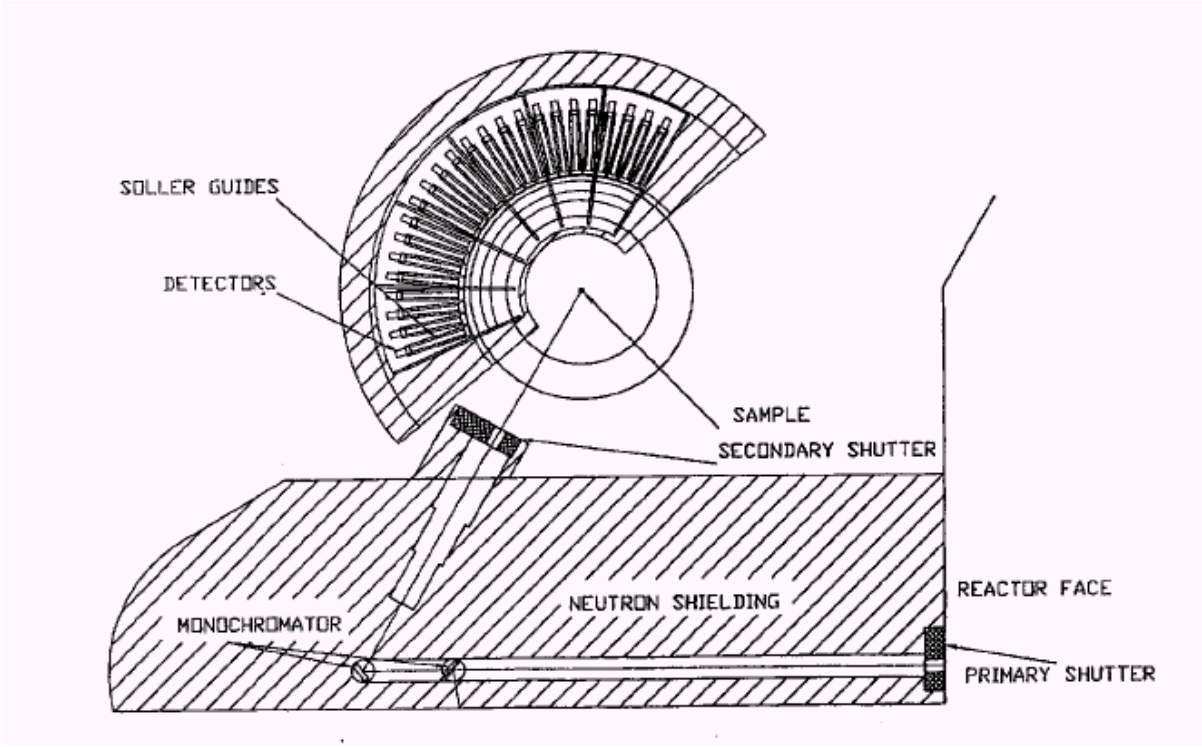

(a)

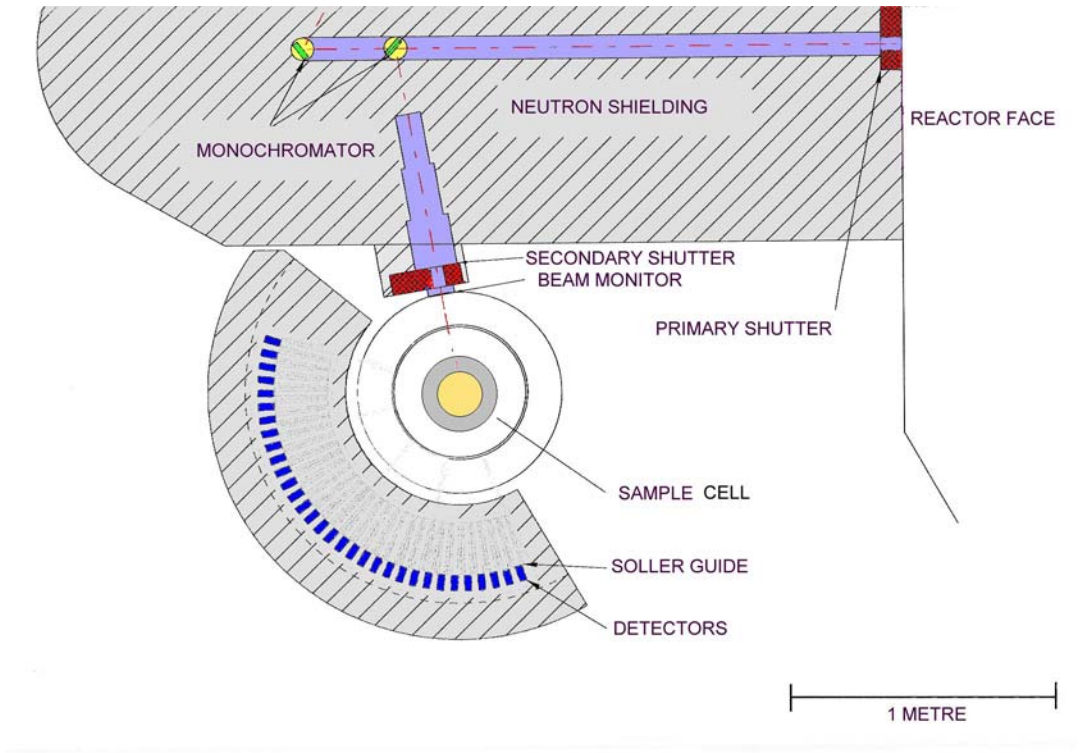

(b)

Figure 3.1 A schematic diagram of (a) HRPD and (b) MRPD

The diffractograms, resulted from both MRPD and HRPD, were refined using the LHPM Rietica refinement method (Howard & Hunter 1997) to extract the lattice parameters (a, b, c, α, β, γ and the volume of unit cells), interatomic distances, and thermal parameters. The input structure for the Rietveld refinement was taken from the ICSD (Inorganic Crystal Structure Database) collections. Details of the ICSD collections used as the input are given in Table 3.6.

Table 3.5 MRPD Pattern Measurement Conditions

Monochromator:	8 Ge single crystal 1 x 5 x 1 cm^3 Take-off angle = 100^o Wavelength = 1665 Å
Optics:	Debye-Scherrer
Specimen:	Vanadium can (10 mm diameter and 60 mm high) placed inside a quartz tube reactor
Detection:	32 ^{3}He detectors, separated by 5^o in 2θ
Acquisition:	Angular range in 2θ, 4^o – 138^o, step size, 0.1^o Six-hour data acquisition for α-$Bi_2Mo_3O_{12}$ and eight hour for β-$Bi_2Mo_2O_9$ and γ-Bi_2MoO_6.
Ancillary:	P1100, a high temperature furnace, able to bring temperature up to 1400^oC

Table 3.6 ICSD collections used for structure input in the refinement

Phase	ICSD Collection Number	Reference
α-$Bi_2Mo_3O_{12}$	2650	Van den Elzen and Rieck (van den Elzen & Rieck 1973a)
β-$Bi_2Mo_2O_6$	201742	Chen and Sleight (Horng-Yih Chen & Sleight 1986)
γ-Bi_2MoO_6	47139	Teller et al. (Teller, Brazdil & Grasselli 1984)

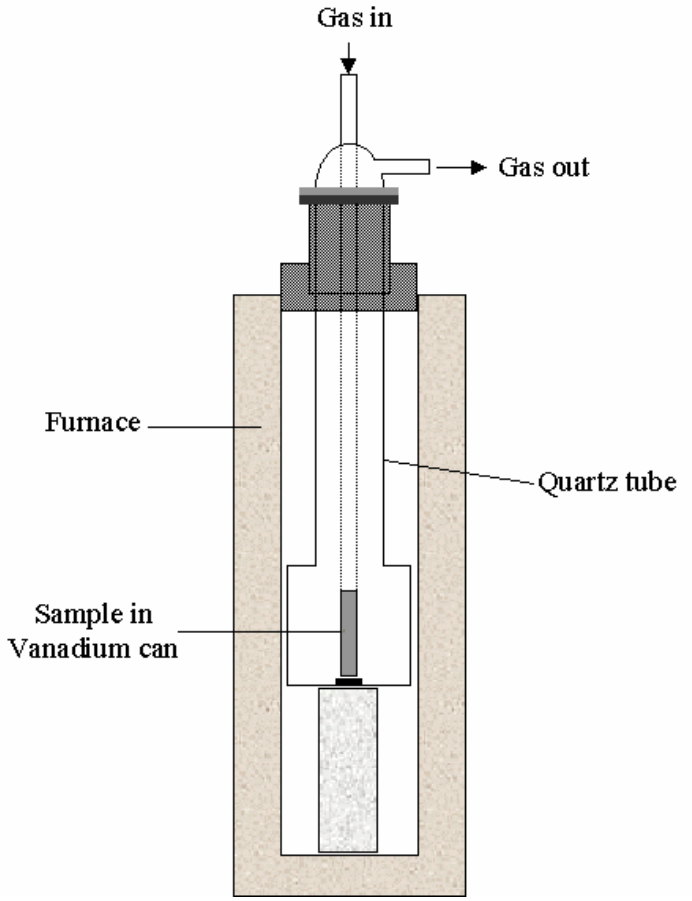

Figure 3.2 A schematic of the special sample cell for the *in-situ* MRPD analyses

3.3 Rietveld Analysis

All x-ray and neutron diffraction data are refined using the Rietveld method with the RIETICA software, freely available on the ANSTO website (Howard & Hunter 1997). To assure the refinement process goes uniformly, the procedures in Table 3.7 is applied in all refinement work. In addition, models and parameters for the refinement work have to be set as close to the actual values. Otherwise the refinement may become unstable. The detailed guidance for successful refinement has been described by Young (Robert Alan Young 1993), Kisi (Kisi 1994) and McCusker et al. (McCusker et al. 1999). In the present thesis, the $2\theta_0$ was fixed at 0.041 for all diffractograms collected from Siemens D500, which was taken from the work by O'Connor and Pratapa (O'Connor & Pratapa 2002). The starting values for U, V, and W for all instruments are tabulated in Table 3.8.

Table 3.7 Refinement sequences in Rietveld refinement work

Sequence No	Parameter(s)
1	Sample displacement, Phase scale
2	Background parameters
3	Unit cell parameters
4	Peak shape factors (U, V, W)
5	Thermal parameters (temperature factors)
6	Atomic coordinate

Table 3.8 Starting values for peak shape parameters

Parameters	**Starting values for**		
	D500	**MRPD**	**HRPD**
U	0.01	0.14	0.07
V	-0.0075	-0.23	-0.15
W	0.01	0.26	0.14

3.4 Kinetic Experiments

3.4.1 Apparatus for Kinetic Experiments

3.4.1.1 The Reactor System

All kinetic experiments as well as catalyst activity and selectivity tests were carried out using a single pass-fixed-bed-quartz reactor, as schematically shown in Figure 3.3. The reactor has two parts, which are tightly coupled by a metallic clamp. The upper part has a small quartz tube (4 mm OD) for thermocouple insertion and as an inlet for reactant gasses. The bottom part uses sintered glass to support the

catalyst, which is placed in the middle of the quartz tube (10 mm ID). A section of 2 mm inner diameter quartz tube was used below the catalyst bed to minimise gas phase reaction (Keulks, Rosyneck & Daniel 1971; Leonard David Krenzke 1977; L. David Krenzke & Keulks 1980b) on the post-catalytic zone. This section was also surrounded by a condensing shell to quench the reacted stream to minimise further oxidation of the products, particularly acrolein. The reactor was heated in a Carbolite™ tubular furnace type CFM 1, controlled by an RKC temperature controller. A type K thermocouple was used to monitor the temperature of the furnace.

High purity oxygen and polymer grade propylene were used as the reactant gasses, both diluted in high purity Helium. All gasses were purchased from BOC Australia and were used without further purification. Three MKS mass flow controllers controlled the flow rate of reactant gasses. Helium and oxygen were controlled by two-model 1159B mass flow controllers with a flow rate range of up to 200 sccm He while an MKS model 1179A with a range of up to 100 sccm N_2 was used for controlling the flow rate of propylene. The inlet pressure for the He mass flow controller was 120 kPa, and oxygen and propylene was 150 kPa. A four-channel MKS readout unit model 247C was used to control all three mass flow controllers. All mass flow controllers were calibrated with a bubble soap flow meter.

The catalyst powder was placed on the top of sintered glass in the reactor. A type *J* thermocouple was fitted just on the top of the catalyst bed to monitor the temperature of the catalyst. The exhaust stream of the reactor was connected to a scrubber, which contained a sodium hydroxide solution with pH 11 to convert all acrolein produced to poly-acrolein, preventing the harmful acrolein from being released to the surrounding. All the reactor assembly was contained in a fume hood to avoid harmful products to be released in the lab.

All connection tubing for the reactor system used was made of 1/8” Teflon. Stainless steel Swagelock connectors were used to connect all tubing except the connection between Teflon tubing and the quartz reactor. The Teflon tubing was connected to the reactor by a flexible silicon tube. A needle valve on the outlet was installed to adjust the pressure of the gas line connected to a gas chromatograph (GC) to analyse for the gas compositions of both inlet and exit streams of the reactor.

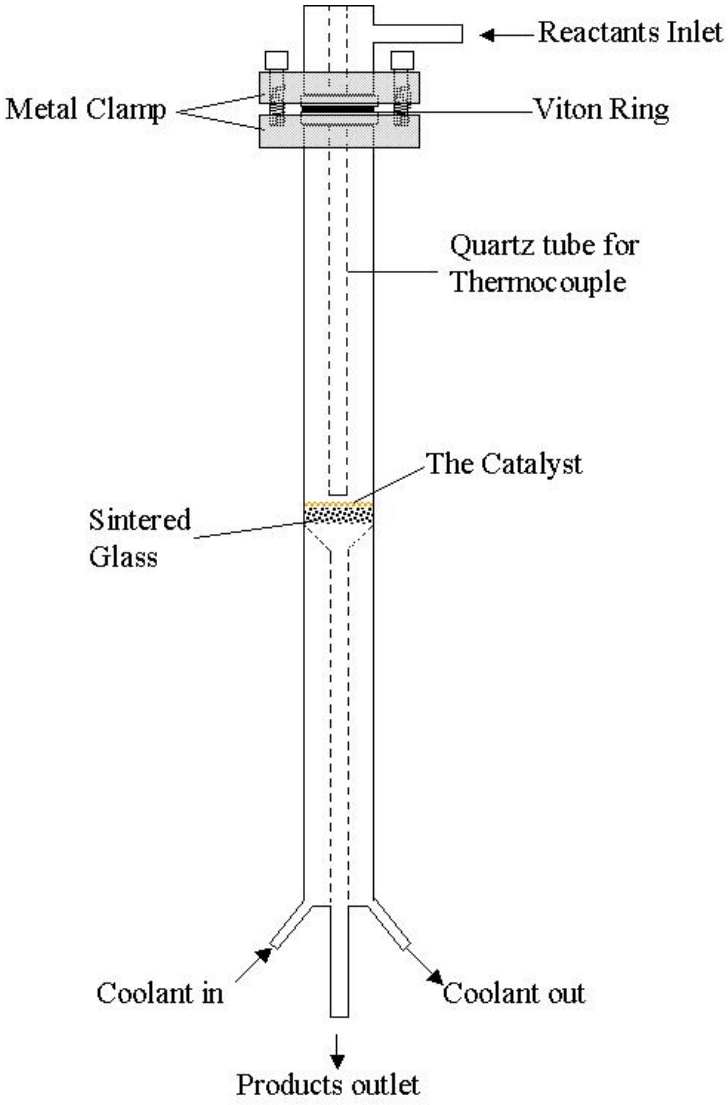

Figure 3.3 A schematic of the quartz reactor

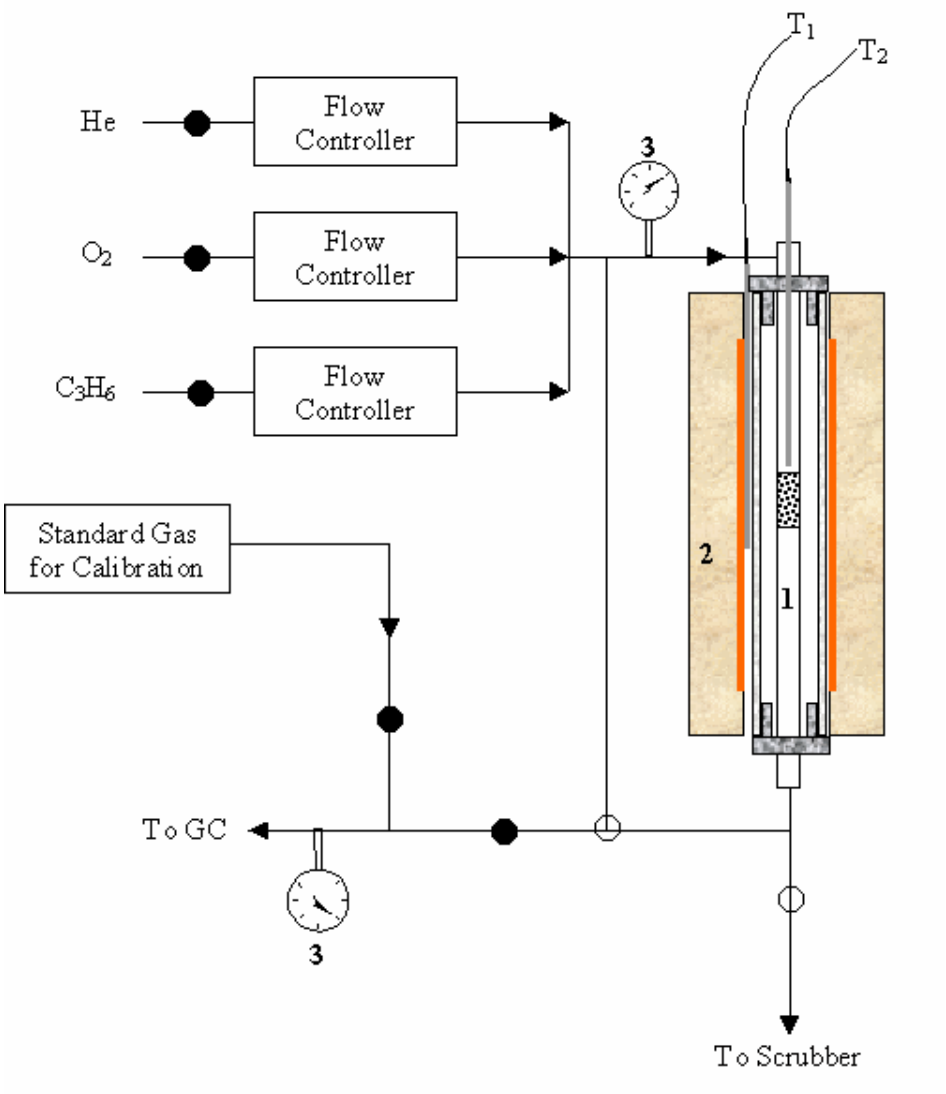

Legend:

1	The Quartz Reactor
2	Furnace
3	Pressure Gauge
T_1	Type K thermocouple for temperature controller
T_2	Type J thermocouple for temperature indicator inside the reactor
	Shut-off valve
	Three-way valve
	Needle valve

Figure 3.4 The reactor system for kinetic and activity experiments.

3.4.1.2 The Gas Chromatograph

A Varian gas chromatograph (GC) model STAR 3400CX was used to analyse gas composition of the inlet reactant and outlet product streams. The GC was fitted with two columns. The first column was a molecular sieve 13X for separating O_2 and the second one was Porapak N for separating Propylene, Acrolein, CO_2, and acetaldehyde. The molecular sieve 13X column was packed with 80 to 100 mesh range of molecular sieve 13 X while the Porapak N column was packed with 80 to 100 mesh Porapak N.

The GC was equipped with two valco valves to automatically control the switching of sample introduction and to alternate the columns for separating both reactants and products from the reactor. It was also equipped with a 167.64 μL sample loops to provide precise and repeatable sample injection to the GC. A schematic diagram of the valve and column system is given in Figure 3.4.

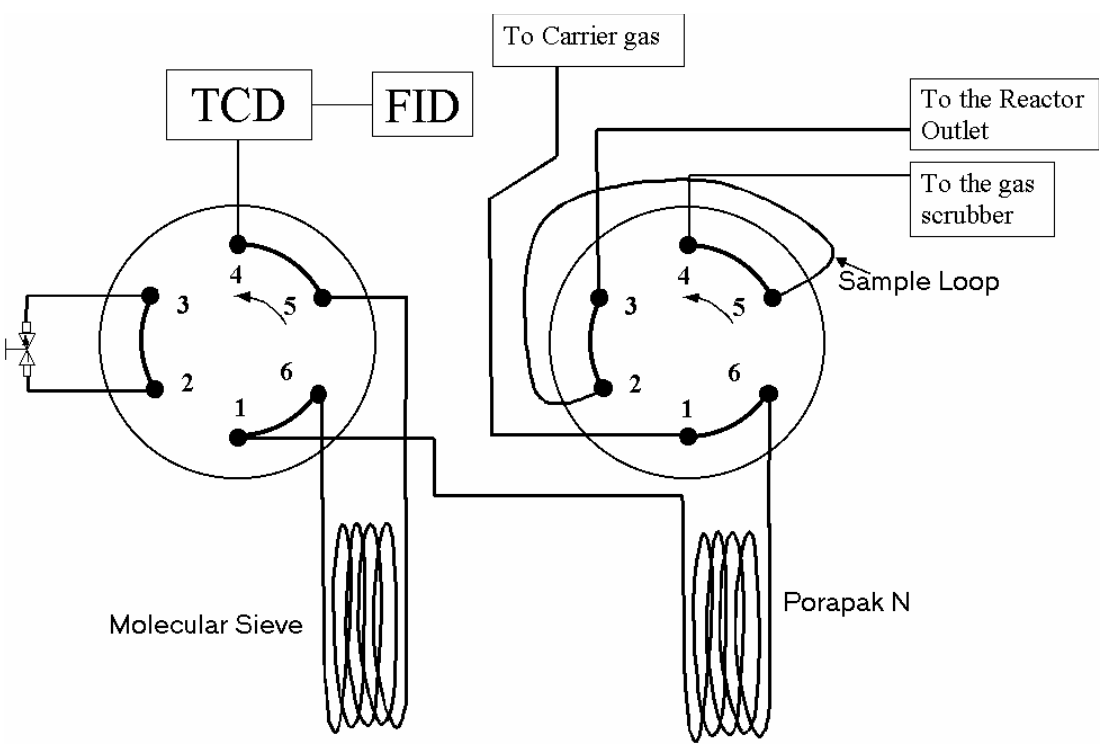

Figure 3.5 A schematic diagram of the valve system of Varian GC model STAR 3400CX.

3.4.2 The Gas Chromatograph Analysis Method

Quantitative analysis of the reactants or products is most important in order to obtain the kinetics of catalytic partial oxidation propylene to acrolein. The analyses of experimental data from differential reactor systems where the conversion of reactant is usually kept very small (less then 10% conversion) require high precision and accuracy of the data. This means that the analysis method has to be able to detect very small changes in concentrations of reactants and products.

A method file to control the GC in performing the quantitative analysis in the STAR software is specially developed for the system. The method programs the temperatures of the GC columns, injector, detectors, and auxiliaries, and the functioning of the GC valves and detectors (FID and TCD). The temperature of the GC columns is programmed to initially start at 110^{o}C and is maintained at this temperature for 5.5 minute. A heating rate of 20^{o} min^{-1} is then applied to increase temperature to 170^{o}C and kept at the temperature for 8 minute. Meanwhile, the temperature of the injector, detectors, and auxiliaries are kept constant. The GC valves are programmed to enable the separation of all reaction products (carbon dioxide, oxygen, carbon monoxide, propylene, acetaldehyde and acrolein). The detectors are set to give the best detection performance. The GC was calibrated weekly to ensure its best performance. The calibration standards were prepared by mixing certain amounts of standard gases in a known volume of a calibration gas bottle.

3.4.3 Procedures of the Kinetic Experiments

3.4.3.1 Procedures

The kinetic experiments were run following a differential reactor model (Levenspiel 1999). To satisfy the conditions of differential reactors, the conversion of propylene was kept below 10%. The low conversion was achieved by using a small amount of the catalysts and a relatively high total flow rate (120 mLmin^{-1}). The catalysts were sieved to a particle size fraction of 45 to 63 μm.

All kinetic experiments on a given catalyst were performed on the same catalyst bed with periodic checks to determine if any deactivation of the catalyst had

occurred. If the catalyst exhibits degradation in their activity, heating the catalyst at 400°C for two hours in oxygen-helium mixture (15% O_2 in 85% He) will regenerate them. Prior to the kinetic experiments, the catalysts were pre-aged by passing through the reactant gas comprising of 5% C_3H_6, 10% O_2 and 85% He at 400°C for six hours or until the catalyst activity became steady.

3.4.3.2 Data Analyses

The data from the kinetic experiments was analysed using the power rate law according to equation 3.1 and 3.2. The model is used because it can give very close approximation of the kinetic parameters such as reaction order, activation energy, and reaction rate constants. Using the differential reactor system, such parameters are obtained straightaway from the experiments.

$$C_3H_6 + O_2 \rightarrow C_3H_4O + H_2O \qquad \text{R.2}$$

$$r = k[C_3H_6]^n[O_2]^m \qquad 3.1$$

$$k = Ae^{-\frac{Ea}{RT}} \qquad 3.2$$

In order to get all apparent kinetic parameters (the reaction rate ***r***, rate constant ***k***, reaction order ***n*** and ***m***, activation energy E_a, and frequency factor ***A***), experiments were carried out with varying reaction temperature and reactant concentration. The temperature range was between 300°C and 450°C with a 30°C interval.

The reaction order of acrolein formation was determined at constant initial concentration (Leonard David Krenzke 1977). In this method, the concentration of one reactant was kept constant while the other varied. The reaction rate as the function of one reactant was then measured and a graphical plot between concentration and reaction rate was drawn. The reaction order was calculated from the plot of *log(**r**)* versus *log(concentration of the reactant varied)*, where, for a bimolecular reaction, has a linear relationship as shown by equation 3.3. For a simple

concentration dependency, the slope will be equal to the reaction order in the reactant and the intercept equal to *log(k)*. The reactant concentrations were varied according to Table 3.2.

$$log(\mathbf{r}) = log(k) + n\ log[C_3H_6] + m\ log[O_2] \qquad 3.3$$

where:

[ ] = concentration of a given reactant

n = reaction order in propylene

m = reaction order in oxygen

Data resulting from these experiments were used to calculate the rate constants, which were subsequently incorporated into an Arrhenius plot to determine the apparent activation energy for acrolein formation.

Table 3.9 Reactant concentrations (%vol at NTP) used in the experiments for determination of reaction orders)

He	**C_3H_6**	**O_2**	**Molar Ratio of C_3H_6 to O_2**
90.00%	5.00%	5.00%	1.0:1.0
88.33%	5.00%	6.67%	1.0:1.3
86.67%	5.00%	8.33%	1.0:1.6
85.00%	5.00%	10.00%	1.0:2.0
80.00%	5.00%	15.00%	1.0:3.0
86.67%	3.33%	10.00%	1.0:3.0
85.00%	5.00%	10.00%	1.5:3.0
83.33%	6.67%	10.00%	2.0:3.0
81.67%	8.33%	10.00%	2.5:3.0
80 %	10.00%	10.00%	3.0:3.0

3.5 Reaction Mechanisms

Two methods were employed to determine the reaction mechanisms of partial oxidation of propylene to acrolein on bismuth molybdate catalysts. The first method is by testing several reaction mechanisms that had been developed by other researchers and fitting them with the present experimental data. The second method was derived from theoretical models based on the results of in-situ characterisation work of the catalysts.

There are four models that have normally been used by different researchers to describe the reaction mechanisms of partial oxidation of propylene to acrolein. The first is the Langmuir-Hinshelwood model, which assumes that the rate-controlling step is the surface reaction between the adsorbed form of propylene and oxygen.

When the adsorption of propylene does not compete with oxygen adsorption, the model is described by equation 3.4. However, if there is a competition for site adsorption between propylene and oxygen, the model is given by equation 3.5.

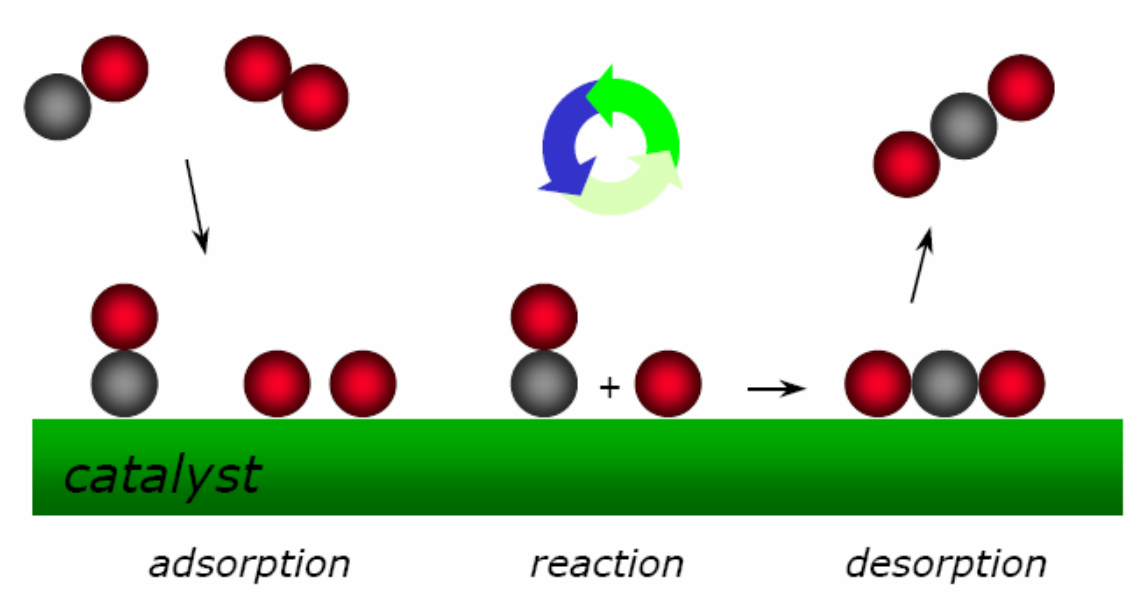

Figure 3.6 A scheme of the Langmuir-Hinshelwood mechanism (Chorkendorf & Niemantsverdriet 2003)

$$r_a = \frac{kK_h P_h (K_O P_O)^n}{\left[1 + K_h P_h + (K_O P_O)^n + K_w P_w\right]^2} \qquad 3.4$$

$$r_a = \frac{kK_h P_h (K_O P_O)^n}{\left[1 + K_h P_h\right]\left[1 + (K_O P_O)^n\right]} \qquad 3.5$$

The second model follows the Eley-Rideal theory, which assumes that only one reactant is adsorbed on the catalyst surface which then reacts with other reactants in the gas phase. The theory acknowledges that the rate-determining step is the reaction between the adsorbed reactant (propylene) and gas phase oxygen. The mechanism leads to equation 3.6.

$$r_a = \frac{kK_h P_h P_O}{1 + K_h P_h + (K_O P_O)^n} \qquad 3.6$$

The third model uses the redox mechanism developed by Mars and van Krevelen (Mars & van Krevelen 1954). In this model, the hydrocarbon is oxidised on the catalyst surface and the reduced form of the catalyst surface is re-oxidised by gas phase oxygen, though not necessarily occurring on the same site as the reduced site. The equation of this model is described in equation 3.7

$$r_a = \frac{k_r P_h^x k_{ox} P_O^y}{k_r P_h^x + k_{ox} P_O^y} \qquad 3.7$$

The final model is the stationary state of adsorption model (Jaswal et al. 1969), which is similar to the redox model. In this model, oxygen for propylene oxidation is from the gas phase rather than from the lattice of the catalyst as the redox model assumes. The rate equation of the model is represented by equation 3.8.

$$r_a = \frac{kP_h k_{ads} P_O^n}{akP_h + k_{ads} P_O^n} \qquad 3.8$$

For all equations, n is ½ or 1, depends on the dissociation of oxygen on the surface. n = 1 indicates that oxygen adsorption is non-dissociative, while n=½ indicates that oxygen is dissociated upon adsorption.

Chapter 4

THE BISMUTH MOLYBDATES CHARACTERISTICS

In this chapter, the experimental results of physical and chemical characterisations are used together to describe the importance of bulk crystalline structure of bismuth molybdate catalysts for propylene to acrolein partial oxidation. There are two major sections in this chapter, first is chemical and physical nature of the catalyst, characterised by several methods such as surface area, chemical composition, and morphology of the catalyst. The second section discusses the results of structural dynamics of the catalysts under real reaction condition, which are mainly come from neutron diffraction work. The structural dynamic study is aimed to look in depth particularly on the dynamics of oxygen ions in the lattice and their role in catalysing partial oxidation of propylene to acrolein.

4.1 Chemical composition of Bismuth Molybdates

The chemical composition of catalysts plays very important role in the catalysts activity, especially in bismuth molybdate. It has been mentioned in the earlier chapters that active bismuth molybdates are those whose chemical composition are within bismuth to molybdenum ratio of 2:1 to 2:3. Beside that reason, the object of this thesis is alpha, beta, and gamma phase of bismuth molybdates, not any other phases. This is the reason why the catalysts composition should be known exactly of their chemical composition.

All catalysts were prepared by coprecipitation method without any washing or filtering procedure. The preparation method assured that the chemical composition of the final catalysts was exactly the same as the composition of the mother liquor composition, i.e. the composition of the liquid mixture in the catalysts preparation.

Chemical analysis results of the catalysts, which were taken by x-ray spectroscopic method using EDS detector running in electron microscope analysis on polished surface of the catalysts, is shown in Table 4.1.

Table 4.1 EDS chemical composition of the catalysts

Catalysts	Bi/Mo molar ratio
α-$Bi_2Mo_3O_{12}$	0.7
β-$Bi_2Mo_2O_9$	0.94
γ-Bi_2MoO_6	1.87

4.2 The Morphology of Bismuth Molybdates

Results of surface area and the pore size distribution analyses of alpha, beta and gamma bismuth molybdate by BET N_2 adsorption method are tabulated in Table 4.2. The surface areas were used to calculate the specific activities and specific rate constant in Chapter Five. The measurement details are given in Appendix C.

Table 4.2 Surface area, Pore volume and Pore size of bismuth molybdates

Catalysts	Specific Area ($m^2.g^{-1}$)	Pore Volume ($cm^3.g^{-1}$)	Average Pore Radius (Å)
α-$Bi_2Mo_3O_{12}$	3.20	3.69×10^{-3}	23.08
β-$Bi_2Mo_2O_9$	4.66	1.76×10^{3}	15.58
γ-Bi_2MoO_6	3.74	4.50×10^{-3}	21.67

The surface area of the beta phase is surprisingly higher than the other bismuth molybdates although its pore volume and distribution are within acceptable

value. Since the beta phase was prepared with higher temperature than the other two, the catalyst should be denser than alpha and gamma phase. Electron microscope images (Figure 4.1), taken by Philips XL-500 SEM using Secondary Electron (SE) detector, show clearly that the β-$Bi_2Mo_2O_9$ is the densest and the less porous catalyst.

The SEM images also show that all bismuth molybdate catalysts are built of microcrystalline. The α-$Bi_2Mo_3O_{12}$ is built of uniform microcrystalline at the size about 0.8 μm. The microcrystalline size of β-$Bi_2Mo_2O_9$ is about ten times larger than the alpha phase and form dense agglomerate. Smaller microcrystalline was clearly shown on the gamma phase than the other catalyst. SEM image of gamma phase also shows sponge like cluster and plate like microcrystalline. The later is consistent with the layer structure of γ-Bi_2MoO_6 unit cell.

The isotherm N_2 BET adsorptions of the catalysts give more information on the pore characteristics of the catalyst. All catalysts follow type IV isotherm adsorption, which means that the pore type of the catalysts is mesoporous as mentioned by Lecloux (Lecloux 1981). Lecloux also mentioned that the isotherm of type IV always have hysteresis loop of the BET isotherm adsorption and desorption curve. The isotherms of the alpha and gamma bismuth molybdate are associated with hysteresis loop type A or C and means that the catalysts have cylindrical (type A) or cone (type C) pore-shapes. The isotherm of beta phase, on the other hand, more likely has type E of hysteresis loops where the pore-shape is correspond to cavities or voids between close-packed spherical-likes particles.

All the pore morphology found from BET adsorption experiments is consistent with the electron microscope images of the catalysts. The images show that the cylindrical and cone pore-shape are only available on alpha and gamma phase, and no pores of such kind were found on the beta phase. The morphology of the catalysts, based on the electron microscopy and surface area analysis, are comparable to those used by previous researcher on pure bismuth molybdate form (Keulks et al. 1974; Leonard David Krenzke 1977; L. David Krenzke & Keulks 1980ab; Monnier & Keulks 1981).

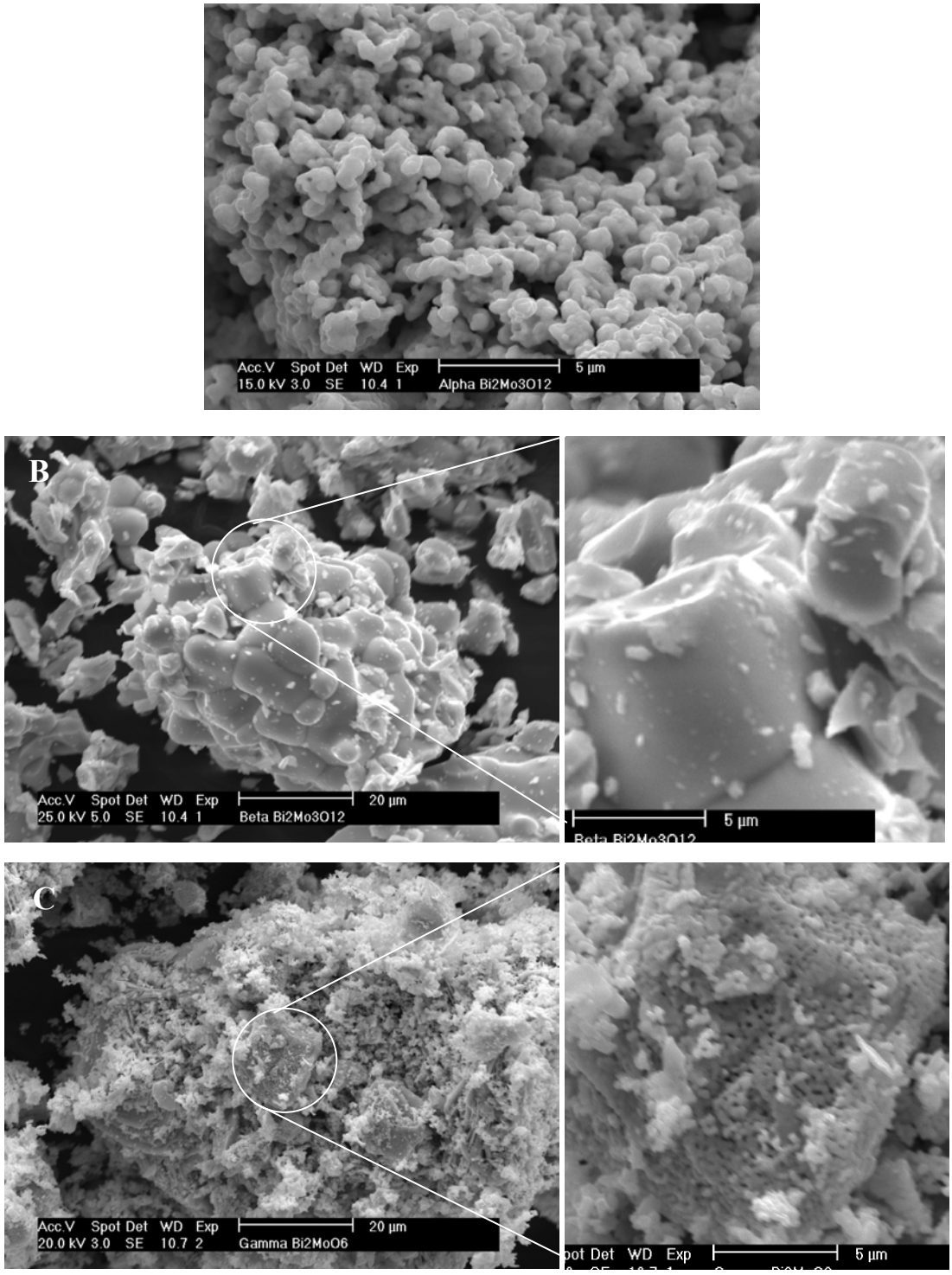

Figure 4.1 SEM images of bismuth molybdate catalysts: A) α-$Bi_2Mo_3O_{12}$, (B) β-$Bi_2Mo_2O_9$ and C) γ-Bi_2MoO_6

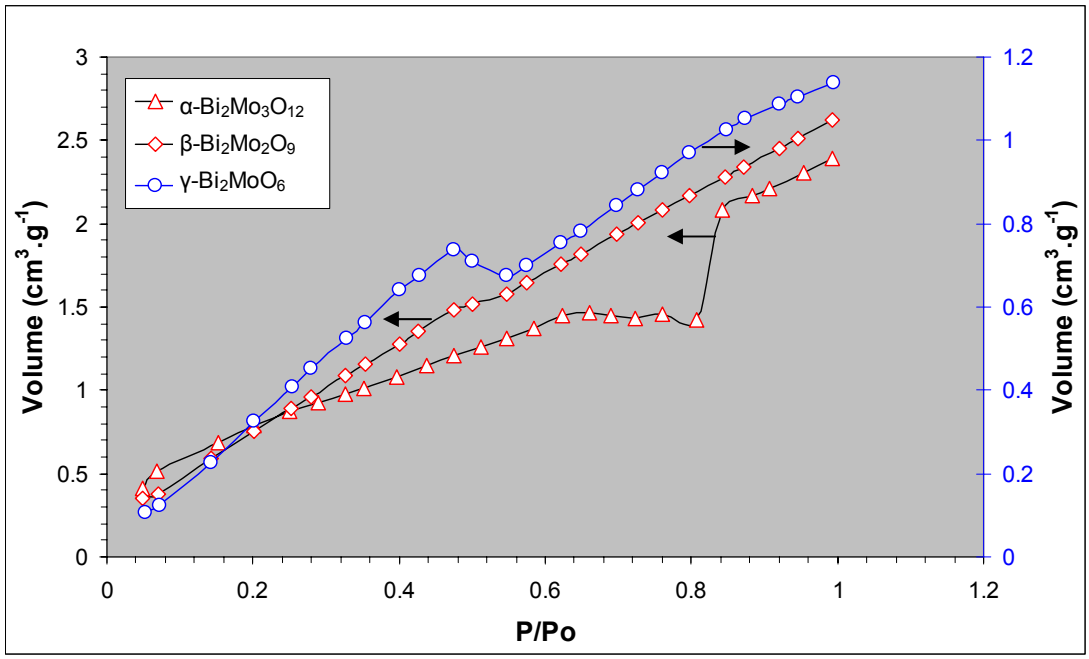

Figure 4.2 BET isotherm adsorption of N_2 on the catalysts

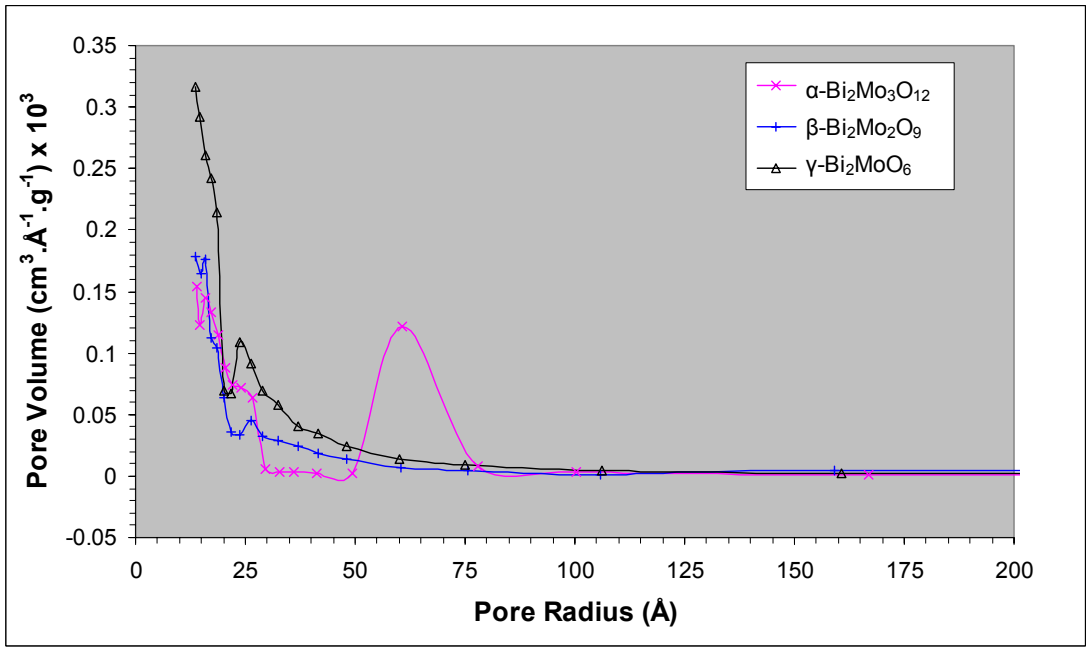

Figure 4.3 BJH Pore size distributions of the catalysts.

4.3 The Room Temperature Crystal Structure of Bismuth Molybdates

Two diffraction methods were employed to study the bulk crystal structure of bismuth molybdate catalysts, namely X-ray and Neutron diffraction. The choice of the methods is to gain more contrast on the atomic coordinate in the crystal lattice. The neutron diffraction would be able to give more accurate coordinate of oxygen than the X-ray. Neutron diffraction patterns are easier to model than X-ray and, as a result, it is easier to refine the crystal structure from neutron pattern. However, neutron beams are normally less intense. The low intensity of neutron beam makes it not sensitive to the existence of contaminant phase (or phases).

Phase analyses on the x-ray diffractograms of bismuth molybdates were taken over by using JADE™ software. No other phase was found on the alpha and beta phase. On the other hand, the gamma phase contain small amount of beta bismuth molybdate. The phase analyses explain effect of chemical composition to the phase formation.

Diffractograms of both X-ray and Neutron were refined by Rietveld method using RIETICA software. All room temperature neutron diffractions were taken with High Resolution Powder Difractometer (HRPD) of neutron diffraction instrument. In performing the refinements, several assumptions were taken into account. First, the 2θ offset ($2\theta_o$) of the X-ray instrument is assumed to be the same as those reported by O'Connor and Pratapa (O'Connor & Pratapa 2002). Second, there was no 2θ offset of neutron diffraction instrument and the wavelength of neutron had carefully calibrated. With those assumptions, no refinement were taken on the $2\theta_o$ and wavelengths of both X-ray and neutron diffraction.

The Rietveld refinement results of unit cell parameters of the room temperature X-ray and HRPD pattern are tabulated in Table 4.3. The result shows that all catalysts prepared in this work are slightly larger than the model reference (ICSD collection number 2650 for α-$Bi_2Mo_3O_{12}$, 201742 for β-$Bi_2Mo_2O_9$, and 47139 for γ-Bi_2MoO_6).

The fitting parameters (Table 4.4) of the refined patterns of neutron diffractogram to the model being used in refinement were within the range where the refinements assumed to be reach their adequate values, i.e. the GOF (Goodness of Fit) values are between 1 and 2.9 (according to Young (Robert Alan Young 1993)). In contrast, only X-ray pattern of the α-$Bi_2Mo_3O_{12}$ which has satisfactory GOF value while the others have high GOF value. Visual identification has also been used to considering the adequacy of fitting as shown in Figure 4.4 and 4.5. The data points (observed patterns) are represented by "+" sign, the model (calculated pattern) by a continues-red line, and the difference between data model are drawn on the bottom of the pattern as a light blue line.

Table 4.3 Refined unit cell parameters of bismuth molybdates of room temperature X-ray and Neutron (HRPD) diffractograms.

Parameters	α-$Bi_2Mo_3O_{12}$		β-$Bi_2Mo_2O_9$		γ-Bi_2MoO_6	
	X-ray	Neutron	X-ray	Neutron	X-ray	Neutron
Volume ($Å^3$)	962.47(2)	963.17(13)	1534.05(9)	1538.27(5)	489.41(3)	490.84(2)
a (Å)	7.714(0)	7.716(1)	11.954(0)	11.965(0)	5.484(0)	5.489(0)
b (Å)	11.527(0)	11.527(1)	10.799(0)	10.810 (0)	16.209(0)	16.225(0)
c (Å)	11.976 (0)	11.977(1)	11.883(0)	11.893 (0)	5.506(0)	5.511(0)
α (^{o})	90.000	90.000	90.000	90.000	90.000	90.000
β (^{o})	115.281(2)	115.276(4)	90.143(3)	90.139(2)	90.000	90.000
γ (^{o})	90.000	90.000	90.000	90.000	90.000	90.000

Table 4.4 Fitting parameters of Riteveld refinement of room temperature X-ray and Neutron diffraction.

Parameters	α-$Bi_2Mo_3O_{12}$		β-$Bi_2Mo_2O_9$		γ-Bi_2MoO_6	
	X-ray	Neutron	X-ray	Neutron	X-ray	Neutron
GOF	2.79	1.30	9.92	1.62	9.02	2.00
R_p	6.79	5.34	15.19	4.63	10.59	5.84
R_{wp}	9.13	6.31	19.9	5.65	16.29	7.44
R_{exp}	5.47	5.53	6.32	4.44	5.42	5.25
R_{Bragg}	2.56	1.28	12.45	1.59	4.94	1.87

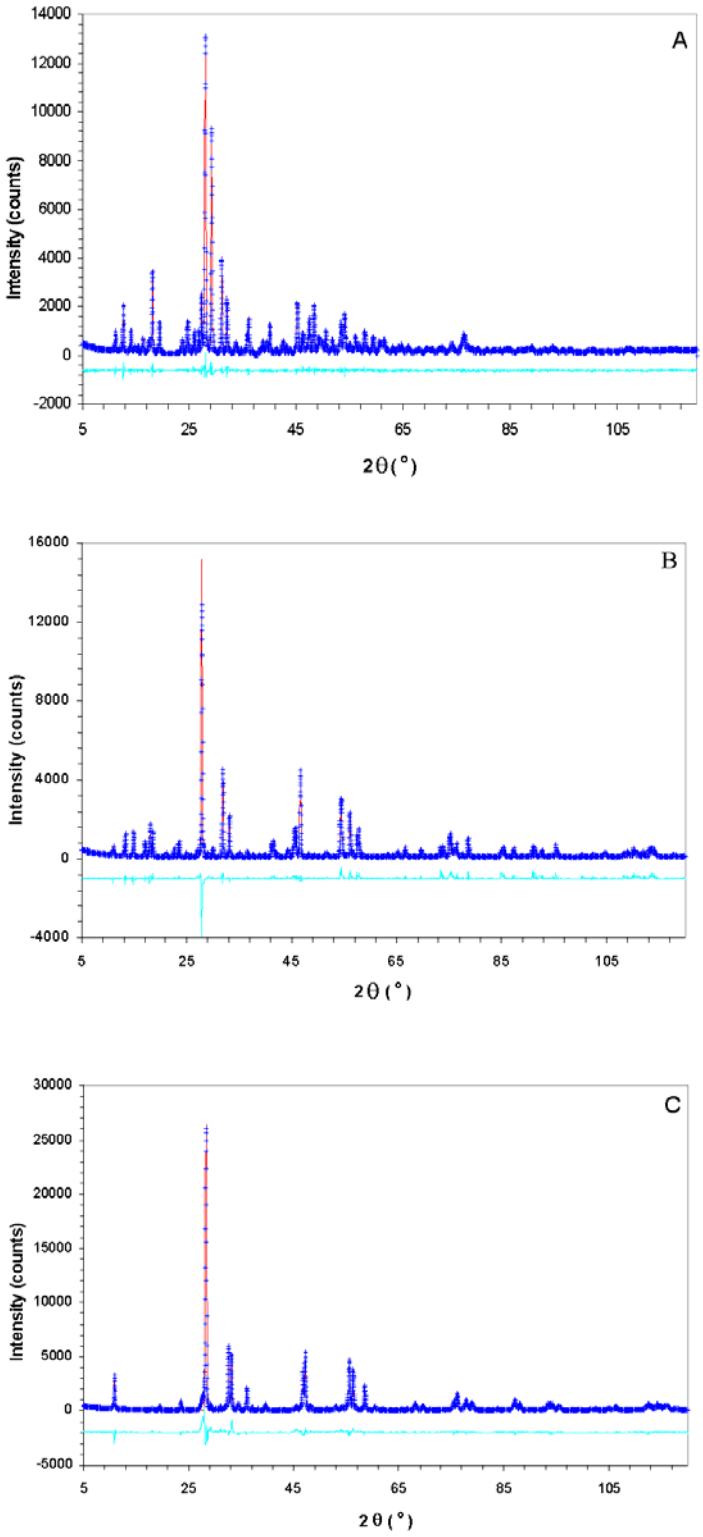

Figure 4.4 Graphical representation of the refinement results of room temperature X-ray diffractograms. (A) α-$Bi_2Mo_3O_{12}$; (B) β-$Bi_2Mo_2O_9$; and (C) γ-Bi_2MoO_6.

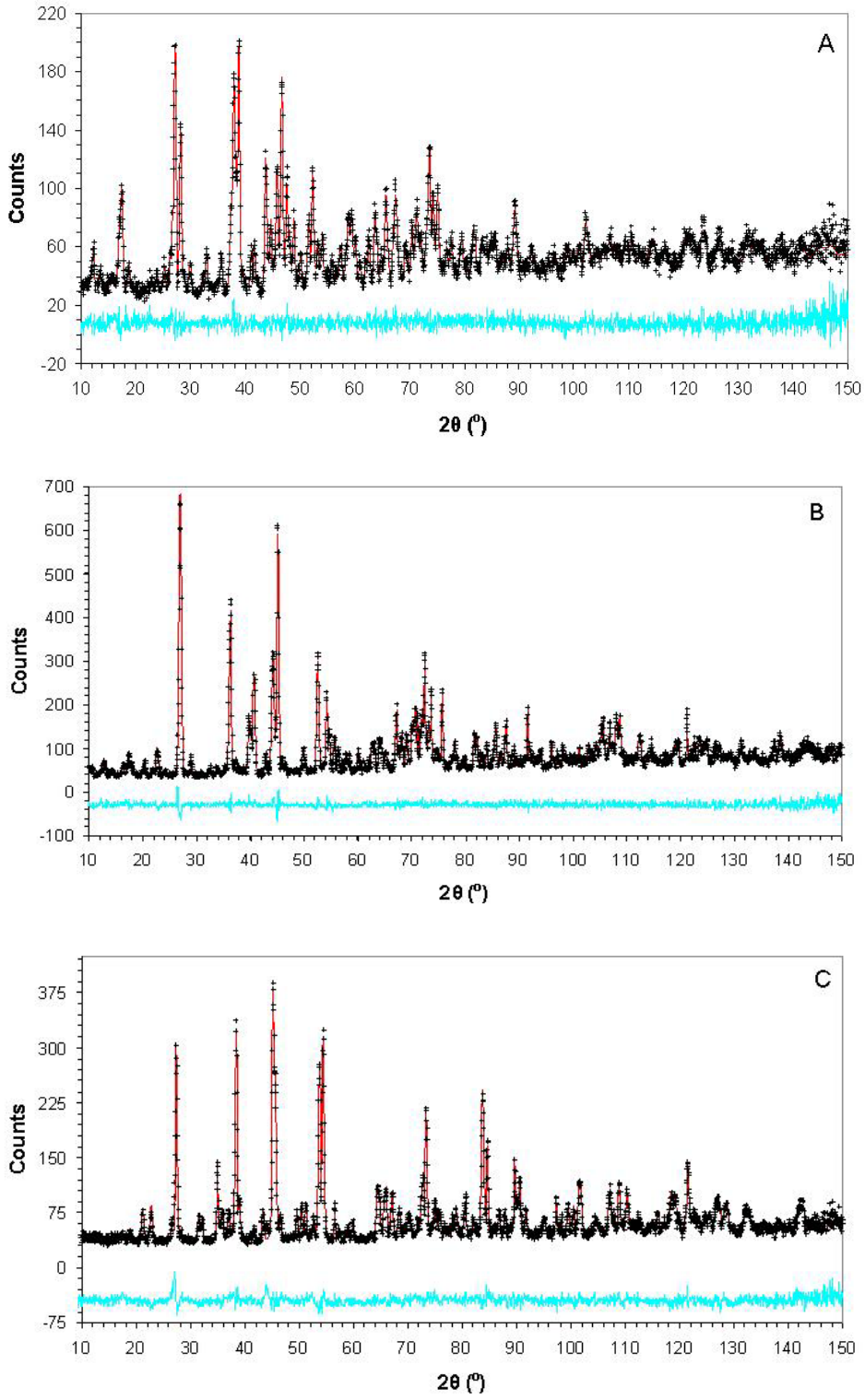

Figure 4.5 Graphical representation of the refinement results of room temperature HRPD diffractograms. (A) α-$Bi_2Mo_3O_{12}$, (B) β-$Bi_2Mo_2O_9$ and (C) γ-Bi_2MoO_6.

4.3.1 Unit cell structure of α-$Bi_2Mo_3O_{12}$

Unit cell structure of the alpha phase of bismuth molybdate prepared in this report is very close to the structure of bismuth molybdate reported by van den Elzen and Rieck (van den Elzen & Rieck 1973a). The volume of unit cell structure, though, is slightly larger than their model as shown in Table 4.5.

Table 4.5 Data for Neutron and X-ray diffraction study of α-$Bi_2Mo_3O_{12}$

Formula weight	897.78			
Crystal system	Monoclinic			
Space group	P 1 2_1/c 1			
Unit Cell	Neutron	X-ray	ICSD 2650	ICSD 63640
a (Å)	7.716(1)	7.7138(2)	7.685(6)	7.7104(3)
b (Å)	11.527(1)	11.5270(3)	11.491(16)	11.5313(4)
c (Å)	11.977(1)	11.9763(3)	11.929(10)	11.9720(5)
β (^{o})	115.276(4)	115.281(2)	115.400(0)	115.276(3)
Volume (Å^3)	963.17(15)	962.89(4)	961.94(5)	962.52(5)
Z	4			
Calculated density (g cm^{-3})	6.186	6.190		

The slight difference of the prepared structure with the van den Elzen model is believed caused by different preparation method. The structure of van den Elzen model was derived from the single crystalline form of alpha bismuth molybdate. Crystallisation of alpha phase has to be carried out at hight temperature, i.e. at its melting point (670^{o}C). In contrast, the powder form in this report was prepared at low temperature (480^{o}C). As a result, the powder structure is more relaxed than the single crystalline one and shown by larger unit cell volume. Atomic coordinates and interatomic distances of α-$Bi_2Mo_3O_{12}$ of its neutron diffractogram refinements are given in Table 4.6 and 4.7, respectively. . The estimated standard deviation (e.s.d) of the last digit of each value is given in parenthesis.

The unit cell structure of the alpha phase prepared in this report was also compared to a powder form of α-$Bi_2Mo_3O_{12}$ reported by Theobald and Laarief (Theobald, Laarif & Hewat 1985). Their structure was determined from powder form of alpha bismuth molybdate which was prepared at 550^{o}C. The model *a, b, c, β*, and unit cell volume are 7.710 Å, 11.531 Å, 11.972 Å, 115.300^o, and 962.50 Å^3, respectively. These values are closer to our structure although they are still slightly smaller.

More relaxed structure, which is a result of lower preparation temperature, is desirable in catalytic reaction. Lower preparation temperature will produce finer catalyst particle and higher surface area. These two parameters contribute to the catalysts activity since the catalytic reactions normally occur on the catalyst surface. In fact, the surface area analysis result of the alpha phase is higher than those in either van den Elzen and Rieck or Theobald and Laarief models.

All polyhedra in the α-$Bi_2Mo_3O_{12}$ are distorted. The oxygen coordination around the two bismuth ions is very similar. The bismuth ions are surrounded by eight oxygen ions with three different groups of bond length. The first group has Bi-O distance around 2.1Å and 2.4Å. The second group has Bi-O distance around 2.6 Å and 2.75 Å, while the third has around 2.9 Å in Bi-O distance. On the other hand, the oxygen coordination around the three molybdenum ion species in the α-$Bi_2Mo_2O_{12}$ are different. As mentioned by van den Elzen and Rieck (van den Elzen & Rieck 1973a), the Mo(1) is surrounded by six oxygen ion while Mo(2) and Mo(3) are clustered together and surrounded by ten oxygen ions. Again, the Mo-polyhedra are distorted as in bismuth polyhedra.

4.3.2 Unit cell structure of β-$Bi_2Mo_2O_9$

The crystal structure the β-$Bi_2Mo_2O_9$ has the same basic structure with the alpha phase, i.e. they were derived from the structure of a mineral called calcite ($CaWO_3$) (D. J. Buttrey, Jefferson & Thomas 1986). The structure of β-$Bi_2Mo_2O_9$ prepared for this thesis resembles very close to the only complete model by Chen and Sleight (Horng-Yih Chen & Sleight 1986). Unit cell parameters and atomic coordinate and thermal parameters are given in Table 4.9 and Table 4.10, respectively. The refined unit cell parameters of HRPD were closer to the model of

Chen and Sleight, while the one of X-ray refinement resembles closer to the structure reported by Antonio at al (Antonio et al. 1988).

Table 4.6 Atomic coordinates of α-$Bi_2Mo_3O_{12}$

Ions	x	y	z	B
Bi(1)	0.2588(13)	0.3623(7)	0.2573(7)	0.84(16)
Bi(2)	0.9802(13)	0.1303(7)	0.0829(8)	0.50(12)
Mo(1)	0.0287(16)	0.1106(8)	0.4162(10)	1.25(18)
Mo(2)	0.4202(16)	0.1511(8)	0.1059(9)	0.70(17)
Mo(3)	0.7332(15)	0.3651(10)	0.1959(9)	1.19(18)
O(1)	0.5404(18)	0.0499(11)	0.2200(11)	1.05(22)
O(2)	0.9327(17)	0.0540(11)	0.2546(10)	0.77(21)
O(3)	0.2196(16)	0.1938(11)	0.1542(9)	0.90(22)
O(4)	0.8598(20)	0.2091(10)	0.4119(12)	1.42(23)
O(5)	0.2214(17)	0.2007(11)	0.4365(9)	0.72(20)
O(6)	0.6201(20)	0.2043(11)	0.0675(12)	1.23(22)
O(7)	0.9552(15)	0.2933(10)	0.1997(10)	0.42(18)
O(8)	0.5046(17)	0.3146(10)	0.1954(10)	0.66(22)
O(9)	0.2869(17)	0.4355(11)	0.4792(11)	0.81(19)
O(10)	0.1258(19)	0.4482(10)	0.0763(11)	1.05(22)
O(11)	0.8377(16)	0.4412(10)	0.3385(10)	0.68(19)
O(12)	0.6933(18)	0.4681(11)	0.0850(13)	1.31(26)

There was not much different found in the atomic coordinate of the prepared β-$Bi_2Mo_2O_9$, compared to the model of Chen and Sleight. The atomic coordinate and thermal parameters are given in Table 4.10. The oxygen coordination around metal ions (Bi and Mo) of refined atomic coordinates from neutron pattern is given in Table 4.11. As in the α-$Bi_2Mo_3O_{12}$, all the bismuth ions are surrounded by eight oxygen ions. The distorted polyhedra were also found in β-$Bi_2Mo_2O_9$ although it is not as severe as those in the alpha phase. There were also three different group of Bi-O bond length. The first bond has the Bi-O bond length of 2.2Å to 2.4Å, the second

has bond length between 2.5Å and 2.7Å while the last group of Bi-O bond distance is around 2.8Å.

Table 4.7 Interatomic distances of α-$Bi_2Mo_3O_{12}$ (in Å).

Atom 1	Atom 2	This work	van den Elzen (van den Elzen & Rieck 1973a)	Theobald (Theobald, Laarif & Hewat 1985)
Bi(1)	O(10)	2.20	2.12	2.22
	O(3)	2.25	2.22	2.23
	O(7)	2.28	2.32	2.31
	O(8)	2.38	2.34	2.41
	O(1)	2.61	2.61	2.63
	O(2)	2.63	2.64	2.62
	O(9)	2.71	2.75	2.71
	O(5)	2.95	2.94	2.95
Mean M(8)		2.50	2.49	2.51
Bi(2)	O(2)	2.17	2.16	2.17
	O(7)	2.28	2.24	2.19
	O(3)	2.30	2.32	2.30
	O(6)	2.31	2.33	2.33
	O(9)	2.63	2.61	2.59
	O(4)	2.67	2.68	2.67
	O(11)	2.81	2.78	2.81
	O(11)	2.86	2.85	2.91
Mean M(8)		2.50	2.50	2.49
Mo(1)	O(4)	1.71	1.69	1.72
	O(5)	1.74	1.72	1.79
	O(2)	1.87	1.85	1.86
	O(10)	1.86	1.91	1.90
	O(10)	2.24	2.25	2.25
	O(12)	2.71	2.69	2.80
Mean M(6)		2.02	2.02	2.05
Mo(2)	O(1)	1.73	1.72	1.72
	O(9)	1.74	1.74	1.75
	O(6)	1.89	1.86	1.78
	O(3)	1.93	1.89	2.05
	O(8)	2.12	2.13	2.18
Mean M(5)		1.88	1.87	1.90
Mo(3)	O(12)	1.71	1.68	1.65
	O(11)	1.78	1.78	1.80
	O(8)	1.85	1.85	1.87
	O(7)	1.89	1.87	1.91
	O(6)	2.32	2.30	2.45
Mean M(5)		1.91	1.90	1.93

Table 4.8 Data for Neutron and X-ray diffraction study of β-$Bi_2Mo_2O_9$

Formula weight	753.83			
Crystal system	Monoclinic			
Space group	P 1 2_1 / n_1 (No. 13)			
Unit Cell	Neutron	X-ray	ICSD 201742	Antonio et al
a (Å)	11.965(0)	11.9542(5)	11.972(3)	11.9515(4)
b (Å)	10.810(0)	10.7995(3)	10.813(4)	10.7993(4)
c (Å)	11.893(0)	11.8828(4)	11.899(2)	11.8805(4)
β (^{o})	90.14 (0)	90.14(0)	90.1(0)	90.142(5)
Volume (Å^3)	1538.27(5)	1534.05(9)	1540.4	1533.38(6)
Z	8			
Calculated density (g cm^{-3})	6.51	6.53	6.50	N/A

Although the structure of beta and alpha phase of bismuth molybdate was derived from fluorite, the oxygen coordination around molybdenum ions is different. All the molybdenum ions in β-$Bi_2Mo_2O_9$ are four coordinated by oxygen and forming tetrahedral of molybdenum oxides. The polyhedra are more regular than those in the alpha phase, which is shown by uniform Mo-O bond distance as shown in Table 4.11. The regularity of Mo-O bond distances support the structure of Chen and Sleight (Horng-Yih Chen & Sleight 1986), and later, supported by Antonio et al (Antonio et al. 1988), rather than those outlined by van den Elzen and Rieck (van den Elzen & Rieck 1975) who mentioned that the Mo-O coordination is strongly distorted.

Table 4.9 Atomic coordinates of β-$Bi_2Mo_2O_9$

Ions	x	y	z	B
Bi(1)	0.1010(10)	0.1233(16)	0.7564(10)	1.10(22)
Bi(2)	0.6009(9)	0.1250(14)	0.7595(8)	0.37(18)
Bi(3)	0.2531(12)	0.1203(13)	0.7575(8)	0.62(9)
Bi(4)	0.2556(10)	0.1244(10)	0.4134(7)	0.60(11)
Mo(1)	-0.0838(11)	0.1243(14)	0.0893(12)	0.45(20)
Mo(2)	-0.0773(11)	0.1266(15)	0.4163(13)	0.65(21)
Mo(3)	0.5867(12)	0.1245(15)	0.0813(13)	1.03(24)
Mo(4)	0.5805(13)	0.1281(16)	0.4153(13)	0.87(22)
O(1)	0.2553(13)	0.2634(14)	0.2853(11)	0.99(23)
O(2)	0.2552(13)	0.4944(14)	0.2266(10)	0.54(20)
O(3)	0.4099(12)	0.2568(16)	0.6916(12)	0.93(29)
O(4)	0.3196(12)	0.2572(19)	0.9028(15)	1.26(28)
O(5)	0.1102(13)	0.4416(17)	0.4457(14)	1.25(26)
O(6)	0.1014(13)	0.2452(15)	0.8198(12)	0.75(24)
O(7)	0.4029(12)	0.4433(15)	0.0519(12)	0.63(25)
O(8)	0.0934(14)	0.4941(17)	0.6837(12)	0.66(25)
O(9)	0.1941(11)	0.2558(17)	0.5954(13)	0.90(26)
O(10)	0.0988(13)	0.3192(15)	0.0550(13)	0.88(28)
O(11)	0.4098(11)	0.3066(15)	0.4538(12)	0.49(25)
O(12)	0.0579(12)	0.1879(15)	0.3868(13)	0.79(23)
O(13)	0.0428(13)	0.0453(16)	0.1119(13)	1.13(26)
O(14)	0.4461(12)	0.0630(16)	0.3829(13)	0.68(22)
O(15)	0.4011(15)	0.4960(17)	0.8139(13)	1.07(28)
O(16)	0.9611(15)	0.2950(18)	0.5957(14)	1.91(32)
O(17)	0.1780(11)	0.4850(15)	0.9019(14)	0.66(24)
O(18)	0.1915(14)	0.9835(18)	0.8995(15)	1.51(33)

Table 4.10 Interatomic distances of β-$Bi_2Mo_2O_9$ (in Å).

		This work	H. Y. Chen (Horng-Yih Chen & Sleight 1986)
Bi(1)	O(2)	2.20	2.15
	O(1)	2.14	2.21
	O(11)	2.47	2.47
	O(13)	2.50	2.48
	O(7)	2.54	2.58
	O(16)	2.77	2.79
	O(6)	2.86	2.87
	O(15)	2.88	2.92
Mean M(8)		2.55	2.56
Bi(2)	O(1)	2.23	2.20
	O(2)	2.26	2.24
	O(5)	2.33	2.34
	O(10)	2.51	2.58
	O(12)	2.58	2.64
	O(14)	2.70	2.71
	O(8)	2.80	2.81
	O(3)	2.81	2.86
Mean M(8)		2.53	2.55
Bi(3)	O(8)	2.39	2.38
	O(18)	2.36	2.39
	O(4)	2.41	2.40
	O(6)	2.38	2.41
	O(3)	2.51	2.48
	O(15)	2.43	2.50
	O(9)	2.52	2.54
	O(17)	2.53	2.56
Mean M(8)		2.44	2.46
Bi(4)	O(1)	2.14	2.13
	O(2)	2.18	2.17
	O(14)	2.40	2.43
	O(12)	2.31	2.48
	O(9)	2.70	2.74
	O(11)	2.74	2.74
	O(7)	2.76	2.75
	O(17)	2.78	2.75
Mean M(8)		2.50	2.52
Mo(1)	O(13)	1.76	1.76
	O(11)	1.77	1.76
	O(3)	1.77	1.77
	O(18)	1.74	1.78
Mean M(4)		1.76	1.77

Table 4.10 continued

		This work	H. Y. Chen (Horng-Yih Chen & Sleight 1986)
Mo(2)	O(4)	1.77	1.71
	O(7)	1.80	1.75
	O(15)	1.82	1.75
	O(12)	1.78	1.77
Mean M(4)		1.79	1.75
Mo(3)	O(16)	1.75	1.73
	O(5)	1.79	1.75
	O(9)	1.83	1.76
	O(8)	1.77	1.80
Mean M(4)		1.79	1.76
Mo(4)	O(10)	1.77	1.72
	O(17)	1.70	1.76
	O(6)	1.80	1.77
	O(14)	1.80	1.77
Mean M(4)		1.77	1.75

4.3.3 Unit cell structure of γ-Bi_2MoO_6

The structure of γ-Bi_2MoO_6 prepared in this project was compared to the model structure of Teller et al (Teller, Brazdil & Grasselli 1984) (ICSD 47139) and Theobald and Laarief (Theobald, Laarif & Hewat 1984) (ICSD 201685). Both model were determined by neutron diffraction from a powder form of synthetic γ-Bi_2MoO_6. Earlier model by van den Elzen and Rieck (van den Elzen & Rieck 1973b) was not used because it had been proven that the model containing very short distance between two unbounded oxygen ions. Unit cell parameters of prepared γ-Bi_2MoO_6 refined by x-ray diffraction were close to the ICSD 47139 while those refined from neutron diffraction was close to ICSD 201685.

The structure of prepared γ-Bi_2MoO_6 was consistence with the structure of both Teller et al and Theobald and Laarief model. Not many differences were noticeable from the refinement result of the prepared γ-Bi_2MoO_6 as given in Table 4.14.

4.3.4 Coordination around metal ions in bismuth molybdates

The coordination around atoms was calculated from the sum of the so-called "bond-strengths" (*s*) calculated by Brown and Wu (Brown & Wu 1957) method. Mathematical equation of the method is given in equation 4.1, where *R* is the interatomic distance; R_1 and N are empirical constants. Values of R_1 and *N* are available in the reference (Brown & Wu 1957). The sum of the bond strengths is the valence charge *S* or also known as total bond order. Table 4.15 to 4.17 show the valence charge of bismuth and molybdenum in α-$Bi_2Mo_3O_{12}$, β-$Bi_2Mo_2O_9$, and γ-Bi_2MoO_6, from this work and some references.

$$s = \left[\frac{R}{R_1}\right]^N \qquad 4.1$$

Table 4.11 Data for Neutron and X-ray diffraction study of γ-Bi_2MoO_6

Formula weight	753.83			
Crystal system	Orthorhombic			
Space group	P c a 2_1 (No. 29)			
Unit Cell	Neutron	X-ray	ICSD 47139	ICSD 201685
a (Å)	5.489(0)	5.484(0)	5.482(0)	5.490(0)
b (Å)	16.225(0)	16.209(0)	16.199(1)	16.227(1)
c (Å)	5.511(0)	5.506(0)	5.509	5.513(0)
Volume ($Å^3$)	490.84(2)	489.41(2)	489.23(3)	491.1
Z	4			
Calculated density (g cm^{-3})	8.25	8.27	8.28	8.26

The valence charges of all bismuth ion species in α-$Bi_2Mo_3O_{12}$ were greater than their expected value (3.00) as Bi is found in its Bi^{3+} state. In the beta and gamma phase, there are mixing valence charge of Bi, one with higher value while the

other less value. On the other hand, the valence charges of all Mo ions in all bismuth molybdate were lower than its expected value, i.e. 6.

The valence charge shows the valence saturation of the relevance ions. Hence, the lager valence charge of Bi ions means that the ions are over saturated, and as a result, they tend to reduce their saturation. In the case of bismuth molybdate, this can be done by adding a proton (H^+) to oxygen ion bounded to bismuth ion. This is the reason why bismuth oxide site is responsible for hydrogen abstraction from propylene.

Table 4.12 Atomic coordinates of γ-Bi_2MoO_6

Ions	x	y	z	B
Bi(1)	0.5212(14)	0.4217(5)	0.9856(19)	0.41(14)
Bi(2)	0.4807(14)	0.0780(5)	0.9840(21)	0.95(15)
Mo	0.0028	0.2488	0.0000	0.81(7)
O(1)	0.0506(22)	0.1411(9)	0.0872(26)	0.51(21)
O(2)	0.2620(15)	-0.0011(9)	0.2752(23)	0.65(30)
O(3)	0.2398(14)	0.5002(9)	0.2680(25)	0.60(28)
O(4)	0.6850(15)	0.2306(6)	0.2499(19)	0.99(16)
O(5)	0.2171(15)	0.2630(6)	0.3514(18)	0.85(13)
O(6)	0.5709(24)	0.3598(11)	0.5761(30)	1.86(32)

.

In contrast to bismuth ions, all molybdenum ions have lower valence charge than what they can handle. This means that the Mo^{3+} species are less saturated and will try to increase their valence saturation by making bonding with donate able electron pair such as those on double bonded of carbon-carbon on propylene. From the valence charge tabulated above, it can be concluded that proton capturing are most likely occur on Bi(1) and Bi(2) in the alpha phase, Bi(3) and Bi(4) in the beta phase and Bi(1) in the gamma phase. The double bond of C=C will interact with more likely with Mo(2) and Mo(3) in both alpha and beta phase because they have smaller valence charge values.

4.4 Structure Dynamic of Bismuth Molybdates

Structural dynamic of bismuth molybdates catalysts were examined using Medium Resolution Powder Diffraction (MRPD) of neutron diffraction. A special furnace and sample cell made of quartz was employed to enable *in-situ* control of temperature and reaction atmosphere as mentioned in Chapter 3.

Table 4.13 Interatomic distances of γ-Bi_2MoO_6 (in Å).

		This work	Teller (Teller, Brazdil & Grasselli 1984)	Theobald (Theobald, Laarif & Hewat 1984)
Bi(1)	$O(3^{iv})$	2.18	2.18	2.11
	$O(3^{ii})$	2.26	2.22	2.27
	$O(3^{iii})$	2.34	2.33	2.33
	O(3)	2.54	2.53	2.57
	O(6)	2.49	2.51	2.49
	$O(6^{ii})$	2.50	2.56	2.52
	O(5)	2.47	2.96	2.38
Mean M(8)		2.50	2.47	2.51
Bi(2)	$O(1^{ii})$	2.42	2.40	2.44
	O(1)	2.64	2.61	2.66
	$O(2^{ii})$	2.18	2.19	2.21
	$O(2^{iv})$	2.21	2.22	2.24
	O(2)	2.38	2.38	2.40
	$O(2^{iii})$	2.55	2.52	2.48
	O(4)	3.10	2.80	3.08
Mean M(8)		2.50	2.50	2.50
Mo	O(1)	1.83	1.85	1.80
	$O(4^{ii})$	1.76	1.75	1.78
	O(4)	2.24	2.22	2.19
	$O(5^{ii})$	1.76	1.77	1.79
	O(5)	2.28	2.28	2.30
	$O(6^{ii})$	1.89	1.86	1.91
Mean M(6)		1.96	1.96	1.96

The furnace and quartz reactor were not purely transparent to neutron beam. Typical background pattern caused by the furnace and sample cell are given in Figure 4.6. These background patterns have to be eliminated from the diffractogram

when refining the structure to obtain information on the structural dynamics. Unfortunately, there is no mathematical model such as polynomial, Cheby, etc which is suitable to model the background because both furnace and quartz cell produce their own specific pattern. The only way to taken out the background pattern is by subtracting the experiment pattern with the background pattern acquired by running several experiment using either furnace only or furnace with the quartz cell without any catalysts.

Table 4.14 Valence charge (*S*) for α-$Bi_2Mo_3O_{12}$

	This Work	**van den Elzen and Rieck** (van den Elzen & Rieck 1973a)	**Theobald and Laarief** (Theobald, Laarif & Hewat 1985)
Bi(1) 8 neighbours	3.07	3.22	3.00
Bi(2) 8 neighbours	3.08	3.16	3.19
Mo(1) 5 neighbours	5.84	5.99	5.43
Mo(2) 5 neighbours	5.58	5.84	5.67
Mo(3) 5 neighbours	5.54	5.82	5.67

Table 4.15 Valence charge (*S*) for β-$Bi_2Mo_2O_9$

	This work	**Chen and Sleight** (Horng-Yih Chen & Sleight 1986)
Bi(1)	2.91	2.85
Bi(2)	2.85	2.81
Bi(3)	3.06	2.96
Bi(4)	3.15	3.01
Mo(1)	5.99	5.83
Mo(2)	5.37	6.32
Mo(3)	5.53	6.01
Mo(4)	5.90	6.10

Table 4.16 Valence charge (*S*) for β-$Bi_2Mo_2O_9$

	This Work	**Teller et al** (Teller, Brazdil & Grasselli 1984)	**Theobald and Laarief** (Theobald, Laarif & Hewat 1984)
Bi(1)	3.04	2.84	3.19
Bi(2)	2.79	2.89	2.71
Mo	5.82	5.86	5.67

The typical background-subtracted patterns are shown in Figure 4.7. The background-corrected pattern, though, still has a background pattern, which need to be modelled in the refinement. In addition, the background-corrected pattern of *in situ* experiments still shows some background residual pattern between 0^o and 25^o 2θ. This fragment of background was unrefined and causing large value in the refinement fit parameters. The same was also happen on the gamma phase. The *in situ* patterns of alpha phase were not affected since they were taken at shorter period of data collection (8 hours, compare to 18 hours for both beta and gamma phase).

Thermal analyses of the catalysts at the temperature being used (i.e. 300, 350, and 400^{o}C) revealed no change in the crystalline phase of the catalysts (Figure 4.8). The thermogram did not show any important phase change which is normally shown by a very sharp peak below their melting point. The thermogram of alpha and beta phase exhibits very sharp and deep endothermic peaks at 658.80^{o}C and 678.74^{o}C, respectively. These temperatures are attributed to their melting point (Tu Chen & Smith 1975). A small endothermic peak was apparent at 633.92^{o}C in the gamma phase which is an evident of the reversible phase transformation of γ to γ" while those at 680.48 is phase transformation of γ" to a stable and irreversible γ' phase (Catlow 1997). The thermal analysis, again, shows that no phase change occurs at the temperature used during *in situ* neutron diffraction analysis. Thus it was also assumed that the crystal structure of all catalysts before and after the *in situ* experiments was identical.

There is not much different in *in-situ* diffractogram patterns and their related room temperature patterns apart of peak shift and peak shape broadening. Due to this reason and the fact that there were no phase change at the temperature employed to study *in situ* structure, it was assumed that no changes were occur to the relative coordinates of ions in the bismuth molybdate lattice regardless the change in their unit change parameters.

With the constrains mentioned above, the refinement of all bismuth molybdates *in situ* patterns were taken by using their respective room temperature refinement results as the starting point. All ions coordinates were not refined while thermal parameters of ions, unit cell parameters, peak shape parameters and backgrounds were all refined. A sixth order of polynomial used to model the residual backgrounds of background-corrected patterns. The comprehensive refinement results are given in Appendices.

The unit cell dynamics, as a result of pattern refinement represented by unit cell parameters in air and under *in situ* condition are represented in Figure 4.9 and 4.10, respectively. The high temperature condition causes an increase on the unit cell volume due to thermal expansion. The percentage of unit cell parameters change relative to its room temperature conditions were calculated according to equation 4.1. In the equation, X represents unit cell parameters (a, b, c, β, and cell volume), subscript T and RT represent the experiment temperature and room temperature, respectively.

$$\text{Unitcell expansion}\,(\%) = \frac{X_T - X_{RT}}{X_{RT}} \times 100\% \qquad (4.1)$$

The symmetry of unit cell structure of alpha and beta phase is the same and thus, according to West (West 1989), they should undergo the same pattern of cell expansion. The unit cell of the gamma phase, on the other hand, is orthorhombic which is more symmetrical than the alpha and beta phase and expected to have uniform expansion rate in all direction of its unit cell axis. However, Figure 4.9 and 4.10 shows that in air, the change in unit cell parameters of beta phase is regular to all direction while the gamma phase experienced uneven unit cell expansion.

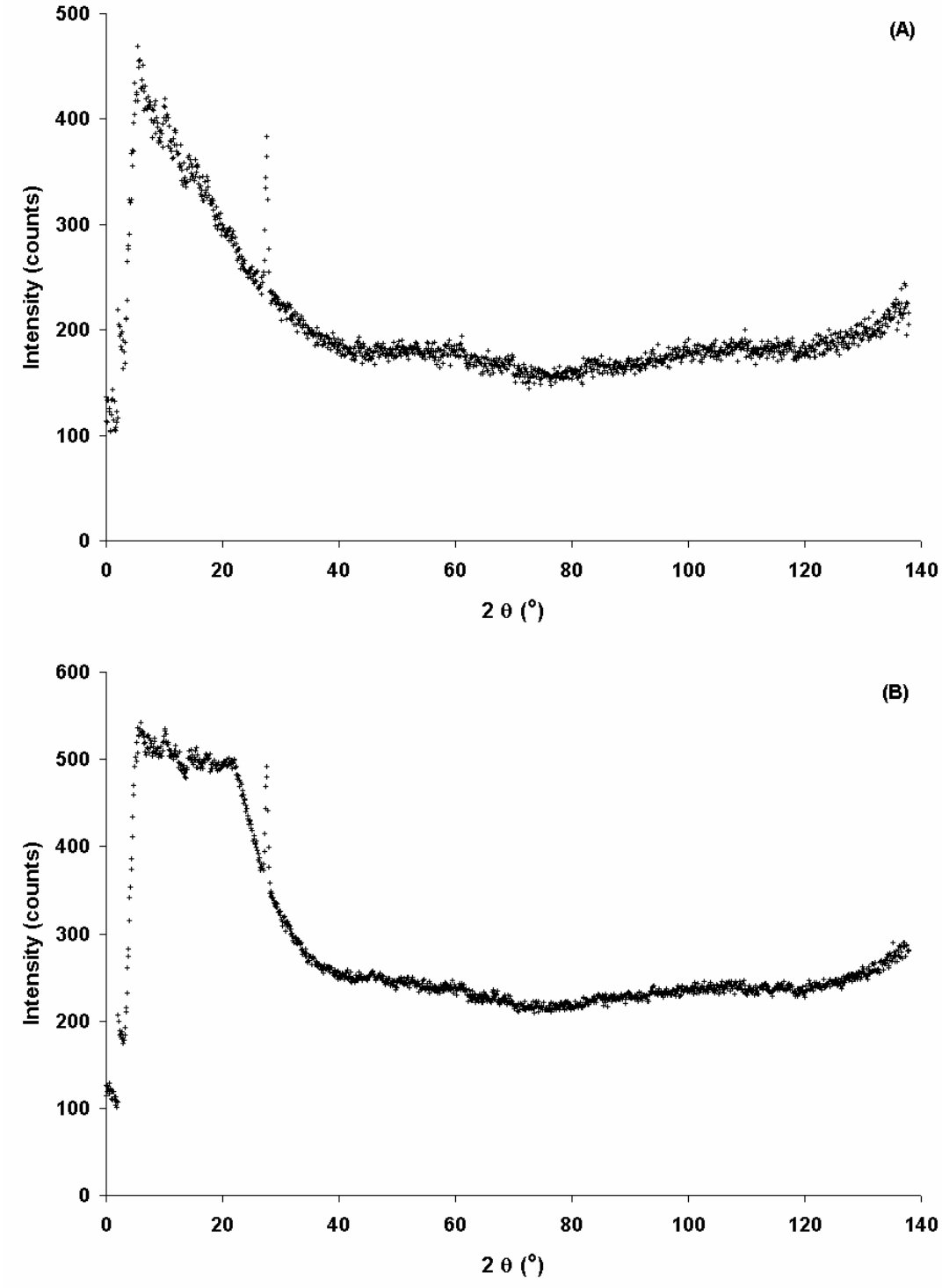

Figure 4.6 Typical background patterns of a) furnace only and b) furnace plus quartz sample cell. The background patterns were taken at room temperature.

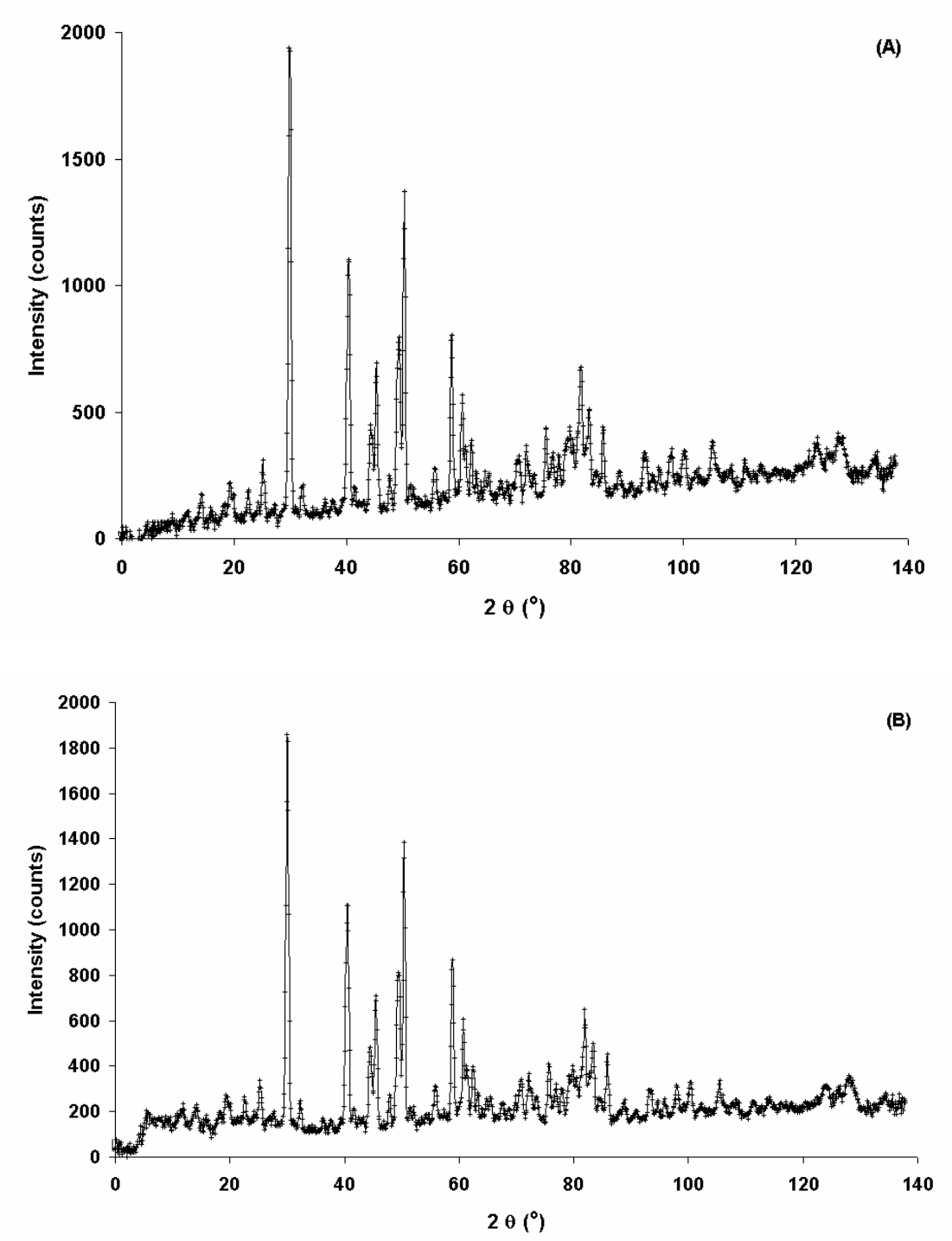

Figure 4.7 An example of background-subtracted patterns of β-$Bi_2Mo_2O_3$: a) at 300°C in air and b) at 300°C in reactant gas atmosphere. The experiment in air was taken without the quartz cell, while those in gas were taken with quartz sample cell.

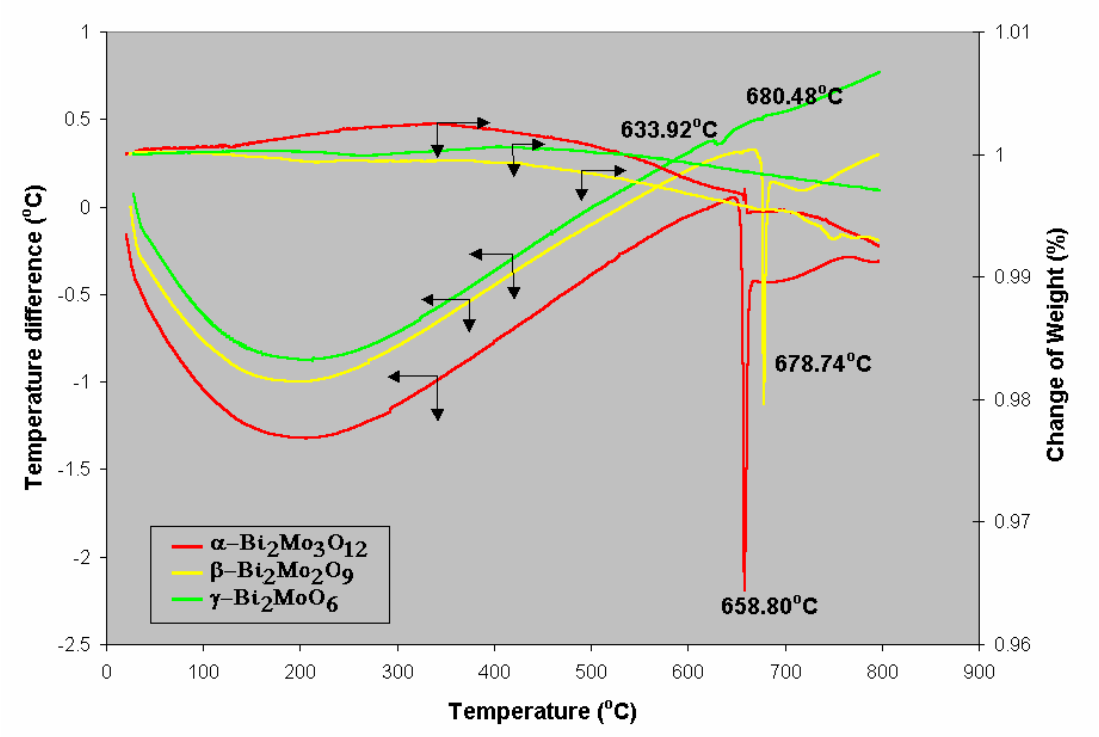

Figure 4.8 DTA-TGA thermogram of a) α-Bi_2Mo3O_{12}, b) β-$Bi_2Mo_2O_9$ and c) γ-Bi_2MoO_6. No sharp peaks are apparent at temperature below 500°C, showing that no phase change was occurring at temperature range below 500°C.

The change in unit cell parameters of α-$Bi_2Mo_3O_{12}$ in air and in reactant gas is anisotropic and actually has the same order of change relative to its room temperature parameters. In both condition, the thermal expansion of α-$Bi_2Mo_3O_{12}$ is mainly attributed to the expansion in b direction and consequently it reduces the β angle (the angle between a and c axis) because the unit cell has monoclinic symmetry. The expansion of the unit cell of β-$Bi_2Mo_2O_9$ in air and under reaction gas atmosphere is also similar. However, the change in β angle in air and reactant gas has opposites direction of change to each other i.e. the β increased at increasing temperature in air but decreased in reactant gas. All unit cell parameters in γ-Bi_2MoO_6 increase at elevating temperature in either air or reactant gas atmosphere. However, the increase rate of unit cell parameters in the gamma phase between 300 and 350°C was slower than those between 350° and 400°C.

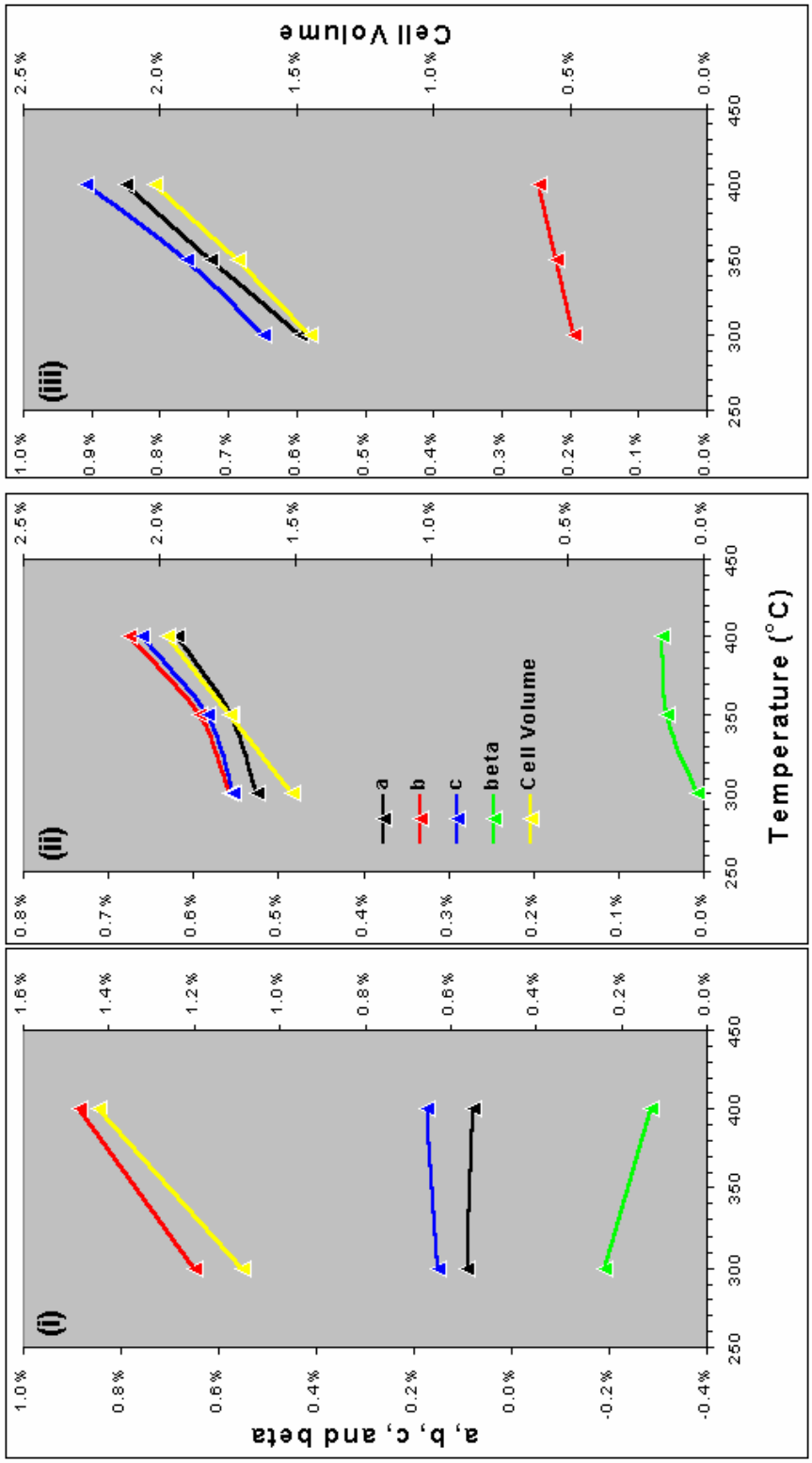

Figure 4.9 The expansion/contraction percentage of unit cell parameters relative to their room temperature condition in air atmosphere of: (i) α-$Bi_2Mo_3O_{12}$, (ii) β-$Bi_2Mo_2O_9$; (iii) γ-Bi_2MoO_6.

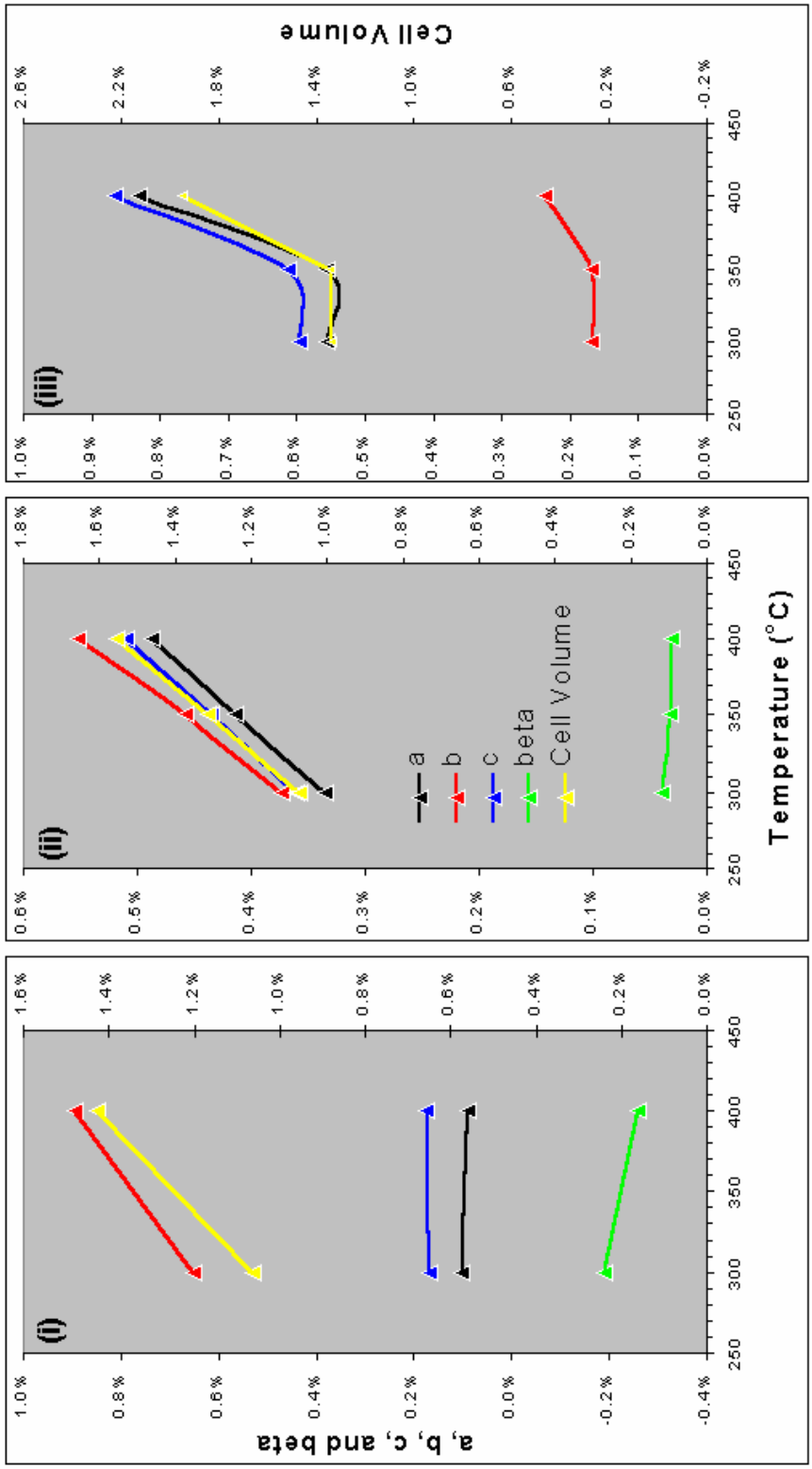

Figure 4.10 The expansion/contraction percentage of unit cell parameters relative to their room temperature condition in reacting gas atmosphere of: (i) α-$Bi_2Mo_3O_{12}$, (ii) β-$Bi_2Mo_2O_9$; (iii) γ-Bi_2MoO_6.

The domination of expansion in b direction over the expansion in a or c in the alpha phase can be explained from the structural point of view. The domination in b direction expansion is caused by oxygen ions available for expansion. At high temperature, oxygen ions in the crystal lattice are expected to have larger vibration amplitude than the heavier ions such as Bi^{3+} and Mo^{6+}. The contributors for the expansion are O1, O2, O9, O10, O11, and O12, which, according to Figure 4.11, stacked in the b direction. These oxygen ions form an oxygen layer, which is separating two layers of bismuth-molybdate in a unit cell.

The β-$Bi_2Mo_2O_9$ was expanded more isotropic in all direction than the alpha phase. Although it has the same symmetry as the alpha phase, the beta phase has less distorted polyhedra in either Bi-O or Mo-O polyhedra than the alpha phase. It also has more even oxygen distribution in the unit cell (see Figure 2.3). As a result, when oxygen ions in the lattice vibrate at elevated temperature, the unit cell will expand to all direction in the cell more uniformly.

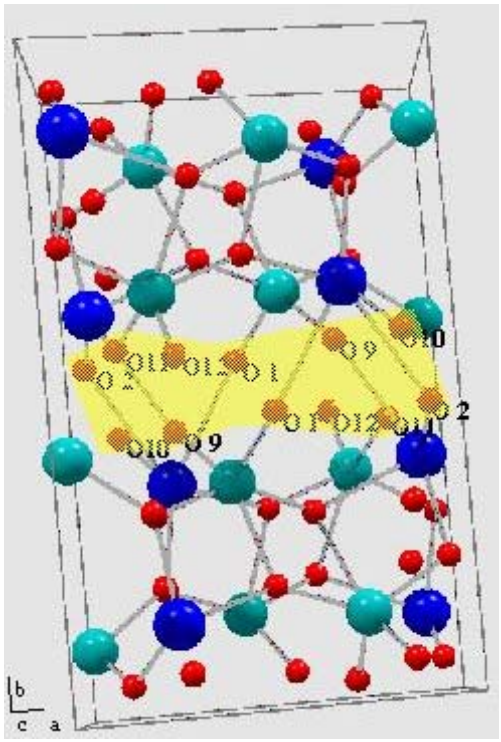

Figure 4.11 A cross section of an α-$Bi_2Mo_3O_{12}$ unit cell from c direction showing the oxygen atoms lying on the interlayer of the bismuth molybdate.

Unit cell expansion in b direction in γ-Bi_2MoO_6 was 50% slower than those in a and c direction. In b direction, Mo-O-Mo networks are dominates the structure while Bi-O-Bi and Bi-O-Mo networks determine the unit cell elongation in **a** and **c** directions. The distance of Mo-O bonds are shorter than Bi-O bond. As a result, when the oxygen ions vibrate at the same vibration amplitude relative to their steady position, the expansion on the direction where cation to oxygen ion distance is larger will experience larger relative expansion. This explain the slower expansion rate in the **b** direction in comparison to in **a** and **c** directions.

There are two consequences of the thermal expansion for the bismuth molybdates structure and their performance in catalysing partial oxidation of alkene to unsaturated aldehyde, in particular, propylene oxidation to acrolein. It has been widely accepted that partial oxidation of alkene over bismuth molybdate catalysts following the Mars and van Krevelen mechanism (Mars & van Krevelen 1954) via the formation of allyl intermediate (Adams & Jennings 1963; Adams et al. 1964; Bettahar et al. 1996; Bielanski & Haber 1991; James D. Burrington, Kartisek & Grasselli 1980; J. D. Burrington, Kartisek & Grasselli 1984; Callahan et al. 1970; Doornkamp, Clement & Ponec 1999; Doornkamp & Ponec 2000; Robert Karl Grasselli 1982; Robert K. Grasselli 19851999; Keulks 1970; Leonard David Krenzke 1977) and need a redox couple to facilitate a selective oxidation process (Batist 1979). For this condition, the activation of alkene to form allyl intermediate required an interaction between the alkene with the catalyst surface in such away that alkene is adsorbed and simultaneously lost its α hydrogen. The adsorption site of the alkene is believed to happen on molybdenum ion site while the α hydrogen was captured by oxygen ions bridging a bismuth and a molybdenum on in the lattice. With this requirement, the expansion of unit cell change in interatomic distances in the crystal lattice which make the distances in Bi-O-Mo become more suitable for the propylene to anchor on to the catalyst surface so as to initiate the formation of allyl intermediate, no matter which mode of hydrogen capturing mechanisms is followed.

The second consequence is that oxygen atoms in the catalyst lattice become less tightly bounded to either the Bi or the Mo sites, thus give them more mobility. With their increased mobility, the oxidations of allyl intermediate become easier.

Both consequences make the catalyst activities and selectivities increase. However, at higher temperatures, where oxygen becomes more and more mobile, the catalysts lost their selectivity just as what had been showed by γ-Bi_2MoO_6 above 400^oC. This may take place since oxygen now becomes so reactive that allyl intermediates are oxidised into complete oxidation product (CO_2) (Fansuri et al. 2003).

A further examination of the refinement results for the atomic temperature parameters gives clearer insight into the lattice dynamic of bismuth molybdate structure and probably its role in determining the catalytic activity and selectivity of bismuth molybdates. Figure 4.12 to 4.14 shows the change in thermal parameters of ions, particularly oxygen ions, in the lattice of bismuth molybdate crystal in air as well as under *in situ* condition.

Thermal parameters of α-$Bi_2Mo_3O_{12}$ at high temperature in either air or under *in situ* condition are given in Figure 4.12. The figure shows not all of the ions in the alpha phase suffer the same heat effect. The Figure clearly shows that O(5) severely affected by high temperature and *in situ* environment while O(11) and (12) are affected moderately in all condition at high temperature. The O(5) is the member of octahedra Mo_2O_8 group containing Mo(1) while O(11) and O(12) are members Mo_2O_8 containing Mo(2) and Mo(3) (van den Elzen & Rieck 1973a).

The high thermal parameters of O(5) is associated with the easiness of the ions to travel inside the lattice. Mean while, the moderate thermal parameter of O(11) and O(12) are associated with their ability to attack the allyl intermediate to form σ-allyl as mentioned by Ono and Kuczkowski (Ono, Ogata & Kuczkowski 1998). From this, it can be concluded that the oxygen ion responsible to provide rapid oxygen exchange is O(5) while those responsible in oxidising the allyl intermediate are O(11) and O(12).

The conclusion support hypothesis that oxygen ions associated with bismuth are responsible for α-hydrogen capture (B. Grzybowska, Haber & Janas 1977; Otsubo et al. 1975) while oxygen ions on molybdenum oxide polyhedra such as O(11) and O(12) are responsible in the abstraction of second hydrogen and oxygen insertion to the olefin group to produce σ-allyl species.

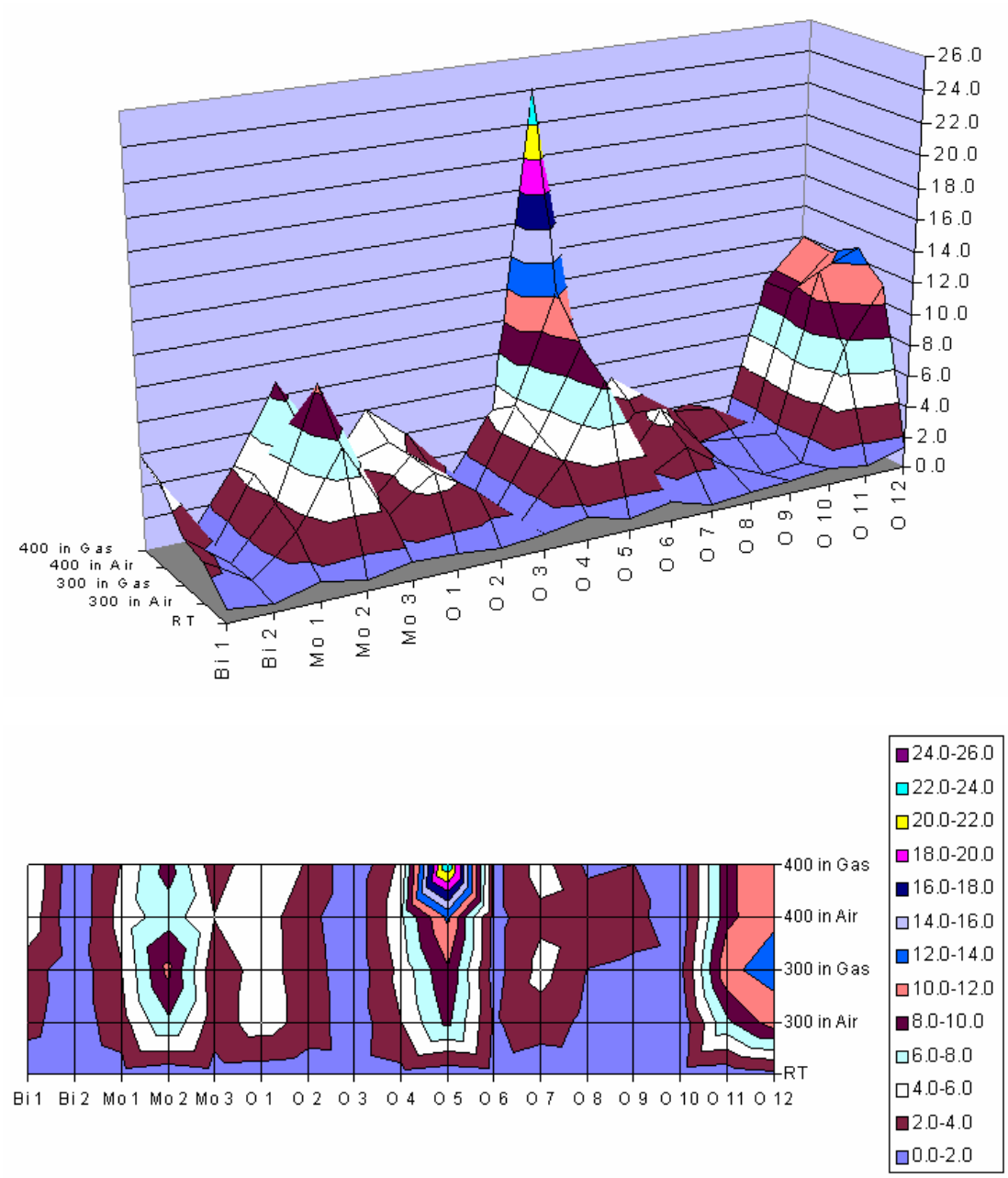

Figure 4.12 Thermal parameter of all ions in α-$Bi_2Mo_3O_{12}$ in various conditions

In β-$Bi_2Mo_2O_9$, there are three oxygen ions that show high thermal parameters at high temperature under either air or *in situ* environment as shown in Figure 4.13. These oxygen ions are O(3), O(11), O(16) and O(18). The O(16) and O(18) are oxygen ions bridged Bi^{3+} and Mo^{6+} ions to form Bi-O-Mo chain. The O(16) is bounded to Bi(1) and Mo(3) while O(18) is bounded to Bi(3) and Mo(1). On

the other hand, each of O(3) and O(11) is bounded to two Bi^{3+} ions and an Mo^{6+} ion. O(3) is bounded to Bi(2), Bi(3) and Mo(1) , while O(11) is bounded to Bi(1), Bi(4) and Mo(1). Moreover, all of these oxygen ions exhibit higher thermal parameters when they were under *in situ* condition. No oxygen ions that solely reside in the so-called Bi_3O_2 chain by Chen and Sleight (Horng-Yih Chen & Sleight 1986) have high thermal parameters. This means that those oxygen ions are inactive for catalytic reaction

Many other oxygen ions in the lattice have similar bonding and environment in the lattice of β-$Bi_2Mo_2O_9$. However, only four ions show their high thermal parameters at high temperature under air or *in situ* atmosphere led to a conclusion that they are the active oxygen in catalysis of partial oxidation of propylene over beta phase of bismuth molybdate. As in the alpha phase, this phase also has a redox couples around active oxygen ions. However, the beta phase does not have oxygen ions that can easily move inside the crustal lattice as O(5) in the alpha phase. This will reduce the ability of the beta phase to facilitate redox reaction without external supply of gaseous phase of oxygen.

Thermal parameters of ions in γ-Bi_2MoO_6 are represented in Figure 4.14. The Figure shows that there are only two oxygen ions have high thermal parameter at high temperature in either air on *in situ* atmosphere. Those oxygen ions are O(1) and O(5) which have similar thermal parameter values over all conditions employed.

Oxygen ions that have high thermal parameters are coordinated to molybdenum ion. The O(1) is bounded to Mo and two Bi(2) ion while O(5) is shared by two Mo^{3+} ion and Bi(1). Oxygen ion O(6) is more or less similar to O(1) and O(4) to O(5). However, O(1) and O(5) have shorter bond distance to Bi^{3+} ions in the lattice compared to their respective companions (O(6) and O(4)). In other word, both oxygen ions are under higher influence by bismuth ion and compose a Bi-O-Mo bridging. In addition, as in the beta phase, no oxygen ion in the gamma phase that as mobile as O(5) in the alpha phase was detected under the experiment condition.

A path of oxygen ions during selective oxidation in `γ-Bi_2MoO_6 has been studied from first principles modelling by Dadyburjour and Ruckenstein (Dadyburjor & Ruckenstein 1978). Their study indicated that the most probable oxygen ion

removed by hydrocarbon when the γ-Bi_2MoO_6 is oxidised, is an oxygen ion associated with the bismuth ion. This oxygen is replaced by oxygen from the mobile layer between $(Bi_2O_2)^{2+}$ and $(MoO2)^{2+}$ layers. This in turn is replaced by an oxygen ion associated with the molybdenum and this is eventually replaced by an oxygen ion derived from reactant gas.

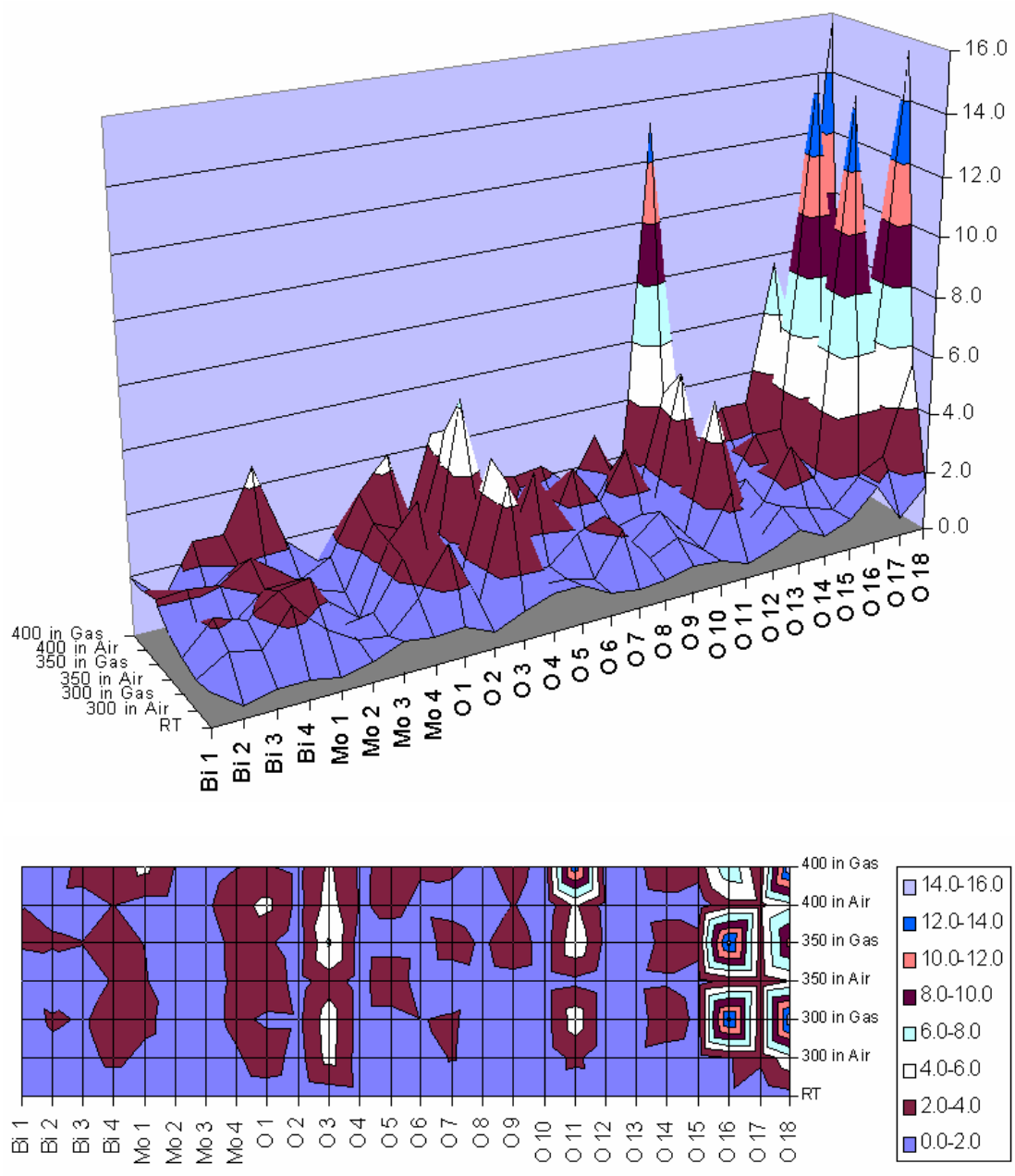

Figure 4.13 Thermal parameter of all ions in β-$Bi_2Mo_2O_{12}$ in various conditions

The oxygen path described by Dadyburjour and Ruckenstein is coherent with the result of *in situ* diffraction results in this work. Figure 4.15 shows a schematic of oxygen path according to Dadyburjour and Ruckenstein. Evident of thermal parameter reveals that path number 2 is associated with oxygen ions O(1) while oxygen in path No. 4 is oxygen ions O(5). The mobility of oxygen ions O(1) and O(5) is evidence from their hight thermal parameters, which was detected as high vibration amplitude.

Dadyburjour and Ruckenstein have also calculated the ease of oxygen removal from $(Bi_2O_2)^{2+}$ layer and found that activation energy for such removal was enormously high $(Bi_2O_2)^{2+}$ (Dadyburjor & Ruckenstein 1980). These oxygen ions are O(2) and O(3), which, according to Figure 4.14, have low thermal parameters. Low thermal parameters mean that such oxygen ions are stable in the lattice and indeed very difficult for direct removal from the lattice. However, since the removal of such oxygen will almost instantly replaced by more mobile oxygen in between $(Bi_2O_2)^{2+}$ and $(Mo_2O_2)^{2+}$ layers, it is somehow reduces the activation energy.

The oxygen path described by Dadyburjour and Ruckenstein and their study in the activation energy of oxygen removal from the γ-Bi_2MoO_6 lattice together with the result of this work, shows that the oxygen ions with less thermal parameter under reaction condition are responsible as the source of oxygen for oxidating propylene to acrolein. On the other hand, oxygen ions with high thermal parameters are mobile ions, which are responsible in supplying rapid oxygen replacement inside the lattice. Thus, all oxygen ions O(5), O(11) and O(12) in α-$Bi_2Mo_3O_{12}$, O(3), O(6), O(16), and O(18) in β-$Bi_2Mo_2O_9$, and O(1) and O(5) in γ-Bi_2MoO_6 are all mobile but not supplied directly to the adsorbed allyl intermediate.

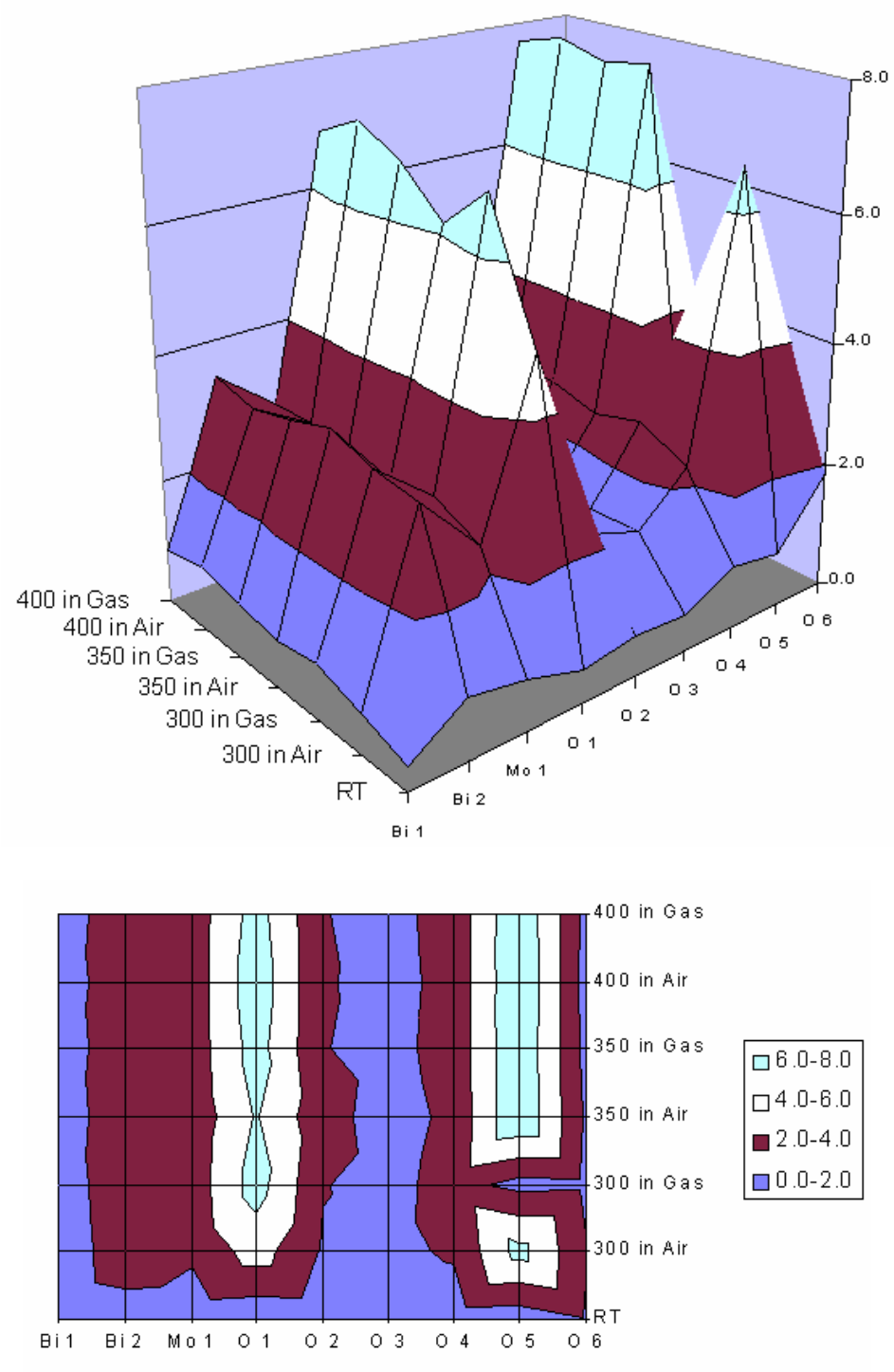

Figure 4.14 Thermal parameter of all ions in γ-Bi_2MoO_6

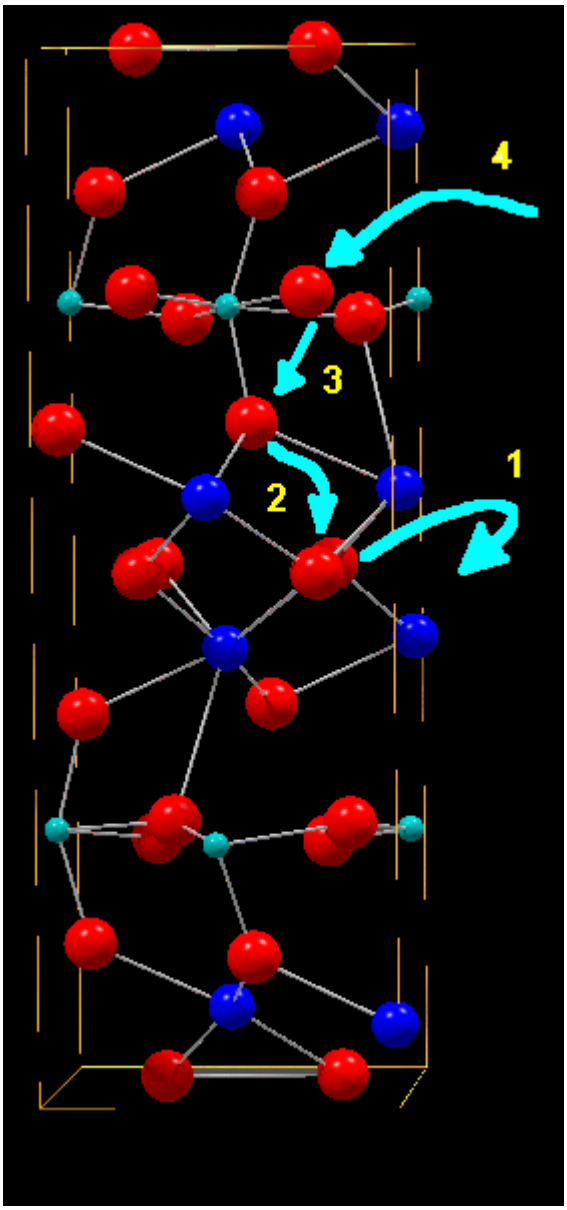

Figure 4.15 Oxygen path in γ-Bi_2MoO_6 according to Dadyburjour and Ruckenstein (Dadyburjor & Ruckenstein 1978)

4.5 Summary

Based on the results presented in this chapter, there are some conclusions that can be taken in the characteristics of the catalysts in this study. First, the bismuth molybdate catalysts prepared in this work are physically and chemically comparable to those used by previous researchers (Keulks et al. 1974; Leonard David Krenzke

1977; L. David Krenzke & Keulks 1980ab; Monnier & Keulks 1981). There are, however, some impurities found in small concentration in beta and gamma.

The structure of all bismuth molybdates is the same as the model structure. The refinement results of the structure at room temperature, particularly the valence charge calculation results, reveals that molybdenum oxides polyhedra in all bismuth molybdates in this work are actually still unsaturated and as a results it plays as an active site for propylene adsorption. On the other hand, bismuth ions have over saturated valence charge. The charge can be reduced by capturing an alpha hydrogen from adsorbed propylene. The information explains the mechanisms of allyl formation as commonly investigated by surface characterisation methods by many of previous researchers.

Study on the lattice dynamic from the results of *in situ* neutron diffraction give better insight to the role of lattice oxygen to the catalytic partial oxidation of propylene to acrolein over bismuth molybdates. The study shows and proves the importance of Bi-O-Mo chain in catalysing partial oxidation of propene. The discussion above shows that certain oxygen ions in the catalyst lattice are the most probable ions controlling the activity of the catalyst.

In case of the alpha phase some oxygen atoms are responsible to keep redox balance in he lattice. These oxygen ions are O1, O11, and O12 which are mobile ions in the lattice. Mobile oxygen in β-$Bi_2Mo_2O_9$ are O(3), O(11), O(16), and O(18), while in γ-Bi_2MoO_6 are O(1) and O(5). There is no direct evidence from the structure dynamic study whether mobile oxygen ions are those responsible to oxidise adsorbed allyl intermediate to become acrolein or not.

Theoretical computation work by Dadyburjour and Ruckenstein (Dadyburjor & Ruckenstein 1978; Dadyburjor & Ruckenstein 1980) on the gamma bismuth molybdate model shows explain that oxygen ions who oxidise the adsorbed allyl intermediate are those who are less mobile although the activation energy needs by such oxygen ions is high. However, due to the availability of mobile oxygen in the lattice, the activation energy might be lower than those calculated. With the analogy taken from the gamma phase, the same might happen on the alpha and beta phase, i.e. the mobile oxygen ions are not those who oxidise the adsorbed allyl intermediate.

Although the mobile oxygen ions are not a direct oxidant to adsorbed allyl intermediate, they play an important role to control the catalysts activity because they lower the activation energy. In addition, according to the oxygen path depicted in Figure 4.15 these mobile oxygen ions, in turn, will become the oxygen which will oxidise the allyl intermediate. This is the possible answer to the fail effort to find which oxygen ions actually responsible for oxidising allyl intermediate by using ^{18}O labelled bismuth molybdate as reported by some researchers (Mestl 1994; Miura et al. 1979; Ono, Ogata & Kuczkowski 1998; Otsubo et al. 1975; Sancier, Wentrcek & Wise 1975), although they could find which from polyhedra are the oxygen ions come from.

The relation between the structure dynamic with the kinetic of propylene oxidation to acrolein and reaction mechanisms will be further discussed in Chapter five and six, respectively.

Chapter 5

THE KINETICS OF PARTIAL OXIDATION OF PROPYLENE TO ACROLEIN

Kinetics of partial oxidation of propylene to acrolein over bismuth molybdate catalysts has been widely explored by many researchers as noted in Chapter 2 Literature Review. The majority of their work was carried out using supported or additive-modified bismuth molybdates. Among the literature reports, those reported by Keulks and co-workers used the powder form of pure bismuth molybdates (Keulks & Lo 1986; Keulks, Rosyneck & Daniel 1971; Leonard David Krenzke 1977; L. David Krenzke & Keulks 1980b; Monnier & Keulks 1981), which are similar to the one used in this work.

Although kinetic data for the catalysts used in this work are available in the literature, all of them were studied separately from the catalysts preparation and characterisation. As a result, the kinetic data were not derived from a well-characterised bismuth molybdate, although they produced quite similar kinetic data. The background mentioned above was the reason for this work to carry out comprehensive work involving characterisation, reaction kinetics and mechanisms in a single research project.

The characteristics of bismuth catalysts used in this work have already been discussed in Chapter 4. This Chapter discusses the results of kinetic experiments mentioned in Chapter 3. This chapter is divided into two sections namely

experimental techniques and procedure and the kinetics of propylene oxidation into acrolein over bismuth molybdates.

5.1 Experimental Techniques and Procedure

The experiments to obtain kinetic data were based on a differential, plug-flow reactor model. To satisfy the differential, plug-flow reactor model, conversions of propylene in all experiments were kept low, i.e. less than 10%. With this reactor model, the rate of conversion was considered constant in all points within the reactor (Levenspiel 1999) and the reaction was not influenced by mass diffusion (Zhang & Agnew 1994). To achieve low conversion, the reactors were fed with small amount of catalyst (ca less than 0.4 g). The plug-flow condition was achieved by using low total flow rate of the feed gas. With this consideration, a total flow rate of 120 ml min^{-1} was employed. All of the reaction conditions above were adapted from the literatures (Kremenic et al. 1987; Kremenic et al. 1988; Leonard David Krenzke 1977; Monnier & Keulks 1981; Hock Seng Tan 1986; H. S. Tan, Downie & Bacon 19881989).

5.1.1 Chromatogram of reactants and products of the kinetic experiments

Gas chromatography (GC) is the main instrument used for quantitatively measuring the concentration of reactants and products of the kinetic experiments. The GC was equipped with two detectors, namely FID and TCD, which are dedicated to detecting organic (C_3H_4O, C_3H_6, and C_2H_4O) and inorganic (CO, CO_2, and O_2) species, respectively. The GC was also equipped with two columns, namely, Porapak-N and Molecular Sieve 13X. A Micro MAT 14 standard gas of Matheson Tri-Gas containing 5% CO_2, 5% CO, 5% O_2, 5% N_2, 4% CH_4 and 4% H_2, balanced with helium, was used to determine retention time of CO_2, CO, O_2 and N_2 on the chromatogram following the GC method as mentioned in Chapter 3. Polymer grade propylene from BOC Gases, a 90% acrolein and acetaldehyde of Sigma-Aldrich were used to determine their retention time. All gasses except N_2, CH_4, and H_2 were involved in the catalytic reaction being studied. For qualitative analysis, a known concentration of the Micro MAT 14 standard gas and propylene were mixed together

in a Teflon plastic bag and diluted with air to reduce their concentration to an acceptable concentration limit of the GC system. The vapour phase of acrolein and acetaldehyde were used in the qualitative GC analyses.

The GC method used in the kinetic experiments successfully separated all gasses involved in the reaction. The separation of each gas is clearly represented in Figures 5.1 and 5.2. In the Figures, the peak of N_2 is three times higher than O_2, which is typical of air composition because the mixture was diluted by air. Retention time of each component, as a result of the qualitative analysis, is given in Table 5.1. Using the method, complete analyses covering all components by the GC method were carried out in 15 minutes.

Table 5.1 Retention time of reactants and products of kinetic experiments using the GC method mentioned in Chapter 3.

Component	**Retention time (minute)**	**Detector**
CO_2	1.49	TCD
O_2	2.20	TCD
CO	2.56	TCD
C_3H_6	4.54	FID
C_2H_4O	8.87	FID
C_3H_4O	13.30	FID

5.1.2 Preliminary tests

Prior to the kinetic experiments, blank runs were carried out to check the performance of the reactor system, particularly the gas phase reaction between propylene and oxygen. The blank runs were carried out with a mixture of reactant gas comprise of 5% C_3H_6, 10% O_2, and 85% He at 120 mL min^{-1} over the temperature range of 300^o – 450^oC. Two reactors were checked in the blank run tests. The first reactor was made of stainless steel while the other was quartz. Under the reaction conditions, no gas phase reaction was detected from the blank runs using

quartz reactor. On the other hand, the runs using stainless steel reactor showed clear evidence of propylene oxidation to carbon oxides at temperature as low as 360°C.

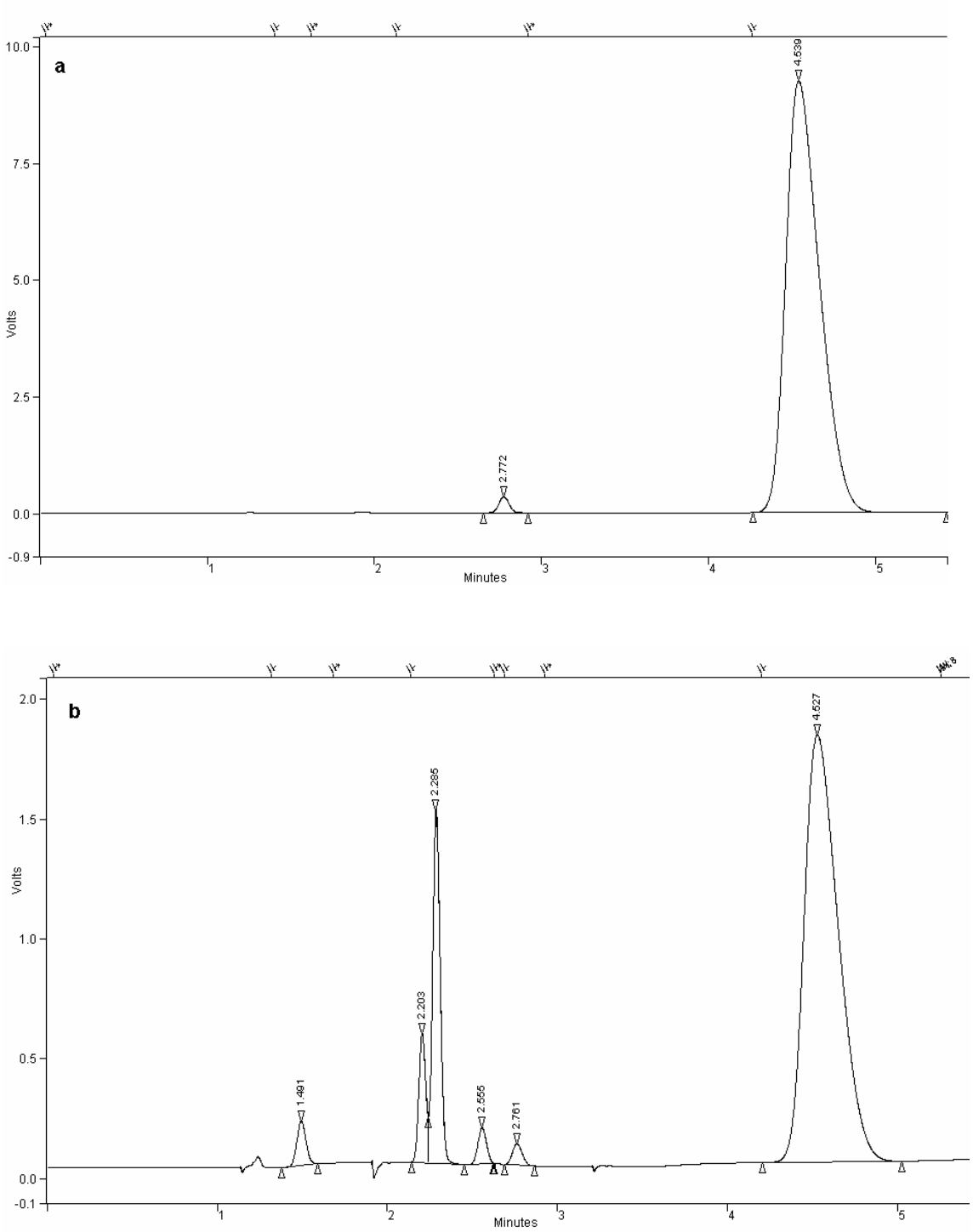

Figure 5.1 Qualitative chromatogram of standard Micromat-14 gas containing CO_2, O_2, N_2, CO, and CH_4 mixed with C_3H_6 detected by a) FID and b) TCD

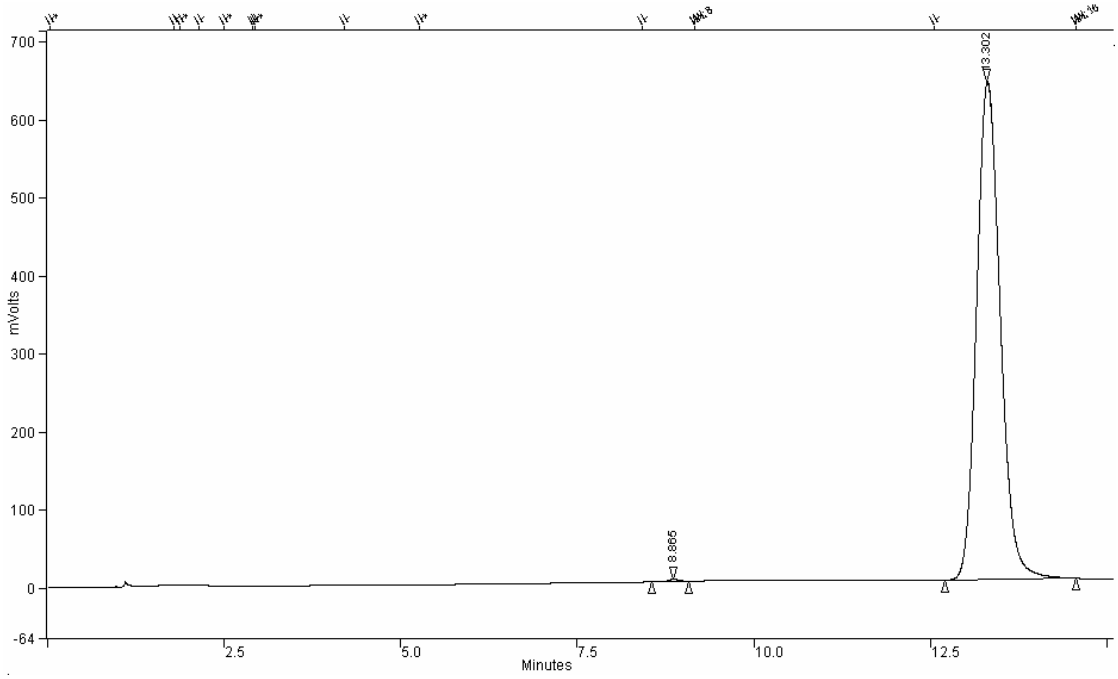

Figure 5.2 Typical chromatogram of sample gas containing acetaldehyde and acrolein

The blank tests at low temperatures were also reported by Tan (Hock Seng Tan 1986) in his thesis. He found that propylene oxidation occurs significantly at temperatures higher than 400^{o}C. Not surprisingly, the reactor used by Tan (Hock Seng Tan 1986) was a stainless steel reactor with a stainless steel mesh in the middle of the reactor to support the catalyst bed. Tan appointed this reaction as catalysed by the reactor wall although no further kinetic data were reported on this reaction. On the other hand, no blank reaction was reported when the reactor is made of quartz glass (Keulks, Rosyneck & Daniel 1971; Kremenic et al. 1987; Kremenic et al. 1988; Leonard David Krenzke 1977; L. David Krenzke & Keulks 1980b; Monnier & Keulks 1981).

The oxidation of propylene into carbon oxides was possibly catalysed by iron oxide formed inside the stainless steel reactor wall. The iron oxides were formed as a result of the high temperature condition and the availability of gas phase oxygen to oxidise metallic iron on the stainless steel wall into iron oxides. Under the reaction condition (at temperature between 300^{o} and 450^{o}C), iron oxides performed as oxidation catalyst for hydrocarbons (Golunski & Walker 2000).

The blank tests were also carried out to check acrolein oxidation without any catalysts in either stainless steel or quartz reactor over a temperature range of 300 to 450^{o}C. The blank tests with the stainless steel reactor showed the formation of carbon oxides from acrolein started at 360^{o}C. Blank tests, carried out using quartz reactor, showed acrolein oxidation to carbon oxides occurred at temperatures higher than 390^{o}C. The result of these blank test runs shows that quartz reactor can be regarded as inert at temperature less than or equal to 390^{o}C.

5.2 The Catalytic Activity and Selectivity

The catalyst activity was obtained at propylene to oxygen ratio of 1:2. The total flow rate was 120 mL.min^{-1} at temperatures between 300^{o}C and 450^{o}C. The temperature range was chosen based on the knowledge that below 300^{o}C the conversion of propylene over the catalysts was negligible and above 450^{o}C, side products were significantly produced. From the catalyst point of view, the temperature range assures that no phase conversion occurs on the catalysts. Phase changes in the gamma phase deactivate the catalyst activity (Barnes, Kitchin & Hriljac ; Douglas J. Buttrey 2001; D. J. Buttrey, Jefferson & Thomas 1986; D. J. Buttrey et al. 1994).

The catalyst activity was determined from their ability to convert propylene to useful product and their selectivity to convert propylene to certain product. The activity of the catalysts was measured based on mol number of carbon atom because the reaction can also produce smaller molecule such as carbon dioxide and carbon monoxide.

The propylene conversion on the catalyst was calculated using equation 5.1, while the selectivity of the catalysts was calculated using equation 5.2.

$$X = \left[1 - \frac{Mole_{C_3H_6 outlet}}{Mole_{C_3H_6 inlet}}\right] \times 100\% \qquad 5.1$$

$$S = \left[\frac{Mole_{C_3H_4O,outlet}}{Mole_{C_3H_6inlet} - Mole_{C_3H_6outlet}} \right] \times 100\% \qquad 5.2$$

The results of the catalyst activity tests are given in Figures 5.3 to 5.5. The figures show that the activity of the catalysts in term of total propylene conversion is in the order of γ>α>β. The alpha and beta phases have similar patterns of catalytic selectivity to acrolein. In contrast, the selectivity of the gamma phase decreased considerably at high temperatures.

The high conversion of propylene over the gamma phase does not mean that the catalyst is the best among the three catalysts as its selectivity is low. Comparing the three catalysts, the catalysts' performance in yielding acrolein will best describe their performance. This can be done by plotting the logarithmic specific rate of acrolein production versus the reaction temperature as shown in Figure 5.6. The figure shows that the catalyst performance decreases in the order of α>γ>β in term of acrolein production rate versus reaction temperature. Figure 5.6 and Figures 5.3 through to 5.5 also show that the alpha and gamma phases have similar activity for propylene conversion to acrolein while the beta phase is always the least active catalyst.

The order of bismuth molybdate activity for propylene conversion to acrolein, particularly the alpha and the gamma phase is very similar to reports by several researchers (Golunski & Walker 2000; Leonard David Krenzke 1977; L. David Krenzke & Keulks 1980b). The beta phase was normally reported as having the same activity as the alpha and gamma phases (Monnier & Keulks 1981; Hock Seng Tan 1986; H. S. Tan, Downie & Bacon 1988). These reports, particularly the activity of the beta phase, are strongly opposed by the results of this research where the activity of the beta phase is the lowest one. The same order of activity was also reported in high conversion tests (Douglas J. Buttrey 2001). The high activity of the beta phase as reported by other researchers (Batist et al. 1968; Beres, Janik & Wasilewski 1969; Cullis & Hucknall 1981; Gorshkov et al. 1968; Millet et al. 1993), might have been caused by the impurities of the catalysts. A recent report by Larsen (Larsen 2003) clearly shows the existence of other bismuth molybdate phases in his catalysts, which

was prepared according to reported preparation procedures (Batist et al. 1968; Beres, Janik & Wasilewski 1969; Cullis & Hucknall 1981; Gorshkov et al. 1968; Millet et al. 1993).

Acetaldehyde, carbon dioxide, and carbon monoxides are the major side products in the propylene to acrolein conversion. The selectiveness of the reaction towards these side products is given in Figures 5.7 to 5.9. The Figures show some very interesting features that the side products of each catalyst are different. On the alpha phase, acetaldehyde is the main side product at temperatures below 390°C. At 390°C to 420°C, the concentration of acetaldehyde decreases and is exceeded by carbon monoxide. At 450°C, carbon dioxide takes over as the dominant side products. In the beta phase, carbon monoxide is the major side product with a small amount of acetaldehyde and a very small amount of carbon dioxide. In the gamma phase, acetaldehyde is the main side product only at 300°C and 330°C, but at higher temperatures, carbon dioxide is the main side product.

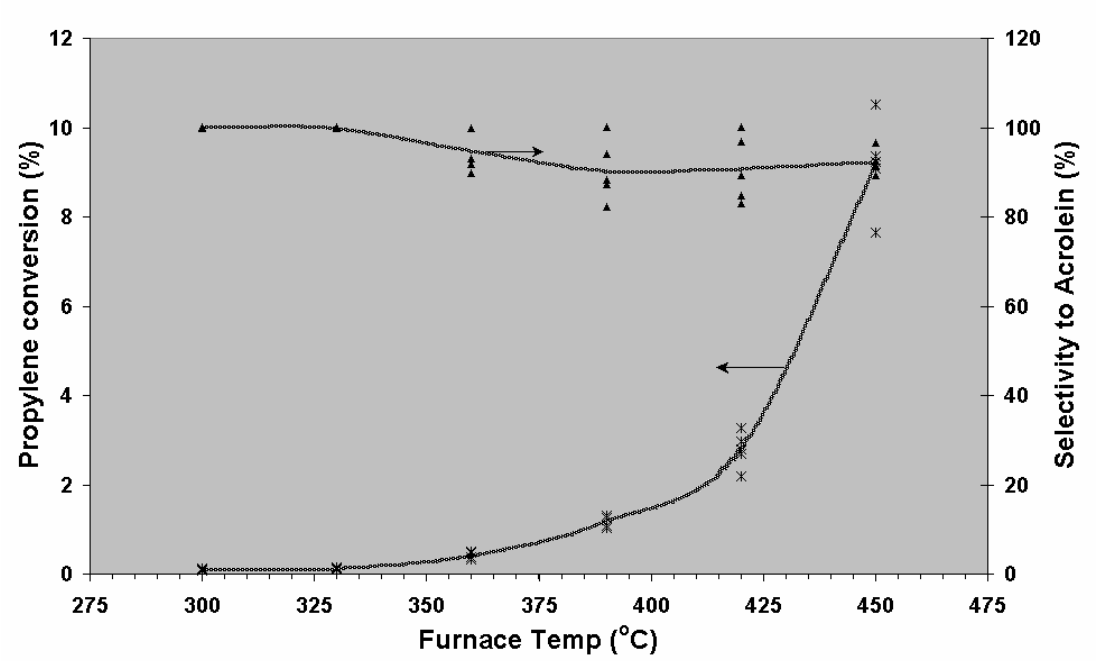

Figure 5.3 Propylene conversion and acrolein selectivity over the α-$Bi_2Mo_3O_{12}$

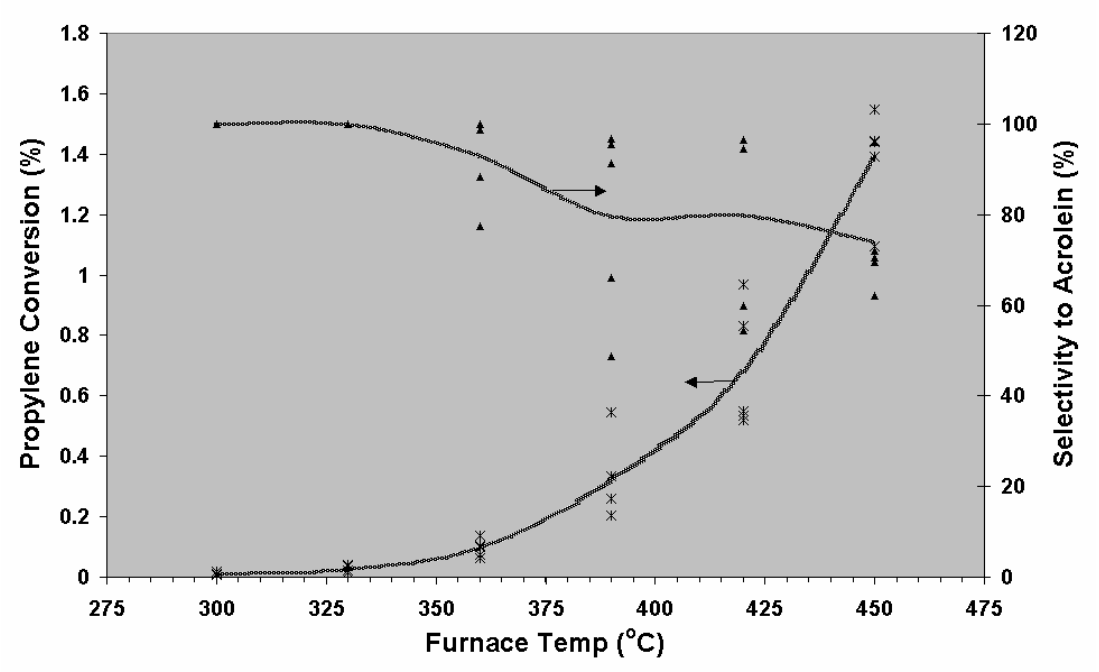

Figure 5.4 Propylene conversion and acrolein selectivity over the β-$Bi_2Mo_2O_9$

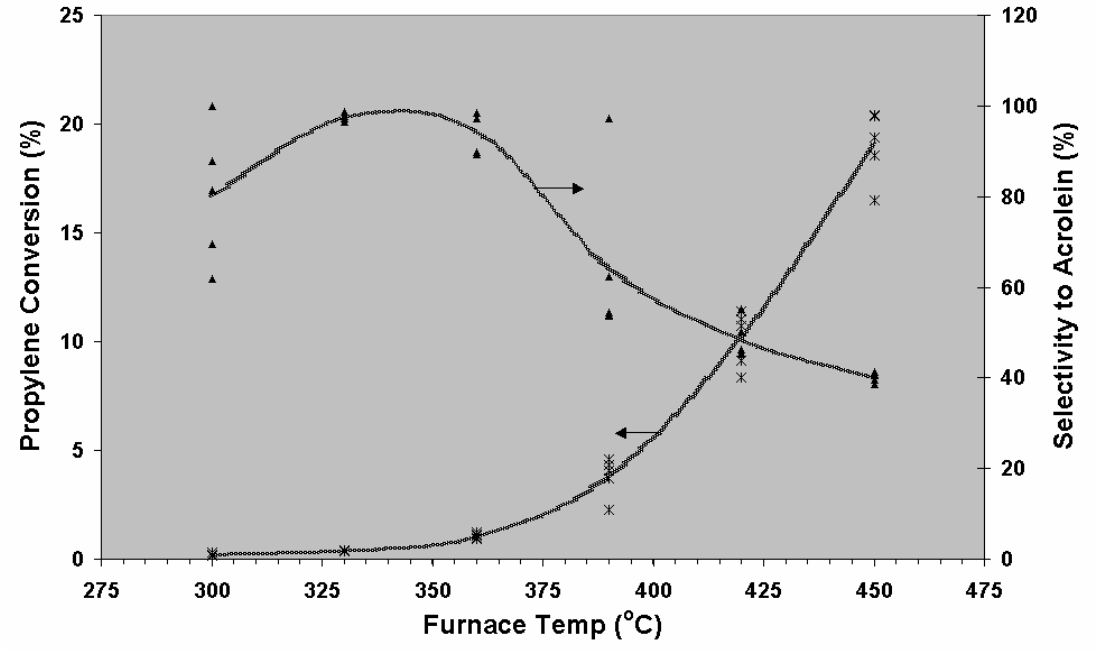

Figure 5.5 Propylene conversion and acrolein selectivity over the γ-Bi_2MoO_6

The change in the catalysts activity and selectivity has very close relation to the change in the crystal structure of the catalyst. As mentioned in section 4 in Chapter 4, the lattice oxygen ions become weakly bonded to metal ions more reactive. The oxygen ions thus more mobile and the oxidations of allyl intermediate become easier. However, at higher temperatures, oxygen ions become too mobile. The high mobility oxygen ions are very reactive but not selective. This is the reason why the catalysts lost their selectivity just as what had been showed by γ-Bi_2MoO_6 above 400^oC. This may take place since oxygen now becomes so reactive that allyl intermediates are oxidised into complete oxidation product (CO_2) (Fansuri et al. 2003).

The nature of oxygen ions in the γ-Bi_2MoO_6 phase is different to those in α-$Bi_2Mo_3O_{12}$ and β-$Bi_2Mo_2O_9$. There is more active oxygen available on the gamma phase per unit cell than in the alpha and beta phase. Therefore, at high temperatures (ca. at 400^oC or higher), more unselective oxygen ions available in the gamma phase. As a result, the selectivity of the gamma phase in converting propylene to acrolein decrease faster than those catalysed by alpha or beta phase. All of these explain the difference activity and selectivity pattern between gamma phase and alpha and beta phase.

The pattern of the catalyst selectivity, though, does not explicitly shows the mechanism of propylene oxidation over the catalyst. Monnier (Monnier & Keulks 1981) revealed that carbon oxides were produced from further oxidation of acrolein and hydrocarbon residue deposited on the surface of the catalysts. Tan (Hock Seng Tan 1986), on the other hand, believed that propylene can be oxidised directly to carbon oxides, while Larsen (Larsen 2003) believes that carbon dioxide was a product of direct oxidation of propylene. Discussion about reaction mechanism deduced from kinetics data collected in this research will be given in Chapter 6.

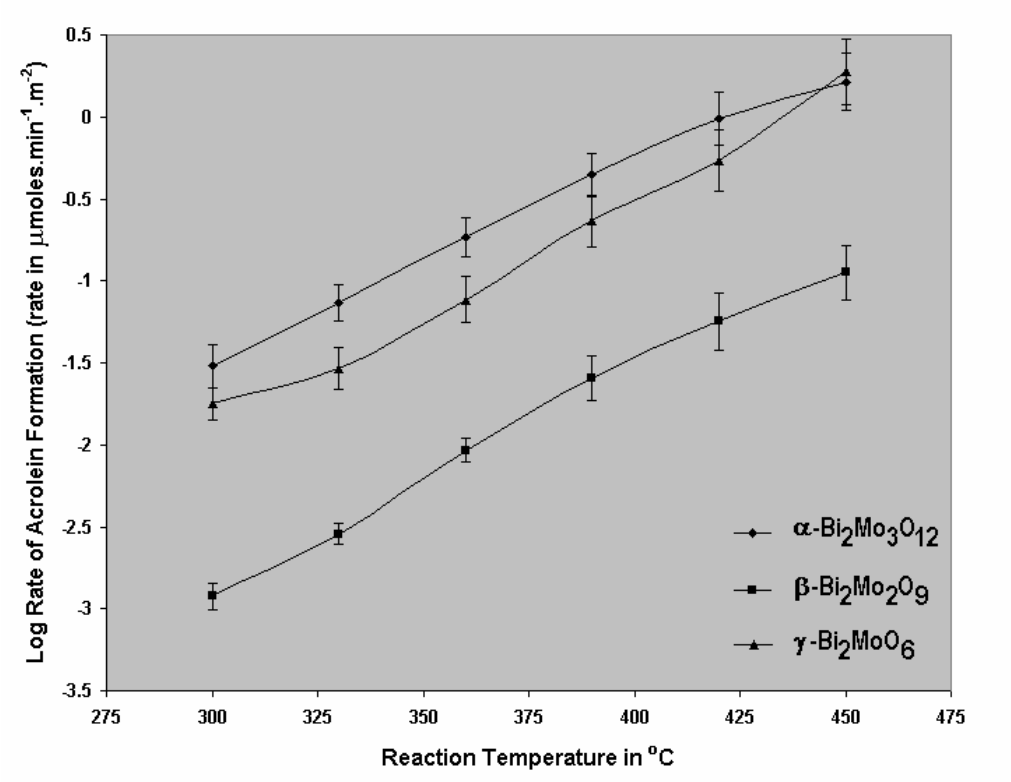

Figure 5.6 Specific rate of Acrolein Formation vs. Reaction Temperature.

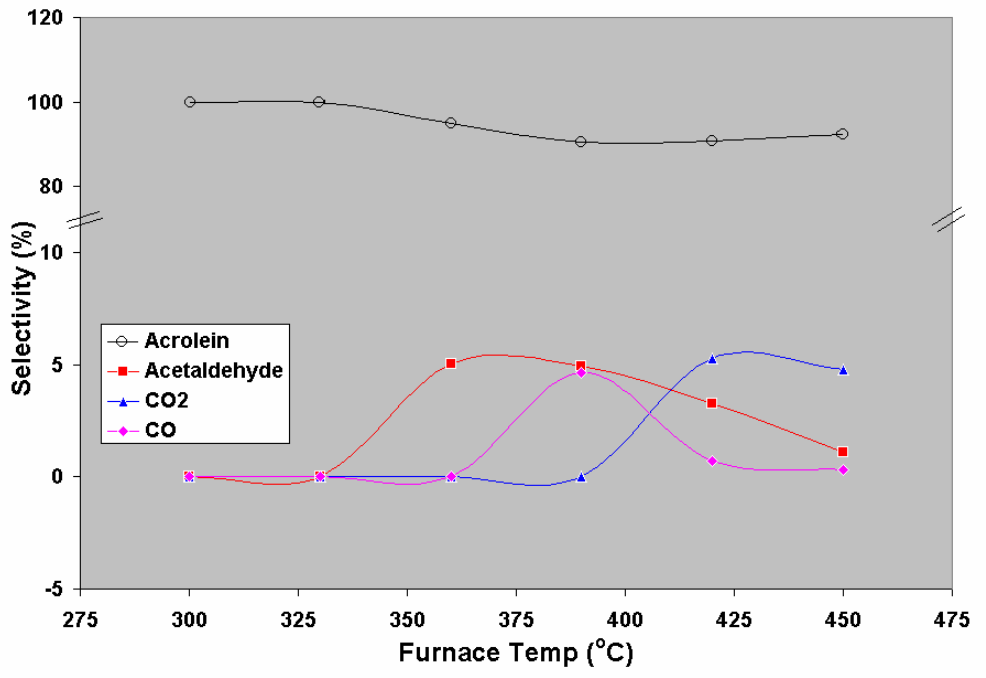

Figure 5.7 Distribution of product selectivity of propylene oxidation over α-$Bi_2Mo_3O_{12}$.

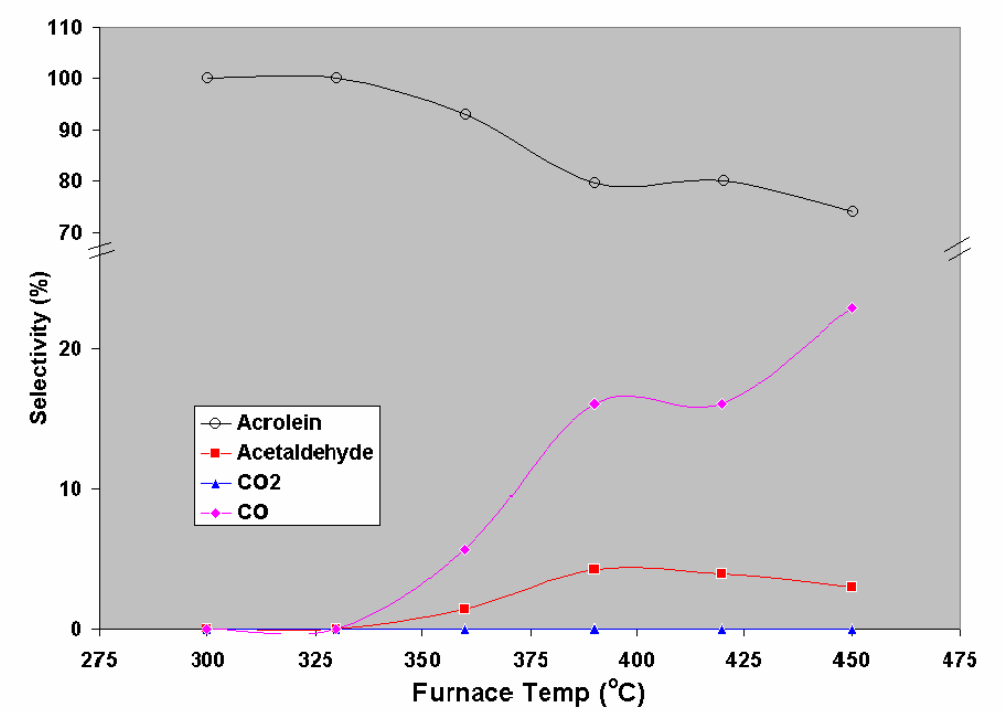

Figure 5.8 Distribution of product selectivity of propylene oxidation over β-$Bi_2Mo_2O_9$.

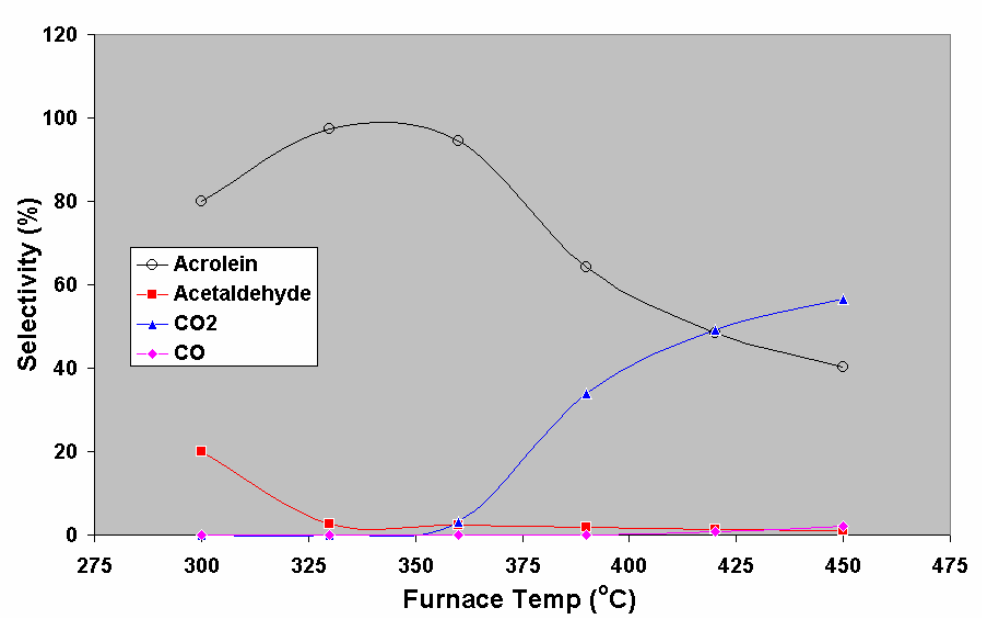

Figure 5.9 Distribution of product selectivity of propylene oxidation over γ-Bi_2MoO_6.

5.3 Kinetics of Partial Oxidation of Propylene into Acrolein

The kinetics of partial oxidation of propylene to acrolein is examined by power rate law (Levenspiel 1999). The reaction orders with respect to propylene and oxygen in the formation of acrolein and carbon oxides were determined at seven different temperatures using the method of constant initial partial concentrations. This method involves holding the concentration of one reactant constant while varying the other and measuring subsequent changes in the rate of reaction. The general relationship between the reaction rate and the reactant concentration for a bimolecular reaction is given by the equations 5.3 and 5.4. In those equations, k is the rate constant, m and n are reaction orders in C_3H_6 and O_2, respectively, and $[C_3H_6]$ and $[O_2]$ are the initial concentrations of propylene and oxygen, respectively.

$$rate = k\,[C_3H_6]^m[O_2]^n \qquad 5.\,3$$

Equation 5.3 can be linearised by taking the logarithmic of both sides. The linear equation is given in equation 5.4.

$$log(rate) = logk + mlog[C_3H_6] + nlog[O_2] \qquad 5.\,4$$

A plot of *log(rate)* versus log of the concentration of one reactant being varied will yield a straight line with the slope being the reaction order in that reactant and the intercept equal to *log(k)*. Such plots are given in Figures 5.10 to 5.15 and the calculated reaction orders in propylene and oxygen towards acrolein formation are given in Table 5.2.

The reaction orders in both propylene and oxygen vary with temperature for all three bismuth molybdate catalysts. For all catalysts, the reaction order in propylene increases from a small fraction or zero order at low temperatures to the first or close to the first order at high temperatures. The reaction order in oxygen decreases from a fractional order at low temperatures to zero or close to zero order at high temperatures.

Table 5.2 Reaction orders in propylene partial oxidation

Temperature (K)	Reaction order of C_3H_6 (m)			Reaction order of O_2 (n)		
	α-$Bi_2Mo_3O_{12}$	β-$Bi_2Mo_2O_9$	γ-Bi_2MoO_6	α-$Bi_2Mo_3O_{12}$	β-$Bi_2Mo_2O_9$	γ-Bi_2MoO_6
573	0.6	0.0	0.6	0.6	0.2	0.3
603	0.6	0.0	0.6	0.6	0.3	0.3
633	0.7	0.4	0.6	0.4	0.4	0.6
663	0.8	0.7	0.7	0.2	0.2	0.6
693	1.0	0.9	0.9	0	0.2	0.0
723	1.0	0.9	0.9	0	0.2	0.0

The dependency of the reaction orders in the propylene and oxygen concentrations is an indication that the catalysts are taking a part in the oxidation reaction. At low temperatures ($\leq 390^oC$), a very small amount of lattice oxygen ions are available for oxidising propylene. As a result, the oxygen ions in the gas phase (from the reactant) are taking a part in the reaction. The less availability of lattice oxygen is also a key reason of the dependency of reaction order in the propylene concentration. Because of insufficient oxygen available for the reaction, adding more propylene to the system would not increase the reaction rate or acrolein yield. The explanation on the reaction mechanisms will be given in Chapter 6.

The specific rate constant for acrolein formation at a given temperature was calculated from the observed specific rate of formation and the calculated reaction orders for oxygen and propylene at that temperature by using equation 5.1. The rate constants obtained at a given temperature were essentially the same. Therefore, the average value was used to calculate the apparent activation energy. The average values of reaction constant are given in Table 5.3.

The apparent activation energy was determined from the Arrhenius relationship between the temperature and the rate constant. This relationship is given by equation 5.3. A plot of *ln(k)* vs 1/T yields a straight line with a slope of ($-E_a/RT$) and an intercept of *ln(A)*. The Arrhenius plots of acrolein formation over all three catalysts studied are given in Figures 5.16 to 5.18.

$$k = Ae^{-Ea/RT} \qquad 5.5$$

The plots of *ln(k)* versus *1/T* of acrolein formation over all bismuth molybdate catalysts give a straight line. The slopes of these lines and the intercepts were determined by a linear regression analysis and the resulting activation energy and pre-exponential factors are given in Table 5.3. The R^2 values for all regressions are more than 90%, indicating the good fit of the data to the model.

The data shown in Table 5.3 compare very well with the results reported by Krenzke (Leonard David Krenzke 1977; L. David Krenzke & Keulks 1980b) for the alpha and gamma phases but different from those reported by Monnier (Monnier & Keulks 1981) for the beta phase. Both Krenzke (Leonard David Krenzke 1977; L. David Krenzke & Keulks 1980b) and Monnier et al. (Monnier & Keulks 1981) reported the evidence of change in activation energy in two temperature regions. The activation energy was high at low temperature region (less than 400) and low at temperatures higher than 400^{o}C. The results from experiments carried out in this thesis, however, did not show clear evidence of the two temperature regions as reported by Krenze and Monnier. Instead, activation energies found from the experiments are within the low and high activation energies reported by both researchers. In the case of the beta phase, the reaction rate parameters are close to high temperature parameters reported by Monnier et al. (Monnier & Keulks 1981).

The kinetic parameters for the beta phase found in this research, however, is slightly different from those reported by Larsen (Larsen 2003). Larsen investigated the kinetics of propylene oxidation to acrolein over β-$Bi_2Mo_2O_9$ under different reaction conditions. He found that the activation energies vary between 72 kJmol^{-1} and 140 kJmol^{-1} and reaction order of propylene and oxygen was 1.0 ± 0.1 and 0.3 ± 0.1, respectively. The β-$Bi_2Mo_2O_9$ used by Larsen, though, is not pure. It also contains alpha and gamma phase. The mixture phase will enhance the catalyst activity as well as selectivity toward selective products as mentioned by some reports (Bettahar et al. 1996; Carrazan et al. 1996b; Carson et al. 1983; Le et al. 2004).

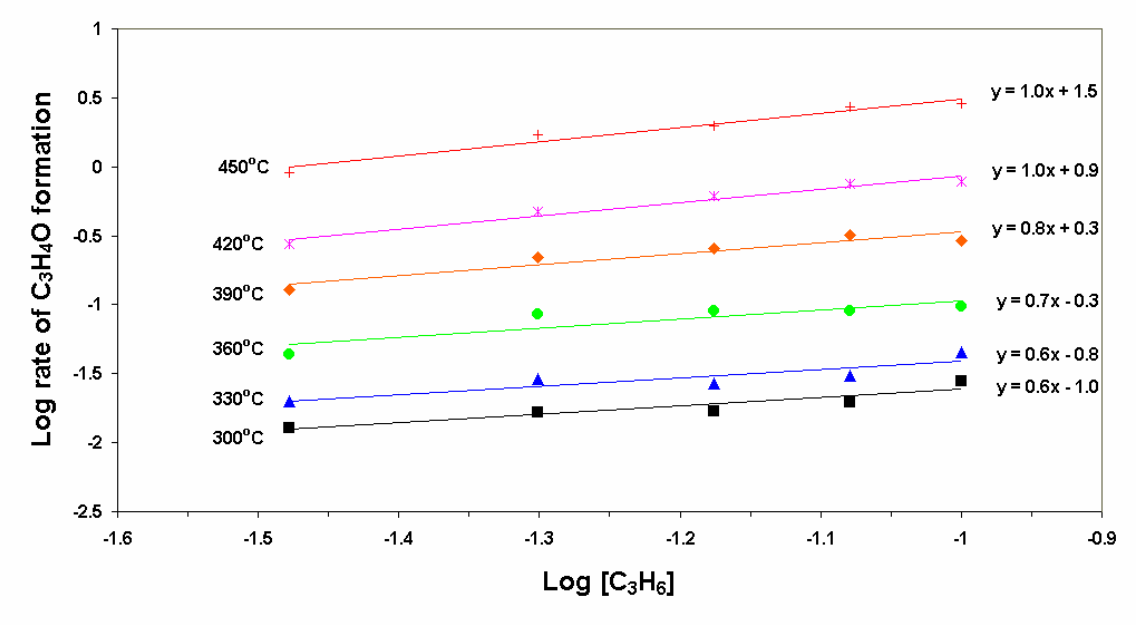

Figure 5.10 Reaction order in propylene over α-$Bi_2Mo_3O_{12}$.

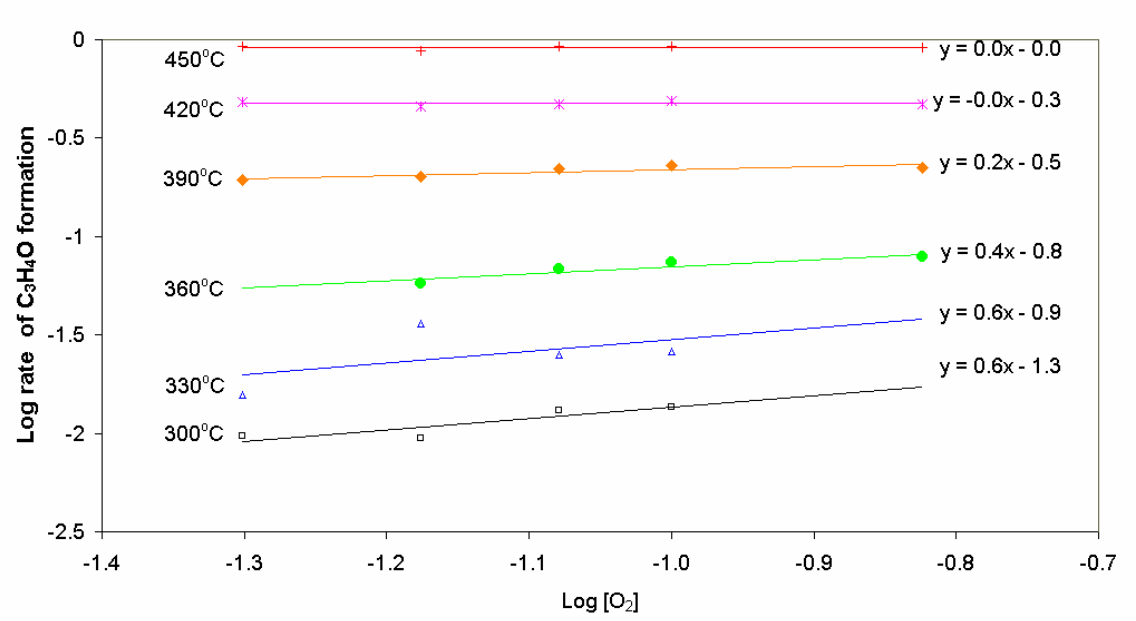

Figure 5.11 Reaction order in oxygen over α-$Bi_2Mo_3O_{12}$.

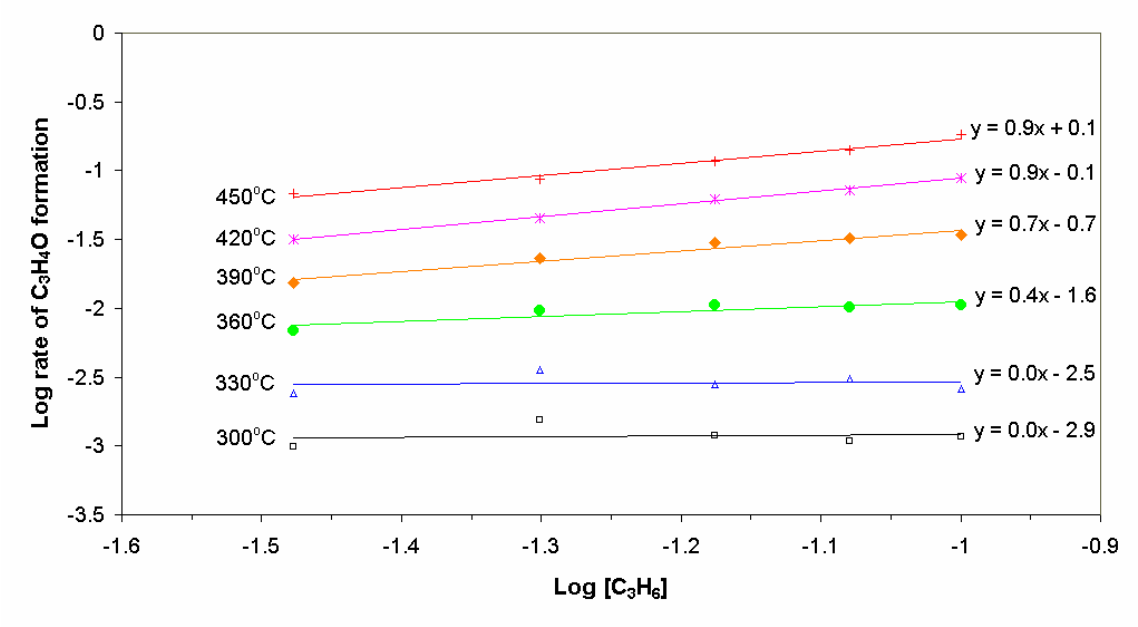

Figure 5.12 Reaction order in propylene over β-$Bi_2Mo_2O_9$.

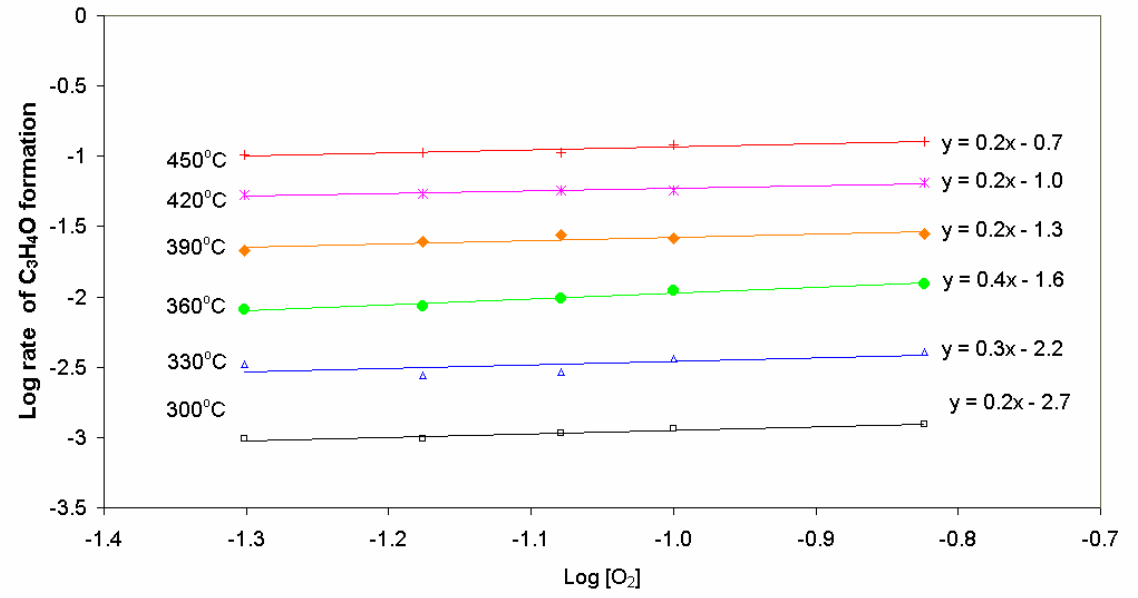

Figure 5.13 Reaction order in oxygen over β-$Bi_2Mo_2O_9$.

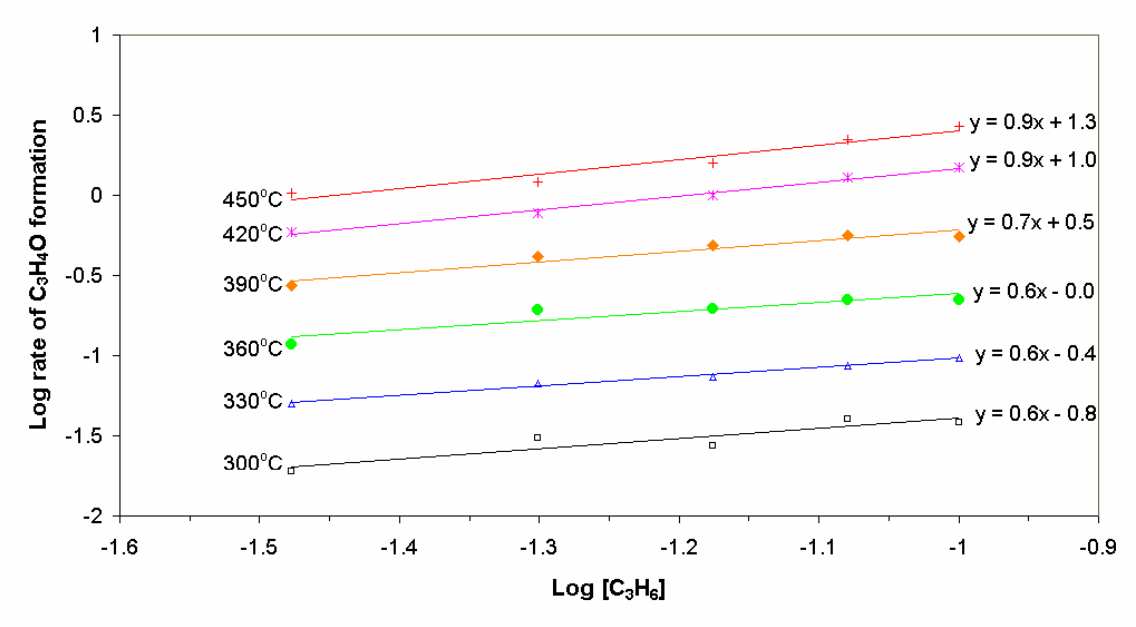

Figure 5.14 Reaction order in propylene over γ-Bi_2MoO_6.

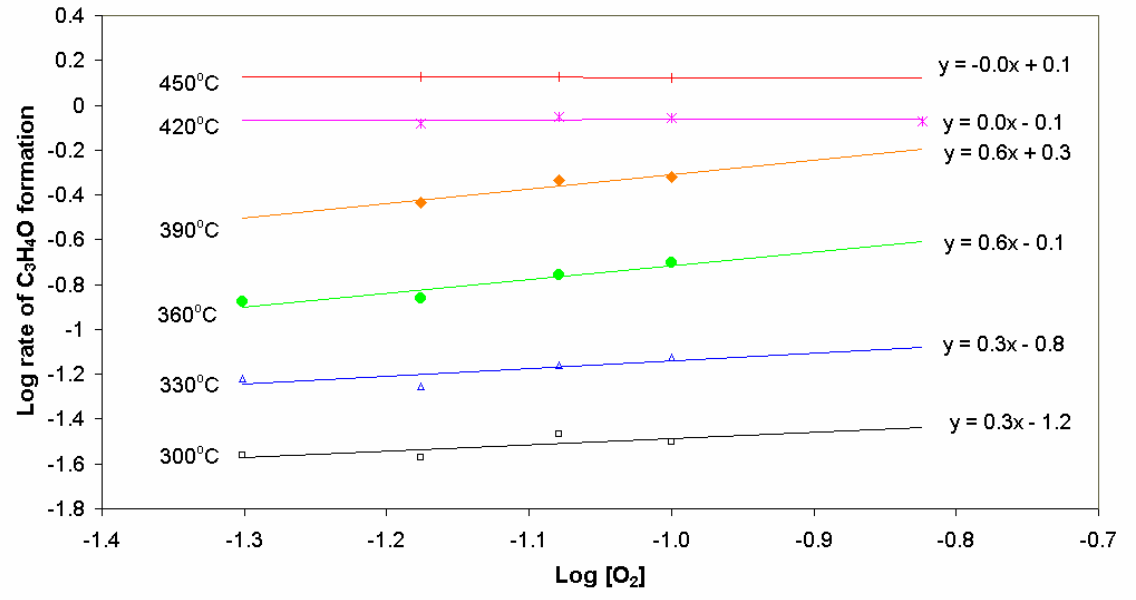

Figure 5.15 Reaction order in oxygen over γ-Bi_2MoO_6.

Table 5.3 Reaction rate constant (k) of acrolein formation calculated using equation 5.1.

Catalyst	Temperature (K)	k ($min^{-1}m^{-2}$)	m	n
α-$Bi_2Mo_3O_{12}$	573	0.4	0.6	0.6
	603	0.6	0.6	0.6
	633	1.4	0.7	0.4
	663	3.4	0.8	0.2
	693	8.7	1.0	0
	723	30.6	1.0	0
β-$Bi_2Mo_2O_9$	573	0.002	0.0	0.2
	603	0.006	0.0	0.3
	633	0.072	0.4	0.4
	663	0.287	0.7	0.2
	693	1.093	0.9	0.2
	723	2.167	0.9	0.2
γ-Bi_2MoO_6	573	0.6	0.6	0.3
	603	1.5	0.6	0.3
	633	3.9	0.6	0.6
	663	9.4	0.7	0.6
	693	20.7	0.9	0.0
	723	34.9	0.9	0.0

Table 5.4 Reaction rate parameters for acrolein formation

Catalyst	A ($min^{-1}.m^{-2}$)	E_a ($kJ.mol^{-1}$)
α-$Bi_2Mo_3O_{12}$	3.05×10^8	99.69
β-$Bi_2Mo_2O_9$	9.62×10^{12}	173.00
γ-Bi_2MoO_6	4.69×10^8	97.66

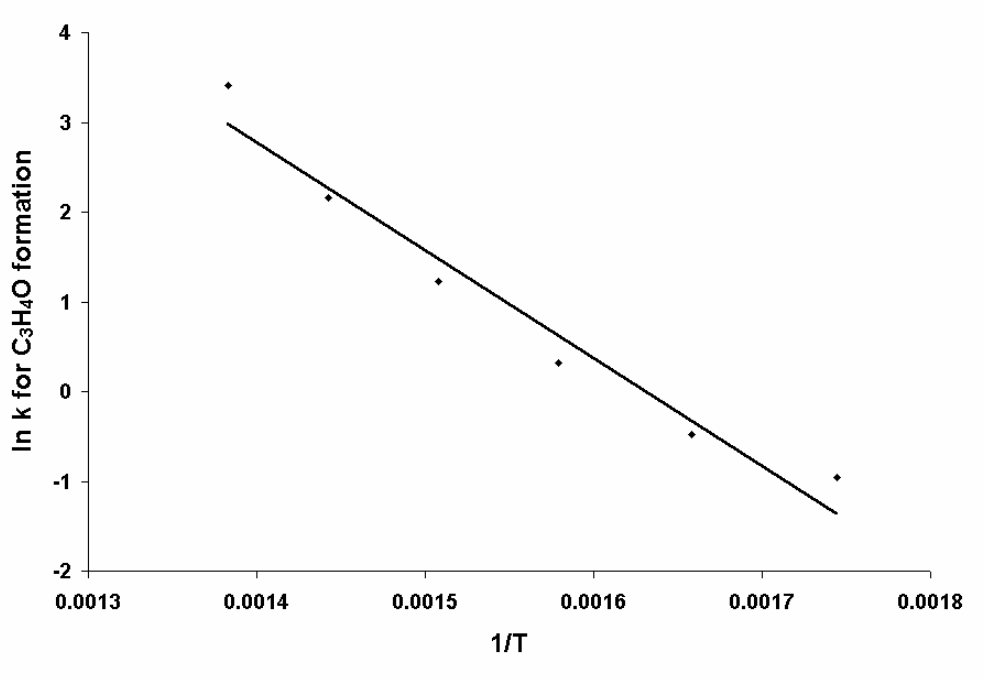

Figure 5.16 An Arrhenius plot for acrolein formation over α-$Bi_2Mo_3O_{12}$

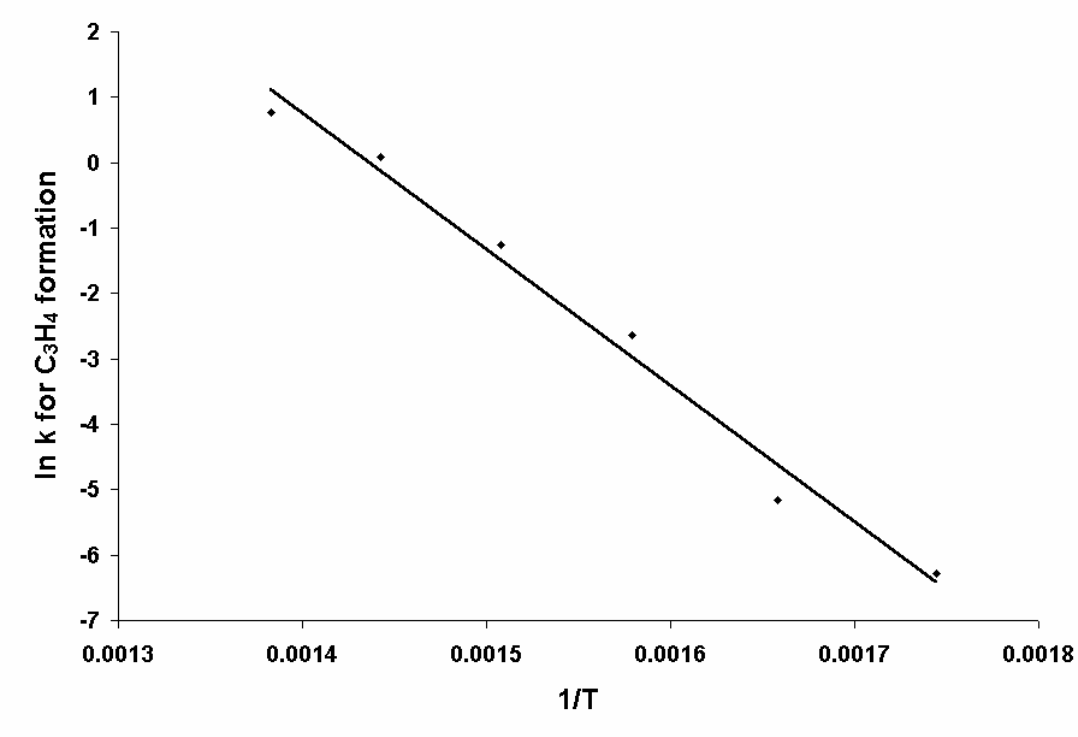

Figure 5.17 An Arrhenius plot for acrolein formation over β-$Bi_2Mo_2O_9$

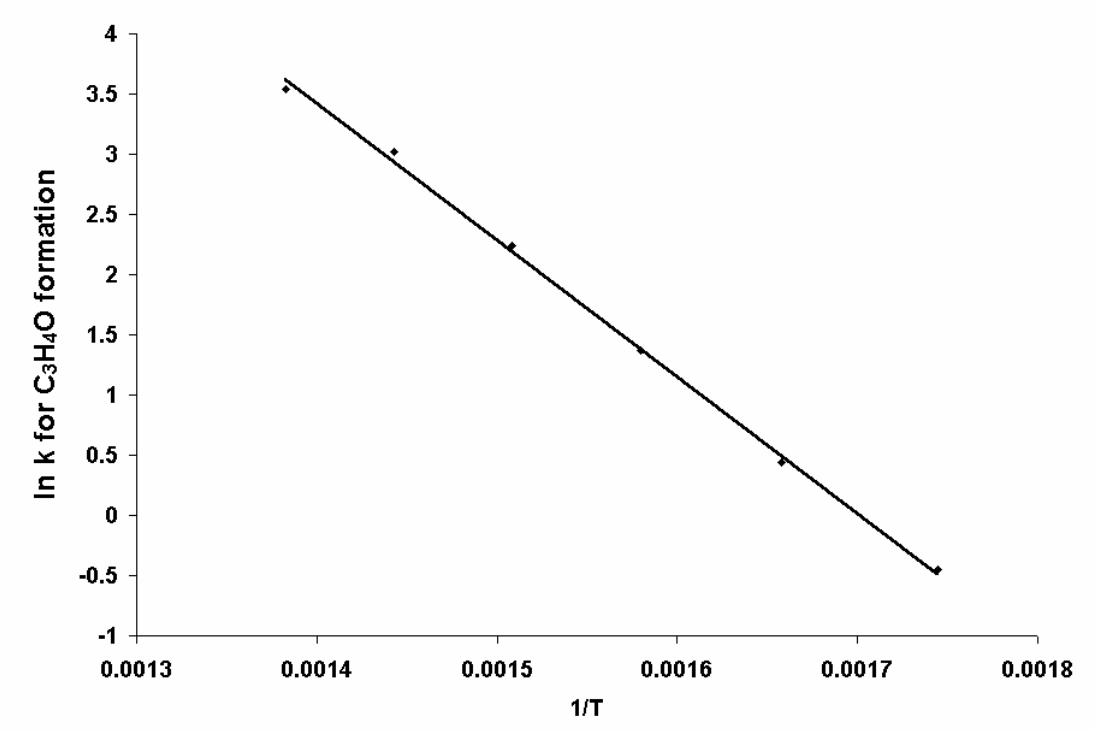

Figure 5.18 An Arrhenius plot for acrolein formation over γ-Bi_2MoO_6

5.4 Kinetics of Formation of Side Products

As mentioned above, the partial oxidation of propylene also produces side products. The side products detected in the present experiments were C_2H_4O (acetaldehyde), CO_2, and CO.

The concentrations of side products were very small and in all cases almost undetectable in the experiments. They were detected in the reaction products in all catalysts at reaction temperature equal or higher than 360^oC.

The kinetic parameters of acetaldehyde formation are given in Table 5.4. As in acrolein, the reaction order of propylene and oxygen in the formation of acetaldehyde is also fractional. Combination of activation energy and pre-exponential factor results in slow overall reaction rate of acetaldehyde formation.

In contrast to acetaldehyde, the formation of CO_2 and CO is very slow at temperatures lower than 390°C. Even at temperatures higher than 390°C, the CO_2 and CO formation is still very slow. Only CO_2 formation over γ-Bi_2MoO_6 is significantly high, from which the kinetic data could be estimated.

The kinetic parameters for CO_2 formation are given in Table 5.5. The parameters are very close to those obtained by Krenzke (Leonard David Krenzke 1977). Although the pre-exponential value is high, its activation energy is high too. As a result, the rate of CO_2 formation is very slow at low temperatures (below 390°C) and significantly increases above that temperature as shown in Figure 5.9.

Table 5.5 Reaction orders of propylene (m) and oxygen (n), activation energies and pre-exponential factors in the formation of acetaldehyde

	α-$Bi_2Mo_3O_{12}$		**β-$Bi_2Mo_2O_9$**		**γ-Bi_2MoO_6**	
Temperature (°C)	**m**	**n**	**m**	**n**	**m**	**n**
360	0.4	1.3	0.3	0	0.9	0.6
390	1.0	0.5	0.6	0.6	0.5	0.5
420	1.2	0.4	0.9	0.6	0.2	0.3
450	1.3	0.3	1.2	0.6	0.1	0.2
E_a (kJ mol^{-1})	33.2		150.4		83.9	
A (min^{-1} m^{-2})	$6.9x10^3$		$2.17x10^{10}$		$7.3x10^5$	

According to Krenzke (Leonard David Krenzke 1977), CO_2 is exclusively produced from further oxidation of acrolein. Tan (Hock Seng Tan 1986), on the other hand, mentioned that the CO_2 is also produced by gas phase oxidation of propylene as experimentally evidenced by the production of CO_2 in blank reactor test. The same was evidenced for CO.

The results of this research support the mechanism proposed by Krenzke (Leonard David Krenzke 1977), where carbon oxides (CO_2 and CO) are formed by further oxidation of propylene partial oxidation products (acrolein and acetaldehyde). The first evidence is shown by the result of blank run in which no carbon oxides

were found when propylene and oxygen were passed through the blank reactor. When acrolein and oxygen were passed through the blank reactor, carbon oxides were found in the product stream. Catalysts selectivity test also showed evidence that carbon oxides were more probably formed from further oxidation of acrolein and acetaldehyde. The selectivity test showed that the acrolein and acetaldehyde selectivity decreased as the selectivity to CO_2 and CO increases. The total reaction order of CO_2 formation being greater than one is also a piece of evidence supporting that carbon oxides are formed from further oxidation of products.

Table 5.6 Kinetic parameters of CO_2 formation over γ-Bi_2MoO_6

	γ-Bi_2MoO_6	
Temperature (^oC)	**m**	**n**
390	0.9	0.3
420	0.9	0.3
450	1.1	0.2
E_a (kJ mol^{-1})	196.9	
A (min^{-1} m^{-2})	$5.3x10^{16}$	

In contrast to CO_2 and CO, not much information are available for the formation of acetaldehyde as a side product of partial oxidation of propylene over bismuth molybdate. Some Russians researchers (Gorshkov et al. 1970; Gorshkov et al. 1969; Gorshkov et al. 1968) reported that the acetaldehyde is formed trough further oxidation of acrolein or from direct oxidation of the π-allyl intermediate, which is rapidly oxidised into carbon oxides. The report, though, did not mention the kinetic of acetaldehyde formation. Even the recent reports (Leonard David Krenzke 1977; Larsen 2003; Monnier & Keulks 1981; Hock Seng Tan 1986) do not mention the formation of acetaldehyde.

5.5 Summary

The discussion on the results of the kinetic studies in this chapter can lead to the following conclusions:

1. The quartz reactor can be regarded as inert for the partial oxidation reaction.
2. The catalyst performance decreases in the order of α>γ>β in term of acrolein production rate versus reaction temperature.
3. There are no clear evidence of two activation energy regions as shown by Krenzke (Leonard David Krenzke 1977) and Monnier (Monnier & Keulks 1981). However, the value of activation energies and pre-exponential factors found in this research are within those reported by Krenzke for alpha and gamma phase and by Monnier for the beta phase.
4. Carbon oxides are produced from further oxidation of acrolein and acetaldehyde.

Chapter 6

REACTION MECHANISMS OF PARTIAL OXIDATION OF PROPYLENE TO ACROLEIN OVER BISMUTH MOLYBDATE CATALYSTS

Reaction mechanisms of partial oxidation of propylene to acrolein over bismuth molybdate catalysts have been investigated by many researchers. However, as mentioned in Chapter 2, the reaction mechanisms are still open to exploration.

There are three approaches that are normally used to investigate the reaction mechanisms, namely, 1) isotope tracing (Adams & Jennings 19631964; Adams et al. 1964; Keulks & Lo 1986; L. David Krenzke & Keulks 1980a; Miura et al. 1979; Voge, Wagner & Stevenson 1963), 2) molecular mechanisms by spectroscopic methods (Ayame et al. 2000; Ayame et al. 2002; Bemis, Douskey & Munson 1997; Boudeville et al. 1979; Burlamacchi, Martini & Ferroni 1971; Carrazan et al. 1996a; Douskey & Munson 1997; Matyshak & Krylov 1995; Uchida & Ayame 1996) and, 3) mechanisms derived from kinetic experiments.

The reaction mechanism investigation using kinetic information can be further divided into two approaches. In the first approach, the reaction mechanisms are deduced from kinetic data. In this method, several models of reaction

mechanisms are proposed and fitted with data from kinetic experiments, respectively. The model, which has the best fit to the experimental data, is chosen and considered to be the *correct* reaction mechanisms.

In the second approach, reaction mechanisms are postulated based on physical and chemical analysis of the catalysts and reactions at molecular level. This is normally achieved with the spectroscopic and isotope-labeling methods to detect and identify reaction intermediates. Based on the intermediates identified, a possible reaction mechanism is postulated.

In this thesis, the reaction mechanisms are investigated using some combinations of the aforementioned methods. The available data for the investigation from own experiments are the kinetic data and time resolved catalysts structure information to rationalise the mechanisms occurring in the catalysts lattice.

6.1 Reaction Mechanisms Derived from Kinetic Data

The kinetic data in this discussion are regarded as products of single reaction, i.e., partial oxidation of propylene to acrolein. The by-products are regarded as a result of direct oxidation of propylene and do not have any interference with acrolein formation.

The experimental data for acrolein formation have been fitted to a linearised form of the power rate law as discussed in Chapter 4. The power rate law was chosen because it is simple and easy to use. In this law, the only parameters described are the rate constant and the dependence on concentrations for the reactants and products.

Although the kinetic data fit well with the power rate law, their kinetic parameters show that the reaction mechanisms are more complex than those suggested by the model. One example is the dependency of the reaction orders of both propylene and oxygen on the reaction temperature. The model also does not explain mechanisms of surface reactions that commonly happen in heterogeneous catalytic reactions.

In order to uncover the reaction mechanisms, the kinetic data obtained are tested with various rate equations given in Chapter 3. The rate equations are derived from commonly used heterogeneous kinetic reaction mechanisms. To discriminate rival mechanisms, the kinetic data are fitted with calculated values of each mechanism. The fitting procedure has been used by several researchers in investigating the kinetics and reaction mechanisms of partial oxidation of propylene over various catalysts (Benyahia & Mearns 19901991; Corberan, Corma & Kremenic 1985; Kremenic et al. 1987; Kremenic et al. 1988). Our experimental measurements are for initial rates. Prior to fitting, the rate equations of various mechanisms models were linearised. The linearised forms of the rate equations are given in Table 6.1 and Table 6.2. In order to compare the different models, the square of correlation coefficients (R^2) are chosen as parameters for discrimination (better fits are indicated by higher R^2 values). The influence of propylene (or oxygen) partial pressure is examined by fitting the rate data versus P_h (or P_O), while keeping P_O (or P_h) constant.

The results of the fitting of the experimental data with the linearised forms of various reaction rate laws under different reaction mechanisms are given in Table 6.3. Model 1 is based on the power rate law as used for estimation of the kinetic data in Chapter 5. The model is excluded from the table because it could not explain the reaction mechanisms of propylene oxidation to acrolein. The results of the use of Model 1 are discussed in Chapter 5.

The R^2 is a square correlation value. This value shows how a change in one variable (eg, the partial pressure of oxygen or propylene according to the linear form of rate equation) affects the other (eg, reaction rate). When there is no correlation between these two variables, the correlation value will be zero. On the other hand, if there is a straight correlation, the value will be 1.

The R^2 values for all catalysts in Table 6.4 reveal that the kinetic data are worst described by models 2a and 2b. These two models are derived with an assumption that oxygen and propylene compete for the same adsorption site. The fact that experimental data do not fit with these two models is an indication that if the reaction follows Langmuir-Hinshelwood mechanisms, the propylene adsorption sites would be different from the oxygen adsorption sites. Kremenic and co-workers (Corberan, Corma & Kremenic 1985; Kremenic et al. 1987; Kremenic et al. 1988)

reported the evidence of different oxygen and propylene adsorption sites from oxygen and propylene adsorption-desorption experiments on Mo-Pr-Bi catalysts. The facts that oxygen and propylene do not compete on the bismuth molybdate surface also supported by numerous reports (Ayame et al. 2000; Ayame et al. 2002; Bielanski & Haber 1991; Cullis & Hucknall 1981; B. Grzybowska, Haber & Janas 1977; R. Grzybowska et al. 1976; Hayden & Higgins 1976; Ono, Ogata & Kuczkowski 1998) indicating that the source of oxygen for selective partial oxidation comes from the lattice oxygen within the catalyst. The *in-situ* characterisation detailed in Chapter 4 also suggested the possibility of the lattice oxygen as active oxygen source for partial oxidation, which provides support the hypothesis that the oxygen and propylene adsorption sites are different and they do not compete with each other. As a result, reaction mechanisms based on competing adsorption site Langmuir-Hinshelwood model is not suitable.

The square of correlation parameters (R^2) of all mechanism models over bismuth molybdate under constant propylene is not as regular as that under constant oxygen pressure. In most cases, the R^2 values are smaller at the lowest and the highest temperatures used in the reaction (573 and 723 K). However, the R^2 indicated that the fit of experimental data with models *a* and *b* of each models (models 3, 4, 5, and 6) are equally well for all catalysts. Hence it means that using the R^2 values alone are not adequate to discriminate which mechanisms are the best to explain the experimental kinetic data.

Table 6.1 Linearised form of Rate Law for Variable Propylene Pressure

Equation No.	Model No.	Linearised form
3.5	2a and 2b	$\left(\frac{P_h}{r_a}\right)^{\frac{1}{2}} = A_h P_h + B_h$ 6. 1
3.6 3.7 3.8 3.9	3a, 3b 4 5a, 5b 6a, 6b	$\frac{1}{r_a} = A_h\left(\frac{1}{P_h}\right) + B_h$ 6. 2

Although model 4 gives a reasonably good fit to the observed kinetic data, it is excluded from further consideration because the model is developed with an assumption that one of the reactants (oxygen or propylene) reacted with a surface intermediate to form the product (acrolein). It has been proven by many researchers that acrolein formed via allyl radical intermediate and oxidation of the radical uses lattice oxygen. With this reason, the assumption that the surface intermediate reacts with gaseous oxygen is inapplicable for the formation of acrolein and hence, model 4 could not be used to explain the reaction mechanisms.

Table 6.2 Linearised form of Rate Law for Variable Oxygen Pressure

Equation No.	Model No.	Linearised form
3.6 3.8 3.9	3a 5a 6a	$\frac{1}{r_a} = A_O\left(\frac{1}{P_O}\right) + B_O$ 6. 3
3.6 3.8 3.9	3b 5b 6b	$\frac{1}{r_a} = A_O\left(\frac{1}{P_O^{\frac{1}{2}}}\right) + B_O$ 6. 4
3.7	4	$r_a = A_O P_O$ 6. 5

In order to further identify the best reaction model to represent the reaction mechanisms, the observed acrolein formation rates are plotted against the calculated reaction rate. The plots are given in Figures 6.1 to 6.3. Kremenic (Kremenic et al. 1987; Kremenic et al. 1988) and Benyahia (Benyahia & Mearns 19901991) used the same methods successfully in the past to discriminate the models under similar condition. Further examination of the best fit by investigating the observed versus calculated reaction rates shows that models 3, 5a and 6a are the best model to describe the reaction mechanisms of partial oxidation over alpha, beta and gamma bismuth molybdates, respectively. Only in the reaction catalysed by γ-Bi_2MoO_6, model 5a and 6a deviated from the 45^o line. The reason for this deviation is the

formation of by-products due to further oxidation of acrolein. At high reaction rates (hence, high propylene conversion at high temperatures), some of the acrolein formed are oxidised further to carbon oxides. As a result, the observed reaction rates become smaller than the calculated one.

Table 6.3 The fitting of experimental data at constant oxygen pressures to Various Reaction Mechanisms Models

Model	Temp (K)	R^2		
		α-$Bi_2Mo_3O_{12}$	β-$Bi_2Mo_2O_9$	γ-Bi_2MoO_6
2a and 2b	573	0.573	0.983	0.648
	603	0.521	0.989	0.965
	633	0.648	0.962	0.870
	663	0.543	0.865	0.886
	693	0.101	0.623	0.593
	723	0.008	0.281	0.084
3a, 3b, 4, 5a, 5b, 6a and 6b	573	0.859	0.739	0.868
	603	0.825	0.973	0.990
	633	0.859	0.866	0.902
	663	0.941	0.981	0.970
	693	0.978	0.997	0.983
	723	0.969	0.971	0.909

It has been proven that oxygen does not dissociate upon adsorption on the surface of bismuth molybdate (Kremenic et al. 1987). This means that although model 3 fits well with the experimental data, it cannot be used to explain the reaction mechanisms since the model contradicts the fact that oxygen does not dissociate on the catalysts surface. Meanwhile, as mentioned earlier, models 5 and 6 are actually only different in the form of oxygen participating in the reaction. Both are derived from the Mars van Krevelen mechanisms. Following this, it can be concluded that the catalytic partial oxidation of propylene over bismuth molybdate follows the redox mechanisms. The redox mechanisms over bismuth molybdate catalysts are further discussed below.

Table 6.4 Fitting of experimental data at constant propylene pressures to Various Reaction Mechanisms Models

Model	Temp (K)	R^2		
		α-$Bi_2Mo_3O_{12}$	β-$Bi_2Mo_2O_9$	γ-Bi_2MoO_6
3a, 5a and 6a	573	0.718	0.866	0.531
	603	0.982	0.931	0.956
	633	0.942	0.929	0.842
	663	0.911	0.866	0.977
	693	0.969	0.812	0.936
	723	0.758	0.833	0.689
3b, 5b and 6b	573	0.746	0.908	0.541
	603	0.972	0.923	0.943
	633	0.895	0.950	0.872
	663	0.932	0.820	0.971
	693	0.978	0.872	0.911
	723	0.824	0.874	0.642
4	573	0.823	0.930	0.510
	603	0.941	0.900	0.719
	633	0.796	0.947	0.930
	663	0.960	0.664	0.941
	693	0.994	0.966	0.821
	723	0.972	0.910	0.482

6.2 Redox Reaction Mechanisms

The basic concept of the redox mechanism is that the lattice oxygen of reducible a metal oxide serves as effective oxidising agent for hydrocarbons. The details of the mechanisms of reduction-reoxidation are described schematically in Figure 6.4. However, a number of investigators (Aykan 1968; Batist et al. 1968; Peacock et al. 1969) have shown quantitatively that product formation and catalyst reduction proceed simultaneously. It was also shown that the rate of this reaction decreases rapidly with an increase in the degree of catalyst reduction. Consequently, in order to maintain a continuous catalytic reaction, the catalyst's oxygen must be

continually replenished via reoxidation from the gas phase. Due to these reasons, the redox mechanisms can be simplified as shown by R.3 and R.4.

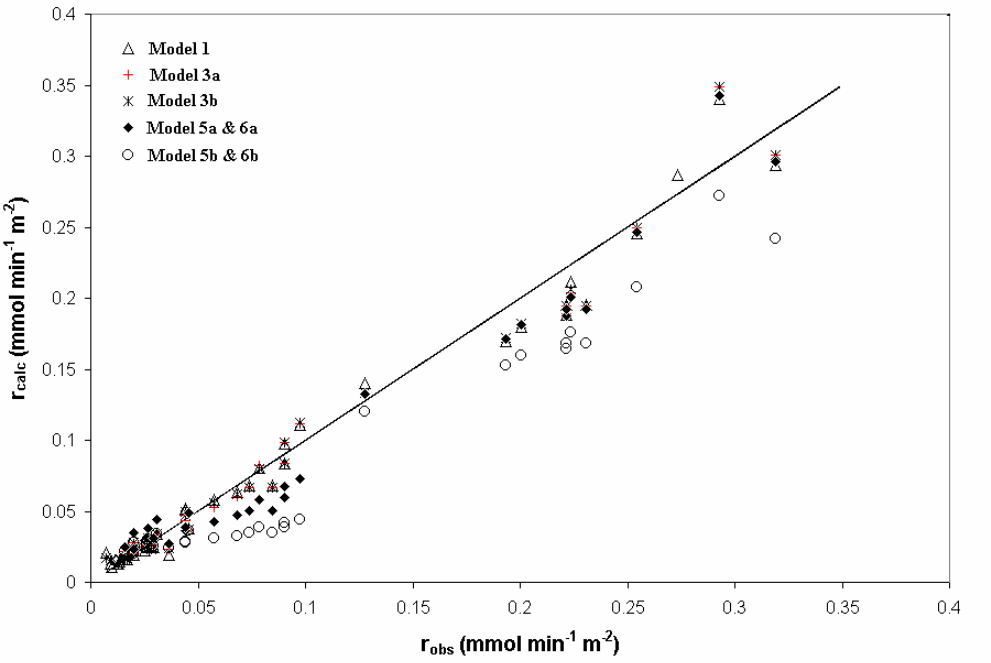

Figure 6.1 Observed versus calculated rates of acrolein formation over α-$Bi_2Mo_3O_{12}$

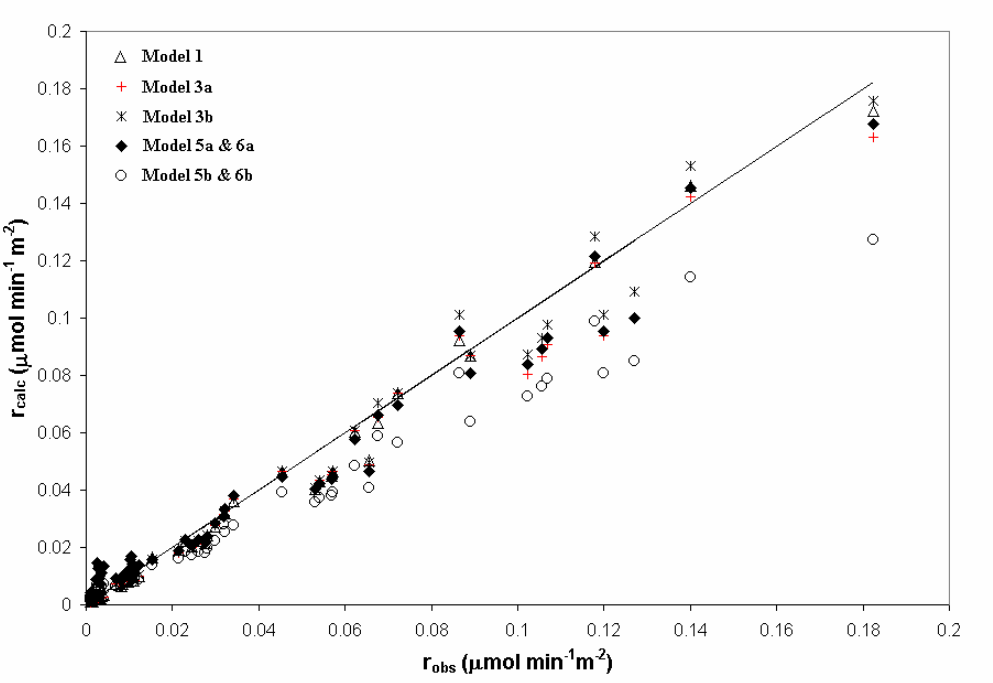

Figure 6.2 Observed versus calculated rates of acrolein formation over β-$Bi_2Mo_2O_9$

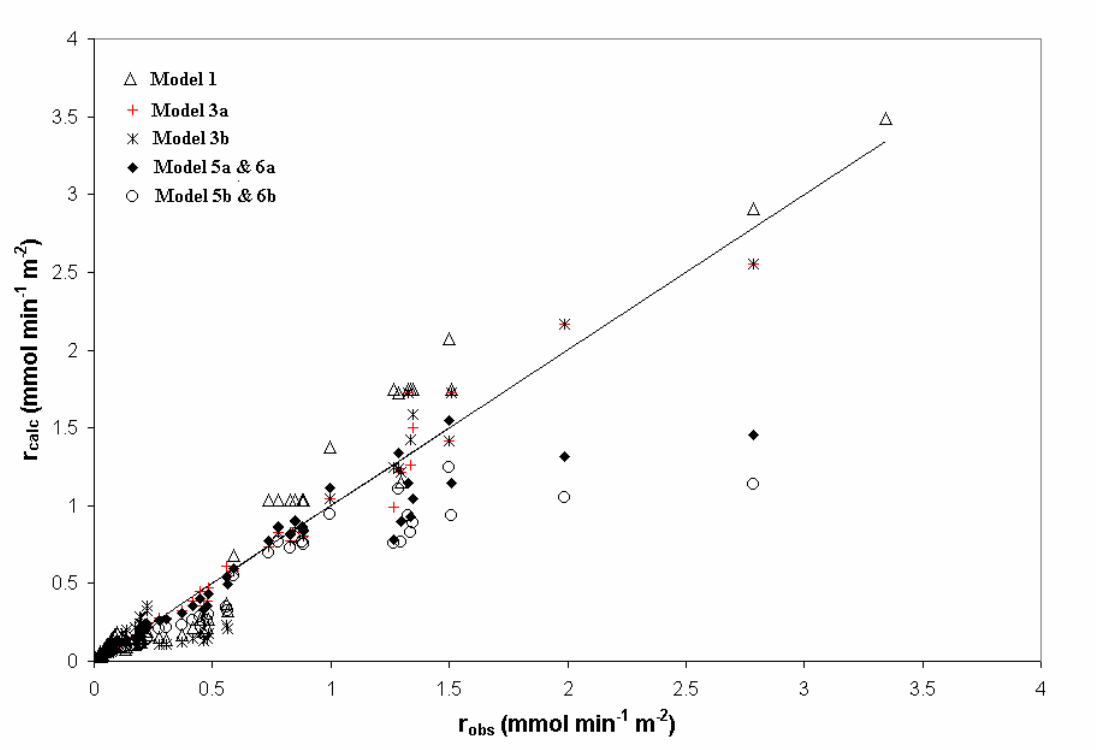

a)

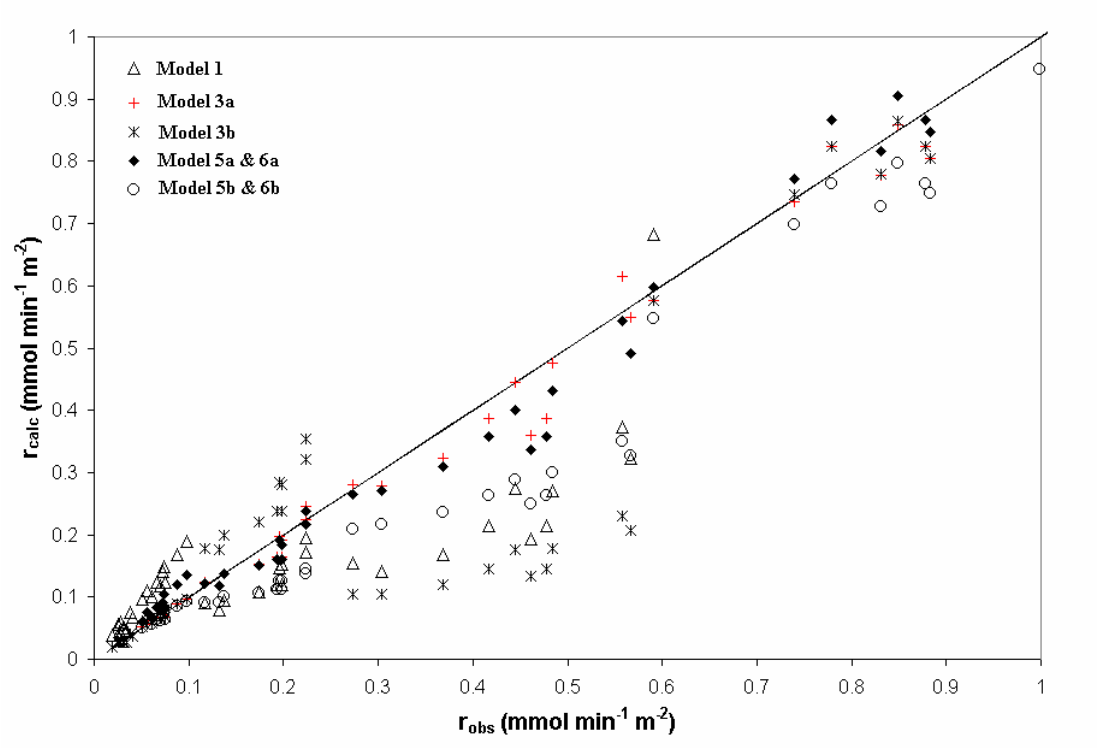

b)

Figure 6.3 Observed versus calculated rates of acrolein formation over γ-Bi_2MoO_6, a) over all observed reaction rate and b) at low propylene conversion

$$C_3H_6 + S_{ox} \xrightarrow{red} C_3H_4O + H_2O + S_{red} \quad \text{R.3}$$

$$S_{red} + O_2 \xrightarrow{ox} S_{ox} \quad \text{R.4}$$

In the above reactions, S_{ox} represents a fully oxidised active site and S_{red} represents a reduced active site. If the total number of active site is N and the fraction of sites, which are fully oxidised, is θ_{ox}, the total number of fully oxidised sites (S_{ox}) is $N\theta_{ox}$ and the total number of reduced sites (S_{red}) is therefore $N(1-\theta_{ox})$.

With this concept and the assumption that the desorption of acrolein is not a rate determining step, the rate equation for propylene oxidation can be written as equation 6.6 and the rate of catalyst reoxidation is written as equation 6.7.

$$-\frac{1}{V}\frac{d[C_3H_6]}{dt} = k_{red} P_{C_3H_6} N\theta_{ox} \quad \text{6. 6}$$

$$-\frac{1}{V}\frac{d[O_2]}{dt} = k_{ox} P_{O_2} N(1-\theta_{ox}) \quad \text{6. 7}$$

where,

k_{red} = Rate constant for catalyst reduction

$P_{C_3H_6}$ = Partial pressure of propylene

θ_{ox} = Fraction of sites which are fully oxidised

k_{ox} = Rate constant for catalyst reoxidation

P_{O_2} = Partial pressure of oxygen

$1-\theta_{ox}$ = Fraction of sites which are reduced

These equations indicate that the rate of reduction or propylene oxidation is dependent on the number of oxidised sites. Both the reduction and reoxidation processes control this number. Under steady-state conditions, the flow of oxygen into

the catalyst equals to the flow of oxygen out of the catalyst as oxygenated products. Therefore, the two rate equations may be equated, yielding equation 6.8.

$$\frac{\theta_{ox}}{(1-\theta_{ox})} = \frac{k_{ox}P_{O_2}}{k_{red}P_{C_3H_6}} \qquad 6.\ 8$$

or

$$\theta_{ox} = \frac{\dfrac{k_{ox}P_{O_2}}{k_{red}P_{C_3H_6}}}{1+\dfrac{k_{ox}P_{O_2}}{k_{red}P_{C_3H_6}}} \qquad 6.\ 9$$

Substituting (6.9) to (6.6) resulting

$$-\frac{1}{V}\frac{d[C_3H_6]}{dt} = \frac{1}{V}\frac{d[C_3H_4O]}{dt} = k_{red}P_{C_3H_6}N\left[\frac{\dfrac{k_{ox}P_{O_2}}{k_{red}P_{C_3H_6}}}{1+\dfrac{k_{ox}P_{O_2}}{k_{red}P_{C_3H_6}}}\right] = \frac{Nk_{ox}P_{O_2}}{1+\dfrac{k_{ox}P_{O_2}}{k_{red}P_{C_3H_6}}} \qquad 6.\ 10$$

Figure 6.5 shows the relation between θ_{ox} with the ratio of the rate of site reoxidation against the rate of site reduction from equation 6.6. When the rate of reoxidation is much higher than the rate of reduction, the fraction of fully oxidised sites is relatively constant. In this condition, the rate of propylene oxidation has positive dependency on the concentration of propylene and zero order in oxygen. On the other hand, when the reoxidation rate is lower than the reduction, the propylene oxidation rate depends on the rate of reoxidation. Hence, the reaction dependency on oxygen concentration will have positive value and zero in propylene concentration.

The redox mechanisms above explain the tendency of dependency of the reaction rate on propylene and oxygen to be varied with the reaction temperature as discussed in Chapter 5. At low temperatures, the rate of reoxidation is slow due to slow oxygen diffusion in the bulk catalyst structure. Therefore, at low temperatures, the dependency of the reaction rate on the concentration of oxygen has positive value

while the dependency on propylene is close to zero. At high temperatures, oxygen is more freely diffused in the catalysts structure. As a result, the propylene oxidation rate is controlled by the rate of catalyst reduction. In this condition, the dependency of the reaction rate on propylene concentration will have positive value and zero on the concentration of oxygen.

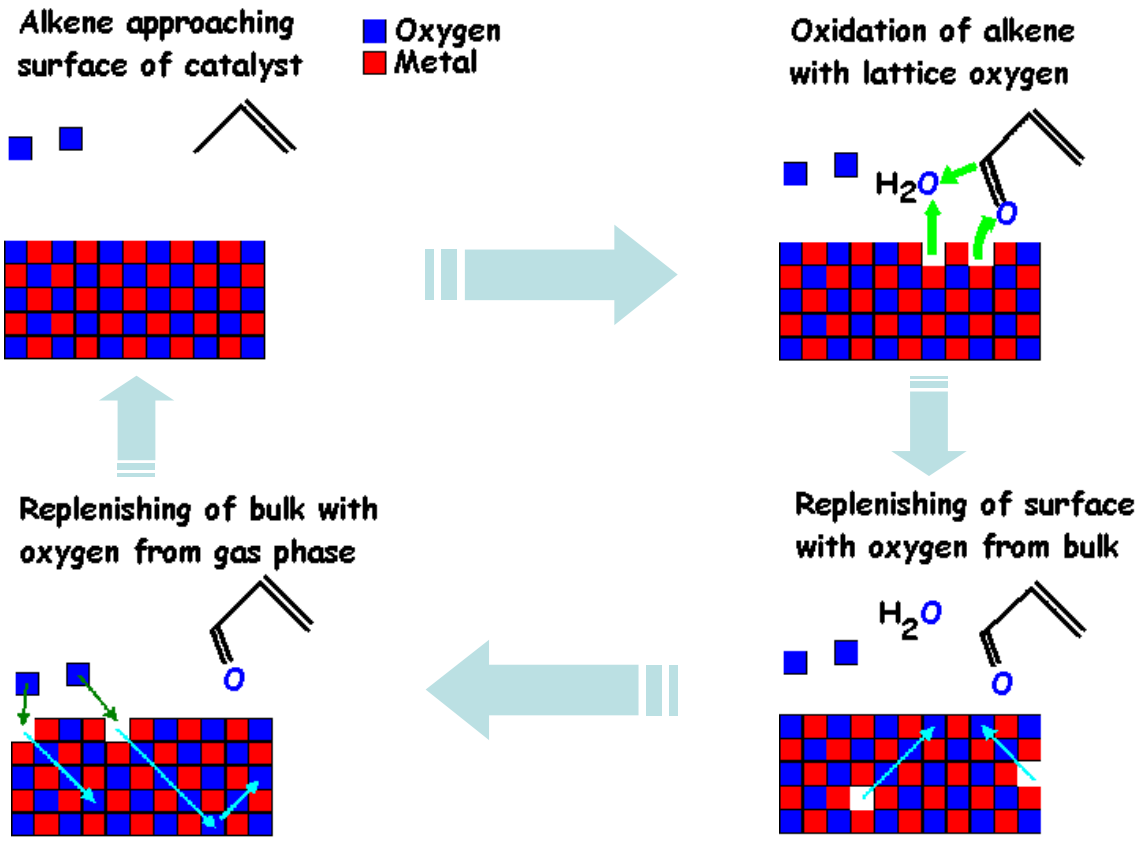

Figure 6.4 A schematic diagram of redox mechanisms over bismuth molybdate catalyst (Ressler 2005).

So far, equations 6.6 to 6.10 assume that reaction orders in propylene and oxygen are unknown and appear in the equations as 1 or ½ as used in kinetic models 3b, 5b, and 6b. Figure 6.5 will show that the reaction orders in both propylene and oxygen are a function of active site concentration. For a reaction such as R5, the

general reaction order in a reactant is given in equation 6.11 (Chorkendorf & Niemantsverdriet 2003).

$$R_1 + R_2 \longrightarrow P \qquad \text{R5}$$

$$n_{C_3H_6} = P_{C_3H_6} x \frac{d \ln \left[\frac{N k_{ox} P_{O_2}}{1 + \frac{k_{ox} P_{O_2}}{k_{red} P_{C_3H_6}}} \right]}{dP_{C_3H_6}} = \frac{\frac{k_{ox} P_{O_2}}{k_{red} P_{C_3H_6}}}{1 + \frac{k_{ox} P_{O_2}}{k_{red} P_{C_3H_6}}} = \theta_{ox} \qquad \text{6. 11}$$

$$n_{O_2} = 1 - \theta_{ox} \qquad \text{6. 12}$$

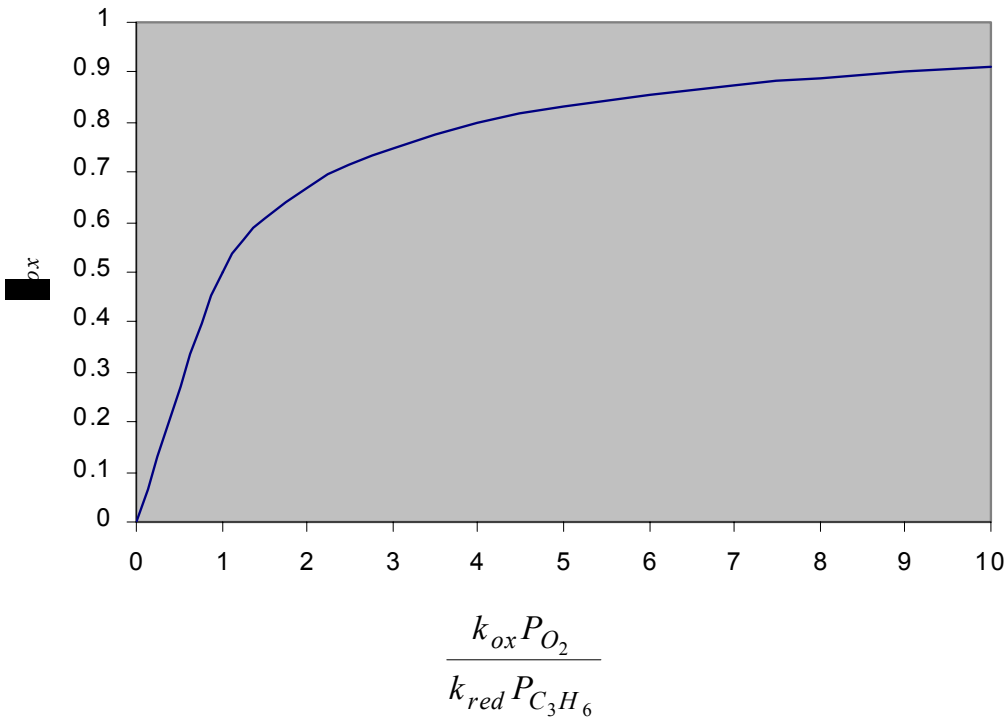

Figure 6.5 Fraction of fully oxidised sites as a function of the rate of sites oxidation to the rate of sites reduction.

With the relation given in equation 6.10, the reaction orders in propylene and oxygen for reactions R3 and R4 are given in equation 6.11. The equation clearly

shows the dependency of the reaction order of the reactants on the concentration of fully oxidised sites of the catalyst. This is also the reason why the correlation of experimental results and the calculated data is not uniform throughout the entire temperature range used in the experiments. Since the maximum value of the fraction of fully oxidised site is 1, the sum of reaction order of propylene and oxygen is normalised. The normalised trends of reaction order are shown in Figure 6.6.

Krenzke (Leonard David Krenzke 1977) calculated the reaction orders in propylene and oxygen over gamma bismuth molybdate. Data for this calculation was taken from oxidation and reduction properties of the gamma bismuth molybdate reported by Uda and co-workers (Uda, Lin & Keluks 1980). The calculated values of the reaction orders in propylene and oxygen are given in Table 6.5. The Table shows that the experimental reaction orders are very close to the calculated values. This means that the redox mechanism is the most probable mechanism occurring in the partial oxidation of propylene to acrolein over bismuth molybdate catalysts.

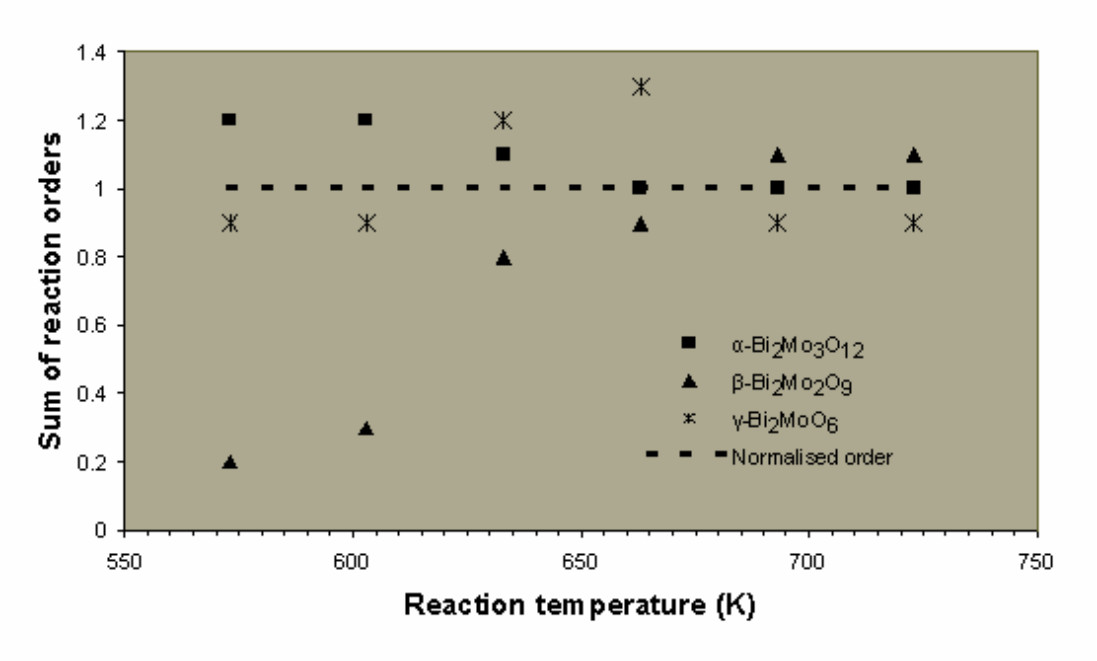

Figure 6.6 The trends of reaction orders to be normalised

Table 6.5 Comparison of reaction orders calculated from redox kinetics with the observed reaction orders for C_3H_6 oxidation of γ-Bi_2MoO_6.

Temperature	Reaction order			
	Experimental		Calculated (Leonard David Krenzke 1977)	
	C_3H_6	O_2	C_3H_6	O_2
450	0.9	0	1	0
435*			1	0
420	0.9	0.0	1	0
400*			0.6	0.2
390	0.7	0.6		
375*			0.4	0.3
360	0.6	0.3		
350*			0.2	0.5
330	0.6	0.3		
325*			0	0.6
300	0.6	0.2		

*Temperatures used in the reaction order calculations

6.3 Reaction Network

Although the redox mechanism explains the partial oxidation of propylene to acrolein, it does not explain other the mechanisms of the formation of by-products. Blank tests of acrolein oxidation show clearly that carbon oxides formed from further oxidation of acrolein. The reaction has to be taken into account especially at high temperatures (T>390^oC) when the rate is high. Under this condition, a reaction network will be required to completely describe the kinetics of propylene oxidation over bismuth molybdates.

Tan (Hock Seng Tan 1986) developed a reaction network model based on silica-supported α-$Bi_2Mo_3O_{12}$ using stainless steel reactor. The reaction network explains the formation of carbon monoxide and acetaldehyde as well as carbon dioxide and acrolein. However, Tan did not break down the reaction network into elementary reactions. The reaction network is schematically shown in Figure 6.7. The calculated values of k_{12}, k_{13}, k_{14}, and k_{23} are given in Table 6.6.

It should be noted here that Tan used the redox mechanisms model in deriving all the kinetic parameters mentioned above. The model used by Tan is the same as model 5.b where the reaction order of oxygen is ½.

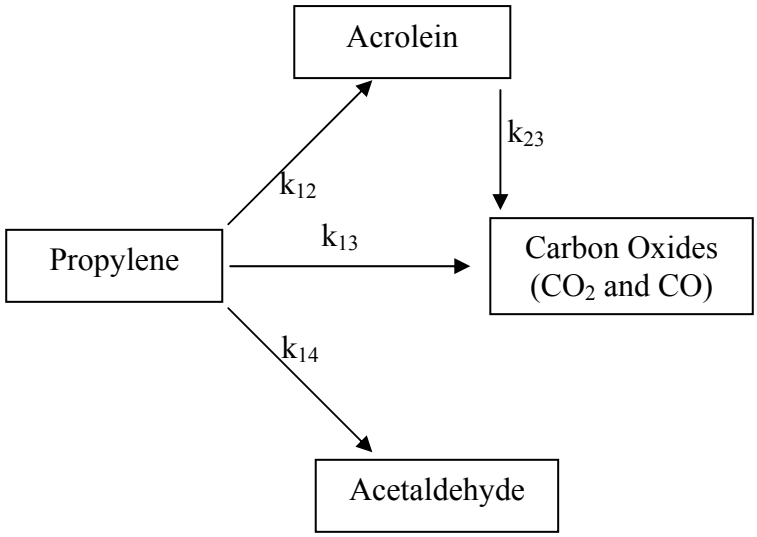

Figure 6.7 A schematic diagram of reaction network studied by Tan (Hock Seng Tan 1986).

Table 6.6 Values of k_{12}, k_{13}, k_{14}, and k_{23} calculated from experimental data according to reaction network given in Figure 6.7.

Temp (^oC)	k_a	k_{12}	k_{13}	k_{14}	k_{23}	k_r
	x 10^{-4}					
325	7.44 ± 1.61				6.77 ± 1.21	
350	16.7 ± 2.0	21.9 ± 1.4	2.70 ± 0.18	2.73 ± 0.21	12.9 ± 12.1	5.18 ± 0.29
365	25.0 ± 6.6			0.45 ± 0.06	19.5 ± 4.9	
370		3.86 ± 0.37	2.94 ± 0.31			7.28 ± 0.48
375	31.5 ± 3.8		2.70 ± 0.27			
390	48.3 ± 3.4	5.38 ± 0.35		0.63 ± 0.07		8.59 ± 0.25

Larsen (Larsen 2003) developed a reaction network over β-$Bi_2Mo_2O_9$. He proposed elementary steps in the formation of C_3H_4O and CO_2 from propylene as shown in Table 6.7. The steps were developed from Mars van Krevelen and Langmuir-Hinshelwood models, respectively. Based on these reactions, He calculated the reaction rate of acrolein formation using quasi equilibrium approximation to solve the equations. The rate expressions and reaction orders in propylene and oxygen in the formation of acrolein are given in Table 6.7.

There are at least two disadvantages of this approach. Firstly, in the Mars van Krevelen model, oxygen comes from the lattice of the catalyst. In contras, Larsen's reaction mechanisms use adsorbed oxygen as the oxygen source for the oxidation reaction. In addition, there is no explanation of the formation of other by-products normally found in the partial oxidation of propylene over bismuth molybdate catalysts such as acetaldehyde and carbon monoxide.

Although Larsen's mechanisms do not consider the formation of CO and C_2H_4O, the reaction order expressions are similar to those in the redox mechanisms, as discussed earlier in this chapter.

To explain the reaction mechanisms of propylene oxidation over bismuth molybdates at the molecular level, a new reaction network is proposed. The network is developed by combining the information available in literatures with information gained from kinetic experiments and catalysts structure investigations. Fundamental concepts in developing the reaction network include:

1. Acrolein is formed exclusively via the redox mechanism and, therefore, the change in kinetics is not due to a change in the reaction mechanism.
2. Carbon oxides are formed solely by the further oxidation of intermediates formed on the bismuth molybdates surface, such as acetaldehyde, formaldehyde, acrolein, and acetic acid.
3. The rate-determining step in acrolein formation is the abstraction of an α-hydrogen from propylene.
4. Oxygen and olefin are adsorbed on different sites. Therefore, the changes in reaction orders cannot be accounted for by competitive adsorption.

5. Desorption of acrolein produced on the catalysts surface is not rate determining step.

Table 6.7 Elementary steps in the formation of C_3H_4O and CO_2 from propylene over β-$Bi_2Mo_2O_9$

React. No.	Reaction
1	$C_3H_6 + * \leftrightarrow C_3H_6*$
2	$C_3H_6* + O* \leftrightarrow C_3H_5* + OH*$ (slow)
3	$C_3H_5* + O* \leftrightarrow C_3H_5O* + *$
4	$C_3H_5O* + O* \leftrightarrow C_3H_4O* + OH*$
5	$C_3H_4O* \leftrightarrow C_3H_4O + *$
6	$H_2O* \leftrightarrow H_2O + *$
7	$O_2 + {}^{*} \leftrightarrow O_2*$
8	$O_2* + * \leftrightarrow 2O*$
9	$OH* + OH* \leftrightarrow H_2O* + O*$
10	$C_3H_6* + O* \leftrightarrow C_3H_6O*$ (slow)
11	$C_3H_6O* + 8O* \leftrightarrow 3\ CO_2* + 3H_2O* + 3*$
12	$CO_2* \leftrightarrow CO_2 + *$

Table 6.8 Reaction rate expression for the formation of acrolein and CO_2, and reaction orders in propylene and oxygen in the acrolein formation (Larsen 2003).

$r_{C_3H_4O} = k_2 K_1 K_7^{0.5} K_8^{0.5} \cdot \left(\frac{p_{C_3H_6} p_{O_2}^{0.5}}{p^{\Theta^{1.5}}} - \frac{p_{C_3H_4O} \cdot p_{H_2O}}{K_{g,C_3H_4O} \cdot p_{O_2}^{0.5} \cdot p_O^{1.5}} \right) \cdot \theta_*^2$
$r_{CO_2} = k_{10} K_1 K_7^{0.5} K_8^{0.5} \cdot \left(\frac{p_{C_3H_6} p_{O_2}^{0.5}}{p^{\Theta^{1.5}}} - \frac{p_{CO_2}^3 \cdot p_{H_2O}^3}{K_{g,CO_2} \cdot p_{O_2}^4 \cdot p_O^2} \right) \cdot \theta_*^2$
$m_{C_3H_4O} = 1 - 2\theta_{C_3H_6}$
$n_{O_2} = 0.5 - 2\theta_{O_2} - \theta_O - 0.5\theta_{OH} + 05\theta_{C_3H_5O} + 1.5\theta_{C_3H_5} + 8\theta_{C_3H_6O}$

The analysis of experimental data on the kinetics of propylene oxidation to acrolein revealed that the reaction follows the Mars van Krevelen (redox) mechanisms. In the mechanisms, the catalysts provide their lattice oxygen for the oxidation reaction. Experimental results on the time-resolved crystal structure elucidation reveal that all bismuth molybdate catalysts are capable of providing the oxygen from their lattice. At the same time, the reduced catalysts should be able to deoxidise their reduced site quickly. This has been shown by the high mobility of lattice oxygen shown by their high lattice thermal parameters as discussed in Chapter 4. Based on the above concepts and information, the reaction mechanisms of partial oxidation of propylene to acrolein and other by-products are proposed. The mechanisms are given in Figure 6.8.

The corresponding elementary reaction steps shown in Figure 6.5, in the form of equilibrium reactions, are given in Table 6.9. The steps No 1 to 8 are similar to Larsen's mechanisms. The difference is the source of oxygen for oxidation of the transition molecules. In the present mechanisms, the oxygen source is the catalyst lattice while in Larsen's mechanism, the oxygen source is the adsorbed oxygen.

Reaction step No. 4 should be very fast and consequently followed by reaction No. 5, i.e, the addition of oxygen into C_4H_4 radical. This step is based on the spectroscopic investigation by Ayame et al. (Ayame et al. 2000; Ayame et al. 2002) who proposed that the second abstraction of hydrogen occurs before the addition of oxygen into the allyl radical. In other publications, these two steps are normally written as a single step where the abstraction of second hydrogen and addition of oxygen occur simultaneously. Therefore, the steps No. 4 and 5 are drawn as a single step in Figure 6.8.

The reactions No 1 to 7 are actually the detailed mechanisms of reaction R.1, i.e a redox mechanisms. Reaction No. 8 is reaction R.2. Therefore, the overall reaction of elementary reactions No 1 to No 8 is the same as the redox mechanisms. Reactions No. 9 to 12 explain the formation of the by-products such as C_2H_4O, CO, and CO_2. They also show how formaldehyde and acetic acids form in the reaction

process. There are several publications reporting the occurrence of these two by-products although they were not detected in the kinetic experiments.

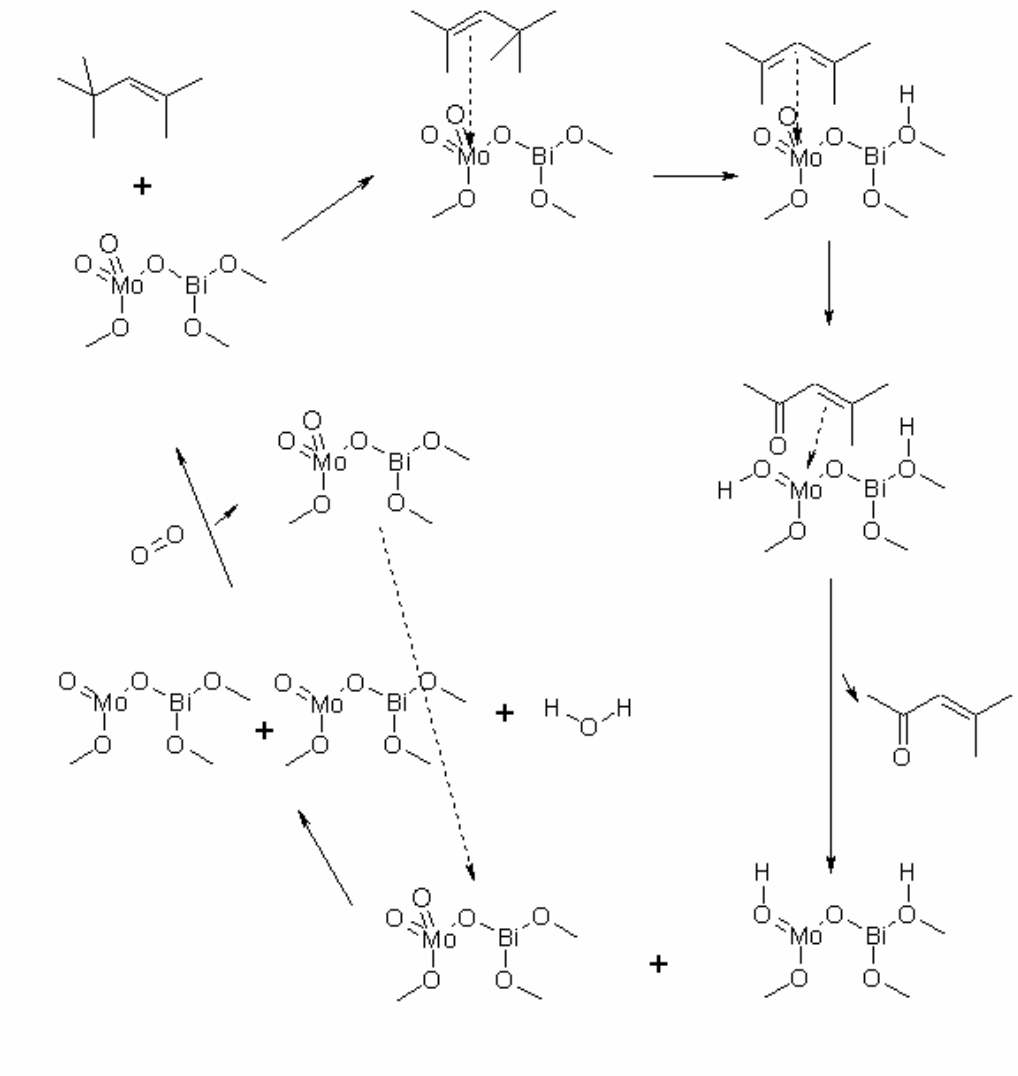

Figure 6.8. continues.....

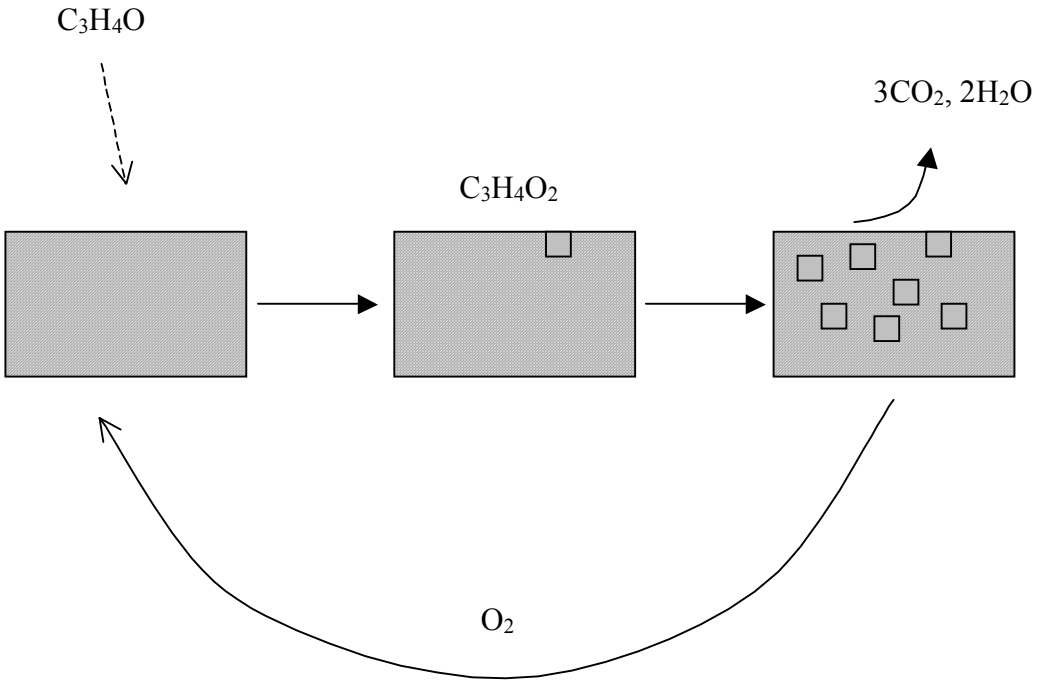

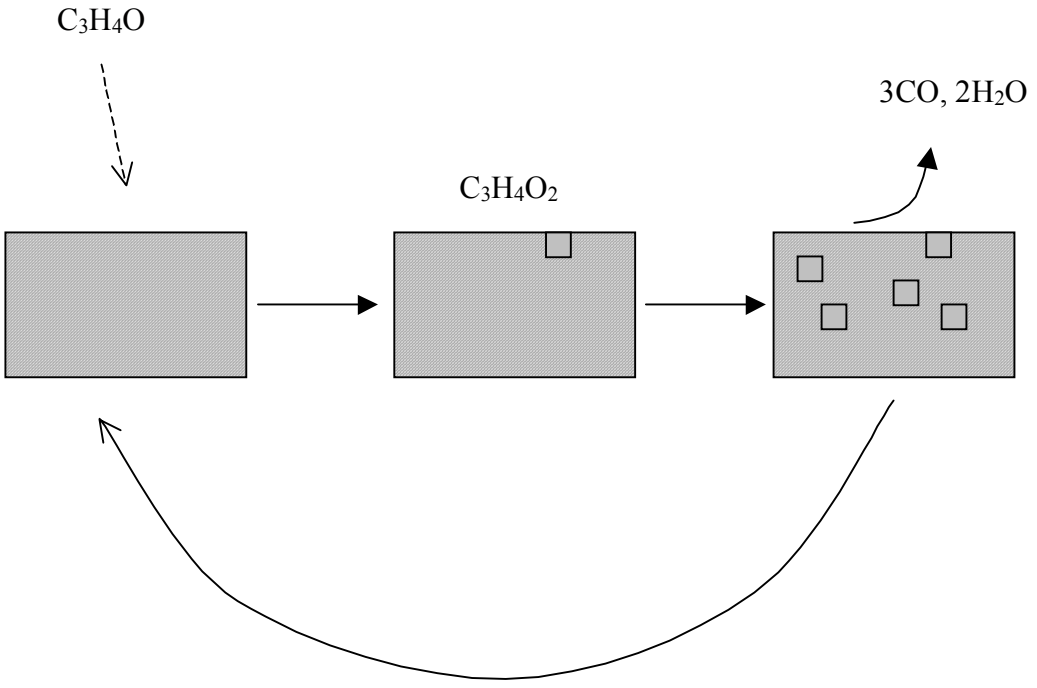

Figure 6.8 continues.....

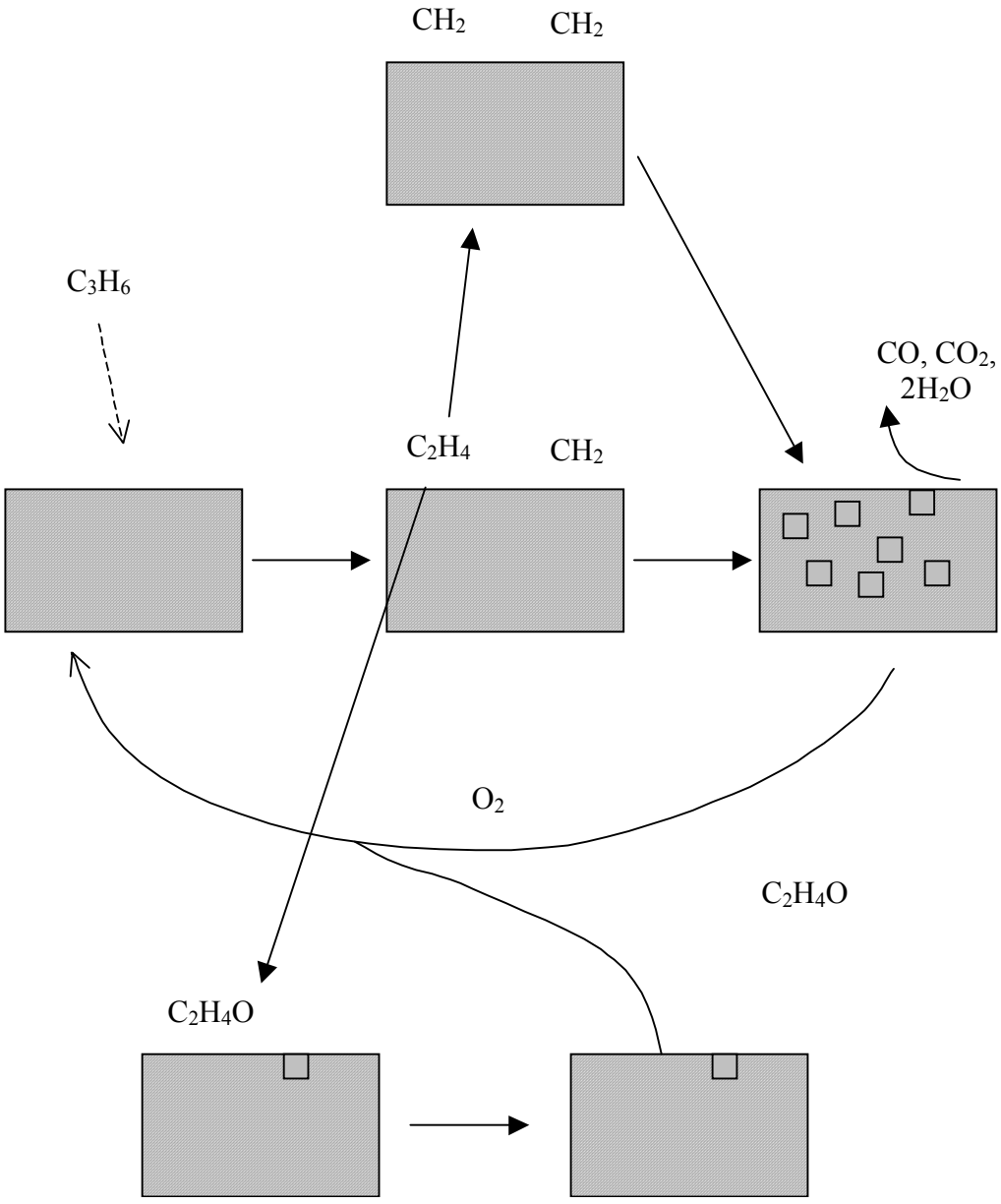

Figure 6.8 The proposed reaction mechanisms of partial oxidation of propylene to acrolein and other by-products over bismuth molybdate catalysts.

Table 6.9 Detailed reaction mechanisms of propylene partial oxidation over bismuth molybdates.

No.	Reaction
1	$C_3H_6 + * \leftrightarrow C_3H_6*$
2	$C_3H_6* + * \leftrightarrow C_3H_5* + H*$ (slow)
3	$C_3H_5* + * \leftrightarrow C_3H_4* + H*$
4	$C_3H_4* + * \leftrightarrow C_3H_4O* + *_{red}$
5	$C_3H_4O* \leftrightarrow C_3H_4O + *$
6	$2H* \leftrightarrow H_2O* + *_{red}$
7	$H_2O* \leftrightarrow H_2O + *$
8	$O_2 + 2*_{red} \leftrightarrow 2*$
9	$C_3H_6* + * \leftrightarrow C_2H_4* + CH_2*$
10	$C_3H_4O* + * \leftrightarrow C_3H_4O_2* + *_{red}$ (slow)
11	$C_3H_4O_2* + 3* \leftrightarrow 3CO + 2H_2O + 3*_{red}$
12	$C_3H_4O_2* + 6* \leftrightarrow 3CO_2 + 2H_2O + 7*_{red}$
13	$C_2H_4* \leftrightarrow C_2H_4O + *_{red}$
14	$CH_2* + * \leftrightarrow CO + H_2O + 2*_{red}$
15	$CH_2* + 2* \leftrightarrow CO_2 + H_2O + 3*_{red}$

6.4 Summary

The reaction mechanisms of propylene oxidation to acrolein have been investigated and derived from the kinetic data, *in-situ* catalyst characterisation data and information from published literatures. Several key conclusions from the discussion can be summarised as follows:

1. The acrolein formation from partial oxidation of propylene over bismuth molybdate catalysts follows redox (or Mars van Krevelen) reaction mechanisms. However, the observed reaction rates on γ-Bi_2MoO_6 deviate from their calculated rates from the mechanisms model due to further oxidation of acrolein to carbon oxides.

2. Mathematical expression purely derived from the Mars van Krevelen mechanisms explains the reaction order dependency on the degree of lattice oxygen saturation of the bismuth molybdate catalysts. The catalysts perform the best activity and selectivity when they are in the highest oxidation state.
3. A detailed reaction mechanisms model derived from the Mars van Krevelen mechanism is proposed. The mechanisms taking into account the possible ways of the formation of by-products (acetaldehyde, carbon monoxide, carbon dioxide and acrylic acid) that are normally found in the catalytic partial oxidation of propylene to acrolein.

Chapter 7

CONCLUSIONS AND RECOMMENDATIONS

7.1 Conclusions

This thesis has addressed the relationship between the crystal structure and the catalytic activity and selectivity of several catalysts for partial oxidation of propylene to acrolein. Catalyst activity and selectivity are represented by their kinetic parameters. The principal results and conclusions from the study are summarised as follows:

7.1.1 Structural characteristics of the catalysts

Three bismuth molybdate catalysts, namely, α-$Bi_2Mo_3O_{12}$, β-$Bi_2Mo_2O_9$ and γ-Bi_2MoO_6, in pure powder form have been successfully prepared in this study. X-ray and neutron diffraction studies revealed that structures of the bismuth molybdates are similar to the model structure from ICSD used in their structural determination and refinement, namely ICSD No. 2650, 201742, and 47139 for α-$Bi_2Mo_3O_{12}$, β-$Bi_2Mo_2O_9$ and γ-Bi_2MoO_6, respectively. The refinements were carried out using the Rietveld method and the RIETICA software. The X-ray diffraction study has also shown no other phases or impurities present in the bismuth molybdates.

In-situ structural characterisation using neutron diffraction has uncovered the possible lattice oxygen ions that control the activity and selectivity of α-$Bi_2Mo_3O_{12}$,

β-$Bi_2Mo_2O_9$ and γ-Bi_2MoO_6 in catalysing partial oxidation of propylene to acrolein. They are O(1), O(11), and O(12) in the α phase; O(3), O(11), O(16), and O(18) in the β phase; and O(1) and O(5) in the γ phase. The oxygen ions have greater thermal parameters, as detected by refining the catalyst structure from the in-situ neutron diffractograms, than others in the catalysts lattice.

One common feature of all mobile oxygen ions, from a catalyst crystal structure point of view, is that they are all related to molybdenum ions rather than bismuth ions in the lattice. It has been widely known that a shear plane, i.e. a transformation of corner sharing to edge sharing molybdenum oxide polyhedra, is a key factor that promotes the catalyst activity for selective partial oxidation reaction on α-$Bi_2Mo_3O_{12}$, β-$Bi_2Mo_2O_9$ and γ-Bi_2MoO_6. Thus, the mobile oxygen ions, which are part of the molybdenum polyhedra, are those who facilitate the "shear plane" formation on the crystal structure of bismuth molybdate.

The diffraction characterisations have also shown that molybdenum oxide polyhedra in all bismuth molybdate are unsaturated. In contrast, the bismuth oxide polyhedra are over charged. The co-existence of molybdenum ions that are co-ordinately unsaturated with bismuth ions that are over valence-charged promote the formation of allyl radical such as those found in the partial oxidation of propylene to acrolein. The molybdenum ions become propylene-adsorbing sites while the bismuth ions are the active sites to attract hydrogen from the adsorbed propylene, leading to the formation of the allyl intermediate.

7.1.2 Kinetics and reaction mechanisms

The catalytic activity and selectivity tests as well as the kinetic experiments were carried out by using a packed bed reactor made of quartz at temperatures between 300 and 400^{o}C. All experiments were carried out at very close to atmospheric pressure. The tests show that all bismuth molybdate catalysts have high selectivity and activity for the catalytic partial oxidation of propylene to acrolein. The activities of α-$Bi_2Mo_3O_{12}$ and γ-Bi_2MoO_9 are similar while the β-$Bi_2Mo_2O_9$ is lower. However, the selectivity of the catalysts to acrolein decreases significantly at reaction temperatures higher than 390^{o}C. The gamma phase suffered the highest lost of selectivity at high temperatures.

The kinetics of the reaction was fitted using the power rate law model. The study showed that the reaction orders in propylene and oxygen in the partial oxidation of propylene to acrolein over α-$Bi_2Mo_3O_{12}$, β-$Bi_2Mo_2O_9$ and γ-Bi_2MoO_9 depend on the reaction temperature. The reaction order in propylene increases with reaction temperature for all the bismuth molybdate catalysts, from 0.6 at 300°C to 1.0 at 450°C while the reaction order in oxygen decreases from 0.6 at 300°C to 0.0 at 450°C. The activation energies are 99.7, 173.0 and 97.7 kJ.mol^{-1} for α-$Bi_2Mo_3O_{12}$, β-$Bi_2Mo_2O_9$ and γ-Bi_2MoO_6, respectively.

The changes in reaction orders with respect to propylene and oxygen as a function of temperature as well as the decrease of the catalyst selectivity at high temperatures are believed as an indication that the reaction occurs through the redox mechanisms using lattice oxygen as the source of oxygen for the reaction. The redox model successfully explains the dependency of the reaction orders in propylene and oxygen on the concentration of the active sites, i.e. the concentration of fully oxidised sites on bismuth molybdate catalysts. A mathematical expression of the redox model is given by the following equations:

$$-\frac{1}{V}\frac{d[C_3H_6]}{dt} = k_{red} P_{C_3H_6} N\theta_{ox}$$

$$-\frac{1}{V}\frac{d[O_2]}{dt} = k_{ox} P_{O_2} N(1-\theta_{ox})$$

$$n_{C_3H_6} = \theta_{ox} \text{ and } n_{O_2} = 1-\theta_{ox}$$

where n_{O_2} and $n_{C_3H_6}$ are the reaction orders in oxygen and propylene, respectively, while n_{O_2} and $n_{C_3H_6}$ are obtained from derivation of the reaction rate expressions.

The examination of several reaction mechanism models has given further evidence that the propylene partial oxidation to acrolein occurs via the redox mechanism. In this mechanism, the rate of acrolein formation depends on the degree of fully oxidised sites in the bismuth molybdate. The oxidised sites affect the apparent reaction orders in propylene and oxygen and thus control the kinetics of partial oxidation of propylene to acrolein. The more easily the reduced catalysts are reoxidised, the more active the catalysts in converting propylene to acrolein.

7.1.3 Relationship between structure and the catalyst selectivity and activity

The change in the catalyst activity and selectivity has very a close relation to the change in the crystal structure of the catalyst. At high temperatures, the lattice oxygen ions become weakly bonded to metal ions and thus become more active. They are more mobile and ease the oxidation of the allyl intermediate until the mobile lattice oxygen ions become too mobile. The ions are very reactive but not selective. This is the reason why the catalysts lost their selectivity above 390^{o}C. This may take place since oxygen now becomes so reactive that allyl intermediates are oxidised into complete oxidation products CO_2 and H_2O. In-situ neutron diffraction study shows not only the increase of the lattice oxygen mobility but also the increase in the number and types of mobile lattice oxygen in bismuth molybdate catalysts.

Lattice oxygen ions in the γ-Bi_2MoO_6 phase are different to those in α-$Bi_2Mo_3O_{12}$ and β-$Bi_2Mo_2O_9$. There is more mobile lattice oxygen available on the gamma phase per unit cell than in the alpha and beta phase. As a result, at high temperatures (greater than 390^{o}C), more unselective oxygen ions become available in the gamma phase. As the unselective, but reactive lattice oxygen ions are more available in the gamma phase, the selectivity of the gamma phase in converting propylene to acrolein decreases faster than those catalysed by the alpha or beta phases.

7.1.4 Reaction network

Although the catalysts are very selective in oxidising propylene to acrolein, some side products such as C_2H_4O, CO_2 and CO still can be found in the reactions. As in acrolein, the reaction order in propylene and oxygen in the formation of C_2H_4O are temperature dependent. The reaction order in propylene increases from 0.3 at 360^{o}C to 1.3 at 450^{o}C on the alpha and beta phases, but it decreases from 0.9 at 360^{o}C to 0.1 at 450^{o}C on the gamma phase. The reaction order in oxygen decreases as reaction temperature increases on the alpha and gamma phases and is relatively constant on the beta phase. Activation energies in the formation of C_2H_4O are 33.2, 150.4 and 83.9 kJ mol^{-1} for α-$Bi_2Mo_3O_{12}$, β-$Bi_2Mo_2O_9$ and γ-Bi_2MoO_6, respectively. For CO_2 and CO, due to their very small concentrations in the product, the kinetics

could not be obtained for the alpha and beta phase. The reaction orders in propylene and oxygen for the formation of CO_2 at temperatures greater than 390^oC on the gamma phase are nearly constant at 1.0 and 0.3, respectively.

A reaction network has been proposed to accommodate the presence of the side products. The network is presented as follows:

1 $C_3H_6 + * \leftrightarrow C_3H_6*$

2 $C_3H_6* + * \leftrightarrow C_3H_5* + H*$ (slow)

3 $C_3H_5* + * \leftrightarrow C_3H_4* + H*$

4 $C_3H_4* + * \leftrightarrow C_3H_4O* + *_{red}$

5 $C_3H_4O* \leftrightarrow C_3H_4O + *$

6 $2H* \leftrightarrow H_2O* + *_{red}$

7 $H_2O* \leftrightarrow H_2O + *$

8 $O_2 + 2*_{red} \leftrightarrow 2*$

9 $C_3H_6* + * \leftrightarrow C_2H_4* + CH_2*$

10 $C_3H_4O* + * \leftrightarrow C_3H_4O_2* + *_{red}$ (slow)

11 $C_3H_4O_2* + 3* \leftrightarrow 3CO + 2H_2O + 3*_{red}$

12 $C_3H_4O_2* + 6* \leftrightarrow 3CO_2 + 2H_2O + 7*_{red}$

13 $C_2H_4* \leftrightarrow C_2H_4O + *_{red}$

14 $CH_2* + * \leftrightarrow CO + H_2O + 2*_{red}$

15 $CH_2* + 2* \leftrightarrow CO_2 + H_2O + 3*_{red}$

In steps No 1 to 8, the lattice oxygen is the primary source of oxygen for the oxidation reaction. Reaction step No. 4 is very fast, followed by reaction No. 5, i.e., the addition of oxygen into the C_4H_4 radical.

7.2 Recommendations

The present work has demonstrated the relationship between catalyst structure and catalytic activity and selectivity of bismuth molybdates for partial oxidation of propylene to acrolein. The results have also provided a much improved understanding of how the selective partial oxidation catalysts work. However, the

thesis has also highlighted several issues that should be addressed in future research. These include:

1. Performing the in-situ structural characterisation using faster diffraction technique such as synchrotron diffraction. The data collection in the in-situ neutron characterisations was too slow in comparison to the catalytic reaction. The reaction only takes several microseconds to completion while the data collection takes several hours. As a result, the resulting structures are actually their steady state structures under the specified condition. The real structure dynamics and oxygen diffusion in the crystal lattice is still not precisely known. The real time structural characterisation under the real reaction conditions can be achieved by synchrotron diffraction technique, which can be performed at the same time scale of the reaction.
2. Isotope tracing study to identify which particular lattice oxygen is participating in the reaction to obtain a better understanding of where the oxygen comes for in the selective oxidation reaction. The current study could not probe which particular lattice oxygen is taken by the allyl intermediate to form selective oxidation products. By placing labelled oxygen into known positions in the catalyst crystal structure, the source of oxygen or the selective oxidation reaction can be affirmatively concluded and the discrepancy between experimental and theoretical results can be resolved. The tracer study using isotope-labelled oxygen will give a better understanding of the relationship between the crystal structure of bismuth molybdates and their activity and selectivity for propylene oxidation to acrolein.
3. CHEMKIN simulations to compare the kinetic results of the proposed reaction mechanisms with the experimental data. The CHEMKIN simulation requires thermodynamic data of all species involved in the mechanisms. It also needs kinetic data for all elementary reactions proposed in the mechanisms. The data is not available at the time this thesis is prepared. Once the thermodynamic data are available, CHEMKIN can be used to simulate the kinetics of the reactions and to compare the simulation results with the experimental results to validate the proposed mechanisms. For the CHEMKIN simulations, the necessary kinetics and thermodynamic data can

be obtained either from experiment results or calculations using first principles approach.

REFERENCES

Adams, CR & Jennings, TJ, 1963, 'Investigation of the mechanism of catalytic oxidation of propylene to acrolein and acrylonitrile', *Journal of Catalysis,* vol. 2, no. 1, pp. 63-68.

Adams, CR & Jennings, TJ, 1964, 'Mechanism studies of the catalytic oxidation of propylene', *Journal of Catalysis,* vol. 3, no. 6, pp. 549-558.

Adams, CR, Voge, HH, Morgan, CZ & Armstrong, WE, 1964, 'Oxidation of butylenes and propylene over bismuth molybdate', *Journal of Catalysis,* vol. 3, no. 4, pp. 379-386.

Antonio, MR, Teller, RG, Sandstrom, DR, Mehicic, M & Brazdil, JF, 1988, 'Structural Characterization of Bismuth Molybdates by X-Ray Absorption Spectroscopy and Powder Neutron Diffraction Profile Analysis', *Journal of Physical Chemistry,* vol. 92, pp. 2939-2944.

Arora, N, Deo, G, Wachs, IE & Hirt, AM, 1996, 'Surface Aspects of Bismuth-Metal Oxide Catalysts', *Journal of Catalysis,* vol. 159, pp. 1-13.

Ayame, A, Iwataya, M, Uchida, K, Igarashi, N & Miyamoto, M, 2000, 'X-Ray Photoelectron Spectroscopic Study on γ-Bismuth Molybdate Surfaces on Exposure to Propene and Oxygen', *Japan Journal of Applied Physics,* vol. 39, no. 7B Part 1, pp. 4335-4339.

Ayame, A, Uchida, K, Iwataya, M & Miyamoto, M, 2002, 'X-Ray Photoelectron Spectroscopic Study on α- and γ-Bismuth Molybdate Surfaces Exposed to hydrogen, Propene, and Oxygen', *Applied Catalysis A: General,* vol. 227, pp. 7-17.

Aykan, K, 1968, 'Reduction of Bi2O3---MoO3 Catalyst during the Ammoxidation of Propylene in the Absence of Gaseous Oxygen', *Journal of Catalysis,* vol. 12, no. 3, pp. 281-290.

Balessi, VC, Trikalitis, PN, Ladavos, AK, Bakas, TV & Pomonis, PJ, 1999, 'Structure and Catalytic Activity of $La_{1-x}FeO_3$ System (x=0.00, 0.05, 0.10, 0.15, 0.20, 0.25, 0.35) for the NO+CO Reaction', *Applied Catalysis A: General,* vol. 177, pp. 53-68.

Barnes, N, Kitchin, S & Hriljac, JA, 1999, 'Progress in the Intercalation of Pyridine and Other Organic Bases into Crystalline Bismuth Molybdenum Oxide Hydrate, $BiMo_2O_7OH.2H_2O$ Catalysts', *Inorganic Chemistry,* vol. 38, no. 26, pp. 6317-6319.

Batist, PA, 1979, 'The Functions of Redox Couples in Catalysts for the Selective Oxidation of Olefins', *Surface Technology,* vol. 9, pp. 443-446.

Batist, PA, Der Kinderen, AHWM, Leeuwenburgh, Y, Metz, FAMG & Schuit, GCA, 1968, 'The catalytic oxidation of 1-butene over bismuth molybdate catalysts : IV. Dependence of activity on the structures of the catalysts', *Journal of Catalysis,* vol. 12, no. 1, pp. 45-60.

Batist, PA, van de Moesdijk, CGM, Matsuura, I & Schuit, GCA, 1971, 'The catalytic oxidation of 1-butene over bismuth molybdates : Promoters for the Bi2O3.3MoO3 catalyst', *Journal of Catalysis,* vol. 20, no. 1, pp. 40-57.

Bemis, JM, Douskey, MC & Munson, EJ 1997, *Investigation of Partial Oxidation Catalysts by Solid-State NMR*, Department of Chemistry, University of Minnesota. Retrieved: 26/03/2003, from http://india.cchem.berkeley.edu/~anant/Public/OldRMCFiles/RMCstuff/rmc97/abstracs/q11.htm.

Benyahia, F & Mearns, AM, 1990, 'Selective Oxidation of Isobutene over Bismuth Molybdate Catalyst', *Applied Catalysis,* vol. 66, pp. 383-393.

Benyahia, F & Mearns, AM, 1991, 'Selective oxidation of isobutene over multicomponent molybdate catalyst', *Applied Catalysis,* vol. 70, no. 1, pp. 149-159.

Beres, J, Janik, A & Wasilewski, J, 1969, 'Preparation of bismuth-molybdenum catalysts', *Journal of Catalysis,* vol. 15, no. 2, pp. 101-105.

Bettahar, MM, Constentin, G, Savary, L & Lavalley, JC, 1996, 'On The Partial Oxidation of Propane and Propylene on Mixed Metal Oxide Catalysts', *Applied Catalysis A: General,* vol. 145, pp. 1-48.

Bielanski, A & Haber, J 1991, *Oxygen in Catalysis*, Marcel Dekker, Inc., New York.

Boudeville, Y, Figueras, F, Forissier, M, Portefaix, J-L & Vedrine, JC, 1979, 'Correlations between X-ray photoelectron spectroscopy data and catalytic properties in selective oxidation on Sb---Sn---O catalysts', *Journal of Catalysis,* vol. 58, no. 1, pp. 52-60.

Brown, ID & Wu, KK, 1957, 'Empirical Parameters for Calculating Cation-Oxygen Bond Valences', *Acta Crystallographica,* vol. B32, pp. 1957-1959.

Burlamacchi, L, Martini, G & Ferroni, E, 1971, 'ESR study of Mo(V) in partially reduced Bi/Mo catalyst', *Chemical Physics Letters,* vol. 9, no. 5, pp. 420-423.

Burrington, JD, Kartisek, CT & Grasselli, RK, 1980, 'Aspects of selective oxidation and ammoxidation mechanisms over bismuth molybdate catalysts : II. Allyl alcohol as a probe for the allylic intermediate', *Journal of Catalysis,* vol. 63, no. 1, pp. 235-254.

Burrington, JD, Kartisek, CT & Grasselli, RK, 1984, 'Surface intermediates in selective propylene oxidation and ammoxidation over heterogeneous molybdate and antimonate catalysts', *Journal of Catalysis,* vol. 87, no. 2, pp. 363-380.

Buttrey, DJ, 2001, 'Compositional and Structural Trends Among the Bismuth Molybdates', *Topics in Catalysis,* vol. 15, no. 2-4, pp. 235-239.

Buttrey, DJ, Jefferson, DA & Thomas, JM, 1986, 'The Structural Relationships Between the Various Phase of Bismuth Molybdates with Special Reference to Their Catalytic Activity', *Philosophical Magazine A,* vol. 53, no. 6, pp. 897-906.

Buttrey, DJ, Vogt, T, Wildgruber, U & Robinson, WR, 1994, 'Structural Refinement of the High Temperature Form of Bi_2MoO_6', *Journal of Solid State Chemistry,* vol. 111, pp. 118-127.

Callahan, JL, Grasselli, RK, Milberger, EC & Strecker, HA, 1970, 'Oxidation and Ammoxidation of Propylene over Bismuth Molybdate Catalyst', *Industrial Engineering Chemical Product: Research and Development,* vol. 9, no. 2, pp. 134-142.

Carrazan, SRG, Martin, C, Rives, V & Vidal, R, 1996a, 'An FT-IR Spectroscopy Study of the Adsorption and Oxidation of Propene on Multiphase Bi, Mo, and Co Catalysts', *Spectrochimica Acta Part A,* vol. 52, p. 11071118.

Carrazan, SRG, Martin, C, Rives, V & Vidal, R, 1996b, 'Selective Oxidation of Isobutene to Methacrolein on Multiphasic Molybdate-Based Catalysts', *Applied Catalysis A: General,* vol. 135, pp. 95-123.

Carson, D, Coudurier, G, Forrisier, M & Vedrine, JC, 1983, 'Synergy Effects in the Catalytic Properties of Bismuth Molybdates', *Journal of The Chemical Society, Faraday Transaction I,* vol. 79, pp. 1921-1929.

Catlow, CRA 1997, *ISIS Experimental Report: Structural Studies of Bismuth Molybdate Catalyst*, Rutherford Appleton Laboratory. Retrieved: 01/05, from.

Centi, G & Perathoner, S, 2001, 'Reaction Mechanis and Control of Selectivity in Catalysis by Oxides: Some Challenges and Open Questions', *International Journal of Molecular Sciences,* vol. 2, pp. 183-196.

Chen, H-Y & Sleight, AW, 1986, 'Crystal Structure of $Bi_2Mo_2O_9$: A Selective Oxidation Catalyst', *Journal of Solid State Chemistry,* vol. 63, pp. 70-75.

Chen, T & Smith, GS, 1975, 'The Compounds and the Phase Diagram of MoO_3-Rich Bi_2O_3-MoO_3 System', *Journal of Solid State Chemistry,* vol. 13, pp. 288-197.

Chorkendorf, I & Niemantsverdriet, JW 2003, *Concepts of Modern Catalysis*, Wiley-VCH, Weinheim.

Corberan, VC, Corma, A & Kremenic, G, 1985, 'Kinetics of the Partial Oxidation of Isobutene over Silica-Supported Molybdenum-Uranium Oxide Catalyst', *Industrial Engineering Chemical Product: Research and Development,* vol. 24, pp. 62-68.

Cullis, CF & Hucknall, DJ 1981, 'Selective Oxidation of Hydrocarbons', in GC Bond & G Webb (eds.), *Catalysis*, vol. 5, The Royal Society of Chemistry, London, pp. 273-307.

Dadyburjor, DB & Ruckenstein, E, 1978, 'Path of Oxygen in a Bismuth Molybdate Lattice During Selective Oxidation', *The Journal of Physical Chemistry,* vol. 82, no. 13, pp. 1563-1575.

Dadyburjor, DB & Ruckenstein, E, 1980, 'Activation Energies to Characterize Ease of Removal of Various Kinds of Oxygen from Bismuth Molybdates', *Journal of Catalysis,* vol. 63, pp. 383-388.

Daniel, C & Keulks, GW, 1972, 'The catalytic oxidation of propylene : I. Evidence for surface initiated homogeneous reactions', *Journal of Catalysis,* vol. 24, no. 3, pp. 529-535.

Doornkamp, C, Clement, M & Ponec, V, 1999, 'The Isotopic Exchange Reaction of Oxygen on Metal Oxides', *Journal of Catalysis,* vol. 182, no. 2, pp. 390-399.

Doornkamp, C & Ponec, V, 2000, 'The universal character of the Mars and Van Krevelen mechanism', *Journal of Molecular Catalysis A: Chemical,* vol. 162, no. 1-2, pp. 19-32.

Douskey, MC & Munson, EJ 1997, *Solid-State NMR Studies of Bismuth Molybdate Catalysts*, Department of Chemistry, University of Minnesota. Retrieved: 26/03/2001, from http://india.cchem.berkeley.edu/~anant/Public/OldRMCFiles/RMCstuff/rmc/abstracts/post11.html.

Driscoll, DJ & Lunsford, JH, 1985, 'Gas-Phase Radical Formation during the Reactions of Methane, Ethane, Ethylene, and

Propylene over Selected Oxide Catalysts', *Journal of Physical Chemistry,* vol. 89, no. 21, pp. 4415-4418.

Egashira, M, Matsuo, K, Kagawa, S & Seiyama, T, 1979, 'Phase diagram of the system Bi2O3---MoO3', *Journal of Catalysis,* vol. 58, no. 3, pp. 409-418.

Evans, BJ, 1976, '121Sb nuclear gamma-ray resonance study of crystal chemical structures in U---Sb---O acrylonitrile catalysts', *Journal of Catalysis,* vol. 41, no. 2, pp. 271-276.

Fansuri, H, Pham, GH, Wibawanta, S, Zhang, D-k & French, D, 2003, 'The Relationship Between Structural and Catalytic Activity of α and γ-Bismuth-Molybdate Catalysts for Partial Oxidation of Propylene to Acrolein', *Surface Review and Letters,* vol. 10, no. 2-3, pp. 549-553.

Fattore, F, Fuhrman, ZA, Manara, G & Notari, B, 1975a, 'Oxidation of Propene in the Abscence of Gasseous Oxygen II. Bismuth Molybdates and Iron Antimonates', *Journal of Catalysis,* vol. 37, pp. 223-231.

Fattore, V, Fuhrman, ZA, Manara, G & Notari, B, 1975b, 'Oxidation of propene in the absence of gaseous oxygen : I. Single metal oxides', *Journal of Catalysis,* vol. 37, no. 2, pp. 215-222.

Gel'bstein, AI, Stroeva, SS, Kul'kova, NV, Bakshi, YM & Lapidus, VL, 1965, 'Mechanism of Partial Oxidation and Oxidative Ammonolysis of Propylene in the Presence of MoO3-Bi2O3', *Neftekhimiya,* vol. 5, no. 1, pp. 118-125.

Golunski, S & Walker, A, 2000, 'Lowering the Operating Temperature of Selective Oxidation Catalysts', *Chem. Commun*, pp. 1593-1594.

Gorshkov, AP, Gagarin, SG, Kolchin, IK & Margolis, LY, 1970, 'Kinetics of Propylene Oxidation on a Bismuth-molybdenum Catalyst', *Neftekhimiya,* vol. 10, no. 1, pp. 59-63.

Gorshkov, AP, Isgulyanats, GV, Derbentsev, YI, Margolis, LY & Kolchin, IK, 1969, 'Mechanism of Propylene Oxidation on a Bismuth-molybdenum Catalyst', *Doklady Akademii Nauk SSSR,* vol. 186, no. 4, p. 827830.

Gorshkov, AP, Kolchin, IK, Gribov, IM & Margolis, LY, 1968, 'Conversion of Oxygen-containing Propene Oxidation Products on Bismuth Molybdate', *Kinetika i Kataliz,* vol. 9, no. 5, pp. 1086-1093.

Grasselli, RK 1982, 'Selective Oxidation and Ammoxidation Catalysis: History of Catalyst Design', in JP Bonnelle, B Delmon & E Derouane (eds.), *Surface Properties and Catalysis by Non-Metals*, D. Reidel Publishing Company, Dordrecht.

Grasselli, RK, 1985, 'Selectivity and Activity Factors in Bismuth-Molybdate Oxidation Catalysts', *Applied Catalysis,* vol. 15, pp. 127-139.

Grasselli, RK, 1999, 'Advances and Future Trends in Selective Oxidation and Ammoxidation Catalysis', *Catalysis Today,* vol. 49, pp. 141-153.

Grasselli, RK & Suresh, DD, 1972, 'Aspects of structure and activity in U---Sb-oxide acrylonitrile catalysts', *Journal of Catalysis,* vol. 25, no. 2, pp. 273-291.

Grzybowska, B, Haber, J & Janas, J, 1977, 'Interaction of allyl iodide with molybdate catalysts for the selective oxidation of hydrocarbons', *Journal of Catalysis,* vol. 49, no. 2, pp. 150-163.

Grzybowska, R, Haber, J, Marczewski, W & Ungier, L, 1976, 'X-ray and Ultraviolet-Photoelectron Spectra of Bismuth molybdate Catalysts', *Journal of Catalysis,* vol. 42, pp. 327-333.

Gualtieri, AF & Venturelli, P, 1999, 'In situ Study of the Goethite-hematite Phase Transformation by Real Time Synchrotron Powder Diffraction', *American Mineralogist,* vol. 84, pp. 895-904.

Haber, J 1985, 'Catalysis by Transition Metal Oxides', in RK Grasselli & JF Brazdil (eds.), *Solid State Chemistry in Catalysis*, American Chemical Society, Washingto, D. C., pp. 1-19.

Han, Y-H, Ueda, W & Moro-Oka, Y, 1999, 'Lattice Oxide Ion-Transfer Effect Demonstrated in the Selective Oxidation of Propene over Silica-Supported Bismuth Molybdate Catalysts', *Applied Catalysis A: General,* vol. 176, pp. 11-16.

Hayden, P & Higgins, GR 1976, 'Selective Oxidation of Hydrocarbons Over Mixed Oxide Catalysts', in C Kemball (ed.), *Catalysis*, vol. 1, The Chemical Society, London, pp. 169-206.

Hearne, GW, Cerrito, E & Adams, ML, *Production of Unsaturated Carbonylic Compounds,* 2451485, Shell Development Company, (patent).

Hoefs, EV, Monnier, JR & Keulks, GW, 1979, 'The investigation of the type of active oxygen for the oxidation of propylene over bismuth molybdate catalysts using infrared and Raman spectroscopy', *Journal of Catalysis,* vol. 57, no. 2, pp. 331-337.

Howard, CJ, Ball, CJ, Davis, RL & Elcombe, MM, 1983, 'The Australian High Resolution Neutron Powder Diffractometer', *Australian Journal of Physics,* vol. 36, pp. 507-518.

Howard, CJ & Hunter, BA 1997, *LHPM Manual, A Computer Program for Rietveld Analysis of X-ray and Neutron Powder Diffraction Patterns*, Australian Institute of Nuclear Science and Engineering, Sydney.

Howard, CJ & Kennedy, SJ, 1994, 'Neutron Diffraction', *Materials Forum,* vol. 18, pp. 155-176.

Hriljac, JA, Torardi, CC & Vogt, T, 1995, 'A High Resolution Powder Neutron Diffraction Study of the Novel Layered Oxide $BiMo_2O_7OD.2D_2O$', *Journal of Physics and Chemistry of Solids,* vol. 56, no. 10, pp. 1339-1343.

International Agency for Research on Cancer 1995, *Dry Cleaning, Some Chlorinated Solvents and Other Industrial Chemical*, IARC*Press*, Lyon.

Jaswal, IS, Mann, RF, Juusola, JA & Downie, J, 1969, 'Vapor-phase Oxidation of Benzene over a Vanadium Oxide Catalyst', *Canadian Journal of Chemical Engineering,* vol. 47, no. 3, pp. 284-287.

Keulks, GW, 1970, 'The mechanism of oxygen atom incorporation into the products of propylene oxidation over bismuth molybdate', *Journal of Catalysis,* vol. 19, no. 2, pp. 232-235.

Keulks, GW, Hall, JL, Daniel, C & Suzuki, K, 1974, 'The catalytic oxidation of propylene : IV. Preparation and characterization of [alpha]-bismuth molybdate', *Journal of Catalysis,* vol. 34, no. 1, pp. 79-97.

Keulks, GW, Krenzke, LD & Notermann, TM, 1978, 'Selective Oxidation of Propylene', *Advances in Catalysis,* vol. 27, pp. 183-225.

Keulks, GW & Lo, M-Y, 1986, 'Catalytic Oxidation of Propylene, 11. An investigation of the Kinetics and Mechanism over Iron-Antimony Oxide', *The Journal of Physical Chemistry,* vol. 90, pp. 4768-4775.

Keulks, GW, Rosyneck, MP & Daniel, C, 1971, 'Bismuth Molybdate Catalysts. Kinetics and Mechanism of Propylene Oxidation', *Industrial Engineering Chemical Product: Research and Development,* vol. 10, no. 2, pp. 138-142.

Khattak, CP & Cox, DE, 1977, 'Profile analysis of X-ray powder diffractometer data: structural refinement of La0.75Sr0.25CrO3', *Journal of Applied Crystallography,* vol. 10, no. 5, pp. 405-411.

Kisi, EH, 1994, 'Rietveld Analysis of Powder Diffraction Patterns', *Materials Forum,* vol. 18, pp. 135-153.

Knott, R, 1998, 'Neutron Scattering in Australia', *Neutron News,* vol. 9, pp. 23-32.

Kobayashi, M & Futaya, R, 1979, 'Mechanism of propylene oxidation over bismuth molybdate revealed by transient response method : I. An intermediate in the complete oxidation of C3H6', *Journal of Catalysis,* vol. 56, no. 1, pp. 73-83.

Krabetz, R, Engelbach, H, Lebert, U, Frey, W, Duembgen, G, Thiessen, F & Willersinn, C-H, *Catalytic Oxidation of α-Olefins,* 4052450, BASF Aktiengesellschaft, (patent).

Kremenic, G, Nieto, JML, Tascon, JMD & Tejuca, LG, 1987, 'Selective Oxidation of Propene on a Mo-Pr-Bi Catalyst', *Industrial Engineering Chemical Research,* vol. 26, pp. 1419-1424.

Kremenic, G, Nieto, JML, Tascon, JMD & Tejuca, LG, 1988, 'Isobutene Oxidation on an Mo-Pr-Bi-O/SiO_2 Catalyst', *Journal of the Less Common Metals,* vol. 138, pp. 47-57.

Krenzke, LD 1977, *The Kinetics and Mechanism of Propylene Oxidation over Bismuth-Molybdate, Bismuth(1)Molybdenum(1)Oxygen(12),*

Bismuth(3)Iron(1)Molybdenum(2)Oxygen(12) and *Uranium(1)Antimony(3)Oxygen(10)*, The University of Wisconsin.

Krenzke, LD & Keulks, GW, 1980a, 'The catalytic oxidation of propylene : VI. Mechanistic studies utilizing isotopic tracers', *Journal of Catalysis,* vol. 61, no. 2, pp. 316-325.

Krenzke, LD & Keulks, GW, 1980b, 'The Catalytic Oxidation of Propylene VIII. An Investigation of the kinetics over $Bi_2Mo_3O_{12}$, Bi_2MoO_6, and $Bi_3FeMo_2O_{12}$', *Journal of Catalysis,* vol. 64, pp. 295-301.

Kumar, J & Ruckenstein, E, 1976, 'Structural Change in Thin Film of the 1:1 Bismuth Molybdate under Reduction and Oxidation Condition', *Journal of Catalysis,* vol. 45, pp. 198-215.

Larsen, JB 2003, *Run in of a Plug Flow Reactor Using the Selective Oxidation of Propene to Acrolein over β-$Bi_2Mo_2O_9$*, Aalborg Universitet Esbjerg.

Le, MT, van Well, WJM, Stoltze, P, van Driessche, I & Hoste, S, 2004, 'Synergy Effects Between Bismuth Molybdate Catalyst Phases (Bi/Mo from 0.57 to 2) for the Selective Oxidation of Propylene to Acrolein', *Applied Catalysis A: General*.

Lecloux, AJ 1981, 'Texture of Catalysts', in JR Anderson & M Boudart (eds.), *Catalysis Science and Technology*, vol. 2, Springer-Verlag, Berlin, pp. 171-230.

Levenspiel, O 1999, *Chemical Reaction Engineering,* 3rd edn, John Wiley & Sons, New York.

Lewis, WK, Gilliland, ER & Reed, WA, 1949, 'Reaction of Methane with Copper Oxide in a Fluidized Bed', *Industrial and Engineering Chemistry,* vol. 41, no. 6, pp. 1227-1237.

Malmros, G & Thomas, JO, 1977, 'Least-squares structure refinement based on profile analysis of powder film intensity data measured on an automatic microdensitometer', *Journal of Applied Crystallography,* vol. 10, no. 1, pp. 7-11.

Mars, P & van Krevelen, DW, 1954, 'Oxidations Carried Out by Means of Vanadium Oxide Catalysts', *Chemical Engineering Science,* vol. 3 (Spec. Suppl.), pp. 41-59.

Martir, W & Lunsford, JH, 1981, 'The Formation of Gas-Phase π-Allyl Radicals from Propylene over Bismuth Oxide and γ-Bismuth Molybdate Catalysts', *Journal of American Chemical Society,* vol. 103, pp. 3728-3732.

Mathematica in Engineering,, eFunda, Inc. Retrieved: 26 April, from http://www.efunda.com/math/leastsquare/leastsquares.cfm.

Matsuura, I, 1974, 'The adsorption of butene, butadiene, and ammonia on UO3---Sb2O3 catalysts', *Journal of Catalysis,* vol. 35, no. 3, pp. 452-459.

Matyshak, VA & Krylov, OV, 1995, 'In Situ IR Spectroscopy of Intermediates in Heterogeneous Oxidative Catalysis', *Catalysis Today,* vol. 25, pp. 1-88.

McCusker, LB, Dreele, RBV, Cox, DE, Louer, D & Scardi, P, 1999, 'Rietveld Refinement Guidelines', *Journal of Applied Crystallography,* vol. 32, no. 1, pp. 36-50.

Mestl, G, 1994, 'Oxygen-Exchange Properties of MoO_3: An in Situ Raman Spectroscopy Study', *Journal of Physical Chemistry,* vol. 98, pp. 11269-11275.

Millet, JMM, Ponceblanc, H, Coudurier, G, Herrmann, JM & Vedrine, JC, 1993, 'Study of Multiphasic Molybdate-Based Catalysts II. Synergy Effect Between Bismuth Molybdate and Mixed Iron and Cobalt Molybdates in Mild Oxidation of Propene', *Journal of Catalysis,* vol. 142, pp. 381-391.

Miura, H, Otsubo, T-o, Shirasaki, T & Morikawa, Y, 1979, 'Tracer studies of catalytic oxidation by bismuth molybdate : II. Propylene reduction of labeled catalysts and catalytic oxidation of propylene', *Journal of Catalysis,* vol. 56, no. 1, pp. 84-87.

Monnier, JR & Keulks, GW, 1981, 'The catalytic oxidation of propylene : IX. The kinetics and mechanism over [beta]-Bi2Mo2O9', *Journal of Catalysis,* vol. 68, no. 1, pp. 51-66.

O'Connor, BH & Pratapa, S, 2002, 'Improving the Accuracy of Rietveld-Derived lattice Parameters by an Order of Magnitude', *Advances in X-Ray Analysis,* vol. 45, pp. 158-165.

Ohara, T, Sato, T, Shimizu, N, Prescher, G, Schwind, H & Weiberg, O 1987, 'Acrolein and Methacrolein', in D Beech (ed.), *Encyclopedia of Chemical Technology*, vol. A1, Ullman Verlag Chemie, Florida, pp. 149-160.

Ohara, T, Ueshima, M, Nishinomiya & Yanagisawa, I, *Process for The Preparation of Unsaturated Carbonyl Compounds,* 3825600, Nippon Shokubai Kagaku Kogyo Co., Ltd., (patent).

Olier, R, Coudurier, G, Jamal, MME, Forrisier, M & Vedrine, JC, 1989, 'Detection and Quantitative Determination of the Composition of Bismuth Molybdate Phases by Various Spectroscopic Techniques', *Journal of The Chemical Society, Faraday Transaction I,* vol. 85, no. 8, pp. 2615-2624.

Ono, T, Ogata, N & Kuczkowski, RL, 1998, 'Tracer Studies of Olefin Oxidation over an [alpha]-Bi2Mo3O12Catalyst Using Laser Raman and Microwave Spectroscopy', *Journal of Catalysis,* vol. 175, no. 2, pp. 185-193.

Otsubo, T-o, Miura, H, Morikawa, Y & Shirasaki, T, 1975, 'Tracer studies of catalytic oxidation by bismuth molybdate : I. Hydrogen reduction of labeled catalysts', *Journal of Catalysis,* vol. 36, no. 2, pp. 240-243.

Peacock, JM, Sharp, MJ, Parker, AJ, Ashmore, PG & Hockey, JA, 1969, 'The oxidation of propene over bismuth oxide, molybdenum oxide, and bismuth molybdate catalysts : II. ESR studies of bismuth molybdate and MoO3 catalysts', *Journal of Catalysis,* vol. 15, no. 4, pp. 379-386.

Perego, G, 1998, 'Characterization of Heterogeneous Catalysts by X-ray Diffraction Techniques', *Catalysis Today,* vol. 41, pp. 251-259.

Pratapa, S 2003, *Diffraction-based Modelling of Microstructural Size and Strain Effects in Sintered Ceramics*, Curtin University of Technology.

Ressler, T 2005, *Geometric Structure - Research Highlight*, Thorsten Ressler. Retrieved: 26/04/2005, from http://w3.rz-berlin.mpg.de~ressler/gs/highlights/gs_highlight_02.htm.

Rietveld, HM, 1967, 'Line Profiles of Neutron Powder-Diffraction Peaks for Structure Refinement', *Acta Crystallographica,* vol. 22, no. 1, pp. 151-152.

Sancier, KM, Wentrcek, PR & Wise, H, 1975, 'Role of sorbed and lattice oxygen in propylene oxidation catalyzed by silica-supported bismuth molybdate', *Journal of Catalysis,* vol. 39, no. 1, pp. 141-147.

Schultz, JC & Beauchamp, JL, 1983, 'Detection of Gas-Phase Organic Radicals Formed in Gas-Surface Reactions by Photoelectron Spectroscopy: Abstraction of Allylic Hydrogen by Bismuth Oxide', *The Journal of Physical Chemistry,* vol. 87, pp. 3587-3589.

Shannon, RD & Prewitt, CT, 1969, 'Effective ionic radii in oxides and fluorides', *Acta Crystallographica Section B,* vol. 25, no. 5, pp. 925-946.

Sitepu, H 1998, *March-Type Models for the Description of Texture in Granular Materials*, Electronic Thesis, Curtin University of Technology.

Stout, GH & Jensen, LH 1989, *X-Ray Structure Determination,* Second edn, John Wiley & Sons, New York.

Takenaka, S, Kido, Y, Shimabara, T & Ogawa, M, *Oxidation Catalyst for Oxidation of Olefins to Unsaturated Aldehydes,* 3778386, Nippon Kayaku Company, Ltd., (patent).

Tan, HS 1986, *Analysis of the Reaction Network for the Catalytic Oxidation of Propylene*, Microfiche, Queen's University at Kingston.

Tan, HS, Downie, J & Bacon, DW, 1988, 'The Kinetics of the Oxidation of Propylene over a Bismuth Molybdate Catalyst', *The Canadian Journal of Chemical Engineering,* vol. 66, pp. 611-618.

Tan, HS, Downie, J & Bacon, DW, 1989, 'The Reaction Network for the Oxidation of Propylene Over a Bismuth Molybdate Catalyst', *The Canadian Journal of Chemical Engineering,* vol. 67, pp. 412-417.

Tan, HS, Downie, J & Bacon, DW, 1990, 'A Dual Response Analysis of the Initial-Rate Data for the Oxidation of Propylene', *Chemometrics and Intelligent Laboratory Systems,* vol. 9, pp. 75-82.

Tanimoto, M, Nakamura, D & Kawajiri, T, *Method for Production of Acrolein and Acrylic Acid from Propylene,* 6545178 B1, Nippon Shokubai Co., Ltd., (patent).

Teller, RG, Brazdil, JF & Grasselli, RK, 1984, 'The Structure of γ-Bismuth Molybdate, Bi_2MoO_6, by Powder Neutron Diffraction', *Acta Crystallographica C,* vol. 40, pp. 2001-2005.

Theobald, F, Laarif, A & Hewat, AW, 1984, 'The Structure of Koechlinite Bismuth Molybdate - A Controversy Resolved by Neutron Diffraction', *Ferroelectrics,* vol. 56, pp. 219-237.

Theobald, F, Laarif, A & Hewat, AW, 1985, 'Redetermination of The Crystal Structure of α-$Bi_2O_3.3MoO_3$ by Neutron Diffraction and The Catalytic Oxidation of Propene', *Material Research Bulletin,* vol. 20, pp. 653-665.

Thomas, JM & Thomas, WJ 1997, *Principles and Practice of Heterogeneous Catalysis*, VCH Verlagsgesellschaft mbH, Weinheim.

Tomasi, C, Spinolo, G, Chiodelli, G & Magistris, A, 1997, 'Phase equilibria in the Bi-rich part of the Bi, Mo/O system', *Solid State Ionics,* vol. 99, no. 3-4, pp. 263-268.

U.S Department of Labor 1989, *Acrolein and/or Formaldehyde*, U.S. Department of Labor, Occupational Safety & Health Administration. Retrieved: 28/9/2004, from http://www.osha.gov/dts/sltc/methods/organic/org052/org052.htm.

Uchida, K & Ayame, A, 1996, 'Dynamic XPS Measurements on Bismuth Molybdate Surfaces', *Surface Science,* vol. 357-358, pp. 170-175.

Uda, T, Lin, TT & Keluks, GW, 1980, 'The Catalytic Oxidation of Propylene VII. The Use of Temperature Programmed Reoxidation to Characterize γ-Bismuth Molybdate', *Journal of Catalysis,* vol. 62, pp. 26-34.

van den Elzen, AF & Rieck, GD, 1973a, 'The Crystal Structure of $Bi_2(MoO_4)_3$', *Acta Crystallographica B,* vol. 29, pp. 2433-2436.

van den Elzen, AF & Rieck, GD, 1973b, 'Redetermination of the Structure of Bi_2MoO_6, Koechlinite', *Acta Crystallographica B,* vol. 29, pp. 2436-2438.

van den Elzen, AF & Rieck, GD, 1975, 'An Outline of the Crystal-Structure of $Bi_2Mo_2O_9$', *Material Research Bulletin,* vol. 10, pp. 1163-1168.

Veatch, F, Callahan, JL, Milberger, EC & Foreman, RW 1960, 'Catalytic Oxidation of Propylene to Acrolein', in *2nd International Congress in Catalysis*, 2nd edn, Paris, pp. 2647-2658.

Voge, HH, Wagner, CD & Stevenson, DP, 1963, 'Mechanism of propylene oxidation over cuprous oxide', *Journal of Catalysis,* vol. 2, no. 1, pp. 58-62.

West, AR 1989, *Solid State Chemistry and Its Application*, John Wiley & Sons, Singapore.

Yamaguchi, G & Takenaka, S, *Process for The Oxidation of Olefin to Aldehyde and Acids,* 3454630, Nippon Kayaku Company, Ltd., (patent).

Young, RA 1993, *The Rietveld Method*, Oxford University Press, New York.

Young, RA, Mackie, PE & von Dreele, RB, 1977, 'Application of the pattern-fitting structure-refinement method of X-ray powder diffractometer patterns', *Journal of Applied Crystallography,* vol. 10, no. 4, pp. 262-269.

Zeeman, J, 1956, 'Die Kristallstruktur von Koechlinit, Bi_2MoO_6', *Beitraege zur Mineralogie un Petrographie,* vol. 5, pp. 139-145.

Zhang, D-k & Agnew, JB 1994, 'A Kinetic Study of Catalytic Decomposition of Nitric Oxide over Cu Ion-Exchange ZSM-5 Zeolite', in *CHEMECA 1994*, Perth, pp. 259-266.

APPENDIX A. Inorganic Crystal Structure Database (ICSD) of Bismuth molybdates

ICSD 2650, α-Bi2Mo3O12

```
 COL  ICSD Collection Code 2650
 DATE Recorded Jan 1, 1980; updated Aug 19, 1992
 NAME Bismuth molybdate
 FORM Bi2 (Mo O4)3
      = Bi2 Mo3 O12
 TITL The crystal structure of Bi2 (Mo O4)3
 REF  Acta Crystallographica B (24,1968-38,1982)

      ACBCA 29 (1973) 2433-2436
 AUT  van den Elzen A F, Rieck G D
 CELL a=7.685(6) b=11.491(16) c=11.929(10) α=90.0 ß=115.4(0) τ=90.0
      V=951.6 Z=4
 SGR  P 1 21/c 1    (14) - monoclinic
 CLAS 2/m   (Hermann-Mauguin) - C2h (Schoenflies)
 PRS  mP68
 ANX  A2B3X12
 PARM Atom__No OxStat  Wyck -----X----- -----Y----- -----Z-----  -
SOF-
      Bi     1  3.000    4e  0.25999(8)  0.36188(5)  0.25584(5)
      Bi     2  3.000    4e  0.90798(10) 0.12976(5)  0.08334(6)
      Mo     1  6.000    4e  0.0320(2)   0.1114(1)   0.4165(1)
      Mo     2  6.000    4e  0.4218(2)   0.1513(1)   0.1089(1)
      Mo     3  6.000    4e  0.7341(2)   0.3669(1)   0.1952(1)
      O      1 -2.000    4e  0.544(2)    0.052(1)    0.224(1)
      O      2 -2.000    4e  0.936(2)    0.054(1)    0.256(1)
      O      3 -2.000    4e  0.222(2)    0.196(1)    0.152(1)
      O      4 -2.000    4e  0.864(2)    0.208(1)    0.412(1)
      O      5 -2.000    4e  0.224(2)    0.199(1)    0.435(1)
      O      6 -2.000    4e  0.620(2)    0.205(1)    0.072(1)
      O      7 -2.000    4e  0.951(2)    0.291(1)    0.197(1)
      O      8 -2.000    4e  0.507(2)    0.316(1)    0.198(1)
      O      9 -2.000    4e  0.287(2)    0.436(1)    0.482(1)
      O     10 -2.000    4e  0.128(2)    0.448(1)    0.082(1)
      O     11 -2.000    4e  0.840(2)    0.442(1)    0.340(1)
      O     12 -2.000    4e  0.692(2)    0.468(1)    0.084(1)
 WYCK e17
 ITF  O   1   B=1.4
 ITF  O   2   B=0.9
 ITF  O   3   B=0.8
 ITF  O   4   B=1.1
 ITF  O   5   B=1.2
 ITF  O   6   B=1.1
 ITF  O   7   B=0.7
 ITF  O   8   B=1.2
 ITF  O   9   B=1.5
 ITF  O  10   B=0.8
 ITF  O  11   B=1.
 ITF  O  12   B=1.9

 TF   Atom   ß(1,1)  ß(2,2)  ß(3,3)  ß(1,2)  ß(1,3)  ß(2,3)
      Bi 1    0.0021  0.0010  0.0014 -0.0000 -0.0001  0.0006
                 (1)     (1)     (1)     (0)     (0)     (0)
      Bi 2    0.0033  0.0010  0.0013 -0.0003 -0.0001  0.0011
                 (1)     (1)     (1)     (0)     (0)     (0)
      Mo 1    0.0039  0.0007  0.0013 -0.0002  0.0001  0.0007
                 (2)     (1)     (1)     (1)     (0)     (1)
```

```
      Mo 2    0.0017  0.0007  0.0020 -0.0000 -0.0001  0.0008
                 (2)     (1)     (1)     (1)     (0)     (1)
      Mo 3    0.0023  0.0012  0.0024 -0.0001 -0.0002  0.0013
                 (2)     (1)     (1)     (0)     (1)     (1)
RVAL 0.037
```

ICSD 201742, β-$Bi_2Mo_2O_9$

```
 COL  ICSD Collection Code 201742
 DATE Recorded Dec 3, 1986; updated May 13, 1997
 NAME Bismuth molybdenum oxide (2/2/9)
 FORM Bi2 Mo2 O9
      = Bi2 Mo2 O9
 TITL Crystal structure of Bi2 Mo2 O9: A selective oxidation
catalyst
 REF  Journal of Solid State Chemistry
      JSSCB 63 (1986) 70-75
 AUT  Chen H-Y, Sleight A W
 CELL a=11.972(3) b=10.813(4) c=11.899(2) α=90.0 ß=90.1(0) τ=90.0
      V=1540.4 Z=8
 SGR  P 1 21/n 1    (14) - monoclinic
 CLAS 2/m   (Hermann-Mauguin) - C2h (Schoenflies)
 PRS  mP104
 ANX  A2B2X9
 PARM Atom__No OxStat  Wyck -----X----- -----Y----- -----Z-----  -
SOF-
      Bi     1  3.000    4e -0.10020(9)  0.1209(2)   0.7564(1)
      Bi     2  3.000    4e  0.60326(9)  0.1229(2)   0.7583(1)
      Bi     3  3.000    4e  0.25585(11) 0.1232(2)   0.7585(1)
      Bi     4  3.000    4e  0.25301(9)  0.1228(1)   0.4122(1)
      Mo     1  6.000    4e -0.0827(2)   0.1230(4)   0.0872(2)
      Mo     2  6.000    4e -0.0784(2)   0.1250(4)   0.4163(2)
      Mo     3  6.000    4e  0.5893(2)   0.1272(4)   0.0814(2)
      Mo     4  6.000    4e  0.5791(2)   0.1321(4)   0.4156(2)
      O      1 -2.000    4e  0.252(2)    0.261(2)    0.285(2)
      O      2 -2.000    4e  0.255(2)    0.493(2)    0.227(2)
      O      3 -2.000    4e  0.409(2)    0.257(2)    0.689(2)
      O      4 -2.000    4e  0.326(2)    0.259(2)    0.901(2)
      O      5 -2.000    4e  0.105(2)    0.437(3)    0.447(2)
      O      6 -2.000    4e  0.101(2)    0.251(2)    0.815(2)
      O      7 -2.000    4e  0.405(2)    0.444(2)    0.048(2)
      O      8 -2.000    4e  0.093(2)    0.494(3)    0.684(2)
      O      9 -2.000    4e  0.194(2)    0.260(2)    0.596(2)
      O     10 -2.000    4e  0.097(2)    0.313(3)    0.050(2)
      O     11 -2.000    4e  0.403(2)    0.308(2)    0.454(2)
      O     12 -2.000    4e  0.056(2)    0.187(2)    0.388(2)
      O     13 -2.000    4e  0.044(2)    0.046(2)    0.112(2)
      O     14 -2.000    4e  0.447(2)    0.066(2)    0.383(2)
      O     15 -2.000    4e  0.399(2)    0.495(3)    0.820(2)
      O     16 -2.000    4e  0.962(2)    0.300(3)    0.599(2)
      O     17 -2.000    4e  0.177(2)    0.489(2)    0.904(2)
      O     18 -2.000    4e  0.192(2)    0.988(3)    0.903(2)
 WYCK e26
 ITF  O   1   B=1.3(5)
 ITF  O   2   B=1.1(5)
 ITF  O   3   B=1.3(5)
 ITF  O   4   B=1.1(5)
 ITF  O   5   B=1.6(5)
 ITF  O   6   B=1.0(4)
 ITF  O   7   B=1.9(4)
 ITF  O   8   B=1.4(5)
 ITF  O   9   B=1.2(5)
 ITF  O  10   B=1.8(5)
 ITF  O  11   B=0.9(4)
 ITF  O  12   B=0.7(4)
```

```
 ITF  O  13   B=0.9(4)
 ITF  O  14   B=1.1(5)
 ITF  O  15   B=1.4(5)
 ITF  O  16   B=1.5(5)
 ITF  O  17   B=1.2(5)
 ITF  O  18   B=1.7(5)

 TF   Atom   ß(1,1)  ß(2,2)  ß(3,3)  ß(1,2)  ß(1,3)  ß(2,3)
      Bi 1    0.0000  0.0019  0.0016  0.0002 -0.0003 -0.0011
                         (1)     (1)     (2)     (1)     (2)
      Bi 2    0.0000  0.0020  0.0014  0.0000 -0.0005  0.0005
                         (1)     (1)     (2)     (1)     (2)
      Bi 3    0.0000  0.0016  0.0012  0.0003 -0.0006  0.0000
                         (1)     (1)     (2)     (1)     (2)
      Bi 4    0.0000  0.0014  0.0010  0.0004 -0.0003  0.0000
                         (1)     (1)     (3)     (1)     (3)
      Mo 1    0.0010  0.0016  0.0008  0.0003 -0.0007  0.0003
                 (1)     (2)     (2)     (2)     (3)     (5)
      Mo 2    0.0010  0.0016  0.0013 -0.0008 -0.0007  0.0008
                 (2)     (2)     (2)     (5)     (5)     (5)
      Mo 3    0.0019  0.0019  0.0014 -0.0005 -0.0002  0.0003
                 (2)     (3)     (2)     (5)     (3)     (5)
      Mo 4    0.0011  0.0023  0.0019 -0.0007 -0.0002  0.0010
                 (2)     (3)     (2)     (5)     (3)     (5)
 REM  H z parameter of Mo1 given incorrectly in paper as -.8722
 RVAL 0.051
 TEST At least one temperature factor is implausible or meaningless
but
      agrees with the value given in the paper. (Code 52)
```

ICSD 47139, γ-Bi_2MoO_6

```
 COL  ICSD Collection Code 47139
 DATE Recorded Jun 11, 1985; updated Nov 30, 1999
 NAME Dibismuth molybdenum oxide
 MINR Koechlinite - synthetic
 FORM Bi2 Mo O6
      = Bi2 Mo O6
 TITL The Structure of gamma-Bismuth Molybdate, Bi2 Mo O6, by Powder
      Neutron Diffraction.
 REF  Acta Crystallographica C (39,1983-)
      ACSCE 40 (1984) 2001-2005
 AUT  Teller R G, Brazdil J F, Grasselli R K, Jorgensen J D
 CELL a=5.482(0) b=16.199(1) c=5.509(0) α=90.0 ß=90.0 τ=90.0
      V=489.2 D=8.28 Z=4
 SGR  P c a 21      (29) - orthorhombic
 CLAS mm2   (Hermann-Mauguin) - C2v (Schoenflies)
 PRS  oP36
 ANX  AB2X6
 PARM Atom__No OxStat  Wyck -----X----- -----Y----- -----Z-----  -
SOF-
      Bi     1  3.000    4a  0.5180(12)  0.4232(4)   0.9814(14)
      Bi     2  3.000    4a  0.4822      0.0783(4)   0.9897(14)
      Mo     1  6.000    4a  0.0028(21)  0.2488(7)   0.
      O      1 -2.000    4a  0.0556(19)  0.1407(8)   0.0959(20)
      O      2 -2.000    4a  0.2594(10) -0.0017(6)   0.2776(14)
      O      3 -2.000    4a  0.2360(13)  0.5006(8)   0.2664(22)
      O      4 -2.000    4a  0.6917(14)  0.2322(5)   0.2524(16)
      O      5 -2.000    4a  0.2121(15)  0.2634(6)   0.3550(16)
      O      6 -2.000    4a  0.5654(22)  0.3589(10)  0.5700(19)
 WYCK a9
 ITF  Bi  1   B=0.3(3)
 ITF  Bi  2   B=1.0(3)
 ITF  Mo  1   B=0.5(1)
 ITF  O   1   B=0.3(2)
 ITF  O   2   B=0.4(2)
 ITF  O   3   B=1.3(3)
 ITF  O   4   B=0.9(2)
 ITF  O   5   B=1.1(2)
 ITF  O   6   B=1.4(4)
 REM  NDP (neutron diffraction from a powder)
 REM  M Not space group Pna21, cp. 201685
 RVAL 0.050
 TEST Calculated density unusual but tolerable. (Code 23)
```

APPENDIX B. Refinement Results

REFINEMENT RESULTS OF α-Bi2Mo3O12

A. Room Temperature Diffractograms

Refinement Parameters	van den Elzen & Rieck (XRD)		Theobald and Laarif (ND)		H5129t (HRPD)		aBiMo009 (Cu RT-XRD)	
	ICSD 2650		ICSD 63640		ICSD 2650		ICSD 2650	
		Esd		Esd		Esd		Esd
Bismuth Molybdate								
R_p					5.34		6.79	
R_{wp}					6.31		9.13	
R_{exp}					5.53		5.47	
R_{Bragg}					1.28		2.56	
GOF					1.30		2.79	
Durbin Unwght					1.80		0.49	
Durbin Wght					1.79		0.78	
N-P					2815.00		5684.00	
Crystal Density (D_x)					6.188		6.190	
MW					3591.120		3591.120	
Cell Volume					963.170	0.150	962.890	0.040
Histogram								
Sample displacement					0.0000	0.0000	0.0061	0.0019
$2\theta_o$					0.13350	0.00568	0.04100	Fixed
B0					63.30	2.07	-101.98	3.08
B1					-1.99	0.11	2.41	0.08
B2					0.04	0.00	-0.01	0.00
B3					0.00	0.00		
B4					0.00	0.00		
B-1					-144.76	11.18	2797.61	27.30
Phases								
Phase scale					0.00966	0.00009	0.00004	0.00000
a	7.685	0.006	7.710	0.000	7.7155	0.0006	7.7138	0.0003
b	11.491	0.016	11.531	0.000	11.5267	0.0008	11.5270	0.0003
c	11.929	0.010	11.972	0.001	11.9768	0.0010	11.9762	0.0003
β	115.400	0.000	115.300	0.000	115.2760	0.0042	115.2810	0.0015
Sample					Voight (How Asy)			
U					0.14609	0.02340	0.16586	0.01060
V					-0.10577	0.03316	-0.00835	0.00710
W					0.11005	0.01243	0.00548	0.00116
Asy1					0.16141	0.00755	0.06276	0.00690
Size/Gam0					0.10121	0.00767	0.06892	0.00090
Particle Size (A)					845.00	64.00	1280.70	16.80
x								
Bi 1	0.25999	0.00008	0.2552	0.0007	0.2588	0.0013	0.2610	0.0002
Bi 2	0.90798	0.00010	0.9055	0.0008	0.9082	0.0013	0.9095	0.0003
Mo 1	0.0320	0.0002	0.0254	0.0009	0.0287	0.0016	0.0313	0.0005
Mo 2	0.4218	0.0002	0.4288	0.0010	0.4202	0.0016	0.4212	0.0006
Mo 3	0.7341	0.0002	0.7325	0.0009	0.7332	0.0015	0.7335	0.0005
O 1	0.544	0.002	0.5436	0.0011	0.5404	0.0018	0.0514	0.0035
O 2	0.936	0.002	0.9362	0.0012	0.9327	0.0017	0.9038	0.0031
O 3	0.222	0.002	0.2158	0.0010	0.2196	0.0016	0.2285	0.0027
O 4	0.864	0.002	0.8525	0.0013	0.8598	0.0020	0.8446	0.0034
O 5	0.224	0.002	0.2308	0.0012	0.2214	0.0017	0.2362	0.0028
O 6	0.620	0.002	0.6068	0.0012	0.6201	0.0020	0.6216	0.0032
O 7	0.951	0.002	0.9491	0.0011	0.9552	0.0015	0.9590	0.0028
O 8	0.507	0.002	0.5052	0.0010	0.5046	0.0017	0.5149	0.0029
O 9	0.287	0.002	0.2877	0.0010	0.2869	0.0017	0.2869	0.0030
O 10	0.128	0.002	0.1294	0.0013	0.1258	0.0019	0.1475	0.0029
O 11	0.840	0.002	0.8313	0.0011	0.8377	0.0016	0.8029	0.0031

Refinement Parameters	van den Elzen & ICSD 2650		Theobald and Laarif ICSD 63640		H5129t ICSD 2650		aBiMo009 ICSD 2650	
		Esd		Esd		Esd		Esd
Bi 1	0.36188	0.00005	0.3612	0.0004	0.3623	0.0007	0.3638	0.0002
Bi 2	0.12976	0.00005	0.1314	0.0004	0.1303	0.0007	0.1296	0.0002
Mo 1	0.1114	0.0001	0.1122	0.0005	0.1106	0.0008	0.1132	0.0003
Mo 2	0.1513	0.0001	0.1896	0.0005	0.1511	0.0008	0.1518	0.0003
Mo 3	0.3669	0.0001	0.3685	0.0006	0.3651	0.0010	0.3693	0.0004
O 1	0.052	0.001	0.0503	0.0007	0.0499	0.0011	0.0608	0.0016
O 2	0.054	0.001	0.0527	0.0008	0.0540	0.0011	0.0546	0.0017
O 3	0.196	0.001	0.1969	0.0007	0.1938	0.0011	0.1878	0.0017
O 4	0.208	0.001	0.2074	0.0006	0.2091	0.0010	0.2002	0.0016
O 5	0.199	0.001	0.2002	0.0007	0.2007	0.0011	0.2018	0.0016
O 6	0.205	0.001	0.2003	0.0008	0.2043	0.0011	0.2181	0.0017
O 7	0.291	0.001	0.2874	0.0007	0.2933	0.0010	0.2923	0.0018
O 8	0.316	0.001	0.3166	0.0007	0.3146	0.0010	0.3042	0.0016
O 9	0.436	0.001	0.4405	0.0008	0.4355	0.0011	0.4322	0.0017
O 10	0.448	0.001	0.4492	0.0006	0.4482	0.0010	0.4565	0.0017
O 11	0.442	0.001	0.4478	0.0007	0.4412	0.0010	0.4439	0.0016
O 12	0.468	0.001	0.4690	0.0007	0.4681	0.0011	0.4541	0.0019
z								
Bi 1	0.25584	0.00005	0.2607	0.0004	0.2573	0.0007	0.2556	0.0002
Bi 2	0.08334	0.00006	0.0840	0.0005	0.0829	0.0008	0.0820	0.0002
Mo 1	0.4165	0.0001	0.4150	0.0005	0.4162	0.0010	0.4171	0.0003
Mo 2	0.1089	0.0001	0.1037	0.0005	0.1059	0.0009	0.1074	0.0003
Mo 3	0.1952	0.0001	0.1943	0.0005	0.1959	0.0009	0.1947	0.0003
O 1	0.224	0.001	0.2189	0.0006	0.2200	0.0011	0.2374	0.0022
O 2	0.256	0.001	0.2556	0.0007	0.2546	0.0010	0.2602	0.0017
O 3	0.152	0.001	0.1543	0.0006	0.1542	0.0009	0.1718	0.0015
O 4	0.412	0.001	0.4126	0.0008	0.4119	0.0012	0.4227	0.0021
O 5	0.435	0.001	0.4441	0.0006	0.4365	0.0009	0.4435	0.0019
O 6	0.072	0.001	0.0588	0.0007	0.0675	0.0012	0.0790	0.0019
O 7	0.197	0.001	0.1968	0.0007	0.1997	0.0010	0.2126	0.0020
O 8	0.198	0.001	0.1974	0.0007	0.1954	0.0010	0.2096	0.0019
O 9	0.482	0.001	0.4811	0.0008	0.4792	0.0011	0.4804	0.0020
O 10	0.082	0.001	0.0783	0.0008	0.0763	0.0011	0.0617	0.0019
O 11	0.340	0.001	0.3372	0.0007	0.3385	0.0010	0.3100	0.0019
O 12	0.084	0.001	0.0873	0.0008	0.0850	0.0013	0.0498	0.0022
B								
Bi 1	*				0.84	0.16	0.50	
Bi 2	*				0.50	0.12	0.50	
Mo 1	*				1.25	0.18	0.50	
Mo 2	*				0.70	0.17	0.50	
Mo 3	*				1.19	0.18	0.50	
O 1	1.40				1.05	0.22	1.40	
O 2	0.90				0.77	0.21	0.90	
O 3	0.80				0.90	0.22	0.80	
O 4	1.10				1.42	0.23	1.10	
O 5	1.20				0.72	0.20	1.20	
O 6	1.10				1.23	0.22	1.10	
O 7	0.70				0.42	0.18	0.70	
O 8	1.20				0.66	0.22	1.20	
O 9	1.50				0.81	0.19	1.50	
O 10	0.80				1.05	0.22	0.80	
O 11	1.00				0.68	0.19	1.00	
O 12	1.90				1.31	0.26	1.90	

B. In-situ Diffractograms

Refinement Parameters	300°C in Air (MRPD) ICSD 2650		400°C in Air (MRPD) ICSD 2650		300°C in Gas (MRPD) ICSD 2650		400°C in Gas (MRPD) ICSD 2650	
		Esd		Esd		Esd		Esd
Bismuth Molybdate								
R_p	2.65		5.34		2.52		5.34	
R_{wp}	3.23		6.31		3.12		6.31	
R_{exp}	2.00		5.53		2.00		5.53	
R_{Bragg}	9.34		1.28		7.64		1.28	
GOF	2.60		1.30		2.42		1.30	
Durbin Unwght	1.01		1.80		1.04		1.80	
Durbin Wght	1.02		1.79		1.06		1.79	
N-P	1207.00		2815.0		1208.00		2815.0	
Crystal Density (D_x)	6.121		6.188		6.119		6.188	
MW	3.591		3591.120		3591.120		3591.120	
Cell Volume	973.848	0.180			974.180	0.188		
Histogram								
Sample displacement	0.0000	0.0000	0.0000	0.0000	0.0000	0.0000	0.0000	0.0000
$2\theta_o$	0.00000	Fixed	0.13350	0.00568	0.00000	Fixed	0.13350	0.00568
B0	*		63.30	2.07	*		63.30	2.07
B1	*		-1.99	0.11	*		-1.99	0.11
B2	*		0.04	0.00	*		0.04	0.00
B3	*		0.00	0.00	*		0.00	0.00
B4	*		0.00	0.00	*		0.00	0.00
B-1	*		-144.76	11.18	*		-144.76	11.18
Phases								
Phase scale	0.07934	0.00085	0.00966	0.00009	0.07156	0.00085	0.00966	0.00009
a	7.2235	0.0008	7.7155	0.0006	7.7237	0.0008	7.7155	0.0006
b	11.6046	0.0012	11.5267	0.0008	11.6063	0.0012	11.5267	0.0008
c	11.9933	0.0014	11.9768	0.0010	11.9928	0.0015	11.9768	0.0010
β	115.0298	0.0096	115.2760	0.0042	115.0209	0.0098	115.2760	0.0042
Sample	Voight (How Asy)		Voight (How Asy)		Voight (How Asy)		Voight (How Asy)	
U	0.21176	0.07797	0.14609	0.02340	0.58150	0.09965	0.14609	0.02340
V	0.05170	0.08243	-0.10577	0.03316	-0.28603	0.10173	-0.10577	0.03316
W	0.07547	0.02346	0.11005	0.01243	0.15730	0.02833	0.11005	0.01243
Asy1	0.20640	0.00693	0.16141	0.00755	0.19303	0.00739	0.16141	0.00755
Size/Gam0	0.11425	0.01218	0.10121	0.00767	0.09909	0.01198	0.10121	0.00767
Particle Size (A)	835.00	89.00	845.00	64.00	962.80	116.40	845.00	64.00
x								
Bi 1	0.2541	0.0027	0.2588	0.0013	0.2618	0.0023	0.2588	0.0013
Bi 2	0.9088	0.0025	0.9082	0.0013	0.8959	0.0025	0.9082	0.0013
Mo 1	0.0327	0.0027	0.0287	0.0016	0.0446	0.0032	0.0287	0.0016
Mo 2	0.4082	0.0036	0.4202	0.0016	0.4521	0.0060	0.4202	0.0016
Mo 3	0.7294	0.0028	0.7332	0.0015	0.7609	0.0024	0.7332	0.0015
O 1	0.5593	0.0058	0.5404	0.0018	0.5380	0.0043	0.5404	0.0018
O 2	0.9508	0.0041	0.9327	0.0017	0.9322	0.0031	0.9327	0.0017
O 3	0.2027	0.0031	0.2196	0.0016	0.2239	0.0027	0.2196	0.0016
O 4	0.8196	0.0051	0.8598	0.0020	0.8682	0.0046	0.8598	0.0020
O 5	0.2134	0.0048	0.2214	0.0017	0.2114	0.0044	0.2214	0.0017
O 6	0.6212	0.0050	0.6201	0.0020	0.6351	0.0042	0.6201	0.0020
O 7	0.9489	0.0027	0.9552	0.0015	0.9410	0.0037	0.9552	0.0015
O 8	0.5052	0.0032	0.5046	0.0017	0.5021	0.0030	0.5046	0.0017
O 9	0.3052	0.0030	0.2869	0.0017	0.2926	0.0036	0.2869	0.0017
O 10	0.1278	0.0031	0.1258	0.0019	0.1231	0.0030	0.1258	0.0019
O 11	0.8597	0.0039	0.8377	0.0016	0.8443	0.0039	0.8377	0.0016
O 12	0.7188	0.0061	0.6933	0.0018	0.6876	0.0044	0.6933	0.0018

Refinement Parameters	300°C in Air		400°C in Air		300°C in Gas		400°C in Gas	
	ICSD 2650		ICSD 2650		ICSD 2650		ICSD 2650	
		Esd		Esd		Esd		Esd
y								
Bi 1	0.3613	0.0017	0.3623	0.0007	0.3575	0.0013	0.3623	0.0007
Bi 2	0.1395	0.0013	0.1303	0.0007	0.1372	0.0016	0.1303	0.0007
Mo 1	0.1142	0.0014	0.1106	0.0008	0.1140	0.0010	0.1106	0.0008
Mo 2	0.1508	0.0017	0.1511	0.0008	0.1342	0.0033	0.1511	0.0008
Mo 3	0.3749	0.0017	0.3651	0.0010	0.3608	0.0018	0.3651	0.0010
O 1	0.0505	0.0031	0.0499	0.0011	0.0632	0.0025	0.0499	0.0011
O 2	0.0665	0.0025	0.0540	0.0011	0.0509	0.0019	0.0540	0.0011
O 3	0.1876	0.0017	0.1938	0.0011	0.1987	0.0019	0.1938	0.0011
O 4	0.2140	0.0022	0.2091	0.0010	0.2084	0.0024	0.2091	0.0010
O 5	0.1947	0.0028	0.2007	0.0011	0.1810	0.0030	0.2007	0.0011
O 6	0.2061	0.0023	0.2043	0.0011	0.2008	0.0020	0.2043	0.0011
O 7	0.2881	0.0018	0.2933	0.0010	0.2962	0.0027	0.2933	0.0010
O 8	0.3110	0.0020	0.3146	0.0010	0.3074	0.0019	0.3146	0.0010
O 9	0.4344	0.0018	0.4355	0.0011	0.4468	0.0022	0.4355	0.0011
O 10	0.4564	0.0018	0.4482	0.0010	0.4494	0.0016	0.4482	0.0010
O 11	0.4399	0.0026	0.4412	0.0010	0.4234	0.0025	0.4412	0.0010
O 12	0.4686	0.0046	0.4681	0.0011	0.4726	0.0020	0.4681	0.0011
z								
Bi 1	0.2495	0.0014	0.2573	0.0007	0.2641	0.0013	0.2573	0.0007
Bi 2	0.0779	0.0018	0.0829	0.0008	0.0774	0.0015	0.0829	0.0008
Mo 1	0.4185	0.0017	0.4162	0.0010	0.4188	0.0022	0.4162	0.0010
Mo 2	0.1085	0.0017	0.1059	0.0009	0.1318	0.0033	0.1059	0.0009
Mo 3	0.1982	0.0015	0.1959	0.0009	0.2112	0.0014	0.1959	0.0009
O 1	0.2234	0.0032	0.2200	0.0011	0.2180	0.0026	0.2200	0.0011
O 2	0.2666	0.0023	0.2546	0.0010	0.2512	0.0020	0.2546	0.0010
O 3	0.1575	0.0016	0.1542	0.0009	0.1502	0.0017	0.1542	0.0009
O 4	0.4036	0.0029	0.4119	0.0012	0.4125	0.0026	0.4119	0.0012
O 5	0.4235	0.0027	0.4365	0.0009	0.4290	0.0029	0.4365	0.0009
O 6	0.0714	0.0028	0.0675	0.0012	0.0719	0.0021	0.0675	0.0012
O 7	0.1926	0.0017	0.1997	0.0010	0.1963	0.0027	0.1997	0.0010
O 8	0.1890	0.0019	0.1954	0.0010	0.1914	0.0018	0.1954	0.0010
O 9	0.4894	0.0020	0.4792	0.0011	0.4926	0.0024	0.4792	0.0011
O 10	0.0753	0.0019	0.0763	0.0011	0.0776	0.0020	0.0763	0.0011
O 11	0.3546	0.0024	0.3385	0.0010	0.3302	0.0024	0.3385	0.0010
O 12	0.0648	0.0046	0.0850	0.0013	0.0892	0.0027	0.0850	0.0013
B								
Bi 1	2.63	0.42	0.84	0.16	1.09	0.27	0.84	0.16
Bi 2	2.30	0.34	0.50	0.12	1.80	0.35	0.50	0.12
Mo 1	1.49	0.31	1.25	0.18	3.03	0.47	1.25	0.18
Mo 2	2.13	0.44	0.70	0.17	11.74	1.37	0.70	0.17
Mo 3	1.45	0.37	1.19	0.18	0.64	0.27	1.19	0.18
O 1	6.51	0.80	1.05	0.22	3.63	0.63	1.05	0.22
O 2	4.00	0.66	0.77	0.21	1.05	0.40	1.05	0.21
O 3	1.72	0.48	0.90	0.22	0.70	0.00	0.70	0.22
O 4	5.12	0.76	1.42	0.23	3.78	0.61	3.78	0.23
O 5	6.35	0.89	0.72	0.20	6.49	1.17	6.49	0.20
O 6	4.81	0.70	1.23	0.22	1.87	0.47	1.87	0.22
O 7	0.67	0.33	0.42	0.18	3.89	0.65	3.89	0.18
O 8	1.60	0.42	0.66	0.22	0.83	0.39	0.83	0.22
O 9	1.66	0.43	0.81	0.19	2.88	0.56	2.88	0.19
O 10	0.80	0.00	1.05	0.22	0.80	0.00	0.80	0.22
O 11	4.07	0.66	0.68	0.19	3.91	0.61	3.91	0.19
O 12	12.56	1.87	1.31	0.26	3.24	0.66	3.24	0.26

REFINEMENT RESULTS OF β-$Bi_2Mo_2O_9$

A. Room Temperature Diffractograms

Refinement Parameters	H.Y.Chen & A.W.Sleight (1986)		H5672 (HRPD)		bBiMo006 (Cu RT-XRD)	
	ICSD 201742		ICSD 201742		ICSD 201742	
		Esd		Esd		Esd
Bismuth Molybdate						
R_p			4.63		15.19	
R_{wp}			5.65		19.90	
R_{exp}			4.44		6.32	
R_{Bragg}			1.59		12.45	
GOF			1.62		9.92	
Durbin UnWght					0.09	
Durbin Wght					0.26	
N-P					5738.00	
Crystal Density (D_x)			6.51		6.525	
MW			6030.720		6030.720	
Cell Volume ($Å^3$)	1540.400		1538.270	0.050	1534.050	0.093
Histogram						
Sample displacement			Fixed	Fixed		
$2\theta_o$			0.00000	Fixed	0.0410	Fixed
B0			23.34520	1.21171	-88.4962	4.7644
B1			0.29534	0.02394	2.1309	0.1165
B2			-0.00035	0.00012	-0.0057	0.0008
B3						
B4						
B-1			168.29100	15.59470	2659.7100	45.9618
Phases						
Phase scale			0.00646	0.00003		
a	11.972		11.9646	0.0002	11.9542	0.0005
b	10.813		10.8104	0.0001	10.7995	0.0003
c	11.899		11.8931	0.0002	11.8828	0.0004
β	90.100		90.1390	0.0018	90.1426	0.0034
Sample			Voight (How Asy)			
U			0.10483	0.00388	0.01700	Fixed
V			-0.26146	0.00745	0.00750	
W			0.18519	0.00401	0.00186	
Asy1			0.06208	0.00175	0.06372	0.00100
Size/Gam0			0.05474	0.00310	0.04881	0.00136
Particle Size (A)			1564.7	88.70000	1808.600	50.50000

Refinement Parameters	H.Y.Chen & ICSD 201742		H5672 (HRPD) ICSD 201742		bBiMo006 ICSD 201742	
		Esd		Esd		Esd
x						
Bi 1	-0.10020		-0.10100	0.00100	-0.1002	
Bi 2	0.60326		0.60090	0.00090	0.6033	
Bi 3	0.25585		0.25310	0.00120	0.2558	
Bi 4	0.25301		0.25558	0.00100	0.2530	
Mo 1	-0.0827		-0.0838	0.0011	-0.0827	
Mo 2	-0.0784		-0.0773	0.0011	-0.0784	
Mo 3	0.5893		0.5867	0.0012	0.5893	
Mo 4	0.5791		0.5805	0.0013	0.5791	
O 1	0.2520		0.2553	0.0013	0.2520	
O 2	0.255		0.2552	0.001	0.255	
O 3	0.409		0.4099	0.0012	0.409	
O 4	0.326		0.3196	0.0012	0.326	
O 5	0.105		0.1102	0.0013	0.105	
O 6	0.101		0.1014	0.0013	0.101	
O 7	0.405		0.4029	0.0012	0.405	
O 8	0.093		0.0934	0.0014	0.093	
O 9	0.194		0.1941	0.0011	0.194	
O 10	0.097		0.0988	0.0013	0.097	
O 11	0.403		0.4098	0.0011	0.403	
O 12	0.056		0.0579	0.0012	0.056	
O 13	0.044		0.0428	0.0013	0.044	
O 14	0.447		0.4461	0.0012	0.447	
O 15	0.399		0.4011	0.0015	0.399	
O 16	0.962		0.9611	0.0015	0.962	
O 17	0.177		0.1780	0.0011	0.177	
O 18	0.192		0.1915	0.0014	0.192	
y						
Bi 1	0.12090		0.12330	0.00160	0.1209	
Bi 2	0.12290		0.12500	0.00140	0.1229	
Bi 3	0.12320		0.12030	0.00130	0.1232	
Bi 4	0.12280		0.12440	0.00100	0.1228	
Mo 1	0.1230		0.1243	0.0014	0.1230	
Mo 2	0.1250		0.1266	0.0015	0.1250	
Mo 3	0.1272		0.1245	0.0015	0.1272	
Mo 4	0.1321		0.1281	0.0016	0.1321	
O 1	0.2610		0.2634	0.0014	0.2610	
O 2	0.493		0.494	0.001	0.493	
O 3	0.257		0.2568	0.0016	0.257	
O 4	0.259		0.2572	0.0019	0.259	
O 5	0.437		0.4416	0.0017	0.437	
O 6	0.251		0.2452	0.0015	0.251	
O 7	0.444		0.4433	0.0015	0.444	
O 8	0.494		0.4941	0.0017	0.494	
O 9	0.260		0.2558	0.0017	0.260	
O 10	0.313		0.3192	0.0015	0.313	
O 11	0.308		0.3066	0.0015	0.308	
O 12	0.187		0.1879	0.0015	0.187	
O 13	0.046		0.0453	0.0016	0.046	
O 14	0.066		0.0630	0.0016	0.066	
O 15	0.495		0.4960	0.0017	0.495	
O 16	0.300		0.2950	0.0018	0.300	
O 17	0.489		0.4850	0.0015	0.489	
O 18	0.988		0.9835	0.0018	0.988	

Refinement Parameters	H.Y.Chen & ICSD 201742		H5672 (HRPD) ICSD 201742		bBiMo006 ICSD 201742	
		Esd		Esd		Esd
z						
Bi 1	0.75640		0.75640	0.00100	0.7564	
Bi 2	0.75830		0.75950	0.00080	0.7583	
Bi 3	0.75850		0.75750	0.00080	0.7585	
Bi 4	0.41220		0.41340	0.00070	0.4122	
Mo 1	0.0872		0.0893	0.0012	0.0872	
Mo 2	0.4163		0.4163	0.0013	0.4163	
Mo 3	0.0814		0.0813	0.0013	0.0814	
Mo 4	0.4156		0.4153	0.0013	0.4156	
O 1	0.2850		0.2853	0.0011	0.2850	
O 2	0.227		0.227	0.001	0.227	
O 3	0.689		0.6916	0.0012	0.689	
O 4	0.901		0.9028	0.0015	0.901	
O 5	0.447		0.4457	0.0014	0.447	
O 6	0.815		0.8198	0.0012	0.815	
O 7	0.048		0.0519	0.0012	0.048	
O 8	0.684		0.6837	0.0012	0.684	
O 9	0.596		0.5954	0.0013	0.596	
O 10	0.050		0.0550	0.0013	0.050	
O 11	0.455		0.4538	0.0012	0.454	
O 12	0.388		0.3868	0.0013	0.388	
O 13	0.112		0.1119	0.0013	0.112	
O 14	0.383		0.3829	0.0013	0.383	
O 15	0.820		0.8139	0.0013	0.820	
O 16	0.599		0.5957	0.0014	0.599	
O 17	0.904		0.9019	0.0014	0.904	
O 18	0.903		0.8995	0.0015	0.903	
B						
Bi 1	*		1.1000	0.2200	1.1000	
Bi 2	*		0.3700	0.1800	0.3700	
Bi 3	*		0.6200	0.0900	0.6200	
Bi 4	*		0.6000	0.1100	0.6000	
Mo 1	*		0.4500	0.2000	0.4500	
Mo 2	*		0.6500	0.2100	0.6500	
Mo 3	*		1.0300	0.2400	1.0300	
Mo 4	*		0.8700	0.2200	0.8700	
O 1	1.3000		0.9900	0.2300	0.9900	
O 2	1.1000		0.5400	0.2000	0.5400	
O 3	1.3000		0.9300	0.2900	0.9300	
O 4	1.1000		1.2600	0.2800	1.2600	
O 5	1.6000		1.2500	0.2600	1.2500	
O 6	1.0000		0.7500	0.2400	0.7500	
O 7	1.9000		0.6300	0.2500	0.6300	
O 8	1.4000		0.6600	0.2500	0.6600	
O 9	1.2000		0.9000	0.2600	0.9000	
O 10	1.8000		0.8800	0.2800	0.8800	
O 11	0.9000		0.4900	0.2500	0.4900	
O 12	0.7000		0.7900	0.2300	0.7900	
O 13	0.9000		1.1300	0.2600	1.1300	
O 14	1.1000		0.6800	0.2200	0.6800	
O 15	1.4000		1.0700	0.2800	1.0700	
O 16	1.5000		1.9100	0.3200	1.9100	
O 17	1.2000		0.6600	0.2400	0.6600	
O 18	1.7000		1.5100	0.3300	1.5100	

B. In-situ Diffractograms

	In Air						in Gas					
Refinement Parameters	**M22472Sum (300°C MRPD) ICSD 201742**		**M22473Sum (350°C MRPD) ICSD 201742**		**M22474Sum (400°C MRPD) ICSD 201742**		**in Gas (300°C MRPD) ICSD 201742**		**in Gas (350°C MRPD) ICSD 201742**		**in Gas (400°C MRPD) ICSD 201742**	
		Esd		Esd		Esd		Esd		Esd		Esd
Bismuth Molybdate												
R_p	5.50		5.27		5.41		6.17		6.27		6.62	
R_{wp}	8.47		7.68		8.52		8.15		8.18		8.60	
R_{exp}	6.47		6.48		6.46		6.39		6.40		6.36	
R_{Bragg}	2.41		2.17		2.37		3.40		3.70		4.00	
GOF	1.72		1.40		1.74		1.63		1.64		1.83	
Durbin UnWght	1.31		1.34		1.30		0.87		0.92		0.86	
Durbin Wght	1.52		1.44		1.51		0.93		0.98		0.92	
N-P	1293		1293		1293		1295		1292		1294	
Crystal Density (D_x)	6.41		6.40		6.38		6.44		6.42		6.41	
Mr	6030.7		6030.7		6030.7		6030.7		6030.7		6030.7	
Cell Volume	1561.52	0.23	1565.06	0.22	1568.55	0.32	1554.66	0.25	1558.35	0.26	1562.10	0.29
Histogram												
Sample displacement												
$2\theta_o$	0.000	Fixed	0.000	Fixed	0.000	Fixed	0.000	Fixed	0.000	Fixed	0.000	Fixed
B0	30.659	1.124	36.129	1.086	28.015	1.118	163.056	2.496	166.911	2.539	170.407	2.728
B1	1.577	0.057	1.474	0.053	1.839	0.052	-1.717	0.164	-1.861	0.167	-1.820	0.180
B2	-0.002	0.000	-0.002	0.000	-0.003	0.000	0.027	0.003	0.030	0.003	0.030	0.003
B3							0.000	0.000	0.000	0.000	0.000	0.000
B4												
B-1												
Phases												
Phase scale	0.029	0.000	0.028	0.000	0.029	0.000	0.028	0.000	0.028	0.000	0.028	0.000
a	12.022	0.001	12.031	0.001	12.045	0.001	12.004	0.001	12.013	0.001	12.021	0.001
b	10.866	0.001	10.874	0.001	10.889	0.001	10.850	0.001	10.859	0.001	10.869	0.001
c	11.954	0.001	11.963	0.001	11.979	0.002	11.937	0.001	11.946	0.001	11.955	0.001
β	90.148	0.015	90.156	0.014	90.162	0.014	90.156	0.017	90.148	0.019	90.151	0.021
Sample												
U	0.460	0.054	0.467	0.052	0.526	0.064	0.594	0.059	0.498	0.058	0.476	0.063
V	-0.523	0.065	-0.507	0.061	-0.602	0.074	-0.726	0.069	-0.600	0.067	-0.569	0.073
W	0.286	0.021	0.279	0.019	0.311	0.023	0.384	0.021	0.352	0.021	0.339	0.023
Asy1	0.150	0.006	0.146	0.005	0.137	0.006	0.059	0.006	0.064	0.006	0.061	0.006
Size/Gam0	0.071	0.009	0.067	0.009	0.069	0.010	0.031	0.010	0.023	0.010	0.032	0.011
x												
Bi 1	-0.1010		-0.1010		-0.1010		-0.1010		-0.1010		-0.1010	
Bi 2	0.6009		0.6009		0.6009		0.6009		0.6009		0.6009	
Bi 3	0.2531		0.2531		0.2531		0.2531		0.2531		0.2531	
Bi 4	0.2556		0.2556		0.2556		0.2556		0.2556		0.2556	
Mo 1	-0.0838		-0.0838		-0.0838		-0.0838		-0.0838		-0.0838	
Mo 2	-0.0773		-0.0773		-0.0773		-0.0773		-0.0773		-0.0773	
Mo 3	0.5867		0.5867		0.5867		0.5867		0.5867		0.5867	
Mo 4	0.5805		0.5805		0.5805		0.5805		0.5805		0.5805	
O 1	0.2553		0.2553		0.2553		0.2553		0.2553		0.2553	
O 2	0.2552		0.2552		0.2552		0.2552		0.2552		0.2552	
O 3	0.4099		0.4099		0.4099		0.4099		0.4099		0.4099	
O 4	0.3196		0.3196		0.3196		0.3196		0.3196		0.3196	
O 5	0.1102		0.1102		0.1102		0.1102		0.1102		0.1102	
O 6	0.1014		0.1014		0.1014		0.1014		0.1014		0.1014	
O 7	0.4029		0.4029		0.4029		0.4029		0.4029		0.4029	
O 8	0.0934		0.0934		0.0934		0.0934		0.0934		0.0934	
O 9	0.1941		0.1941		0.1941		0.1941		0.1941		0.1941	
O 10	0.0988		0.0988		0.0988		0.0988		0.0988		0.0988	
O 11	0.4098		0.4098		0.4098		0.4098		0.4098		0.4098	
O 12	0.0579		0.0579		0.0579		0.0579		0.0579		0.0579	
O 13	0.0428		0.0428		0.0428		0.0428		0.0428		0.0428	
O 14	0.4461		0.4461		0.4461		0.4461		0.4461		0.4461	
O 15	0.4011		0.4011		0.4011		0.4011		0.4011		0.4011	
O 16	0.9611		0.9611		0.9611		0.9611		0.9611		0.9611	
O 17	0.1780		0.1780		0.1780		0.1780		0.1780		0.1780	
O 18	0.1915		0.1915		0.1915		0.1915		0.1915		0.1915	

Refinement Parameters	In Air						in Gas					
	M22472Sum		M22473Sum		M22474Sum		in Gas		in Gas		in Gas	
	ICSD 201742		ICSD 201742		ICSD 201742		ICSD 201742		ICSD 201742		ICSD 201742	
		Esd		Esd		Esd		Esd		Esd		Esd
y												
Bi 1	0.1233		0.1233		0.1233		0.1233		0.1233		0.1233	
Bi 2	0.1250		0.1250		0.1250		0.1250		0.1250		0.1250	
Bi 3	0.1203		0.1203		0.1203		0.1203		0.1203		0.1203	
Bi 4	0.1244		0.1244		0.1244		0.1244		0.1244		0.1244	
Mo 1	0.1243		0.1243		0.1243		0.1243		0.1243		0.1243	
Mo 2	0.1266		0.1266		0.1266		0.1266		0.1266		0.1266	
Mo 3	0.1245		0.1245		0.1245		0.1245		0.1245		0.1245	
Mo 4	0.1281		0.1281		0.1281		0.1281		0.1281		0.1281	
O 1	0.2634		0.2634		0.2634		0.2634		0.2634		0.2634	
O 2	0.4944		0.4944		0.4944		0.4944		0.4944		0.4944	
O 3	0.2568		0.2568		0.2568		0.2568		0.2568		0.2568	
O 4	0.2572		0.2572		0.2572		0.2572		0.2572		0.2572	
O 5	0.4416		0.4416		0.4416		0.4416		0.4416		0.4416	
O 6	0.2452		0.2452		0.2452		0.2452		0.2452		0.2452	
O 7	0.4433		0.4433		0.4433		0.4433		0.4433		0.4433	
O 8	0.4941		0.4941		0.4941		0.4941		0.4941		0.4941	
O 9	0.2558		0.2558		0.2558		0.2558		0.2558		0.2558	
O 10	0.3192		0.3192		0.3192		0.3192		0.3192		0.3192	
O 11	0.3066		0.3066		0.3066		0.3066		0.3066		0.3066	
O 12	0.1879		0.1879		0.1879		0.1879		0.1879		0.1879	
O 13	0.0453		0.0453		0.0453		0.0453		0.0453		0.0453	
O 14	0.0630		0.0630		0.0630		0.0630		0.0630		0.0630	
O 15	0.4960		0.4960		0.4960		0.4960		0.4960		0.4960	
O 16	0.2950		0.2950		0.2950		0.2950		0.2950		0.2950	
O 17	0.4850		0.4850		0.4850		0.4850		0.4850		0.4850	
O 18	0.9835		0.9835		0.9835		0.9835		0.9835		0.9835	
z												
Bi 1	0.7564		0.7564		0.7564		0.7564		0.7564		0.7564	
Bi 2	0.7595		0.7595		0.7595		0.7595		0.7595		0.7595	
Bi 3	0.7575		0.7575		0.7575		0.7575		0.7575		0.7575	
Bi 4	0.4134		0.4134		0.4134		0.4134		0.4134		0.4134	
Mo 1	0.0893		0.0893		0.0893		0.0893		0.0893		0.0893	
Mo 2	0.4163		0.4163		0.4163		0.4163		0.4163		0.4163	
Mo 3	0.0813		0.0813		0.0813		0.0813		0.0813		0.0813	
Mo 4	0.4153		0.4153		0.4153		0.4153		0.4153		0.4153	
O 1	0.2853		0.2853		0.2853		0.2853		0.2853		0.2853	
O 2	0.2266		0.2266		0.2266		0.2266		0.2266		0.2266	
O 3	0.6916		0.6916		0.6916		0.6916		0.6916		0.6916	
O 4	0.9028		0.9028		0.9028		0.9028		0.9028		0.9028	
O 5	0.4457		0.4457		0.4457		0.4457		0.4457		0.4457	
O 6	0.8198		0.8198		0.8198		0.8198		0.8198		0.8198	
O 7	0.0519		0.0519		0.0519		0.0519		0.0519		0.0519	
O 8	0.6837		0.6837		0.6837		0.6837		0.6837		0.6837	
O 9	0.5954		0.5954		0.5954		0.5954		0.5954		0.5954	
O 10	0.0550		0.0550		0.0550		0.0550		0.0550		0.0550	
O 11	0.4538		0.4538		0.4538		0.4538		0.4538		0.4538	
O 12	0.3868		0.3868		0.3868		0.3868		0.3868		0.3868	
O 13	0.1119		0.1119		0.1119		0.1119		0.1119		0.1119	
O 14	0.3829		0.3829		0.3829		0.3829		0.3829		0.3829	
O 15	0.8139		0.8139		0.8139		0.8139		0.8139		0.8139	
O 16	0.5957		0.5957		0.5957		0.5957		0.5957		0.5957	
O 17	0.9019		0.9019		0.9019		0.9019		0.9019		0.9019	
O 18	0.8995		0.8995		0.8995		0.8995		0.8995		0.8995	
B												
Bi 1	0.96	0.53	1.47	0.58	1.98	0.68	1.20	0.00	2.10	0.80	1.92	0.62
Bi 2	1.56	0.62	0.96	0.53	1.50	0.67	2.20	0.53	2.21	0.77	0.98	0.85
Bi 3	1.35	0.23	1.30	0.21	1.38	0.25	1.86	0.24	2.03	0.26	2.61	0.31
Bi 4	2.52	0.43	2.15	0.38	2.04	0.42	2.53	0.43	2.68	0.46	2.57	0.48
Mo 1	1.45	0.74	2.13	0.61	1.20	0.00	2.66	0.99	1.96	0.69	4.58	1.07
Mo 2	0.90	0.57	1.22	0.50	1.05	0.65	0.90	0.00	1.18	0.81	1.89	0.79
Mo 3	0.75	0.63	0.43	0.00	1.56	0.66	1.03	0.70	0.80	0.00	1.00	0.00
Mo 4	1.71	0.74	2.67	0.82	3.42	1.02	2.54	0.71	2.84	1.07	1.98	1.16
O 1	3.19	0.85	3.71	0.84	4.50	1.09	1.58	0.73	2.38	0.84	2.13	0.95
O 2	1.08	0.45	1.10	0.42	1.36	0.52	1.64	0.63	0.82	0.57	1.41	0.65
O 3	4.70	1.17	3.18	0.83	4.83	1.35	5.05	1.53	6.28	1.87	4.38	1.55
O 4	1.08	0.73	1.07	0.63	1.73	0.87	1.00	0.00	1.00		1.70	0.00
O 5	1.03	0.71	3.76	1.03	2.56	1.05	1.00	0.00	1.00		2.50	0.00
O 6	0.79	0.63	0.70	0.00	1.51	0.81	1.92	0.90	0.84	0.79	2.25	1.06
O 7	2.17	0.87	0.62	0.59	1.17	0.77	2.27	0.95	3.06	1.27	2.34	1.01
O 8	1.00	0.00	1.20	0.00	0.50	0.00	1.12	0.82	1.68	0.93	1.50	0.00
O 9	1.41	0.70	1.40	0.65	2.15	0.84	1.94	0.77	3.25	1.09	2.99	1.16
O 10	0.80	0.00	1.00	0.00	0.50	0.00	0.91	0.00	1.07	0.80	1.00	0.00
O 11	2.52	0.87	1.58	0.67	4.37	1.25	5.23	1.48	5.47	1.61	13.21	3.29
O 12	0.50	0.00	0.50	0.00	1.16	0.68	0.50	0.00	1.36	0.76	0.97	0.87
O 13	1.58	0.85	1.71	0.79	1.40	0.85	1.30	0.77	1.06	0.76	1.76	1.08
O 14	1.29	0.64	1.84	0.68	1.58	0.77	3.05	1.01	2.70	1.16	2.90	1.02
O 15	1.00	0.00	1.20	0.00	0.82	0.71	1.62	0.93	2.69	1.22	2.88	1.14
O 16	1.94	0.76	2.73	0.82	3.40	1.03	14.38	3.32	14.59	3.40	7.72	2.25
O 17	2.43	0.83	2.62	0.82	3.47	1.06	2.58	1.02	3.11	1.14	2.24	1.09
O 18	5.44	1.27	4.04	1.00	5.62	1.42	15.56	3.77	10.07	2.88	15.63	4.20

REFINEMENT RESULTS OF γ-Bi_2MoO_6

A. Room Temperature Diffractograms

Refinement Parameters			H5673t (HRPD)		RT-XRD (g-BiMo009)	
	ICSD 47139		ICSD 47139			
		Esd		Esd		
Bismuth Molybdate						
R_p			5.84		10.59	
R_{wp}			7.44		16.29	
R_{exp}			5.25		5.42	
R_{Bragg}			1.87		4.94	
GOF			2.00		9.02	
Durbin UnWght			1.12		0.17	
Durbin Wght			1.11		0.26	
N-P			2794		5429	
Crystal Density (D_x)	8.28		8.25		8.27	
Mr			2439.6		2439.6	
Cell Volume	489.23	0.03	490.84	0.02	489.41	0.02
Histogram						
Sample displacement						
$2\theta_o$			0.0000	Fixed	0.0410	
B0			30.409	1.022	-5.640	2.173
B1			0.102	0.020	0.715	0.023
B2			0.000	0.000		
B3						
B4						
B-1			98.732	12.397	2035.10	31.25
Phases						
Phase scale			0.033	0.000	0.000	0.000
a	5.482	0.000	5.489	0.000	5.484	0.000
b	16.199	0.001	16.225	0.000	16.209	0.000
c	5.509	0.000	5.511	0.000	5.506	0.000
x						
Bi 1	0.5180	0.0012	0.5212	0.0014	0.5180	
Bi 2	0.4822		0.4807	0.0014	0.4822	
Mo 1	0.0028	0.0021	0.0028	Fixed	0.0028	
O 1	0.0556	0.0019	0.0506	0.0022	0.0556	
O 2	0.2594	0.0010	0.2620	0.0015	0.2594	
O 3	0.2360	0.0013	0.2398	0.0014	0.2360	
O 4	0.6917	0.0014	0.6850	0.0015	0.6917	
O 5	0.2121	0.0015	0.2171	0.0015	0.2121	
O 6	0.5654	0.0022	0.5709	0.0024	0.5654	
y						
Bi 1	0.4232	0.0004	0.4217	0.0005	0.4232	
Bi 2	0.0783	0.0004	0.0780	0.0005	0.0783	
Mo 1	0.2488	0.0007	0.2488	Fixed	0.2488	
O 1	0.1407	0.0008	0.1411	0.0009	0.1407	
O 2	-0.0017	0.0006	-0.0011	0.0009	-0.0017	
O 3	0.5006	0.0008	0.5002	0.0009	0.5006	
O 4	0.2322	0.0005	0.2306	0.0006	0.2322	
O 5	0.2634	0.0006	0.2630	0.0006	0.2634	
O 6	0.3589	0.0010	0.3598	0.0011	0.3589	
z						
Bi 1	0.9814	0.0014	0.9856	0.0019	0.9814	
Bi 2	0.9897	0.0014	0.9840	0.0021	0.9897	
Mo 1	0.0000	Fixed	0.0000	Fixed	0.0000	
O 1	0.0959	0.0020	0.0872	0.0026	0.0959	
O 2	0.2776	0.0014	0.2752	0.0023	0.2776	
O 3	0.2664	0.0022	0.2680	0.0025	0.2664	
O 4	0.2524	0.0016	0.2499	0.0019	0.2524	
O 5	0.3550	0.0016	0.3514	0.0018	0.3550	
O 6	0.5700	0.0019	0.5761	0.0030	0.5700	
B						
Bi 1	0.3000	0.3000	0.4100	0.1400	0.3000	
Bi 2	1.0000	0.3000	0.9500	0.1500	1.0000	
Mo 1	0.5000	0.1000	0.8100	0.0700	0.5000	
O 1	0.3000	0.2000	0.5100	0.2100	0.3000	
O 2	0.4000	0.2000	0.6500	0.3000	0.4000	
O 3	1.3000	0.3000	0.6000	0.2800	1.3000	
O 4	0.9000	0.2000	0.9900	0.1600	0.9000	
O 5	1.1000	0.2000	0.8500	0.1300	1.1000	
O 6	1.4000	0.4000	1.8600	0.3200	1.4000	
Sample						
U			0.129	0.009	0.024	0.005
V			-0.260	0.015	0.006	0.006
W			0.175	0.007	0.004	0.001
Asy1			0.065	0.003	0.053	0.001
Size/Gam0			0.120	0.005	0.089	0.001
Particle Size (A)			713.20	29.20	994.90	15.80

B. In-situ Diffractograms

Refinement Parameters	In Air							In Gas					
	300°C		350°C		400°C			300°C		350°C		400°C	
		Esd		Esd		Esd			Esd		Esd		Esd
Bismuth Molybdate													
R_p	9.28		9.98		8.83			6.94		6.98		7.82	
R_{wp}	14.02		15.80		12.68			10.24		10.31		11.82	
R_{exp}	8.14		8.19		8.23			5.49		5.49		5.57	
R_{Bragg}	5.09		5.53		5.11			3.65		3.66		4.43	
GOF	2.97		3.72		2.37			3.49		3.53		4.51	
Durbin UnWght	0.98		0.84		0.89			0.74		0.73		0.56	
Durbin Wght	1.49		1.30		1.29			1.14		1.13		0.90	
N-P	1296		1293		1297			1298		1298		1299	
Crystal Density (D_x)	8.13		8.11		8.09			8.14		8.14		8.09	
Mr	2439.6		2439.6		2439.6			2439.6		2439.6		2439.6	
Cell Volume	497.96	0.10	499.28	0.12	500.75	0.10		497.41	0.06	497.43	0.06	500.41	0.08
Histogram													
Sample displacement													
$2\theta_o$	0.0000	Fixed	0.0000	Fixed	0.0000	Fixed		0.0000	Fixed	0.0000	Fixed	0.0000	Fixed
B0	4.417	1.793	-2.622	1.968	5.775	1.513		25.553	1.796	25.466	1.807	17.036	1.996
B1	3.388	0.141	3.385	0.163	3.201	0.125		3.777	0.091	3.795	0.092	4.297	0.103
B2	-0.046	0.003	-0.044	0.003	-0.043	0.002		-0.016	0.001	-0.016	0.001	-0.019	0.001
B3	0.000	0.000	0.000	0.000	0.000	0.000							
B4													
B-1													
Phases													
Phase scale	0.162	0.003	0.166	0.004	0.162	0.003		0.394	0.005	0.393	0.005	0.361	0.006
a	5.522	0.001	5.529	0.001	5.536	0.001		5.520	0.005	5.520	0.000	5.535	0.001
b	16.256	0.000	16.261	0.002	16.265	0.001		16.252	0.001	16.252	0.001	16.263	0.001
c	5.547	0.001	5.553	0.001	5.561	0.001		5.544	0.000	5.545	0.000	5.559	0.001
x													
Bi 1	0.5212	0.0000	0.5212	0.0000	0.5212	0.0000		0.5212	0.0014	0.5212	0.0014	0.5212	0.0014
Bi 2	0.4807	0.0000	0.4807	0.0000	0.4807	0.0000		0.4807	0.0014	0.4807	0.0014	0.4807	0.0014
Mo 1	0.0028	0.0000	0.0028	0.0036	0.0028	0.0000		0.0028	Fixed	0.0028	Fixed	0.0028	Fixed
O 1	0.0506	0.0045	0.0506	0.0049	0.0506	0.0051		0.0506	0.0022	0.0506	0.0022	0.0506	0.0022
O 2	0.2620	0.0045	0.2620	0.0000	0.2620	0.0000		0.2620	0.0015	0.2620	0.0015	0.2620	0.0015
O 3	0.2398	0.0038	0.2398	0.0046	0.2398	0.0042		0.2398	0.0014	0.2398	0.0014	0.2398	0.0014
O 4	0.6850	0.0037	0.6850	0.0042	0.6850	0.0040		0.6850	0.0015	0.6850	0.0015	0.6850	0.0015
O 5	0.2171	0.0046	0.2171	0.0049	0.2171	0.0046		0.2171	0.0015	0.2171	0.0015	0.2171	0.0015
O 6	0.5709	0.0032	0.5709	0.0039	0.5709	0.0040		0.5709	0.0024	0.5709	0.0024	0.5709	0.0024
y													
Bi 1	0.4217	0.0000	0.4217	0.0000	0.4217	0.0000		0.4217	0.0005	0.4217	0.0005	0.4217	0.0005
Bi 2	0.0780	0.0000	0.0780	0.0000	0.0780	0.0000		0.0780	0.0005	0.0780	0.0005	0.0780	0.0005
Mo 1	0.2488	0.0000	0.2488	0.0010	0.2488	0.0000		0.2488	Fixed	0.2488	Fixed	0.2488	Fixed
O 1	0.1411	0.0012	0.1411	0.0014	0.1411	0.0014		0.1411	0.0009	0.1411	0.0009	0.1411	0.0009
O 2	-0.0011	0.0015	-0.0011	0.0000	-0.0011	0.0000		-0.0011	0.0009	-0.0011	0.0009	-0.0011	0.0009
O 3	0.5002	0.0015	0.5002	0.0015	0.5002	0.0014		0.5002	0.0009	0.5002	0.0009	0.5002	0.0009
O 4	0.2306	0.0019	0.2306	0.0021	0.2306	0.0019		0.2306	0.0006	0.2306	0.0006	0.2306	0.0006
O 5	0.2630	0.0013	0.2630	0.0016	0.2630	0.0015		0.2630	0.0006	0.2630	0.0006	0.2630	0.0006
O 6	0.3598	0.0010	0.3598	0.0013	0.3598	0.0013		0.3598	0.0011	0.3598	0.0011	0.3598	0.0011
z													
Bi 1	0.9856	0.0000	0.9856	0.0000	0.9856	0.0000		0.9856	0.0019	0.9856	0.0019	0.9856	0.0019
Bi 2	0.9840	0.0000	0.9840	0.0000	0.9840	0.0000		0.9840	0.0021	0.9840	0.0021	0.9840	0.0021
Mo 1	0.0000	0.0000	0.0000	Fixed	0.0000	0.0000		0.0000	Fixed	0.0000	Fixed	0.0000	Fixed
O 1	0.0872	0.0055	0.0872	0.0062	0.0872	0.0065		0.0872	0.0026	0.0872	0.0026	0.0872	0.0026
O 2	0.2752	0.0046	0.2752	0.0000	0.2752	0.0000		0.2752	0.0023	0.2752	0.0023	0.2752	0.0023
O 3	0.2680	0.0042	0.2680	0.0040	0.2680	0.0036		0.2680	0.0025	0.2680	0.0025	0.2680	0.0025
O 4	0.2499	0.0047	0.2499	0.0051	0.2499	0.0047		0.2499	0.0019	0.2499	0.0019	0.2499	0.0019
O 5	0.3514	0.0043	0.3514	0.0046	0.3514	0.0047		0.5813	0.0042	0.3514	0.0018	0.3514	0.0018
O 6	0.5761	0.0034	0.5761	0.0041	0.5761	0.0042		0.5761	0.0030	0.5761	0.0030	0.5761	0.0030
B													
Bi 1	0.6300	0.2600	0.7500	0.2900	1.0100	0.2800		2.0000	0.3300	2.0600	0.3200	2.3600	0.4600
Bi 2	3.3400	0.4400	3.6500	0.5000	3.2500	0.4200		1.6200	0.3100	1.6600	0.2900	1.9200	0.4200
Mo 1	2.3600	0.2400	2.5400	0.2800	2.7000	0.2300		1.5800	0.1400	1.6100	0.1500	1.7600	0.1800
O 1	4.8800	0.9900	6.1700	1.1700	7.2500	1.0200		3.3000	0.6400	3.2000	0.6300	3.2900	0.8700
O 2	1.8400	0.6200	2.6000	0.7200	2.1900	0.6200		1.7800	0.5700	1.7500	0.5700	1.5800	0.7100
O 3	1.5400	0.5500	1.3100	0.5400	1.3900	0.5000		1.5700	0.5400	1.6200	0.5300	2.0300	0.7200
O 4	2.2400	0.5200	2.3900	0.6000	2.5500	0.5100		2.1400	0.3300	2.1200	0.3400	2.5100	0.4500
O 5	6.7200	0.9900	7.8600	1.2700	7.9000	1.0200		4.5200	0.4900	4.6800	0.5100	5.2700	0.6900
O 6	2.1200	0.6700	1.7300	0.6500	1.4300	0.4900		2.3700	0.5700	2.1400	0.5300	3.0500	0.8400
Sample													
U	0.117	0.060	0.143	0.072	0.192	0.060		0.088	0.036	0.090	0.037	0.112	0.048
V	-0.041	0.088	-0.089	0.102	-0.160	0.085		0.033	0.054	0.028	0.054	0.015	0.069
W	0.139	0.032	0.147	0.036	0.171	0.030		0.071	0.019	0.073	0.020	0.085	0.024
Asy1	0.222	0.011	0.215	0.012	0.209	0.010		0.311	0.007	0.310	0.007	0.292	0.008
Size/Gam0	0.100	0.016	0.116	0.017	0.110	0.014		0.125	0.010	0.125	0.010	0.108	0.012
Particle Size (A)	954.10	155.30	819.90	122.90	867.80	111.00		760.90	59.70	762.00	60.30	882.30	98.50

APPENDIX C. The Determination of Surface Area, Pore Volume and Pore Size of Bismuth Molybdates

Surface areas, pore volume and pore size distribution of the catalysts prepared for this study were determined using the BET method with N_2 as the adsorbate at the liquid nitrogen temperature. The measurements were carried out at *Pusat Penelitian Tenaga Nuklir (PPTN)* Yogyakarta, Indonesia. The instrument used for these measurements was a NOVA 1000 *Surface Area Analyser* (Quantachrome Instruments). All catalysts were oven dried at 105^{o}C for 24 hours, allowed to cool down in a desiccator and then vacuum-sealed before shipping for measurements.

The surface areas were determined using the multi point BET method while the pore size distributions were evaluated using the BJH method from the adsorption isotherm. Average pore radiuses were calculated with an assumption that the pore geometry is cylindrical. The pore volumes were calculated according to the following equation:

$$r_p = \frac{2P_a V_{ads} V_m}{RT}$$

where,
P_a = ambient pressure
V_{ads} = volume of nitrogen adsorbed
V_m = molar volume of the liquid adsorbate (34.7 $cm^3.mol^{-1}$ for nitrogen)
T = ambient temperature

All calculations of surface area, pore volume, and pore size distribution were carried out by application software accompanying the instrument (NOVADRP version 2.00). The experimental results are given in Tables C.1 to C.3.

Table C.1 α-$Bi_2Mo_3O_{12}$

Sample ID = abimo
Adsorbate = N_2
Adsorption tolerance = 0.1000 mm Hg
Adsorption Equil Time = 60 sec
Adsorption Dwell Time = 180 Sec

Sample Weight = 0.2384 g
P_o = 784.27 mm Hg
Bath Temperature = 77.40 ^oK

Multi BET (adsorption)

P/P_o	BET Transform $(1/\{W[P_o/P - 1]\})$
0.48040	97.159489
0.068820	114.042079
0.153116	210.161812
0.201007	254.106036
0.250925	306.121330

Surface Area	0.763264 m^2
Specific Surface Area	3.201478 m^2 g^{-1}

BJH (Adsorption)

Pore Radius (Å)	Cumulative Pore Volume (cc g^{-1} 10^{-3})
715.341689	3.549832
166.725841	3.404021
100.313498	3.24338
78.033001	3.160523
60.859476	2.989983
49.424781	1.516226
41.183703	1.494194
36.195337	1.483466
32.658333	1.46959
29.628589	1.458727
26.618066	1.440058
24.133795	1.261238
22.107304	1.106805
20.328903	0.966874
18.749532	0.821001
17.290948	0.648384
15.855395	0.4603
14.754369	0.250358
13.866719	0.158572

Total Pore Volume is 3.694904x10^{-03} cc g^{-1} for all pore less than 1178.593734 Å
Average pore radius is 23.082490 Å

Table C.2 β-$Bi_2Mo_2O_9$

Sample ID = Beta Bimo
Adsorbate = N_2
Adsorption tolerance = 0.1000 mm Hg
Adsorption Equil Time = 60 sec
Adsorption Dwell Time = 180 Sec

Sample Weight = 0.3428 g
P_o = 750.33 mm Hg
Bath Temperature = 77.40 ^oK

Multi BET (adsorption)

P/P_o	BET Transform $(1/\{W[P_o/P - 1]\})$
0.105301	306.858308
0.142002	325.298358
0.204744	356.129456
0.241696	373.994787

Surface Area	9.020623 m^2
Specific Surface Area	4.660135 $m^2 g^{-1}$

BJH (Adsorption)

Pore Radius (Å)	Cumulative Pore Volume (cc g^{-1} 10^{-3})
931.053456	2.122919
159.124512	2.066356
105.871378	2.038831
75.532598	1.971715
60.399872	1.909436
48.029024	1.794714
41.48486	1.68478
36.994075	1.58539
32.585777	1.499373
28.958741	1.353603
26.21481	1.281895
23.783664	1.134932
21.838197	1.082711
20.077756	1.001041
18.554337	0.924805
17.165934	0.734089
15.840241	0.628847
14.793266	0.362074
13.746309	0.233773

Total Pore Volume is 1.759221x10^{-03} cc g^{-1} for all pore less than 1639.733899 Å
Average pore radius is 15.576319 Å

Table C.3 γ-Bi_2MoO_6

Sample ID = Gamma Bimo
Adsorbate = N_2
Adsorption tolerance = 0.1000 mm Hg
Adsorption Equil Time = 60 sec
Adsorption Dwell Time = 180 Sec

Sample Weight = 0.5397 g
P_o = 751.50 mm Hg
Bath Temperature = 77.40 ^oK

Multi BET (adsorption)

P/P_o	BET Transform $(1/\{W[P_o/P - 1]\})$
0.070664	161.145982
0.141794	223.748945
0.201835	269.578549

Surface Area	2.016675 m^2
Specific Surface Area	3.736381 $m^2 g^{-1}$

BJH (Adsorption)

Pore Radius (Å)	Cumulative Pore Volume (cc g^{-1} 10^{-3})
814.989479	4.211614
160.850173	4.03251
106.216649	3.929396
74.945447	3.715394
60.121336	3.591567
48.194609	3.363503
41.543763	3.167965
37.000637	2.982252
32.603068	2.829688
28.965029	2.537139
26.258014	2.38445
23.82944	2.09091
21.841507	1.910043
20.112715	1.75543
18.581563	1.67703
17.150425	1.262867
15.916384	1.03682
14.76672	0.637315
13.730276	0.413731

Total Pore Volume is $4.049085x10^{-03}$ cc g^{-1} for all pore less than 1406.934593 Å
Average pore radius is 21.673831 Å